

THE ROLE OF RECEPTOR ACTIVITY
MODIFYING PROTEIN 1 IN PROSTATE
CANCER

Jessica Warrington

PhD

Department of Oncology and Metabolism

February 2018

Acknowledgements

I would like to firstly thank my excellent supervisors and mentors Professor Tim Skerry and Dr Gareth Richards. Both of you have been incredibly helpful throughout my postgraduate degree and I definitely could not have done it without you. Tim has taught me how to never forget the reason for my experiments and to step back sometimes to see the bigger picture. Although terrifying, your “grilling” during lab meetings has led me to become a better scientist and I thank you for that. Also, a big thank you to Gareth for always being on hand to answer my questions and give advice as well as being a great friend. I also could not have completed this PhD without the help of Ning Wang and his excellent *in vivo* knowledge. Thank you, Ning, for your help and patience during my project and for your feedback when I have been preparing oral presentations. I would like to thank Mark Kinch for his efforts in preparing tissue sections from my *in vivo* studies. I would also like to thank Sue Clarke and the Flow Cytometry Core Facility for helping me with sorting my CRISPR cells. Thank you to Alison Gartland, my personal tutor and friend, your advice has always been incredibly useful. I must also thank Karan Shah, who will always go above and beyond to help others including myself. I am grateful to Karan also for the amount of shots we have shared over the last few years. I would also like to thank my PhD partners, Paris Avgoustou and Ameera Al Jailani for their support and help throughout my own PhD. Thank you to our new PhD students, Joe Holmes, Kamilla Bigos and Ewan Lilley for making me laugh on the tough days. I am grateful to my family for their continuing support throughout university and now you finally have a record of what it is I actually do! Lastly, I want to generally thank everybody within the department for creating such a friendly atmosphere and amiable working environment.

Abstract

Prostate cancer affects 1 in 8 men in the UK. Treatment options for advanced prostate cancer patients with hormone refractory and metastatic disease are limited and therefore investigations are required to identify novel therapeutic targets. Receptor activity modifying protein 1 (RAMP1) is a vital component for many different G protein-coupled receptors (GPCRs) from the calcitonin peptide family. It also has been linked with the clinical progression of prostate cancer and found to be an important driver of tumour growth in prostate cancer cell lines.

To further investigate the role of RAMP1 in prostate cancer, CRISPR/Cas9 was used to generate RAMP1 knockouts in a PC3 cell line. RAMP1 knockouts were validated using endpoint and quantitative PCR with Sanger sequencing. These RAMP1 knockouts were then tested *in vitro* and showed to have significant reductions in cell viability, invasion, adhesion and colony formation abilities. Increased levels of apoptosis were also found in RAMP1 knockouts. *In vivo*, deletion of RAMP1 resulted in almost complete inhibition of subcutaneous tumour growth. Immunohistochemistry staining revealed no differences in markers for Ki67 and CD31, respectively suggesting alternative causes for tumour growth inhibition. Treatment with human CGRP antagonists had no effect on tumour growth. These results may suggest that RAMP1 is acting in a CGRP-independent manner. Analysis of downstream signaling pathways in RAMP1 KO cells also revealed an association with Akt and STAT3.

These results show that RAMP1 may be vital for the survival of aggressive prostate cancer cells and that this protein plays an important role in the development of tumour growth. Although it remains unknown through which mechanism RAMP1 is promoting prostate cancer, the dysregulation of phosphorylated Akt and STAT3 implicates RAMP1 as an important instigator of oncogenic pathways associated with promoting hormone refractory and metastatic prostate cancer. Future investigations may focus on which GPCR RAMP1 is acting

with to promote prostate cancer and whether this receptor protein can be targeted therapeutically to aid advanced prostate cancer patients.

Table of Contents

Acknowledgements	2
Abstract	3
Table of Contents	5
List of Figures	8
List of Tables	11
CHAPTER 1: General Introduction	12
1.1. Hallmarks of Cancer	12
1.2. Prostate Cancer	14
1.2.1. Incidence and Diagnosis.....	14
1.2.2. Staging and Treatment	17
1.3. G Protein-Coupled Receptors (GPCRs): The Calcitonin Peptide Family	23
1.3.1. Structure of Adrenomedullin and CGRP	26
1.1 Adrenomedullin and Prostate Cancer	27
1.2 CGRP and Prostate Cancer	31
1.3 GPRC6A and Prostate Cancer	33
1.4 Adrenomedullin and CGRP: The Bone Microenvironment	34
1.5 Hypothesis and Objectives	35
CHAPTER 2: Characterisation of the PC3 Cell line	37
2.1 Introduction	37
2.2 Hypotheses:	40
2.3 Research Questions:	40
2.4 Methods and Materials	40
2.4.1 Maintenance of Cell Lines	40
2.4.2 Passage of Cells	41
2.4.3 Cell Counting	41
2.4.4 RNA Extraction.....	41
2.4.5 cDNA Synthesis.....	42
2.4.6 Endpoint Polymerase Chain Reaction (PCR).....	43
2.4.7 Gel Electrophoresis.....	45
2.4.8 Sanger Sequencing.....	45
2.4.9 Protein Extraction	46
2.4.10 Bicinchoninic Acid (BCA) Assay.....	46
2.4.11 Western Blotting: Gel Electrophoresis and Transfer	48
2.4.12 Western Blotting: Blocking and Probing.....	49
2.4.13 Western Blotting: Detection	50
2.4.14 Western Blotting: Optimisation	51
2.4.15 CGRP (Human) Fluorescent Immunoassay	51
2.4.16 cAMP LANCE Ultra TR-FRET	54
2.5 Results	60
2.5.1 Endpoint PCR.....	60
2.5.2 Western Blot	63
2.5.3 CGRP Fluorescent Immunoassay	63
2.5.4 Cyclic AMP Assays.....	65

2.6	Discussion	68
	CHAPTER 3: GENERATION OF CRISPR/CAS9 KNOCKOUT IN PC3 CELLS	71
3.1	Introduction	71
3.2	Hypothesis:	77
3.3	Research Aims:.....	77
3.4	Methods & Materials	78
3.4.1	Transfection of CRISPR Vectors into PC-3 Cells.....	78
3.4.2	Fluorescence-Activated Cell Sorting of CRISPR Cells	79
3.4.3	Endpoint Polymerase Chain Reaction.....	80
3.4.4	Reverse Transcription for Quantitative Polymerase Chain Reaction (qPCR) ..	80
3.4.5	Quantitative Polymerase Chain Reaction (qPCR)	82
3.4.6	Genomic DNA Polymerase Chain Reaction	83
3.4.7	Genomic DNA Extraction.....	84
3.4.8	Genomic PCR Reaction.....	84
3.5	Results.....	86
3.5.1	Transfection of PC3 Cell Line with HDR CRISPR/Cas9 Constructs.....	86
3.5.2	Fluorescent activated cell sorting of CRISPR transfected cells.....	87
3.5.3	Validation of CRISPR Clones with Endpoint PCR.....	91
3.5.4	Validation of CRISPR Clones with Genomic DNA and Endpoint PCR	94
3.5.5	Validation of CRISPR Clones with Quantitative PCR.	96
3.5.6	Levels of RAMP2 and RAMP3 mRNA in RAMP1 CRISPR Clones Measured with Endpoint PCR.	100
3.5.7	Validation of RAMP1 CRISPR Clones with Western Blotting.....	101
3.6	Discussion	102
	CHAPTER 4: FUNCTIONAL EFFECTS OF RAMP1 DELETION IN PC3 CELLS <i>IN</i>	
	<i>VITRO</i>.	108
4.1	Introduction	108
4.2	Hypotheses	112
4.3	Research Aims.....	112
4.4	Materials and Methods.....	114
4.4.1	Viability Assays	114
4.4.2	Apoptosis Caspase 3/7 Assays.....	116
4.4.3	Migration “Scratch” Assays.....	119
4.4.4	Transwell Invasion Assays	119
4.4.5	Colony Formation Assays	121
4.4.6	Adhesion Assays	122
4.4.7	Multiplex Magnetic Bead Assay	122
4.4.8	Statistical Analysis.....	126
4.5	Results.....	126
4.5.1	Viability Assays	126
4.5.2	Migration “Scratch” Assays.....	130
4.5.3	Transwell Invasion Assays	133
4.5.4	Colony Formation Assays	135
4.5.5	Adhesion Assays	138
4.5.6	Apoptosis Assays	139
4.5.7	Multiplex Magnetic Bead Assay: Multi-Pathway 9 Plex.....	141
4.6	Discussion	144
	CHAPTER 5: FUNCTIONAL EFFECT OF RAMP1 DELETION <i>IN VIVO</i>.	152
5.1	Introduction	152
5.2	Hypothesis:	157

5.3	Research Aims:	158
5.4	Methods and Materials	158
5.4.1	Mice	158
5.4.2	CGRP Antagonist Preparation	158
5.4.3	Preparation of Cells for Subcutaneous Injection.....	159
5.4.4	Subcutaneous Injection of Cells	159
5.4.5	Measurement of Tumour Growth	160
5.4.6	Experiment Endpoint	160
5.4.7	Immunohistochemistry Staining of Tumour Tissues	160
5.4.8	Ki67 Immunohistochemistry Staining.....	161
5.4.9	CD31 Immunohistochemistry Staining	162
5.4.10	ImageJ Analysis of CD31 Staining	163
5.4.11	cAMP LANCE TR-FRET Assays.....	166
5.4.12	Statistical Analysis	168
5.5	Results	169
5.5.1	Tumour Development.....	169
5.5.2	Immunohistochemistry.....	174
5.5.3	cAMP LANCE TR-FRET	181
5.6	Discussion	183
	CHAPTER 6: GENERAL DISCUSSION	189
6.1	Future Work	203
6.2	Conclusion	205
	CHAPTER 7: APPENDIX	206
	BIBLIOGRAPHY	230

List of Figures

Figure 1.1.1 The hallmarks of cancer.	13
Figure 1.2 Genetic mutations that increase familial risk of prostate cancer.	16
Figure 1.3 Histological staining of prostatic tumours with their Gleason score.	18
Figure 1.4 CGRP and AM1/2 Receptors.	24
Figure 1.5 The role of CGRP in physiology and pathology.	25
Figure 1.6 The role of adrenomedullin in physiology and pathology.	26
Figure 1.7 Structure of the adrenomedullin gene.	27
Figure 2.1 BCA standard curve.	48
Figure 2.2 CGRP immunoassay peptide standard concentrations.	52
Figure 2.3 CGRP immunoassay standard curve.	53
Figure 2.4 LANCE Ultra cAMP assay principle.	54
Figure 2.5 Forskolin dose response. All values are mean \pm SEM, n=3.	55
Figure 2.6 Dose response of cAMP standards. All values are mean \pm SEM, n=3.	56
Figure 2.7 cAMP stimulation buffer recipe.	56
Figure 2.8 Endpoint PCR GAPDH.	60
Figure 2.9 Endpoint PCR RAMPs 1-3, CLR and AM.	61
Figure 2.10 RAMP1 sanger sequencing.	62
Figure 2.11 Western blotting RAMP1-3 and CLR.	63
Figure 2.12 CGRP fluorescent immunoassay.	64
Figure 2.13 Forskolin dose response on PC3 cells.	65
Figure 2.14 Dose response of CGRP stimulation on PC3 cells.	66
Figure 2.15 Dose response of AM stimulation on PC3 cells.	66
Figure 2.16 Dose response of Amylin stimulation on PC3 cells.	67
Figure 3.1 Diagrams of gene editing techniques.	73
Figure 3.2 Prokaryote adaptive immunity.	75
Figure 3.3 CRISPR/Cas9 HDR system.	79
Figure 3.4 Genomic PCR primers.	83
Figure 3.5 Thermal cycler protocol for genomic DNA extraction.	84
Figure 3.6 Transfection images.	86
Figure 3.7 FlowJo analysis of cell sorting.	87
Figure 3.8 Bright field images of RAMP1 single cell colonies.	88
Figure 3.9 Bright field images of RAMP2 single cell colonies.	89
Figure 3.10 Bright field images of RAMP3 single cell colonies.	90
Figure 3.11 Endpoint PCR GAPDH for RAMP1 and RAMP2 CRISPR clones.	91
Figure 3.12 Endpoint PCR RAMP1.	92
Figure 3.13 Endpoint PCR RAMP2.	92
Figure 3.14 Endpoint PCR GAPDH for RAMP3 CRISPR clones.	93
Figure 3.15 Endpoint PCR RAMP3.	93
Figure 3.16 Endpoint PCR with RAMP1 genomic DNA.	94
Figure 3.17 CRISPR edited RAMP1 gene.	95
Figure 3.18 CRISPR edited RAMP1 crystal structure.	96
Figure 3.19 qPCR amplification plot for ACTB.	97
Figure 3.20 qPCR ACTB expression levels.	98
Figure 3.21 qPCR RAMP1 expression.	99

Figure 3.22 Endpoint PCR GAPDH, RAMP2 and RAMP3 on RAMP1 KO clones.....	100
Figure 3.23 RAMP1 western blot for CRISPR knockouts.....	101
Figure 4.1 Principle of cell viability assay.....	114
Figure 4.2 Cell density optimisation for viability assay.....	116
Figure 4.3 Caspase 3/7 assay principle.....	117
Figure 4.4 Optimisation of incubation time for caspase 3/7 assay.....	118
Figure 4.5 Transwell control and Matrigel-coated membranes.....	120
Figure 4.6 Optimisation of cell density for colony formation assay.....	121
Figure 4.7 Schematic diagram of multiplex magnetic bead immunoassay.....	123
Figure 4.8 Schematic diagram of multiple pathways targeted in multiplex bead assay.....	124
Figure 4.9 Viability assays comparing PC3 wild type and RAMP1 KO cells.....	127
Figure 4.10 CGRP and antagonist cell viability.....	129
Figure 4.11 Migration (scratch) assay.....	131
Figure 4.12 ImageJ analysis of migration assay.....	132
Figure 4.13 Transwell migration assay.....	133
Figure 4.14 Transwell invasion assay.....	134
Figure 4.15 Colony formation images.....	135
Figure 4.16 Number of colonies in colony formation assay.....	136
Figure 4.17 Percentage area of colonies in colony formation assay.....	137
Figure 4.18 Adhesion assay.....	138
Figure 4.19 Caspase 3/7 activity.....	140
Figure 4.20 Multiplex multi-pathway magnetic bead assay A-D.....	142
Figure 4.21 Multiplex multi-pathway magnetic bead assay (E-I).....	143
Figure 5.1 ImageJ analysis settings.....	164
Figure 5.2 ImageJ analysis for CD31 IHC staining.....	165
Figure 5.3 Forskolin dose response on Panc02 cells.....	166
Figure 5.4 CGRP dose response on Panc02 cells.....	167
Figure 5.5 Tumour volume measurements.....	169
Figure 5.6 Tumour mass measurements.....	170
Figure 5.7 Tumour volume measurements for all experimental groups.....	171
Figure 5.8 Tumour mass measurements for all experimental groups.....	172
Figure 5.9 Endpoint liver mass measurements for all experimental groups.....	173
Figure 5.10 Endpoint total mice weights for all experimental groups.....	173
Figure 5.11 Images of H&E staining of PC3 WT tumour.....	175
Figure 5.12 Image of H&E staining for RAMP1 KO tumour.....	176
Figure 5.13 Images of H&E staining for wild type and RAMP1 KO PC3 tumours...	177
Figure 5.14 Image of Ki67 staining for wild type and RAMP1 KO PC3 tumours.....	178
Figure 5.15 Analysis of Ki67 positive cells.....	179
Figure 5.16 Images of CD31 staining of wild type and RAMP1 KO PC3 tumours...	180
Figure 5.17 Quantification of CD31 analysis.....	181
Figure 5.18 cAMP dose response curves for CGRP antagonists.....	182
Figure 7.1 Sanger sequencing PC3 WT and RAMP1.....	206
Figure 7.2 Sanger sequencing PC3 and RAMP3.....	207
Figure 7.3 Sanger sequencing PC3 and CLR.....	208
Figure 7.4 Sanger sequencing PC3 and AM.....	209

Figure 7.5 Sanger sequencing of CRISPR clone A7 and EF1-alpha promoter region	210
Figure 7.6 BLAST alignment for CRISPR clone A7	211
Figure 7.7 Sanger sequencing for CRISPR clone A7 and left homology arm.....	212
Figure 7.8 BLAST alignment of RAMP1 CRISPR clone A7 and left homology arm..	213
Figure 7.9 Sanger sequencing of CRISPR clone C1 and left homology arm.	215
Figure 7.10 BLAST alignment of CRISPR clone C1 and EF1-alpha promoter	216
Figure 7.11 BLAST alignment of CRISPR clone C1 and left homology arm.	217
Figure 7.12 Sanger sequencing for PC3 and RAMP2	218
Figure 7.13 BLAST alignment of PC3 for RAMP2	219
Figure 7.14 BLAST alignment of CRISPR clone A7 and PC3 wild type.....	219
Figure 7.15 Sanger sequencing for CRISPR clone A7 and RAMP2	220
Figure 7.16 BLAST alignment for CRISPR clone A7 and RAMP2	221
Figure 7.17 Sanger sequencing for CRISPR clone C1 and RAMP2	222
Figure 7.18 BLAST alignment of CRISPR clone C1 and PC3 wild type.....	223
Figure 7.19 BLAST alignment of CRISPR clone C1 and RAMP2.....	223
Figure 7.20 Sanger sequencing for CRISPR clone D5 and RAMP2.....	224
Figure 7.21 BLAST alignment of CRISPR clone D5 and PC3 wild type.....	225
Figure 7.22 BLAST alignment of CRISPR clone D5 and RAMP2	225

List of Tables

Table 1.1 Tumour Node Metastasis (TNM) classification is used for staging of prostate cancer.	19
Table 1.2 The calcitonin peptide family and the G protein-coupled receptors.	24
Table 1.3 The roles of adrenomedullin and CGRP in prostate cancer.	33
Table 2.1 Reverse transcription reaction recipe.....	42
Table 2.2 Reverse transcription reaction cycle.....	43
Table 2.3 Endpoint PCR primers.	44
Table 2.4 Endpoint PCR recipe.....	44
Table 2.5 Endpoint PCR cycle.....	45
Table 2.6 Protein standard concentrations for BCA assay.....	47
Table 2.7 Western blotting primary antibodies.	50
Table 2.8 Western blotting secondary antibodies.....	50
Table 2.9 cAMP forskolin concentrations.	57
Table 2.10 cAMP ligand concentrations.....	58
Table 2.11 Enight plate reader settings for cAMP assays.....	59
Table 3.1 Endpoint PCR primers for RAMP1 CRISPR validation.	80
Table 3.2 cDNA synthesis primer annealing reaction.	81
Table 3.3 cDNA synthesis total reaction	81
Table 3.4 qPCR primers designed to target RAMP1.	82
Table 3.5 qPCR Mastermix recipe.	82
Table 3.6 qPCR amplification protocol.....	83
Table 3.7 Genomic PCR primers	85
Table 3.8 Genomic PCR recipe.....	85
Table 3.9 CT values for PC3 wild type and CRISPR samples.....	100
Table 4.1 Plate reader settings for viability assays.....	115
Table 4.2 Percentage differences in cell viability.	128
Table 4.3 Percentage differences in migration.....	132
Table 4.4 Percentage differences in migration and invasion.	134
Table 4.5 Percentage differences in colony formation.....	137
Table 4.6 Percentage differences in adhesion.	139
Table 4.7 Percentage differences in caspase 3/7 activity.....	141
Table 5.1 Best fit values for forskolin curves.....	167
Table 5.2 Best fit values for CGRP curve.	168
Table 5.3 Best fit values for CGRP antagonist curves.	183
Table 7.1 List of manufacturers and reagents.....	226

CHAPTER 1: General Introduction

1.1. Hallmarks of Cancer

It is now estimated that there are more than 200 types of cancer and that 1 in 2 people in the UK will get cancer at some point in their lifetime. Cancers of the lung, bowel, breast and prostate accounted for almost half of all cancer deaths in the UK in 2012. Statistics show that cancer has become increasingly prevalent over the last 50 years, rising in males and females 23% and 47% respectively, since the 1970s [1]. This increase in incidence does not necessarily represent a higher prevalence of cancer but rather the advances made in diagnosing disease and also the fact that people are living longer and therefore survive previous causes of death e.g. stroke, heart failure. Cancer is strongly associated with old age and therefore an ageing population creates a higher incidence of cancer [2].

Over the last few decades great strides have been made in translation research that provides clinical treatments and improved survival rates. However, it has become increasingly clear that the complex biology of tumours cannot be fully understood by focusing on the cancer cells alone but requires understanding of the 'tumour microenvironment' [3]. This includes non-cancerous or stromal cells such as fibroblasts, immune cells and the proteins they secrete which may influence cancer progression both positively and negatively. Cross-talk between stromal cells can occur through the extracellular matrix which provides a structural scaffold for cells. Tissues can communicate through a complex network of interactions using autocrine, paracrine or juxtacrine signaling. This provides information needed to maintain a healthy cellular environment. If these intercellular signals get disrupted it can lead to functional disorder. Abnormal interactions can result in the genomic instability of the stromal cells providing them with a tumourigenic potential. Proliferating cancer cells can interact with their microenvironment and further enhance abnormal signaling to promote tumour growth [4].

A pivotal review by Hanahan and Weinberg first described what is now famously known as the ‘hallmarks of cancer’ [5]. A second review accompanied this ten years later detailing the mechanisms used by cancer cells to alter the function of stromal cells and promote tumorigenesis (see Fig 1.1) [6]. These hallmarks include the ability of cancer to evade immune detection, even when promoting inflammation and invading surrounding tissues. Cancer cells can also avoid growth suppressors and resist apoptosis whilst initiating processes such as angiogenesis and proliferation to further promote their survival. Their effect on the surrounding stroma creates genomic instabilities and mutations which ultimately lead to the deregulation of cell metabolism [6]

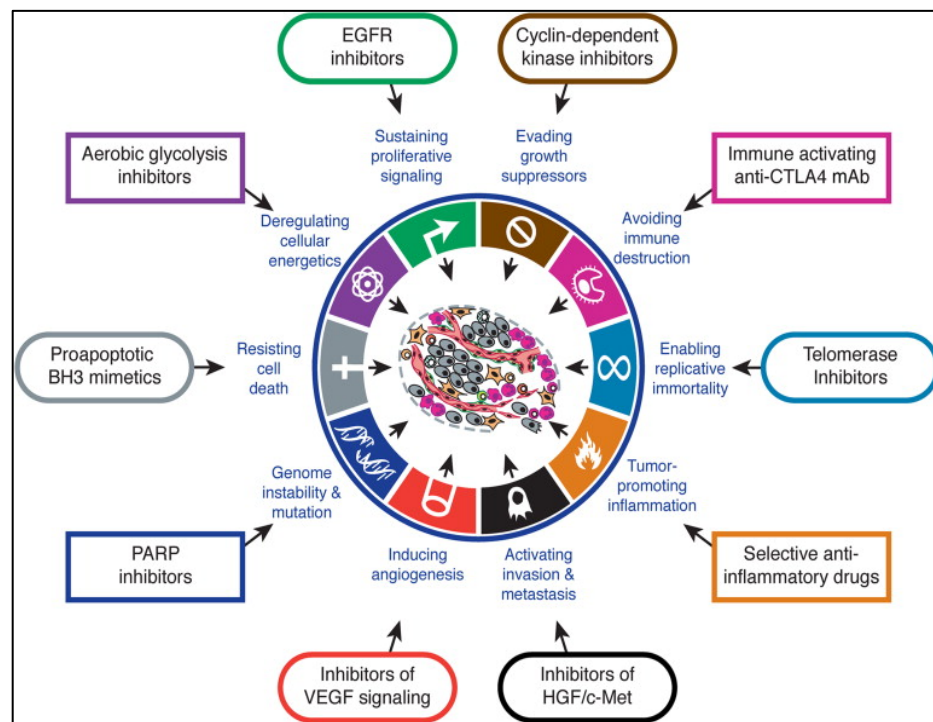


Figure 1.1.1 The hallmarks of cancer.

Diagram showing the different hallmarks of cancer and drugs that are in development or in some cases approved for clinical use for inhibiting these processes. (Reprinted from Hardy & Weinberg with permission from Elsevier [6].)

Cancer is not one disease but many different ones sharing the same inherited loss of inhibition of proliferation, so that many different tumour types interact with the wide range of tissues within the body whether as primary tumours within those

tissues or as secondary tumours that have spread to a new site. While some tumours occur in primary sites that are in themselves innocuous e.g. skin melanomas, which are problematic because they metastasize to vital organs, others arise in sites where the presence of a primary tumour poses a health risk in the site itself. This creates a plethora of potential therapeutic targets and often these targets will have important physiological functions and their inhibition will often have disastrous consequences. Care must therefore be taken when selecting possible targets for therapeutic intervention. Often this is achieved by investigating the molecular mechanisms associated with cancer and determining the signaling pathways that may be affected by pharmacological intervention.

1.2. Prostate Cancer

1.2.1. Incidence and Diagnosis

The prostate is a male sexual gland, situated anterior to the rectum and between the bladder and penis [7]. Its dual function is to produce a number of secretory products that condition the urethral surface for spermatozoa and to contribute to the production of semen [8]. Prostate cancer is the most common cancer in men with 1 in 8 men in the UK begin diagnosed within their lifetime [1]. The most significant risk factor associated with prostate cancer is age, with the average age of diagnosis being 72 [9]. In the UK, 54% of prostate cancer cases are diagnosed in males aged 70 or over [1]. A genetic risk also exists and it is estimated that a man may be 2-3 times more likely to develop prostate cancer if a close family member has also suffered from the disease [1]. Common genetic mutations that predispose to prostate cancer include BRCA1, BRCA2, HOXB13 and many others (see Fig 1.2) [10]. Prostate cancer can often be asymptomatic but the most common complaint in both malignancy and benign tumours is urinary problems such as disrupted micturition, increased frequency and nocturia [11]. Often, these symptoms can be caused by benign prostate hyperplasia or an enlarged prostate instead of cancer. Diagnostic tests must differentiate between benign or malignancy and include tools such as for digital rectal examination (DRE) and transrectal

ultrasound (TRUS)-guided biopsy [12]. It has been estimated that in 18% of patients, prostate cancer is detected by DRE alone, irrespective of blood test results [13]. These results must then be confirmed with ultrasound or biopsies to differentiate between benign or malignant disease. TRUS has now become the standard method of obtaining material for biopsy in prostate cancer patients. Blood tests are available and look for biomarkers such as prostate specific antigen (PSA) a glycoprotein produced by prostate gland cells (benign or malignant) [14]. This protein is encoded by the prostate-specific gene kallikrein 3 (KLK3) and in its mature form is secreted into the semen [15]. Under normal conditions, low levels of PSA are detected in the blood but increased serum levels may represent disruption to the prostate gland caused by prostate cancer although exact mechanisms still remain unclear [16]. In fact, PSA screening has become widely used since its discovery in 1979 and thereby promoted earlier detection of prostate cancer cases before significant clinical symptoms have manifested [17].

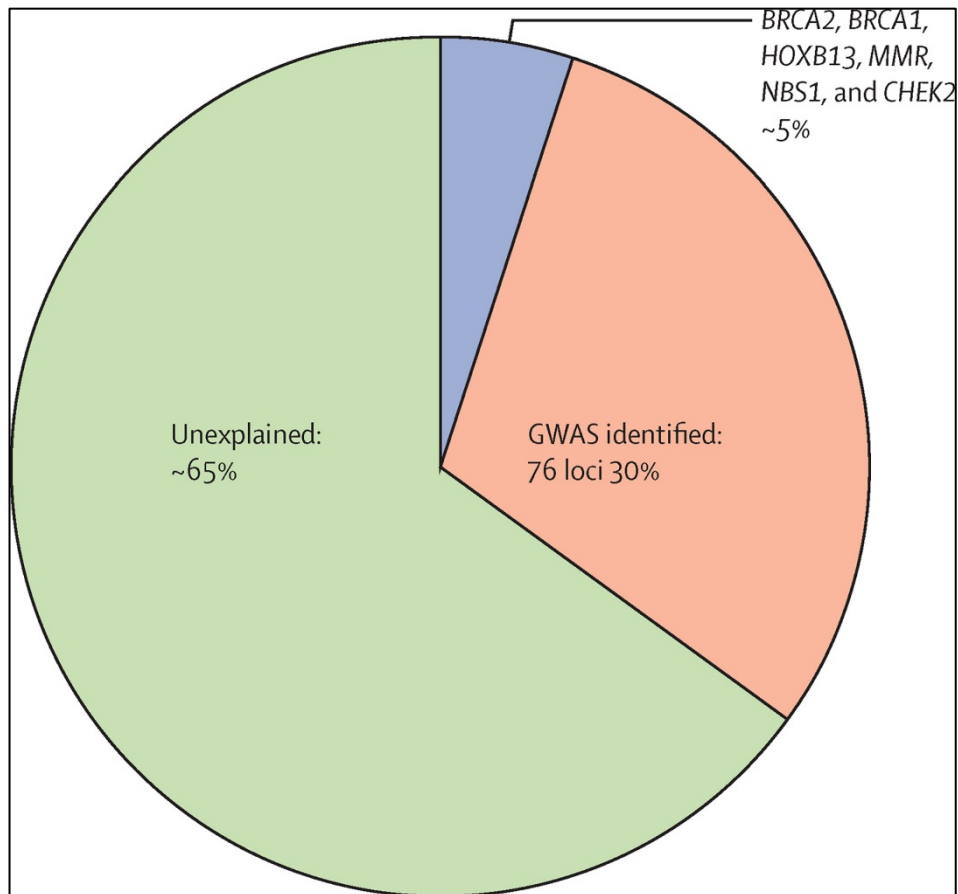


Figure 1.2 Genetic mutations that increase familial risk of prostate cancer.

Reprinted from Attard et al with permission from Elsevier [10].

PSA was regarded as a relatively useful biomarker for prostate cancer for some years before its limitations became evident. A lack of specificity was found, as PSA can become elevated by noncancerous events such as inflammation or infection leading to incorrect diagnoses [15, 16]. This has sparked a search for new biomarkers of prostate cancer, using “-omics” technologies such as deep sequencing of DNA and RNA transcriptome profiling. These investigations aim to profile prostate tumours by investigating alterations in DNA, RNA and epigenetic methylation [18]. Many new biomarkers have been found using this method including PCA3, a long non-coding RNA shown to be elevated in more than 90% of PC cases and has emerged as a new non-PSA based diagnostic test [19, 20]. Other candidates such as TMPRSS2-ERG [21] and AMACR [22] have also been identified but found only useful when used in

combination with other biomarker tests due to their low specificity to prostate cancer [18].

1.2.2. Staging and Treatment

After diagnosis, local staging of the disease is often determined with further biopsies and using magnetic resonance imaging (MRI). This is because TRUS-guided biopsies are often not specific enough for accurate staging and have a tendency to underestimate progression of the disease. The 2009 Tumour Node Metastasis (TNM) classification is used for staging both primary prostate tumours and regional lymph nodes (See Table 1.1) [12]. Another method for grading prostate cancer is the Gleason score. This system was developed after a study from 1979 to 1964 enrolled 270 prostate cancer patients and Dr Donald Gleason created a grading system based on the different histological patterns seen in patient biopsies [23]. He observed that most tumours displayed two distinct patterns and so a score was created that added the two most common grade patterns in a tumour (scores range from 2-10) to achieve a "Gleason score" (see Fig 1.3.) Revisions have since been made to the Gleason's scoring system however it is still commonly used for grading histological prostate tumour sections. Although these modifications add to the specificity of the system, diagnosis has now become very complex and can be confusing to both patients and clinicians. Nevertheless the Gleason scoring system remains a robust predictor of prostate cancer prognosis and therefore plays a significantly important role in the management and treatment of the disease [24] .

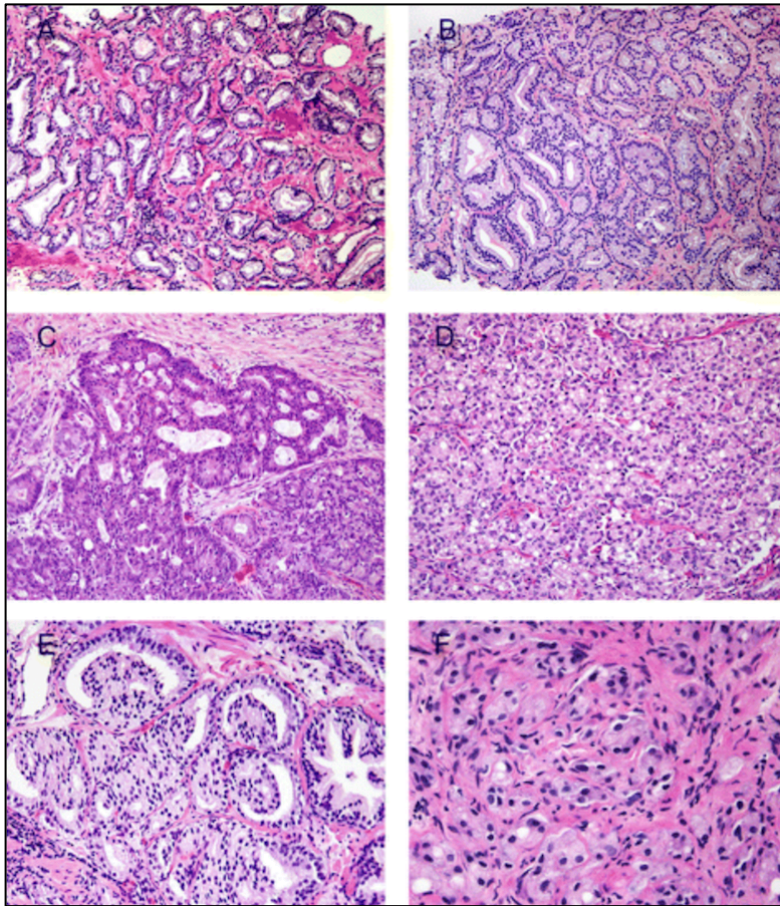


Figure 1.3 Histological staining of prostatic tumours with their Gleason score.

Histological staining of prostatic tumours with their Gleason score. (A) Gleason grade group 1 (3 + 3 = 6). (B) Gleason grade group 2 with cribriform glands. (C) Gleason grade group 4 (4 + 4 = 8) with irregular cribriform glands. (D) Gleason grade group 4 (4 = 4 = 8) with fused cytoplasmic vacuoles. (E) Gleason grade group 4 (4 + 4 = 8) with glomeruloid glands (F) Gleason grade group 4 (4 + 4 = 8) with poorly formed glands. Gordetsky and Epstein Copyright[©] with permissions [24].

T – Primary Tumour	
TX	Primary tumour cannot be assessed
T0	No evidence of primary tumour
T1	Clinically unapparent tumour not palpable or visible by imaging
T1a	<i>Tumour incidental histological finding in 5% or less of tissue resected</i>
T1b	<i>Tumour incidental histological finding in more than 5% of tissue resected</i>
T1c	<i>Tumour identified by needle biopsy (e.g. because of elevated PSA level)</i>
T2	Tumour confined within prostate
T2a	<i>Tumour involves one half of one lobe or less</i>
T2b	<i>Tumour involves one more than half of one lobe</i>
T2c	<i>Tumour involves both lobes</i>
T3	Tumour extends through prostatic capsule
T3a	<i>Extracapsular extension (unilateral or bilateral) including bladder neck involvement</i>
T3b	<i>Tumour invades seminal vesicle(s)</i>
T4	Tumour is fixed or invades adjacent structures other than seminal vesicles: external sphincter, rectum, levator muscles and/or pelvic wall
N – Regional Lymph Nodes	
NX	Regional lymph nodes cannot be assessed
N0	No regional lymph node metastasis
N1	Regional lymph node metastasis

Table 1.1 Tumour Node Metastasis (TNM) classification is used for staging of prostate cancer.

Staging of prostate cancer can then inform on appropriate treatment options either of the local primary tumour or metastatic disease. Many low risk PC patients are put under active surveillance (AS) and are initially not treated unless a threat of progression occurs in follow-up testing. AS was put into action to avoid unnecessary treatment of patients with clinically confined low risk prostate cancer. This decision is based on findings that show men with well differentiated PC have a 20-year survival rate of 80-90% and as prostate cancer often occurs in men aged 70+ years old this may be pragmatic [25, 26]. Radical prostatectomy (RP) a surgical treatment for localised prostate cancer and has been shown to have an increased survival in a subset of patients when compared with AS in two different randomised trials [27, 28]. However, this benefit in survival has a negative correlation with age, as patients less than 65 years of age were found to benefit in overall and metastasis-free survival [27]. The Prostate Cancer Intervention Versus Observation Trial recruited 731 patients from 1992 to 2002 and found that this effect was only deemed statistically

significant in patients with high-risk PC or PSA levels of <10ng/mL. These patients experienced a 31% increase in overall survival ($p = 0.02$) and an absolute risk reduction of 10.5% ($P = < 0.01$). Significant reductions in the development of bone metastases was also seen in patients who were treated with RP compared with AS (4.7% versus 10.6%, $P = < 0.01$). Nerve-sparing radical prostatectomy is a preferred treatment to RP as it avoids many of the side effects such as urinary incontinence and erectile dysfunction. This technique is becoming more common and can be performed by a method known as robot-assisted laparoscopic RP (RALP). This new technique is yet to be critically evaluated due to the lack of long-term follow up studies [29].

Three-dimensional conformal radiation therapy (3D-CRT) is considered the gold standard radiotherapy method for many cancers [12]. Its value in treating prostate cancer patients was first shown almost 20 years ago when a randomised controlled trial was conducted to compare toxicity of 2D and 3D-CRT. It was concluded that 3D-CRT not only was as sufficient as 2D techniques but also had lower risks of late radiation-induced proctitis for patients [30]. However, since then further advancements have led to the development of intensity-modulated radiation therapy, a more optimised form of 3D-CRT. This technique is widely used because of its advantage of allowing doses to be altered without any corresponding toxicity [31]. Active surveillance, radical prostatectomy and radiotherapy treatments are considered useful for low-intermediate risk patients however no consensus is found when determining treatment for high-risk, clinically localised prostate cancer. Radical prostatectomy is suggested as a reasonable first step for patients with tumours of a small volume however further management of high-risk patients may be determined on a case-by-case basis [12].

Metastatic prostate cancer patients have been recommended for androgen deprivation therapy (ADT) for many decades [32]. Originally, surgical castration (specifically bilateral orchidectomy) was regarded as a successful treatment for advanced prostate cancer patients [33]. However, the majority of patients would prefer not to undergo surgical castration due to the psychologically traumatic impact

on erectile function and libido [34]. Since the days of surgical castration, Gonadotropin-releasing hormone (GnRH) antagonists have proved to achieve and maintain levels of serum testosterone equivalent to surgical castration [35]. GnRH antagonists have many advantages over surgical castration and represent a common method of treatment for advanced prostate cancer patients who have a high risk of metastatic disease that may include neurological manifestation, urinary obstruction and bone pain all relating to metastasis. GnRH treatment has been described as the mainstay of treatments for advanced prostate cancer patients by the European Association of Urology (EAU) [36]. However, a few years later, guidelines published by the EAU also recognised the use of luteinising hormone-releasing hormone (LHRH) agonists as a standard of care [37]. Recent studies found that LHRH antagonists can be used to induce a more rapid decrease in testosterone levels compared with previous hormone treatments without any flare. Testosterone flare is a phenomenon seen where levels are transiently increased in patients treated with GnRH agonists creating symptoms such as bone pain and urinary problems during the first few weeks of treatment courses [38]. Long term treatment of ADT can lead to reductions in bone mineral density and increase fracture risk, requiring patients to be monitored regularly [39].

Unfortunately, despite the effectiveness of ADT, all patients' prostate cancers will eventually become castration resistant if they do not die of other causes. This is defined as either development of metastatic disease or three consecutive increases in PSA levels in the presence of castrate levels of testosterone [40, 41]. Studies have tried to show the molecular mechanisms responsible for castration resistance. It appears that the androgen receptor itself is involved directly and may be mutated when cancer becomes resistant to ADT. These mutations may amplify androgen receptor gene expression allowing it to become sensitive to lower doses of androgens or other steroids [42]. However, indirectly coactivators may increase this sensitivity of the receptor through a variety of signalling mechanisms [43]. Prostate cancer cells have also been found to bypass the androgen receptor pathway entirely and promote proliferation through alternative signalling pathways [44]. One potentially relevant pathway is the neuroendocrine (NE) differentiation of tumours

which may allow secretion of neurotransmitters that promote proliferation in prostate cancer [45, 46].

Despite reports that relapsing patients can survive 5 years with ADT, the majority will die from castration resistant metastases [47]. Patients who advanced to progressive metastatic castration resistant prostate cancer have a median survival time of 9-12 months [48]. 80% of these advanced patients will have bone metastases which are a major cause of disability and death and represent increasing costs in treatment [37]. Zoledronic acid is the sole bisphosphonate that has been shown to reduce bone pain and skeletal metastases in prostate cancer patients [49]. Alternatively, Radium-223 can act as a calcium mimic and target bone growth around bone metastasis sites with heavy alpha particles that have an ultra-short range [50]. A study of 921 castration-resistant prostate cancer patients found overall survival to be increased 25% ($P = < 0.0001$) [51]. Docetaxel is a current standard of care for castration resistant patients and is a heavily studied chemotherapeutic that is used in the treatment of a variety of cancers [52]. However, castration resistant patients eventually become also resistant to docetaxel due to drug efflux [53]. EAU guidelines suggest that due to the lack of evidence on timing or sequence of therapies, clinicians should try to include advanced metastatic patients in clinical trials for the best chance of survival. In fact, it is estimated that any patient with castration-resistant prostate cancer is currently involved in a clinical trial [37].

Prostate cancer prognosis may be good for patients diagnosed with low risk localised tumours however it still remains poor for advanced patients. All therapies including ADT, radio- and chemo-therapy only act to slow the progression of prostate cancer metastasis. Therefore, it is imperative to study the mechanisms of this process and identify key proteins that may be targeted therapeutically.

1.3. G Protein-Coupled Receptors (GPCRs): The Calcitonin Peptide Family

Adrenomedullin (AM) and calcitonin gene-related peptide (CGRP) are members of the calcitonin peptide family. This family is so named as all members share structural similarities with calcitonin (CT) a hypocalcemic hormone secreted from the thyroid gland. The Calcitonin Gene-Related Peptide (CGRP) is appropriately named as it is an alternative splicing of the CT gene [54]. CGRP is mostly expressed in the central and peripheral nervous systems often in nerves innervating vasculature [55]. Adrenomedullin was first described in 1993 when identified in a human pheochromocytoma patient. It is a potent vasodilator, acting directly on renal, cerebral and lung circulation systems as well as the vascular supply of bone [56]. The physiological and pathological functions of both AM and CGRP are summarised in Figures 1.5 & 1.6. The receptors for these peptides are unusual in that they are formed by two separate proteins, a seven-transmembrane domain G protein-coupled receptor and a receptor activity modifying protein (RAMP). In the case of AM and CGRP, the receptor is the calcitonin-like receptor (CLR). This receptor binds with RAMP1 to form a CGRP receptor and with RAMP2 and RAMP3 to form two distinct AM receptors (AM1 and AM2) (See Fig 1.4) [57]. RAMPs share 30% amino acid sequence homology and can also interact with other receptors to form GPCRs for multiple ligands. All RAMPs can traffic the calcitonin receptor (CTR) to the cell surface forming three distinct amylin receptors (AMY1, AMY2, AM3) [54].

RAMP1 and RAMP3 have been shown to interact with the calcium sensing receptor (CaSR) [58]. Unpublished work in our group has also provided evidence that RAMP1 may traffic a receptor known as GPRC6A to the cell membrane. GPRC6A is named from the GPCR, class C, group 6 subtype A receptor (and previously described as a second calcium sensing receptor) [59, 60]. It is a receptor that can be activated by multiple ligands including cations, L-amino acids and osteocalcin [59, 61]. GPRC6A also plays an important role in the regulation of testosterone in both physiology and pathology [62]. RAMPs 2 and 3 have also been shown to interact with two distinct parathyroid hormone receptors (PTH1 and PTH2) at the cell surface [63] (See Table 1.2). The calcitonin family and their receptors have a wide range of physiological and

pathological functions which have been widely discussed in the literature [64-68]. Due to their well-established roles in vital cellular mechanisms it is therefore unsurprising that they also feature as promoters of tumorigenesis across many different cancer types.

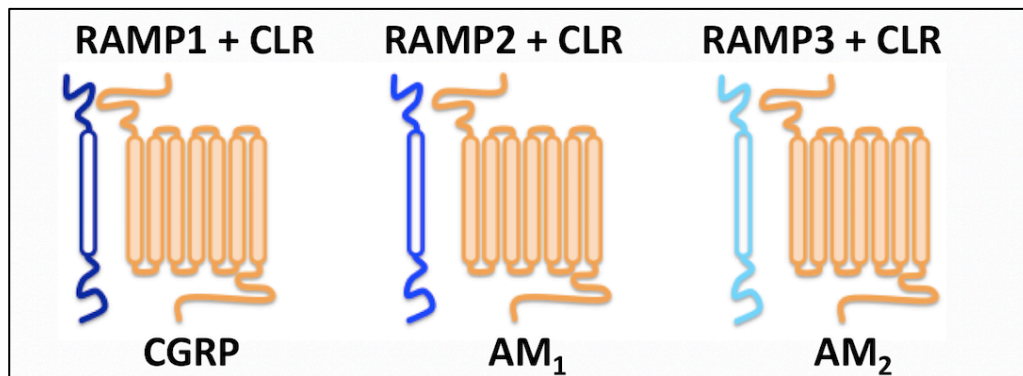


Figure 1.4 CGRP and AM1/2 Receptors.

The CGRP and Adrenomedullin (AM) receptors are composed of the calcitonin-like receptor (CLR) bound with a receptor activity modifying protein (RAMP).

Ligand	Receptor	Receptor Components
Calcitonin	CTR	CTR
Calcitonin Gene-Related Peptide	CGRP	CLR + RAMP1
Adrenomedullin	AM1	CLR + RAMP2
Adrenomedullin	AM2	CLR + RAMP3
Amylin	AMY1	CTR + RAMP1
Amylin	AMY2	CTR + RAMP2
Amylin	AMY3	CTR + RAMP3
Calcium	CaSR	CaSR + RAMP1/3
Calcium	GPRC6A	GPRC6A + RAMP1
Parathyroid hormone	PTH1/2	PTH1/2 + RAMP2/3

Table 1.2 The calcitonin peptide family and the G protein-coupled receptors.

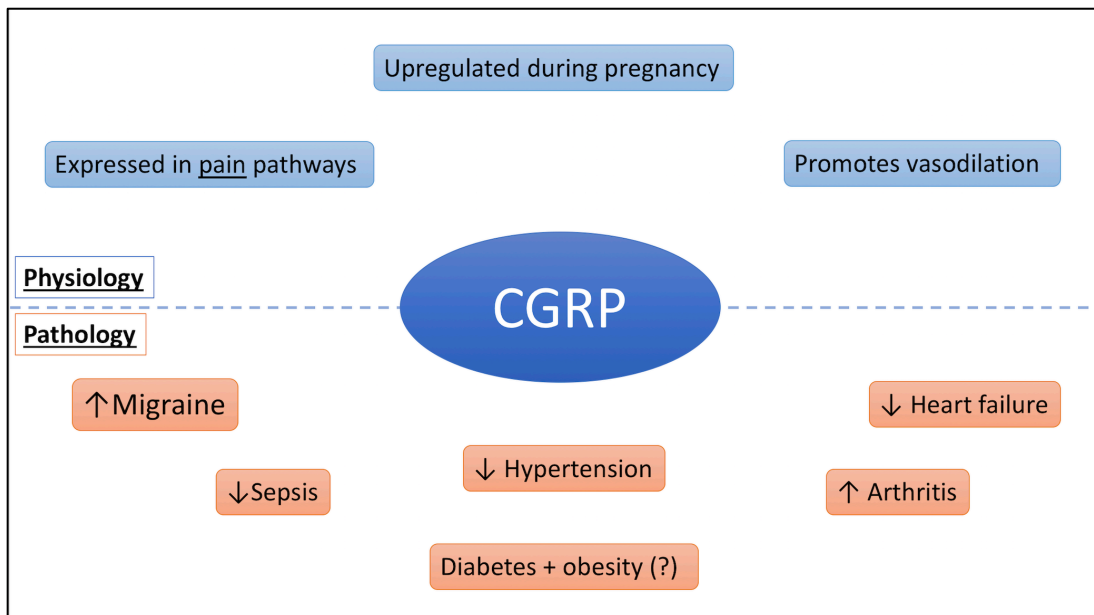


Figure 1.5 The role of CGRP in physiology and pathology.

CGRP is known to activate vasodilation by acting on both vascular smooth muscle and endothelial cells. It is also expressed and released from the trigeminal ganglion and associated with pain pathways. CGRP is upregulated during pregnancy but its effect remains unknown [55].

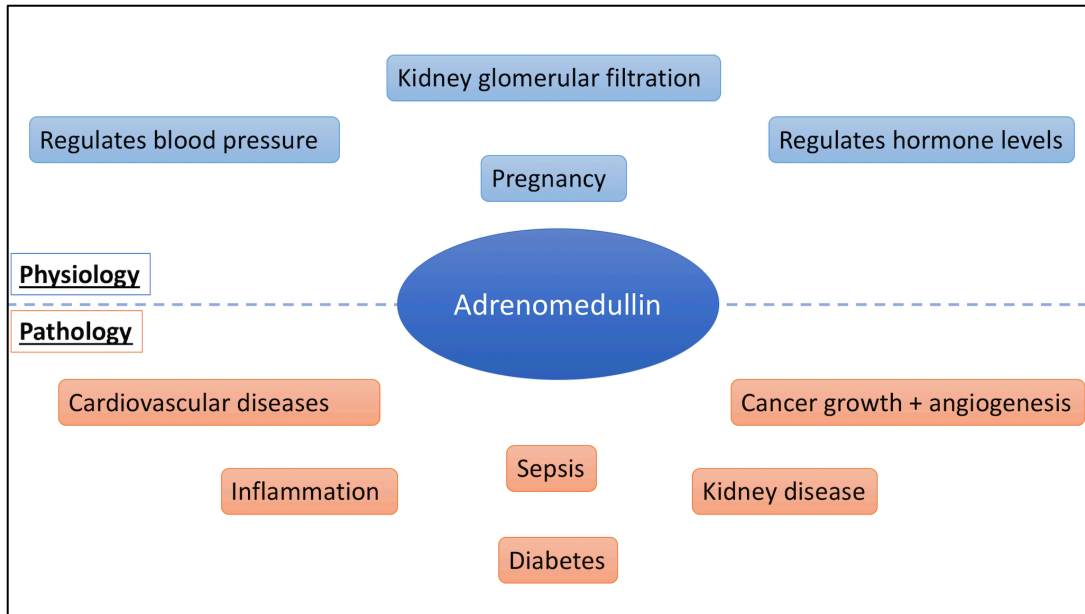


Figure 1.6 The role of adrenomedullin in physiology and pathology.

Adrenomedullin is a vasodilator that regulates blood pressure and hormone levels. It is also involved in glomerular filtration and blood pressure in the kidney and is upregulated during pregnancy to aid placentation [69].

1.3.1. Structure of Adrenomedullin and CGRP

Adrenomedullin (AM) consists of 52 amino acids and has one intramolecular disulfide bond [56]. Structural features important for biological activity such as the ring and carboxyl terminal amide structures remain preserved across species [70]. The human AM precursor (preproAM) is 185 amino acids in length and gives rise to either proAM (PAMP) or mature adrenomedullin, the former can be found to be expressed *in vivo* regulating hypotension in rats [71]. The human AM gene consists of 4 exons and 3 introns, the mature AM peptide being transcribed from exon 4, whereas PAMP is coded in intron 2 (see Fig 1.5) [70].

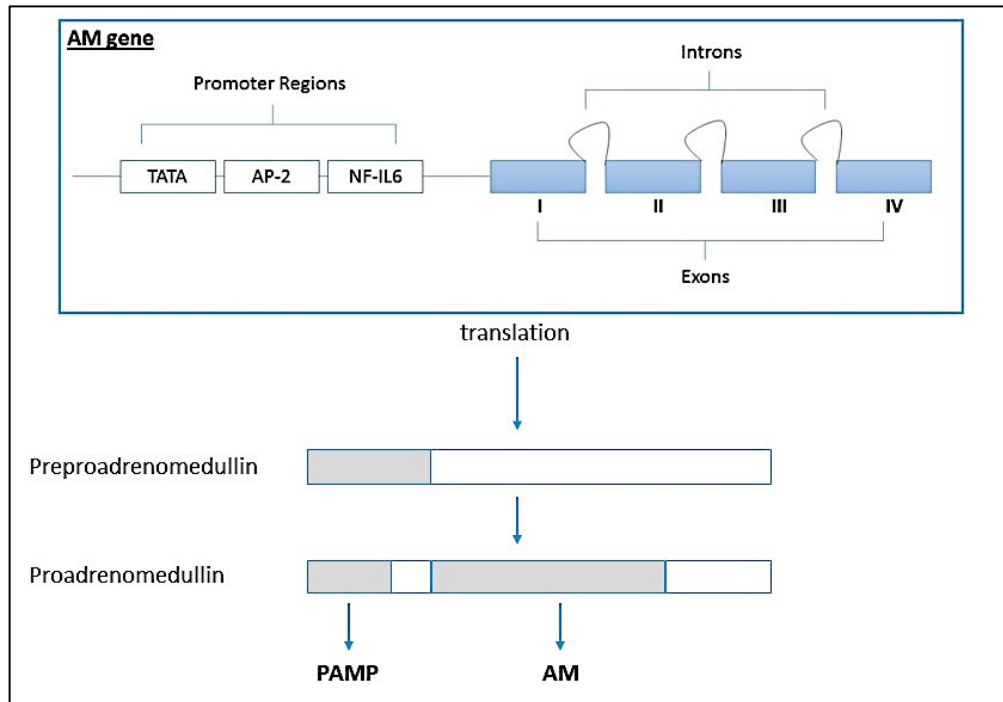


Figure 1.7 Structure of the adrenomedullin gene.

AM has four exons and three introns which are translated to the precursor molecules preproAM and proAM which are then processed into mature AM and PAMP.

Although two CGRP peptides have been described (α CGRP and β CGRP) they differ from each by three amino acids and have proved so far to be indistinguishable in physiological function [72]. Unless otherwise stated α CGRP is predominantly described as CGRP. The amino acid sequences for CGRP also are well preserved across many different species [73]. This 37-amino acid peptide has a disulfide bond between residues 2 and 7 and a carboxyl terminal amide. Studies using proton nuclear magnetic resonance (^1H NMR) show that residues 8-18 form an alpha helix and that conformation of both alpha and beta peptides are identical [74].

1.1 Adrenomedullin and Prostate Cancer

Adrenomedullin has been implicated in many different solid cancers including lung, breast, ovarian, adrenal and brain tumours [56, 75-78]. It has also been found to be upregulated at an mRNA level in human prostate cancer cell lines

after androgen deprivation and can act as a growth factor in DU145 cells suggesting an autocrine loop which could potentially drive tumour growth [79, 80]. Expression of AM is significantly higher in malignant tissues and correlates with high Gleason scores in prostate cancer when compared with adjacent healthy tissue controls [80]. AM has also been associated with neuroendocrine differentiation, a reported early marker of androgen independence [81]. AM was also shown to induce a neuroendocrine phenotype in LNCaP cells via both AM1 and AM2 receptors characterized by observed increases in neuritic processes and expression of neuro-specific enolase (NSE). *In vivo* studies also show that in castrated animals, treatment with AM results in up to 250% increase in tumour volume [82].

An important trait of prostate cancer cells is the ability to proliferate uncontrollably. The current literature features discrepancies when investigating whether AM has influence on the proliferation of prostate cancer cells. It would appear that the effect of AM *in vitro* can be heavily dependent on cell culture conditions. One study has found that treatment with AM in DU145 cells results in a 20% increase in proliferation after 4 days ($P = 0.05$), however no effect was found in PC3 and LNCaP cell lines. The authors suggest that because these cell lines were also found to secrete AM peptide, they may not be susceptible to treatment as maximal proliferative effects have already been achieved [80]. Conversely, a separate study found that treatment with AM results in decreases in proliferation in PC3 (20%) and LNCaP (50%) cell lines. The reported effect was dose-dependent with significant decreases in proliferation only occurring at a range of 10nM-1 μ M [83]. These results are contrary to previously reported data by Rocchi et al. and the authors argue this is due to differences in experimental conditions. They claim that previous reports used serum-free medium in proliferation experiments whereas they used a 1% fetal calf serum (FCS) concentration. Therefore, it may be that prostate cancer cell lines only display this effect when grown in “stress-free” conditions.

Interestingly, it has been shown that in the mammary cell line T47D, overexpression of AM results in cells growing at lower rates in low serum concentrations compared with mock transfected controls. The same overexpressing

cells, when grown in serum-free conditions showed increases in proliferation [84]. The authors also comment on unpublished work which shows results that are concomitant with Rocchi et al. It is reported that prostate cancer cells cultured in serum-free media did not show the same inhibition on cell growth. This is also represented in work by Rocchi et al. which shows that expression of AM mRNA is much higher in prostate cancer cell lines that have been injected into athymic mice xenografts compared with cell lines cultured *in vitro* [80]. Other studies have found that blocking of the AM receptors using a cocktail of antibodies leads to reduced growth of DU145 *in vitro* and in mouse xenografts. This reduction was also seen in LNCaP xenografts but only in castrated animals, suggesting that not only may AM be regulating tumour growth *in vivo* but also play an important role in androgen independence [85].

The effect of AM gene knockdown or knockout on proliferation in prostate cancer cells has yet to be explored. However, *in vivo* studies have found the knockdown of AM results in reduced growth of SW480 colon tumour xenografts. Immunohistochemistry analysis of these tumours showed no significant differences in Ki67 between control and knockdown sections. This is reflective of studies *in vitro* which found that the proliferation of SW480 cells was only minimally effected by silencing of AM. Findings indicate that the reduced growth was attributed to the effect of AM depletion on tumour angiogenesis and apoptosis. These conclusions were drawn from knockdown tumours showing higher levels of staining for CD31 an endothelial marker and cleaved caspase 3 [86]. It can therefore be hypothesized that AM may affect tumour growth *in vivo* through non-proliferative mechanisms or by influencing the tumour microenvironment rather than tumour growth directly.

Although the effect of AM on proliferation in prostate cancer remains ambiguous, in other cell lines it has been shown that variation of ERK1/2 levels are seen after treatment with AM and that after stimulation of proliferation with AM, levels of phosphorylated ERK are increased [87-89]. Although AM receptors, like many GPCRs, have been associated with elevation of cAMP following activation, reports have found that in prostate cancer cells, AM receptors can function

independently from cAMP and stimulate ERK1/2 signaling instead. In order to hypothesise AM's role in proliferation of prostate cancer cells it is apt to also look at its effect on cell signaling pathways associated with this process. Activation of the MAPK signaling has also been shown in DU145 cells when stimulated with different doses of recombinant AM. Phosphorylation of CRAF, MEK1/2 and ERK1/2 was achieved after treatment with 10^{-7} mol/L AM for 5 minutes. Interestingly, inhibition of MEK (an upstream ERK1/2 activator) disrupts AM activated phosphorylation of ERK1/2. These effects were reversed by pretreatment with an anti-AM antibody cocktail (for both AM1 and AM2 receptors). The MAPK cell signaling pathways has been implicated with many hallmarks of cancer including cell proliferation, migration and apoptosis [90]. AM may therefore be influencing proliferation and metastasis of prostate cancer cells by influencing this survival pathway.

Prostate cancer cells must evade apoptotic mechanisms in order to promote tumour growth. Studies have been able to show that AM promotes survival of prostate cancer cell lines when apoptosis is induced with either serum deprivation or treatment with chemotherapeutic agent etoposide (a topoisomerase II inhibitor). Overexpression of AM in PC3 cell lines protects against etoposide effects and maintains a Bcl2/Bax expression level consistent with untreated cells [91]. Blocking of AM has also shown to increase the number of apoptotic cells in DU145 prostate orthotopic tumours 6-fold compared with controls ($P = < 0.001$). Apoptosis was observed to occur mostly in tumour-associated lymphatic vessels thereby preventing the prostate tumours from inducing lymphoangiogenesis [85]. This process is key to tumour growth as lymph and blood vessels are recruited to increase nutrient supply for growing cancer cells. AM has been predicted as a key protein involved in angiogenesis for many cancers, this is precedent when considering AM was first identified as a potent vasodilator and is expressed in endothelial cells [92, 93]. In prostate cancer, AM has also been found both *in vitro* and *in vivo* to upregulate IL-13, an interleukin also implicated in angiogenesis [94, 95].

Cellular migration and invasion also plays a pivotal role in metastasis of prostate cancer and many of the components responsible for cellular migration rely

on intracellular calcium levels [96]. Transient receptor potential (TRP) channels are a family of calcium channels and have been shown to be involved with carcinogenesis, including prostate cancer specifically [97, 98]. Specifically, TRPV2 channel is involved with cellular migration and promoting androgen dependence in prostate cancer [99]. It has been reported that TRPV2 modulates AM stimulation of cell motility in PC3 cells and that when this gene is knocked down, the effect of AM on adhesion, migration and invasion is also removed. The authors also show that AM can increase the invasive phenotype of PC3 cells through β 1-integrin and FAK activation [100]. It is clear that AM regulates many of the hallmarks of cancer including proliferation, apoptosis, lymphoangiogenesis, migration, adhesion and invasion. However, there is little evidence of which AM receptors are responsible if not both, as most studies use AM peptide to treat prostate cancer cells *in vitro* or alter AM gene expression to use cells in *in vivo* studies. Previous *in vivo* studies have found that RAMP3 knockout in mice has no adverse effects on physiology whereas RAMP2 knockout mice die *in utero*. This shows that RAMP2 and RAMP3 have distinct physiological functions which may be reflected also in pathology. By studying the individual receptor components (CLR, RAMP2 and RAMP3) in prostate cancer, the mechanism of AM-associated tumorigenesis may be explored further.

1.2 CGRP and Prostate Cancer

Clinical evidence exists linking CGRP with prostate cancer. It was first reported that CGRP serum levels correlate with prostate cancer stage and histological grade ($P = 0.01$). However, years later the same group reported interesting findings when analysing samples from patients who had received hormonal therapy (HT). Highest levels of serum CGRP were again found to be in patients with late stage disease but in patients treated with HT this was not the case. The authors therefore suggest that care should be taken when considering CGRP as a potential biomarker of prostate cancer (as was originally mentioned in the previous paper) [101, 102]. *In vitro* studies have investigated the relationship between many neuropeptides, including CGRP, and prostate cancer cell lines. Invasion across

Matrigel membranes (an extracellular matrix reconstituted substance) of LNCaP and PC3 cells after stimulation with 10^{-7} mol/L was increased by 30% ($P = < 0.01$). This effect was reflected when exploring haptotactic migration (experiments tested the ability of cells to adhere to ECM proteins and then degrade them to migrate towards a fibronectin substrate) [103]. CGRP was also seen to promote invasion in DU145 cell lines by 30% after treatment with 10^{-8} mol/L, however doses of 10^{-6} mol/L were required to elicit significant effects on haptotactic migration of DU145 cells ($P = < 0.01$). CGRP doses of 10^{-7} resulted in 48% increase in LNCaP cells when testing haptotactic migration ability [104].

There is a significant lack of evidence implicating CGRP in prostate cancer, although it has been shown that this is a clinically relevant peptide to study. In order to more fully understand mechanisms by which CGRP may be promoting prostate cancer growth, it is important to investigate its receptors components as well. RAMP1 knockdown in PC3 and LNCaP cells results in decreases in proliferation and the number of colonies grown on soft agar plates is halved compared with control wild type cell lines ($P < 0.05$). RAMP1 knockdown xenografts also result in reduced tumour growth by 30% after 30 days and histological analysis of tumour sections reveals fewer numbers of Ki67 (a proliferative marker) positive cells in RAMP1 knockdown tumours [105]. RAMP1 is a key component of the CGRP receptor, ensuring the calcitonin-like receptor (CLR) is trafficked to the cell surface [57]. It is therefore possible that the effect seen after RAMP1 gene deletion is due to insufficient CGRP receptor expression. However, RAMP1 has been shown to be involved in other receptors, such as the CaSR and GPRC6A both of which have been shown to correlate with prostate tumour progression [58, 60, 106, 107]. RAMP1 knockdowns resulted also in reduced phosphorylation of ERK1/2 and MAPK mRNA transcripts. However, all aforementioned receptors have been reported to signal through ERK pathways, so this does not provide evidence of which upstream effector is responsible for the effect of RAMP1 depletion [107-109].

CGRP correlates with prostate cancer progression and has a pro-tumorigenic effect on prostate cancer cell lines *in vitro*. However, further evidence is still required

to link CGRP to mechanisms of metastasis such as proliferation and apoptosis and also to further elucidate its role *in vivo*. It may be that this neuropeptide is indirectly affecting prostate tumours by influencing the tumour microenvironment. In the case of prostate cancer, 90% of metastases are skeletal, therefore when considering targets, the bone environment should also be explored [110].

Effects in prostate cancer	Adrenomedullin	CGRP
Castration resistance	AM secreted by castration resistant cell lines [79].	Unknown
Correlation with tumour stage	AM tissue expression correlates with Gleason's score [79].	CGRP serum levels correlate with Gleason's score [100-101].
Neuroendocrine phenotype	AM promotes NE phenotype in LNCaP [81].	Unknown
Tumour growth	AM promotes growth of DU145 and LNCaP (castrated mice) xenografts [84].	CGRP promotes proliferation of prostate cancer cell lines [103].
Apoptosis inhibition	AM protects against apoptosis through Bcl2/Bax regulation [90].	Unknown
Angiogenesis	AM promotes angiogenesis via IL-13 [94].	Unknown
Invasion / Migration	Promotes invasion via β 1-integrin + FAK also migration and adhesion in PC3 [99].	Promotes invasion and migration of PC3, DU145 and LNCaP cell lines [102-103].

Table 1.3 The roles of adrenomedullin and CGRP in prostate cancer.

1.3 GPRC6A and Prostate Cancer

GPRC6A has been shown to traffic with RAMP1 in thyroid human carcinoma cells in unpublished work [60]. This receptor has been shown to be activated by many ligands including osteocalcin, which in high serum levels is a biomarker for prostate cancer [111]. GPRC6A also interacts with testosterone and has also been linked with promoting androgen independence in aggressive prostate cancer cell lines, such as PC3 cells [62]. It is highly expressed in human prostate cancer tumours and stimulates proliferation of prostate cancer cells *in vitro*. In addition, knockdown of GPRC6A results in inhibition of prostate cancer cell migration and invasion [107]. Knockout of GPRC6A in transgenic mouse models of prostate cancer, results in reduced hyperplasia and a 23% increase in survival rates [107]. Intriguingly, human genome wide association studies (GWAS) have found single nucleotide

polymorphisms (SNPs) in GPRC6A that are linked with the development of prostate cancer in Asian populations and an individual SNP (rs1606365) which is associated with aggressive prostate cancer [112-114]. This GPCR is therefore clinically relevant to advanced prostate cancer patients and its involvement with RAMPs should be further investigated.

1.4 Adrenomedullin and CGRP: The Bone Microenvironment

The calcitonin peptide family and their receptors have long been associated with the regulation of bone metabolism. CGRP can inhibit osteoclast motility and cause quiescence through cAMP-dependent mechanisms [115]. Alternatively, both CGRP and AM have been shown to influence osteoblast activity by stimulating proliferation and triggering bone formation *in vivo* [116]. Specifically, AM treatment results in increases in mouse tibial cortical width and trabecular bone volume, suggesting it has a strong anabolic effect in the regulation of bone mass. It is therefore unsurprising that AM may be able to influence the bone environment to promote tumour growth. Breast cancer also commonly metastasizes to bone in advanced stages and therefore lessons may be learned from studies of this disease. Findings show that AM may be capable of aiding tumour growth after metastasis to the bone has occurred. *Ex vivo* models using co-cultures of breast cancer cell lines with mice calvarial bone showed that receptor activator nuclear factor- κ B ligand (RANKL) is decreased in bone but upregulated in tumour cells. This is not surprising as RANKL has long been known to be involved in regulation of bone remodeling and in pathology can influence the bone microenvironment to promote carcinogenesis [117, 118]. Interestingly, this effect was then reversed after treatment of co-cultures with 10^{-8} mol/L AM. Addition of an AM antagonist (16311) blocked expression of RANKL in both bone and tumour cells. Previous research has shown that crosstalk between breast and prostate tumour cells and osteoblasts aids to increase metastatic growth via a vicious cycle in which IL-6 and RANKL can upregulate each other in metastatic environment [119, 120]. It has not been investigated what role AM may play on IL-6 but by upregulating RANKL in tumour cells it is promoting the vicious cycle of bone metastasis growth in breast cancer. These findings may be

applicable in prostate cancer, as bone metastasis mechanisms are often similar [121, 122].

Due to its neuropathic properties, CGRP is often associated with bone pain induced by cancer metastasis [123]. When labelling sensory nerves with an anti-CGRP antibody, it was observed that following injection of prostate cancer cells into mouse femurs, nerves began to grow around the injection site. In tumour-bearing mice, these fibres grew in a disorganized manner compared with control animals which showed a linear structure with clear single fibre morphology. The fibres also seemed to sprout directly from prostate cancer cell colonies [124]. The presence of CGRP positive nerves in *in vivo* prostate cancer models such as this, suggest that secretion may influence the bone environment. Growth factors such as nerve growth factor (NGF) were found to be expressed in prostate cancer cells *in vivo* when normally NGF is not expressed in these cells. It may be possible that tumour-associating factors such as CGRP can trigger pathological sprouting of sensory neurons in prostate tumours to promote a neuroendocrine phenotype, a characteristic of advanced prostate cancer and androgen independence [81].

Taken together these findings suggest that both AM and CGRP may be influencing prostate tumour growth and metastasis either directly or indirectly. A lack of evidence exists investigating the individual receptor components of the GPCRs these peptides signal through. In order to understand the mechanisms involved in both the bone microenvironment and prostate tumour growth, these components can be explored in both *in vitro* and *in vivo* models. Prostate cancer cell lines may shed light on expression and influence of this peptide family but ultimately *in vivo* models may be better designed to test hypotheses in a realistic setting of prostate cancer metastasis.

1.5 Hypothesis and Objectives

Given the current evidence of AM and CGRP in promoting prostate cancer progression, it is hypothesized that these peptides, with their corresponding

receptors (CLR, RAMP1, 2 and 3) are involved in prostate tumour growth and metastasis. To test this hypothesis the following objectives have been set:

Objective 1: To determine the expression of AM, CGRP, RAMPs 1-3 and CLR in PC3 prostate cancer cells.

Objective 2: To use CRISPR/Cas9 gene editing to delete RAMPs 1-3 in PC3 cells and to validate this gene knockout using RT-PCR, qPCR and Sanger sequencing.

Objective 3: To determine the effect of RAMP deletion in PC3 cells *in vitro* by measuring proliferation, migration, invasion, adhesion, colony formation and responses to apoptosis.

Objective 4: To determine the effect of RAMP deletion in PC3 cells *in vivo* by using a subcutaneous xenograft mouse model and investigating tumours with immunohistological analysis targeting Ki67 and CD31 markers.

Objective 5: To determine if effects of RAMP deletion are due to CGRP stimulation by using CGRP antagonist Telcagepant in *in vivo* experiments.

CHAPTER 2: Characterisation of the PC3 Cell line

2.1 Introduction

In order to investigate the molecular mechanisms involved in prostate cancer (PC), robust, relevant models are often required. Although animal models are often the more beneficial, prostate cancer is a disease that only occurs naturally in mature male canines which, in addition to many limiting factors, can rarely be obtained for research investigations [125]. Researchers have therefore made great efforts in the past to develop prostate cancer cell lines that can mimic various stages of the disease and also with tissue specific metastasis sites. These cell lines are often selected for their aggressiveness and ability to form tumours *in vivo* (most commonly in mouse models). The first initial tissue culture cell lines used by PC researchers were LNCaP, PC-3 and DU-145 and still today these cell lines are the most widely used in published research. A PubMed search in 2017 for these terms generated 1,912, 6,239 and 7,760 published articles respectively.

The first of these tissue culture cell lines to be established was DU145. These are epithelial cells isolated from a brain tumour mass from a 69 year old white man with PC and lymphocytic leukemia [126]. This cell line lacks the androgen receptor for 5α -dihydrotestosterone produced by testosterone. Androgen sensitivity is characteristic of early PC development and patients can be treated with androgen therapy but often experience remission by which point the PC cells have become androgen insensitive [127]. DU-145 therefore represent a late stage PC and mimic this with the ability to metastasise. Subcutaneous injection of DU145 cells into NOD SCID mice produced metastatic sites in the liver, lung, lymph nodes and spleen [128]. The ability of DU-145 cells to home to bone has also been investigated using

humanized SCID mice. DU-145 (and PC-3) cells colonise to implanted fragments of human bone and form osteolytic lesions [129].

LNCaP cells were first isolated from a needle aspiration biopsy of a lymph node metastatic lesion from a 50 year old white man [130]. Interestingly, this cell line was first solely used to demonstrate androgen sensitivity and displayed poor tumorigenesis in mouse models without the use of Matrigel or co-injection of mesenchymal or stromal cell [131, 132]. This emphasises the importance of the extracellular matrix and paracrine growth factors in PC growth and metastasis. Sub cell lines were obtained by culturing LNCaP cells after being grown in castrated mice, as a result the C4-2 and C4-2B lines show metastasis to lymph nodes and bone following subcutaneous injection in mice [133].

The PC3 cell line was derived from a lumbar vertebral metastasis found in a 62 year old white man in 1979 [134]. This is a highly metastatic cell line which has been reported to establish lymph node metastases after intravenous injection and orthotopic implantation in mice [135, 136]. Intracardiac injection of PC3 cells yields bone metastases with osteolytic responses, specifically in the spine and long bones [137]. PC3 cells are also androgen insensitive and do not express the androgen receptor [138]. This cell line therefore represents a high invasive clinical state seen in PC patients who often show increased incidence of bone metastases [139]. This is a common metastasis site in PC and consequently researchers are focused on investigating models of PC in order to understand the molecular mechanisms behind this characteristic of the disease.

Calcitonin gene related peptide (CGRP) and adrenomedullin (AM) are two hormones reported to be linked with prostate cancer. They both signal through different G protein-coupled receptors (GPCRs) (See Table 1.) and the individual receptor components such as calcitonin-like receptor (CLR) and receptor activity modifying proteins (RAMPs) also have been associated with the development of prostate cancer both in the clinic and bench side. Evaluation of 129 PC patient blood samples reported CGRP serum levels significantly higher in patients with higher

clinical stages and histological grades. Authors of this publication predicted CGRP may be a useful biomarker for untreated PC patients in the future [101]. Another publication searching for prostate cancer biomarkers found RAMP1 to be differentially expressed when comparing benign and malignant prostate tissue mRNA [140].

Prostate cancer cell lines have been used to investigate the role of these targets. For example, PC3 cells have an increased invasive and migratory capacity when stimulated with CGRP *in vitro* [103, 104, 125]. Using the genomics tool OncoPrint, a cancer-specific database, researchers were able to report that RAMP1 mRNA is upregulated in prostate cancer most significantly when comparing data from other human cancers. This led the group to develop a RAMP1 knockdown in PC3 cells and were able to show reduced proliferation and decreased tumour growth and volume *in vivo* [105].

The role of adrenomedullin and its receptor components CLR, RAMP2 and RAMP3 have not been fully investigated in prostate cancer. Blocking of AM with an antibody cocktail for these components shows reduction of prostate cancer cell growth and migration [85]. AM can regulate these effects by acting on calcium channels, for example the transient receptor potential channel, TRPV2. Knockdown of this channel with siRNA abolished all effects seen on PC cells after AM treatment such as increased migration and invasion. AM is known to be associated with other metastatic cancers such as breast and lung. It is therefore worth investigating its potential in promoting prostate cancer progression.

In order to measure functional CGRP and AM expression in the PC3 cell line it is important to investigate all receptor components of CGRP and AM at both a mRNA and protein level, using RT-PCR and Western blotting. There is a lack of publications on the expression of receptor components such as RAMP1, 2, 3 and CLR at the surface of PC3 cells. It is therefore not known whether these receptors and corresponding ligands are functional in this cell line. To investigate this flow cytometry can be used to measure protein levels both inside and at the surface of

the cells. Many GPCRs including CGRP and AM can often activate via cAMP mechanisms. This means that when the receptor is stimulated with the ligand cAMP is released and this can be detected using LANCE cAMP TR-FRET assays. PC3 cells will therefore be stimulated with CGRP or AM and responses in cAMP activity measured.

2.2 Hypotheses:

1. PC3 cells express RAMP1, RAMP2, RAMP3, CLR and AM at both a mRNA and protein level *in vitro*.
2. PC3 cells express functional CGRP and AM receptors *in vitro*

2.3 Research Questions:

1. Do PC3 cells express RAMPs 1-3, CLR and AM at an mRNA and protein level?
2. Do PC3 cells express RAMPs 1-3 at the cell surface?
3. Are CGRP and AM receptors functional in PC3 cells?

2.4 Methods and Materials

2.4.1 Maintenance of Cell Lines

PC-3 cells were maintained in T-175 cm² culture flasks (Nunclon, Thermo Scientific) in RPMI 1640 medium supplemented with Glutamax™ (Gibco), 1% Penicillin and Streptomycin (5,000 units/mL, Sigma-Aldrich) and 10% fetal calf serum (Sigma-Aldrich) at 37°C in a 5% CO₂ incubator. These cell culture conditions have been previously reported in the literature to be sufficient in support growth of PC3 cells [80, 100, 105]. Media was changed twice a week until cells were observed to be 70% confluent under an INVERSO inverted microscope (Medline Scientific Ltd) and deemed ready for passaging.

2.4.2 Passage of Cells

Cells were washed once with sterile Phosphate Buffered Saline (PBS, GIBCO) and then incubated with 1X TrypLE Express Enzyme (Gibco) for 5 minutes at 37°C in a 5% CO₂ incubator to allow cells to detach from the bottom of the culture flask. Cells were then centrifuged at 300 x RPM for 5 minutes to form a pellet and then resuspended in 10mL fresh media. Cell suspension was added to a new flask with the appropriate media at a ratio of 1:10. Cells were then maintained as described above.

2.4.3 Cell Counting

Cells were detached and suspended as described above and 10µL cell suspension was mixed with 10µL 0.4% Trypan blue solution. 10µL of this mix was pipetted into a Countess chamber slide (Invitrogen) and inserted into a Countess™ Automated Cell Counter (Invitrogen).

2.4.4 RNA Extraction

Cells were grown to 70% confluency in T-75 culture flasks and then counted as described previously (Section 2.4.1-3). 5×10^5 cells were harvested for RNA extraction and were first washed with 1mL ice cold PBS and centrifuged at 300 x G for 5 minutes. RNA extraction was performed with the Reliaprep RNA Cell Miniprep System using protocols provided. The supernatant was discarded and cells were resuspended in 250µL BL + TG Buffer containing guanidine thiocyanate, guanidine hydrochloride and 1-Thioglycerol to lyse cells and release RNA by denaturing nucleoprotein complexes. Samples were then stored at -20°C. RNA was extracted using the ReliaPrep™ RNA Cell Miniprep System (Promega) following protocols provided. This included inactivation of endogenous ribonuclease (RNase) activity and the removal of contaminating DNA and proteins. Lysates were added to columns and centrifuged at 14,000 x G for 1 minute, liquid was then discarded from the collection tube. 500uL RNA wash buffer was then added to the column and then centrifuged again for 30 seconds. Liquid from the collection tube was discarded once more and

DNase I treatment was prepared by adding 24µL Yellow Core Buffer, 3µL 0.09M MnCl₂ and 3µL DNase I enzyme per sample. Samples were then incubated at room temperature with DNase treatment for 15 minutes before being washed with 200µL column wash. Columns were centrifuged again and liquid from the collection tube discarded, this was repeated twice more with 500µL RNA wash buffer. Extracts were then eluted in 30µL nuclease-free water and quantified using a Nanodrop 2000 spectrophotometer at 260nm and 260nm (Thermo Fisher).

2.4.5 cDNA Synthesis

cDNA was synthesised from RNA samples using the High Capacity RNA-to-cDNA kit (Applied Biosystems). 2µg of RNA was quantified with Nanodrop and then used for each reaction, a negative control or RT- reaction contained no reverse transcriptase to determine any genomic DNA contamination in RNA samples. Reagents were thawed on ice and then mixed as per protocol provided (see Table 2.1). Tubes were briefly centrifuged to remove air bubbles and placed in a ProFlex PCR System thermocycler (Life Technologies). Conditions were programmed as was described in the manufacturers protocol (see Table 2.2) and then samples were stored at -20°C.

Component	Volume/Reaction (µL)	
	RT +	RT -
2X RT Buffer	10.0	10.0
20X RT Enzyme Mix	1.0	0.0
RNA Sample	2µg	2µg
Nuclease-free water	To 20µL	To 20µL
Total per reaction	20.0	20.0

Table 2.1 Reverse transcription reaction recipe.

	Step 1	Step 2	Step 3
Temperature (°C)	37	95	4
Time	60 minutes	5 minutes	∞

Table 2.2 Reverse transcription reaction cycle.

2.4.6 Endpoint Polymerase Chain Reaction (PCR)

Primers were designed using the Primer3 web tool (ELIXIR) for each target, including a housekeeping gene, GAPDH (See Table 2.3) GAPDH was used as a negative control to determine environmental contamination of samples rather than as a loading control. Although this is commonly used in RT-PCR the expression of targets was not quantified and was only investigated for either presence or absence in PC3 cell mRNA. Primer3 shortlisted possible primer pairs for each target and then these were selected based on a few different criteria. Primer pairs with similar melting temperatures were preferably selected and with a high GC content. Guanine and cytosine form three hydrogen bonds together creating a stronger match compared with adenosine and thymine (only two bonds). This creates a stronger annealing process during PCR and ensures a higher level of success when targeting DNA with primers. Primers were also preferably no more than 20 nucleotides long as this has been found to be an optimal length.

cDNA samples were amplified using GoTaq G2 polymerase using protocols provided and temperatures optimised for each pair of primers (see Table 2.4). Reagents were all thawed on ice and mixed in autoclaved PCR reaction tubes using sterile pipette tips. Reactions were vortex to mix contents and then briefly centrifuged to avoid air bubbles. Reactions were run on a ProFlex PCR System thermal cycler (Life Technologies) using conditions listed in Table 2.5.

Target	Sense	Sequence 5' to 3'	Tm (°C)	Annealing Temperature (°C)	Amplicon Size (bp)
RAMP1	Forward	ATGCAGAGGTGGACAGGTTTC	59	52	193
RAMP1	Reverse	GCCTACACAATGCCCTCAGT	60		
RAMP2	Forward	CTGTCCTGAATCCCCACGAG	61	65	256
RAMP2	Reverse	CTCTCTGCCAAGGGATTGGG	60		
RAMP3	Forward	AAGGTGGACGTCTGGAAGTG	60	56	227
RAMP3	Reverse	ATAACGATCAGCGGGATGAG	57		
AM	Forward	TACCGAGAGCATGAACAA	57	54	276
AM	Reverse	CTAAAGAAAGTGGGGAGCACTTC	60		
CLR	Forward	CTGGCTGGGGATTCCACT	59	54	302
CLR	Reverse	CCTTCAGGTCGCCATGGAAT	59		
GAPDH	Forward	TTGTCAGCAATGCATCCTGC	57	52	354
GAPDH	Reverse	GCTTCACCACCTTCTTGATG	57		

Table 2.3 Endpoint PCR primers.

These primers target RAMP1, 2, 3, CLR, AM and GAPDH were synthesised by Eurofins and diluted with nuclease-free water on arrival to 100pmol/μL and stored at -20°C.

Component	Final Volume	Final Concentration
5X GoTaq G2 Green Buffer	10μL	1X
MgCl ₂ (25mM)	1.5μL	0.75mM
dNTP mix (10mM each)	1μL	0.2mM each dNTP
Forward primer	5μL	1μM
Reverse primer	5μL	1μM
GoTaq G2 DNA Polymerase (5 units/μL)	0.25μL	1.25 units
Template DNA	1μL	0.2μg
Nuclease-free water	--	--
Total	50μL	

Table 2.4 Endpoint PCR recipe

PCR Step	Temperature	Time	Cycle Number
Denaturation	95°C	2 min	x1
	95°C	1 min	x35
Annealing	--°C	1 min	
Extension	72°C	1 min	
	72°C	5 min	x1
Hold	4°C	∞	

Table 2.5 Endpoint PCR cycle

2.4.7 Gel Electrophoresis

PCR products were visualised on 1.5% agarose gels prepared with 1.5g agarose (Fisher Scientific) and 100mL 1X TBE (Tris-borate-EDTA, Scientific Laboratory Supplies) buffer heated in a 750W microwave oven for 120 seconds. The solution was then stirred to dissolve agarose and heated again for 40 seconds. 0.5µg/mL (final concentration) ethidium bromide (Sigma-Aldrich) was added to the agarose mixture in order to bind to DNA and be detected using a UV light source. Then the solution was poured into an electrophoresis gel casting tray with a 16-well comb to set for 15 minutes. The gel was then transferred to an electrophoresis gel chamber containing 1X TBE buffer. 10µL of PCR product was loaded to each well. A 10µL FullRanger 1kb DNA Ladder (Geneflow) was loaded to the first lane of each agarose gel. GoTaq G2 Mastermix buffer was sufficient density for PCR products to be loaded straight into agarose gels. The gel was run at 200 volts for 45 minutes and then visualised using a Gel Doc XR+ Gel Documentation System (Bio-Rad).

2.4.8 Sanger Sequencing

PCR products were validated with Sanger sequencing to confirm correct targets were amplified. Products were provided at 50ng/µL with forward and reverse primers diluted to 1µM and sequencing was performed by the University of

Sheffield Core Genomic Facility using BigDye™ Terminator v3.1 Cycle Sequencing Kit (Thermo Fisher) and run on an Applied Biosystems 3730 DNA Analyser. Sequencing data was generated in “abi” file format and analysed using 4Peaks v1.8 software (Nucleobytes). Sequences were then compared to NCBI target sequences using BLAST (Basic Local Alignment Search Tool, NCBI).

2.4.9 Protein Extraction

Cells were grown to 70% confluency in T-75 flasks and then incubated on ice for 10 minutes. Halt™ Protease and Phosphatase Inhibitor Cocktail (Thermo Scientific) was diluted 1:100 with NP-40 buffer (150mM NaCl, 50mM Tris Base pH 8.0, 1% NP-40) to form the cell lysis buffer. Protease inhibitors included in lysis buffer were aprotinin, bestatin and leupeptin which inhibit serine and cysteine proteases. Phosphatase inhibitors included sodium fluoride and sodium orthovanadate which inhibit serine, threonine and tyrosine phosphatases. Culture medium was removed from cells and then washed with 10mL ice cold PBS. 1mL lysis buffer was added and cells were incubated on ice for 5 minutes. Cells were scraped from the flask and lysate transferred to a cold 1.5mL Eppendorf tube. The cell lysate was kept on ice and sonicated at input 60 for 30 seconds before being centrifuged at 13,000 x G for 20 minutes at 4°C. Lysate supernatant was then transferred to a fresh tube and aliquoted before being stored at -20°C.

2.4.10 Bicinchoninic Acid (BCA) Assay

Protein extracts were quantified using a DC Protein Assay kit (Bio-Rad). This is a colorimetric assay that can quantify proteins after they are solubilised in detergent. The experiment relies on the reaction of protein samples with alkaline copper tartrate solution and Folin reagent. Samples first react with copper tartrate and then reduce Folin reagent by the loss of 1-3 oxygen atoms, this creates several reduced species which have a characteristic blue colour with a maximum absorbance of 750nm and minimum 405nm. A working solution was made by adding 20µL reagent S per mL of reagent A (an alkaline copper tartrate solution). Bovine serum

albumin was prepared at 5 different dilutions in lysis buffer to produce a standard curve for each assay (See Table 2.6).

Protein Standard Concentration (mg/mL)	Lysis Buffer Amount (μ L)	Protein Standard Amount (μ L)
1.43	0	20
1.14	4	16
0.86	8	12
0.57	12	8
0.29	16	4
0	20	0

Table 2.6 Protein standard concentrations for BCA assay.

Serial dilutions were performed starting from stock concentration of 1.43mg/mL and including a blank of only lysis buffer to account for background signal.

Protein samples were added in triplicates at 5 μ L to a 96-well microplate either neat or diluted 1:10 with lysis buffer. Protein standards were also added in duplicates at 5 μ L. 25 μ L working solution (reagent A + reagent S) was then added. 200 μ L reagent B (a dilute Folin reagent) was added to each well and gently mixed. Any bubbles that were formed were popped with a dry pipette tip. After 15 minutes incubation at room temperature absorbance was read using a Ensignt Perkin Elmer plate reader at 750nm. A standard curve was plotted using GraphPad Prism 7 and unknown values of protein samples were interpolated from the standard curve linear equation: $y = mx + c$ (see Fig 2.1.)

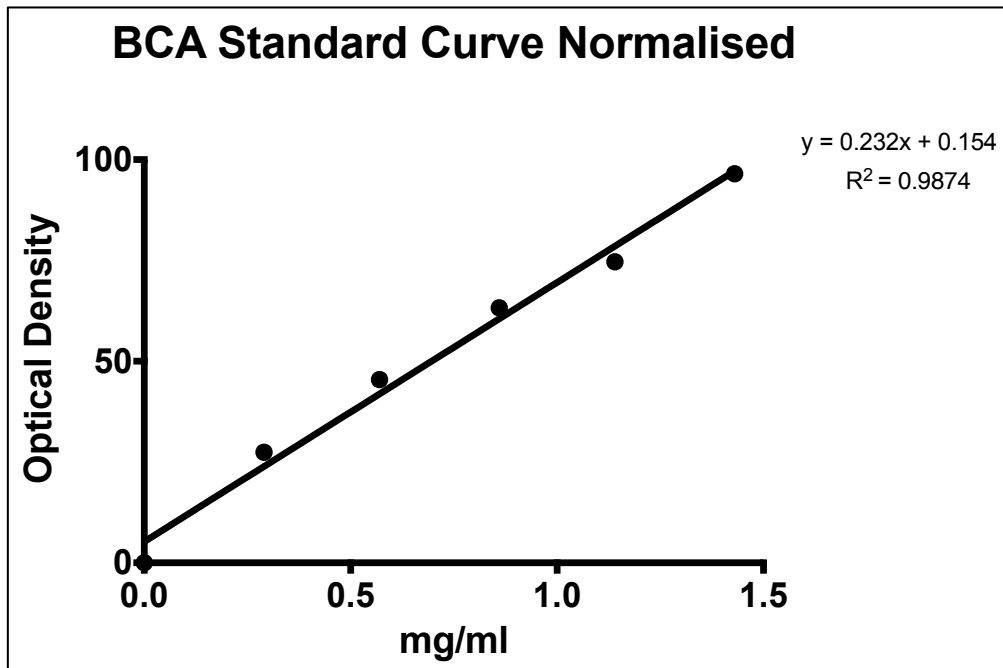


Figure 2.1 BCA standard curve.

2.4.11 Western Blotting: Gel Electrophoresis and Transfer

Western blotting is an efficient method for measuring protein expression in cell lysates. After protein concentrations have been quantified the samples can be diluted in Laemmli buffer and mixed with DTT (dithiothreitol) to aid denaturation of protein by reducing disulfide bonds. Proteins are then separated by size when loaded onto an electrophoresis gel and a charge is placed on the gel. Proteins are then transferred from the gel to a “transfer membrane” in order to probe with antibodies. Blocking of the membrane prevents non-specific protein interactions before a primary antibody is added which binds to the protein of interest. A secondary antibody is then added to bind to the primary and is often conjugated to an enzyme e.g. horse radish peroxidase (HRP). The bands can then be detected using chemiluminescence substrates and a film or photo imager.

Once quantified, protein samples were diluted with distilled water and Laemmli buffer (Bio-Rad) (containing 62.5mM Tris-HCl, pH 6.8, 25% glycerol, 2% SDS and 0.01% Bromophenol Blue) with a reducing agent, 350mM DTT (dithiothreitol) (Fisher Scientific) to a final volume of 50 μ L. Protein samples were then denatured using a heat block at 95°C for 10 minutes. 10 μ L of Precision Plus Protein™ Dual Colour Standards (Bio-Rad) and 50 μ L of protein samples were loaded onto 4-20% Mini-PROTEAN® TGX™ Precast Protein Gels (Bio-Rad) and placed in a Vertical Electrophoresis Cell (Bio-Rad) filled with 1x Tris/Glycine/SDS running buffer (Bio-Rad). The gels were then run at 150 volts for 45 minutes – 1 hour. Gels were then transferred onto Trans-Blot PVDF membranes (Bio-Rad) using a Trans-Blot® Turbo™ Rapid Transfer System (Bio-Rad). A mixed molecular weight pre-programmed transfer protocol was used at 25 volts for 7 minutes.

2.4.12 Western Blotting: Blocking and Probing

Transfer membranes were then placed in shallow containers filled with the appropriate blocking buffer (see Table) and incubated for 1 hour at room temperature on a plate shaker at 600rpm. Primary antibody was diluted in blocking buffer at the appropriate concentration (see Table 2.7.) and then incubated with the transfer membrane overnight at 4°C on a plate shaker at 600rpm. The blot was then washed with 1X TBS-T (NaCl 150mM, Tris base 20mM, 0.1% Tween-20, pH 7.6) for 10 minutes on the plate shaker at 600rpm. This washing was repeated three times. The blot was then incubated for 1 hour at room temperature on a plate shaker at 600 rpm in a blocking buffer containing the appropriate secondary antibody at the appropriate concentration (see Table 2.8.) The blot was then washed three times for 5 minutes with 1X TBS-T buffer and then three times for 5 minutes with distilled water.

Target	Antibody	Species	Company	Protein Amount	Primary Concentration	Block
RAMP1	Monoclonal	Anti-rabbit	AbCam 156575	10µg	1:1000	3% BSA – 0.1% Tween 20
RAMP2	Monoclonal	Anti-mouse	Santa Cruz 365240	10µg	1:100	3% BSA – 0.1% Tween 20
RAMP3	Monoclonal	Anti-mouse	Santa Cruz 365313	10µg	1:1000	5% Skimmed Milk
CLR	Monoclonal	Anti-mouse	Santa Cruz 30028	20µg	1:100	2.5% Skimmed Milk
Vinculin	Monoclonal	Anti-rabbit	AbCam 129002	10µg	1:10,000	3% BSA – 0.1% Tween 20

Table 2.7 Western blotting primary antibodies.

Details of primary antibodies and the optimised concentrations and blocking conditions.

Secondary Antibody	Antibody	Company	Secondary Concentration
Goat IgG anti-rabbit HRP	Polyclonal	Dako P0449	1:15,000
Goat IgG anti-mouse HRP	Polyclonal	Dako P0447	1:2000

Table 2.8 Western blotting secondary antibodies.

Details of secondary antibodies and the optimised concentrations.

2.4.13 Western Blotting: Detection

Blots were detected using a SuperSignal West Femto Maximum Sensitivity Substrate (Thermo Scientific) by mixing 250µL Stable Peroxide Solution with 250µL Luminol/Enhancer Solution (per blot). The oxidation of luminol in the presence of horse radish peroxidase (HRP) and peroxide produces prolonged chemiluminescence when can then be visualised with a photo imaging system. The combined substrates are used to cover both sides of the blot and the blot is then placed in transparent plastic film for detection using a Gel Doc XR+ Gel Documentation System (Bio-Rad).

2.4.14 Western Blotting: Optimisation

Antibodies were optimised by first using any recommended concentrations or conditions from the manufacturers. Conditions were then optimised to reduce non-specific signal by changing the blocking buffer from 3% BSA to 1-5% skimmed milk. Primary antibodies were then also titrated to find an optimal concentration. In some cases, denaturing temperatures were also changed but this rarely improved antibody performance. The secondary antibodies were kept at a constant concentration throughout all optimisation experiments.

2.4.15 CGRP (Human) Fluorescent Immunoassay

Levels of CGRP peptide were measured in conditioned media of PC3 cells using a fluorescence enzyme immunoassay (EIA) kit (Phoenix Pharmaceuticals). First, 2×10^5 PC3 cells were plated in 6 well plates and left to adhere for 24 hours in an incubator at 37°C. The cells were then washed once with 500µL PBS and 1% RPMI was added for another 24 hours. This conditioned media was then collected and treated with Halts protease inhibitor cocktail (Thermo Fisher) and stored at -80°C. The principle of the immunoassay uses an immunoplate pre-coated with a secondary antibody with blocked non-specific binding sites. First, 50µL of either sample, standard peptides or a positive control (CGRP peptide) were mixed with 25µL of the anti-CGRP primary antibody and incubated at 4°C overnight. The fc fragment of the primary antibody binds to the secondary antibody on the pre-coated immunoplate and any unbound material was then removed with four washes of 300µL assay buffer. 25µL of biotinylated peptide was then added to the plate and incubated for 1.5 hours on a shaker (400 rpm) at room temperature. The primary antibody has a biotinylated Fab fragment that is competitively bound by both the biotinylated peptide and peptide standard or targeted peptide in the samples.

After four washes with 300 μ L assay buffer, 100 μ L of streptavidin-horseradish peroxidase (SA-HRP) was added to each well. The biotinylated peptide then interacts with SA-HRP which then catalyses the substrate. The plate was then read using an Enight plate reader (Perkin Elmer) at 340nm excitation and 470nm emission wavelengths. The intensity of the fluorescent signal generated is inversely proportional to the amount of peptide in standard solutions or samples. This is because competitive binding of the biotinylated peptides with the standard or sample peptide to the primary antibody. A standard curve of known concentrations (see Fig 2.2) of CGRP peptide was generated and unknown concentrations of the conditioned media samples were extrapolated.

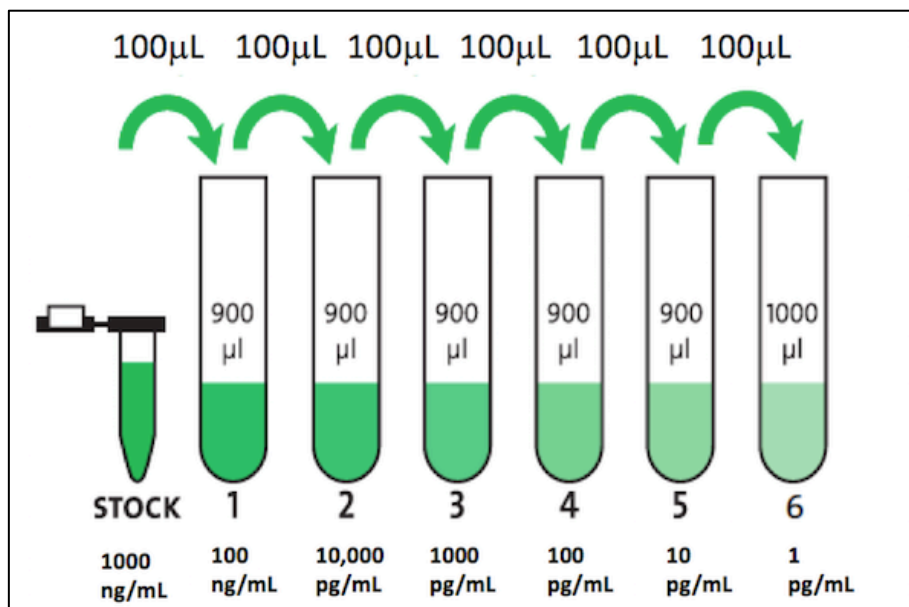


Figure 2.2 CGRP immunoassay peptide standard concentrations.

Standard solutions were generated using serial dilution of stock concentration 100 ng/mL and diluted with 1X assay buffer.

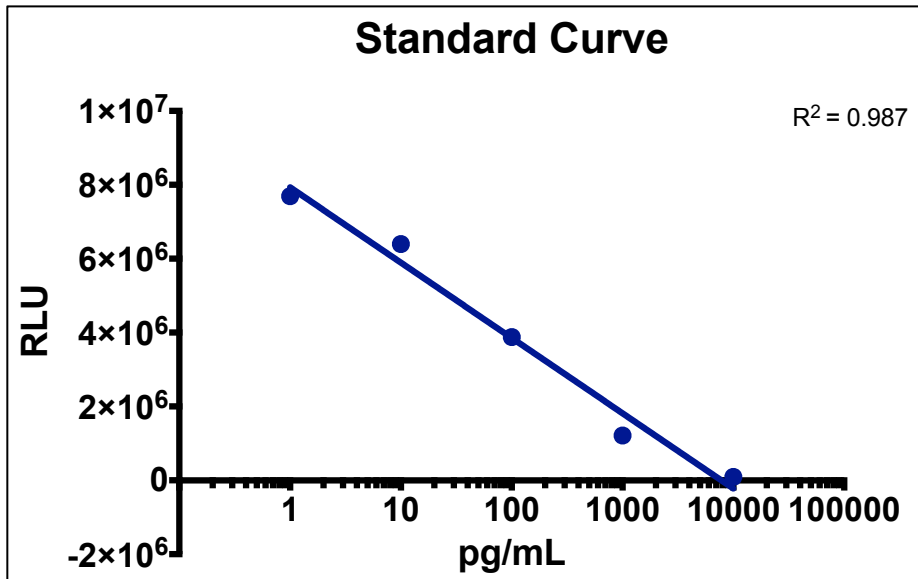


Figure 2.3 CGRP immunoassay standard curve.

Unknown concentrations of CGRP in PC3 conditioned media was extrapolated from the standard curve. Fluorescence intensity is inversely proportional to the level of CGRP peptide.

2.4.16 cAMP LANCE Ultra TR-FRET

To measure cAMP activity in PC3 cells the LANCE Ultra cAMP assay (Perkin Elmer) was used. This is a time-resolved fluorescence resonance energy transfer (TR-FRET)

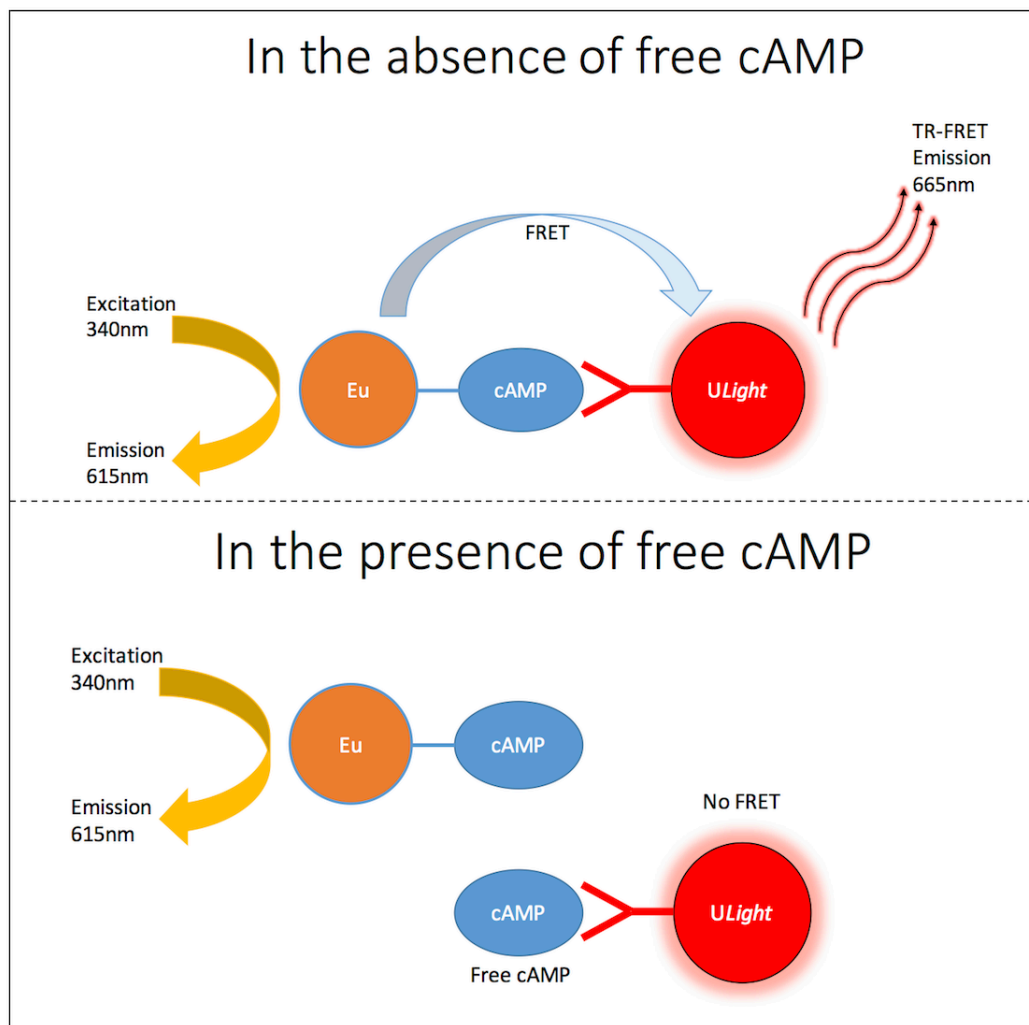


Figure 2.4 LANCE Ultra cAMP assay principle.

immunoassay which measures cAMP produced after modulation of adenylyl cyclase activity by GPCRs. The principle utilises the competition between a europium (Eu) chelate-labelled cAMP tracer and sample cAMP for binding sites on cAMP-specific monoclonal antibodies labelled with a *ULight* dye. When the Eu-labelled cAMP tracer binds to these antibodies a light pulse at 320-340nm excites the Eu molecule. The energy emitted by the excited Eu molecule is transferred by FRET to *ULight*

molecules on the antibodies themselves, which in turn emit light at 665nm (see Fig 2.4.)

To determine the optimal cell number and stimulation conditions, forskolin dose response curves were generated (see Fig 2.5.) Forskolin is a cell permeable diterpenoid isolated from the Indian Coleus plant and can activate adenylyl cyclase producing intracellular cAMP. cAMP standards were also used to generate dose response curves to optimise stimulation conditions (see Fig 2.6.) It was found that 250 PC3 cells per well produced a curve that covers the most dynamic range compared with the cAMP standard curve. This suggests that the cell density is giving the highest signal to background ratio, calculated using maximal signal (untreated cells) and the minimal signal obtained with a saturating concentration of forskolin (fully activated cells). cAMP standard dose response curves showed the optimal stimulation buffer which are shown in Table 2.7.

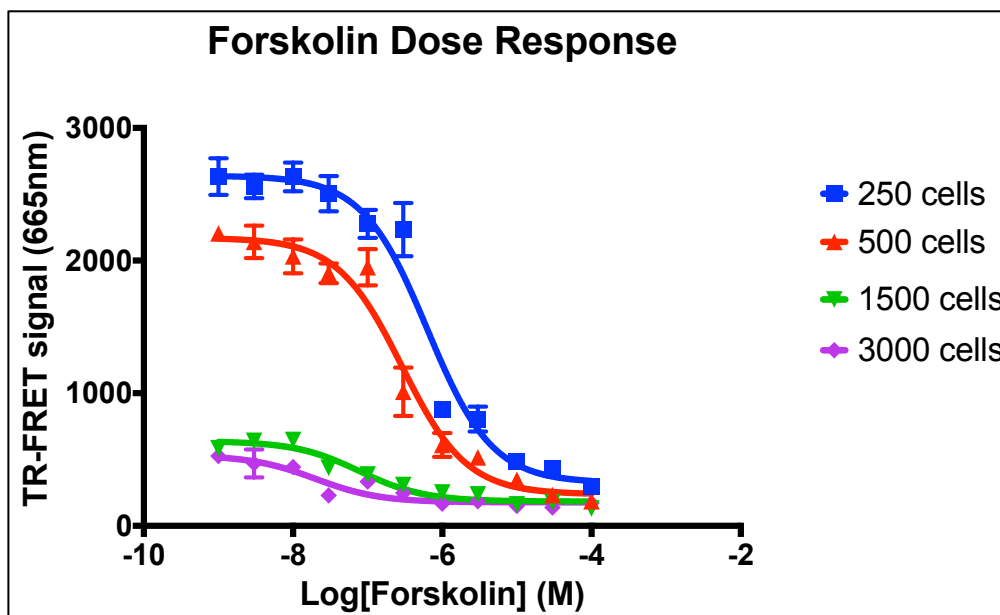


Figure 2.5 Forskolin dose response. All values are mean \pm SEM, n=3.

Dose response of Forskolin on PC3 cells to optimise cell number.

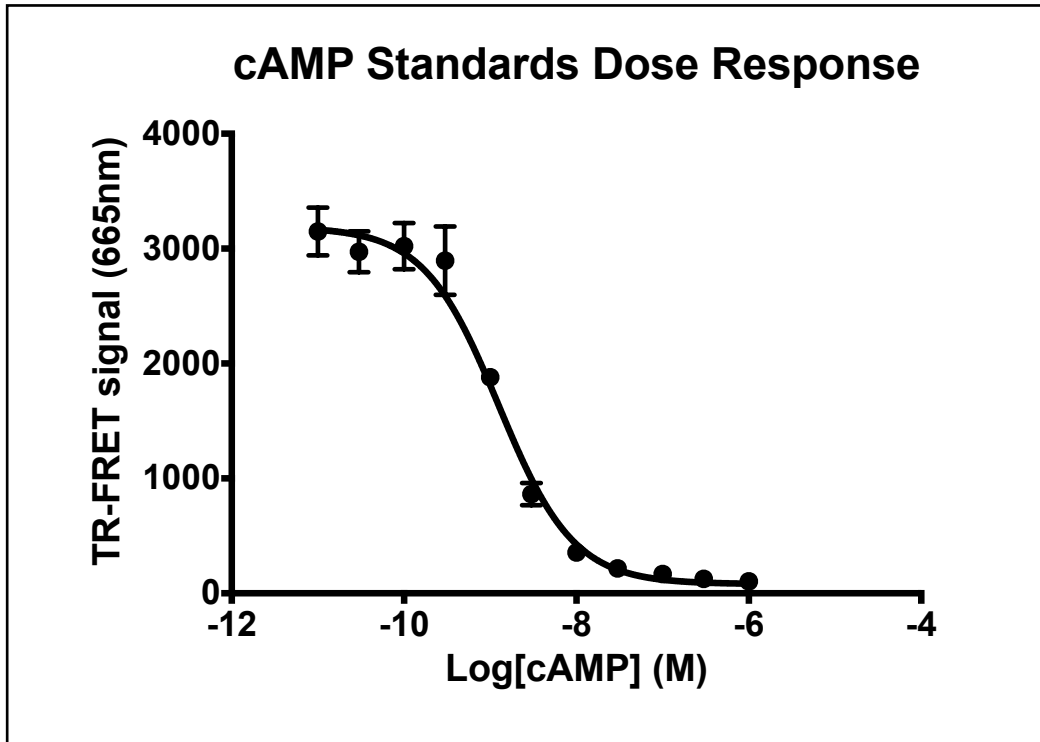


Figure 2.6 Dose response of cAMP standards. All values are mean \pm SEM, n=3.

Component	Volume
Hank's Balanced Salt Solution 1X (-CaCl ₂ -MgCl ₂)	14mL
HEPES Buffer (1M)	75 μ L
IBMX 250mM	30 μ L
BSA Stabiliser (7.5% solution)	100 μ L

Figure 2.7 cAMP stimulation buffer recipe.

Serial dilutions of ligands or forskolin for each assay were made first (See Tables 2.9 & 2.10) in stimulation buffer. Siliconized pipette tips were used at all times in the preparation of ligands or forskolin. Blanks of buffer alone were added to untreated cells to allow measurement of background signal. These were then transferred to a white opaque 384 microtiter plate (5 μ L per well) and centrifuged at

300 x G for 1 minute. Cells were either used live or from -80°C frozen aliquots and counted using methods described previously. Overexpressing (OE) cell lines were used as positive controls, either expressing CGRP or AM and their receptor subcomponents (RAMP1-3 and CLR). 2,500 OE cells were added per well 250 PC3 cells were added per well as was optimized previously. Cell suspensions were made in stimulation buffer and volumes of 5µL per well were added on top of ligand or forskolin dilutions. Plates were then centrifuged at 300 x G for 1 minute and incubated at room temperature for 30 minutes.

Dilution	Final Concentration	2X Concentration	Volume of dilution	Stimulation buffer
1	1x10 ⁻⁴	2x10 ⁻⁴	80µL	120µL
2	3x10 ⁻⁵	6x10 ⁻⁵	60µL	140µL
3	1x10 ⁻⁵	2x10 ⁻⁵	60µL	120µL
4	3x10 ⁻⁶	6x10 ⁻⁶	60µL	140µL
5	1x10 ⁻⁶	2x10 ⁻⁶	60µL	120µL
6	3x10 ⁻⁷	6x10 ⁻⁷	60µL	140µL
7	1x10 ⁻⁷	2x10 ⁻⁷	60µL	120µL
8	3x10 ⁻⁸	6x10 ⁻⁸	60µL	140µL
9	1x10 ⁻⁸	2x10 ⁻⁸	60µL	120µL
10	3x10 ⁻⁹	6x10 ⁻⁹	60µL	140µL
11	1x10 ⁻⁹	2x10 ⁻⁹	60µL	120µL
12 (Blank)	---	---		140µL

Table 2.9 cAMP forskolin concentrations.

Forskolin serial dilutions in stimulation buffer ranging from 1x10⁻⁴ to 1x10⁻⁹ final concentration. Dilutions were made up 2X and then added to cell suspension 1:1.

A working solution containing the 4X Eu-cAMP tracer was prepared by making a 1:50 dilution of Eu-cAMP tracer stock solution in cAMP detection buffer. 4X *ULight* anti-cAMP working solution was prepared by making a 1:150 dilution of the *ULight* anti-cAMP stock solution in cAMP detection buffer. Both these working solutions were prepared in the dark and stored in foil covered tubes until use. After the cells were incubated with ligand or forskolin, 5µL of Eu-cAMP tracer working solution was added to each well and the plate was centrifuged at 300 x G for 1 minute. Then 5µL *ULight* anti-cAMP working solution was added to each well and the plate was centrifuged at 300 x G for 1 minute and then incubated at room temperature in the dark for 1 hour. After incubation, the plate was read using an Ensign multimode plate reader (Perkin Elmer) under the conditions described in Table 2.11.

Dilution	Final Concentration	2X Concentration	Volume of dilution	Stimulation buffer
1	1×10^{-6}	2×10^{-6}	3.3µL	96.7µL
2	3×10^{-7}	6×10^{-7}	30µL	70µL
3	1×10^{-7}	2×10^{-7}	30µL	60µL
4	3×10^{-8}	6×10^{-8}	30µL	70µL
5	1×10^{-8}	2×10^{-8}	30µL	60µL
6	3×10^{-9}	6×10^{-9}	30µL	70µL
7	1×10^{-9}	2×10^{-9}	30µL	60µL
8	3×10^{-10}	6×10^{-10}	30µL	70µL
9	1×10^{-10}	2×10^{-10}	30µL	60µL
10	3×10^{-11}	6×10^{-11}	30µL	70µL
11	1×10^{-11}	2×10^{-11}	30µL	60µL
12 (Blank)	---	---		70µL

Table 2.10 cAMP ligand concentrations.

Ligand serial dilutions in stimulation buffer ranging from 1×10^{-6} to 1×10^{-11} final concentration.

Parameter	Instrument Settings
Excitation Filter	Lamp: 111 (UV2 320)
Emission	1) 615 2) 665
Delay Time	70 μ s
Number of Flashes	100
Window Time	100 μ s
Total Time	170 μ s

Table 2.11 Ensign plate reader settings for cAMP assays.

2.5 Results

2.5.1 Endpoint PCR

cDNA samples taken from PC3 cells, including reverse transcription (RT) negative controls were amplified using endpoint PCR with GAPDH (housekeeping) primers to check RT negative controls for genomic DNA contamination. These samples were then used to check for the expression of RAMP1, 2, 3, CLR and AM. Reverse transcription negative controls showed no clear bands indicating no DNA contamination (see Fig 2.8.)

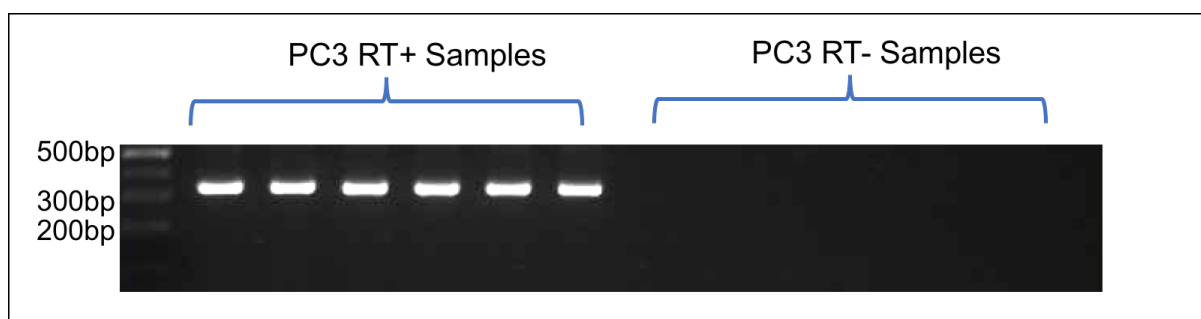


Figure 2.8 Endpoint PCR GAPDH.

cDNA samples taken from PC3 cells amplified using endpoint PCR and GAPDH primers (354 bp). Reverse transcription negative controls show no bands, indicating no genomic DNA contamination.

PC3 cDNA samples were then amplified using primers designed for RAMP1, 2, 3, CLR and AM (see Table 2.3.) After experimental repeats, PC3 samples showed bands for all targets and RAMP1-3, CLR and AM (see Fig 2.9). Negative controls were used to assess environmental contamination, these reactions contained nuclease free water instead of a DNA template and did not show any bands. Endpoint PCR products were then analysed using Sanger sequencing to validate correct target amplification. All targets were successfully sequenced and matched correctly to NCBI database sequences using Basic Local Alignment Search Tool (BLAST) (for RAMP1 as an example see Fig 2.10 or Appendix for RAMP2, 3, CLR and AM).

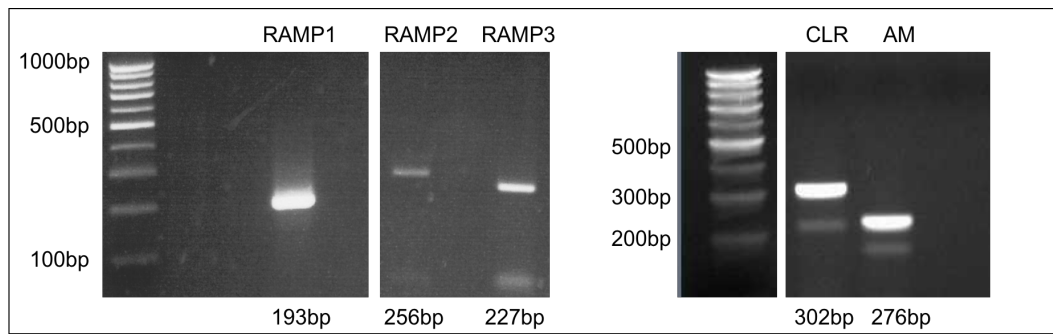
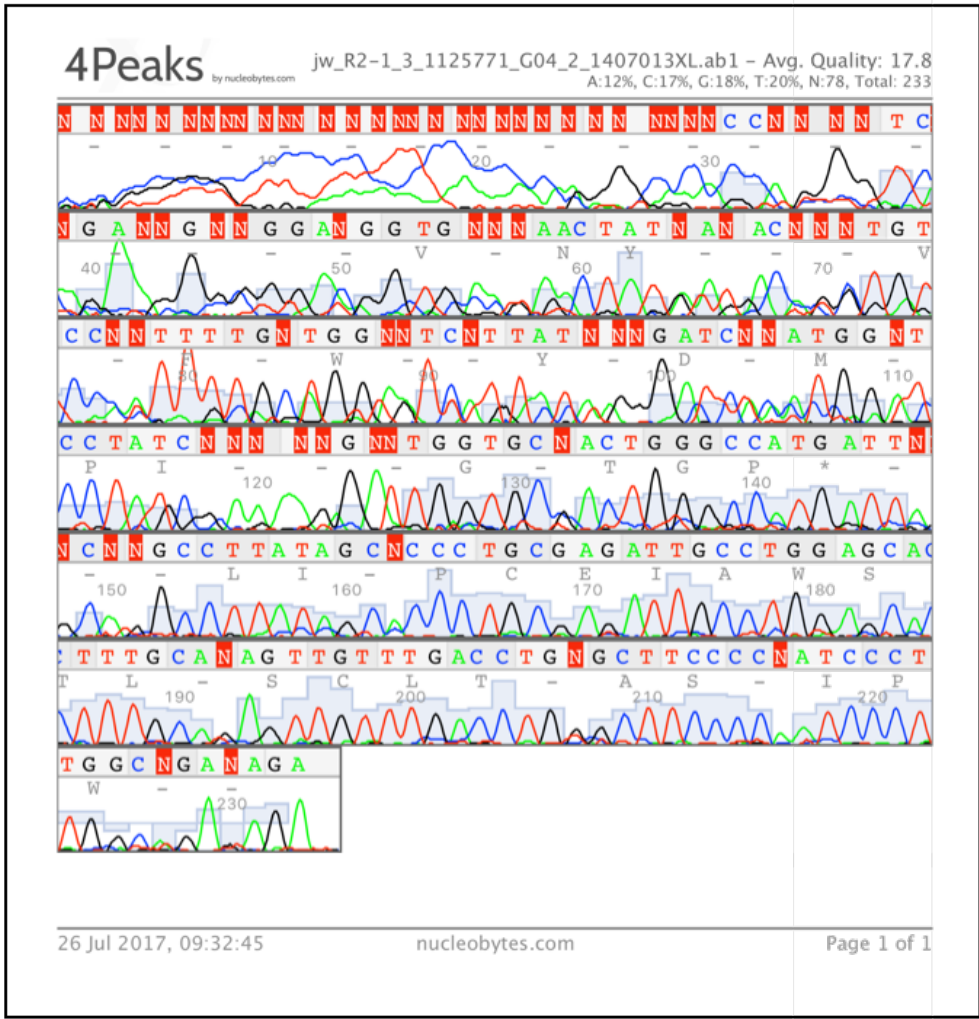


Figure 2.9 Endpoint PCR RAMPs 1-3, CLR and AM.

PC3 cDNA samples amplified using endpoint PCR and primers targeting RAMP1 (193bp), RAMP2 (256bp), RAMP3 (227bp), CLR (302bp) and AM (276bp). All targets showed visible bands at different levels of intensity when repeated three times.



Homo sapiens receptor activity modifying protein 1 (RAMP1), transcript variant 1, mRNA
 Sequence ID: **gi|816197636|NM_005855.3** Length: 920 Number of Matches: 1
 Range 1: 184 to 283

Score	Expect	Identities	Gaps	Strand	Frame
167 bits(90)	1e-38()	96/100(96%)	1/100(1%)	Plus/Plus	

Features:

Query	96	GCCCATCACCTCTTCATGACCACTGCCTGCCAGGAGGCTAACTACGGTGCCCTCCTCCGG	155
Sbjct	184	GCCCATCACCTCTTCATGACCACTGCCTGCCAGGAGGCTAACTACGGTGCCCTCCTCCGG	243
Query	156	GAGCTCTGCCTCACCCAGTTCAGGTANN-ATGNAGGCCG	194
Sbjct	244	GAGCTCTGCCTCACCCAGTTCAGGTAGACATGGAGGCCG	283

Figure 2.10 RAMP1 sanger sequencing.

(A) Sanger sequence for RAMP1 analysed using 4Peaks software shows 78% accurate base calling. Background noise found 1-20bp and 330-380bp, target size = 193bp. **(B)** Screenshot of Sanger sequence for RAMP1 aligned with NCBI NM_005855.3 RAMP1 mRNA sequence. 96% identity match was found.

2.5.2 Western Blot

Expression of RAMP1, RAMP2, RAMP3 and CLR total protein was measured by Western Blotting. PC3 protein was extracted and quantified using a BCA assay (see Section 2.4.10) before probed with different target antibodies including a vinculin loading control (see Section 2.4.11-13.) After visualisation using a chemiluminescence substrate, bands were detected in all targets at the predicted monomer size. RAMP1 was detected at ~17kDa, RAMP2 at ~20kDa, RAMP3 at ~28kDa and CLR was detected at ~55kDa (see Fig 2.11.)

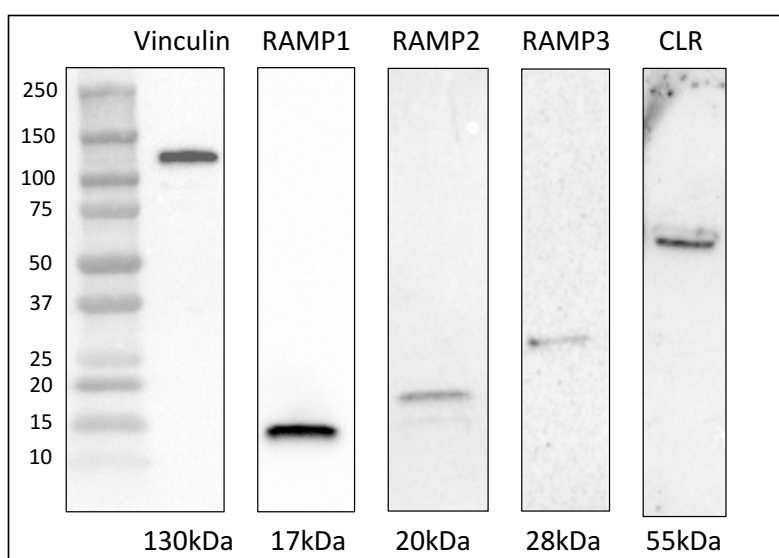


Figure 2.11 Western blotting RAMP1-3 and CLR.

Western blot on PC3 total protein extracts to measure RAMP1 (17kDa), RAMP2 (20kDa), RAMP3 (28kDa) and CLR (55kDa) expression (n = 3). Vinculin was used as a positive control.

2.5.3 CGRP Fluorescent Immunoassay

Conditioned media from PC3 cells was tested for levels of CGRP peptide using a fluorescent immunoassay. Concentrations were interpolated from a standard curve of known concentrations of CGRP peptide. Positive controls (CGRP peptide alone) ensured quality control of all assays. Three separate samples of PC3

conditioned media were tested with 1% RPMI used as a negative control and to account for any background signal. Results show that PC3 conditioned media contained on average 35pg/mL of CGRP, 1% RPMI media alone had consistent results of only 1pg/mL (see Fig 2.12). The positive control was estimated to contain 40-120 pg/mL CGRP and results show an average of 131 pg/mL confirming the quality of the immunoassay.

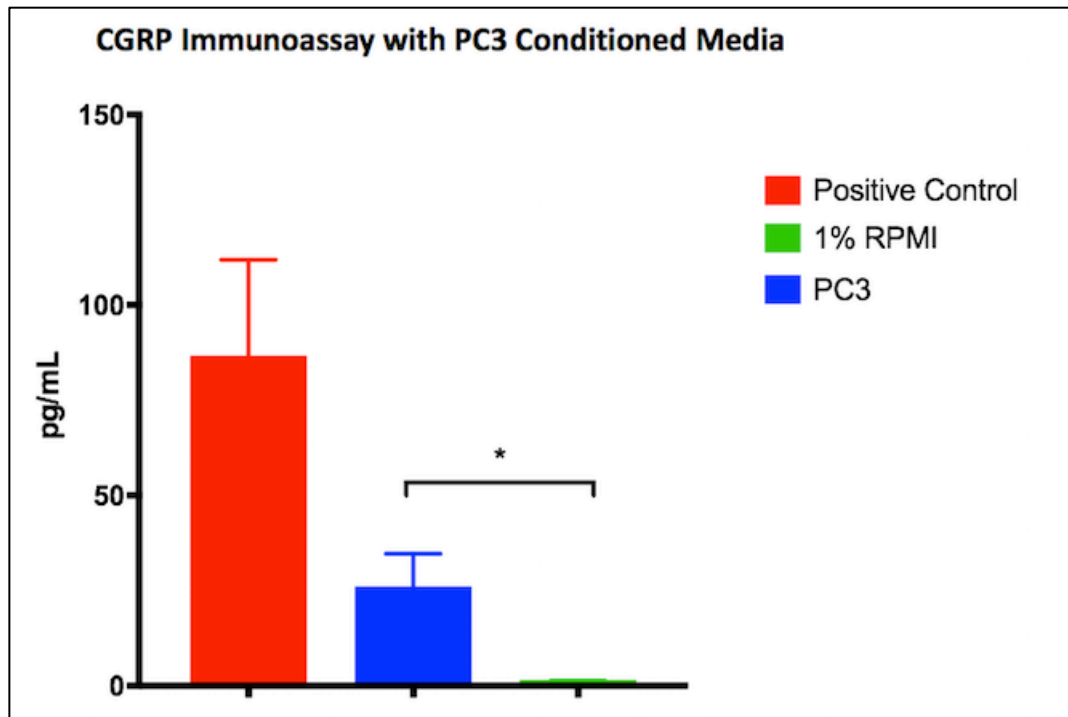


Figure 2.12 CGRP fluorescent immunoassay.

Levels of CGRP were measured using a fluorescent immunoassay. Levels of CGRP were calculated to be 35 pg/mL in PC3 conditioned media compared with 1 pg/mL in 1% RPMI alone. Positive controls were found to contain 131 pg/mL CGRP. All values are mean \pm SEM, n=3. $P < 0.05$, (Students unpaired t-test).

2.5.4 Cyclic AMP Assays

To assess whether CGRP or AM receptors are functional in PC3 cells, LANCE Ultra cAMP assays were used to detect changes in intracellular cAMP levels following stimulation with either CGRP or AM ligand and forskolin was used as a positive control. It was found that PC3 cells when stimulated with forskolin always produce an increase in cAMP levels that was detected in a dose dependent manner (see Fig 2.13). However, when stimulated with either CGRP or AM, PC3 cells did not show any increases in intracellular cAMP (see Fig 2.15 and 2.16). PC3 cells were stimulated also with Amylin as this also uses RAMP1 along with calcitonin-like receptor (CTR) as its functional receptor, however no changes in cAMP levels were detected (see Fig 2.16).

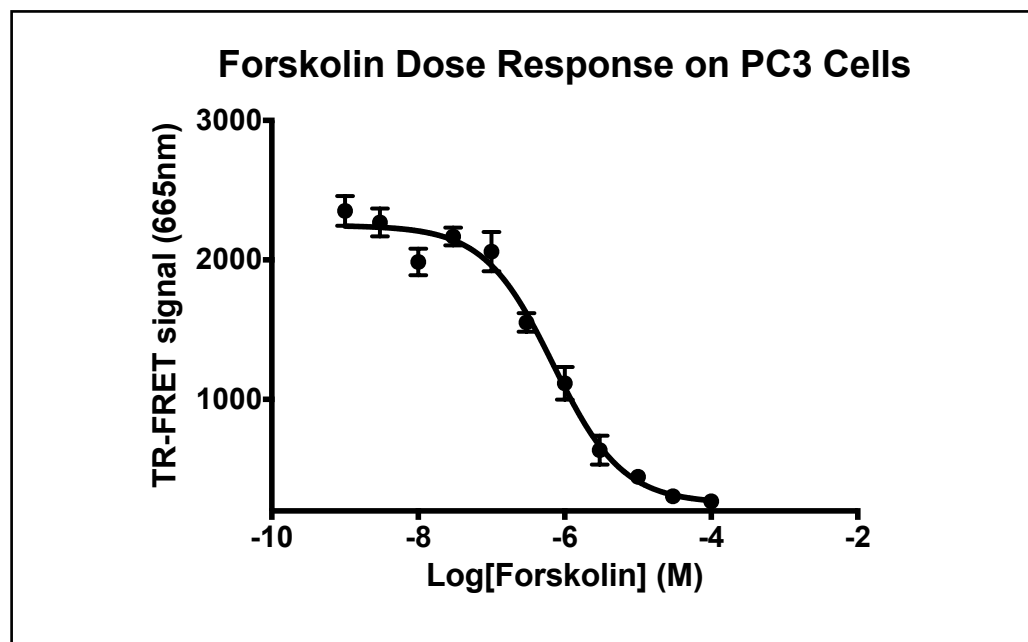


Figure 2.13 Forskolin dose response on PC3 cells.

All values are mean \pm SEM, n=3.

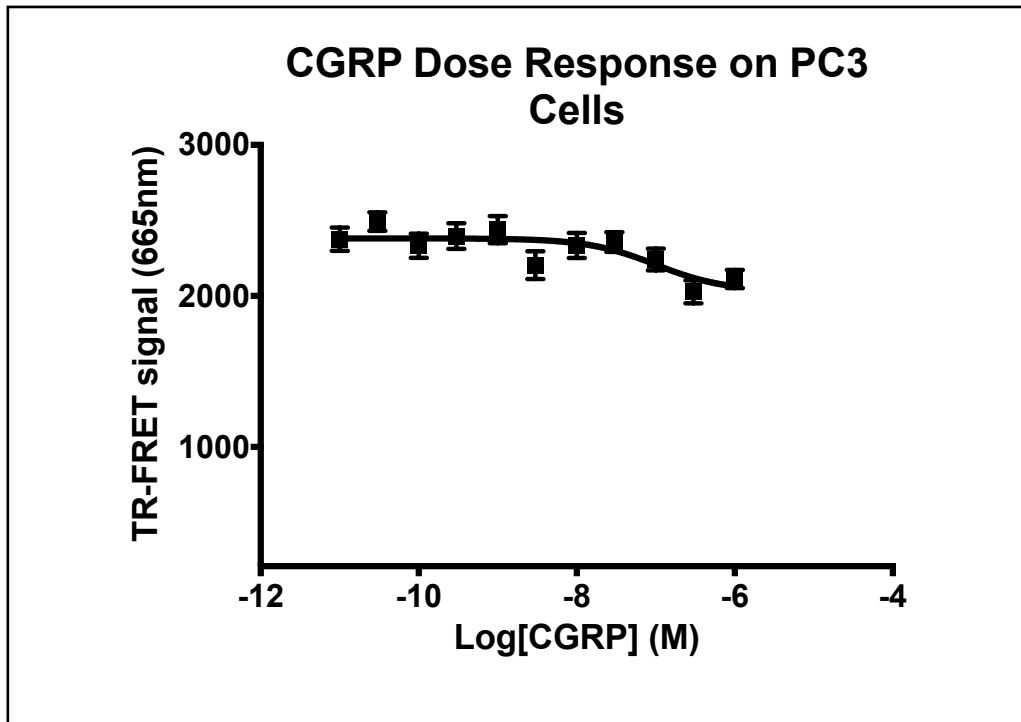


Figure 2.14 Dose response of CGRP stimulation on PC3 cells.

All values are mean \pm SEM, n=3.

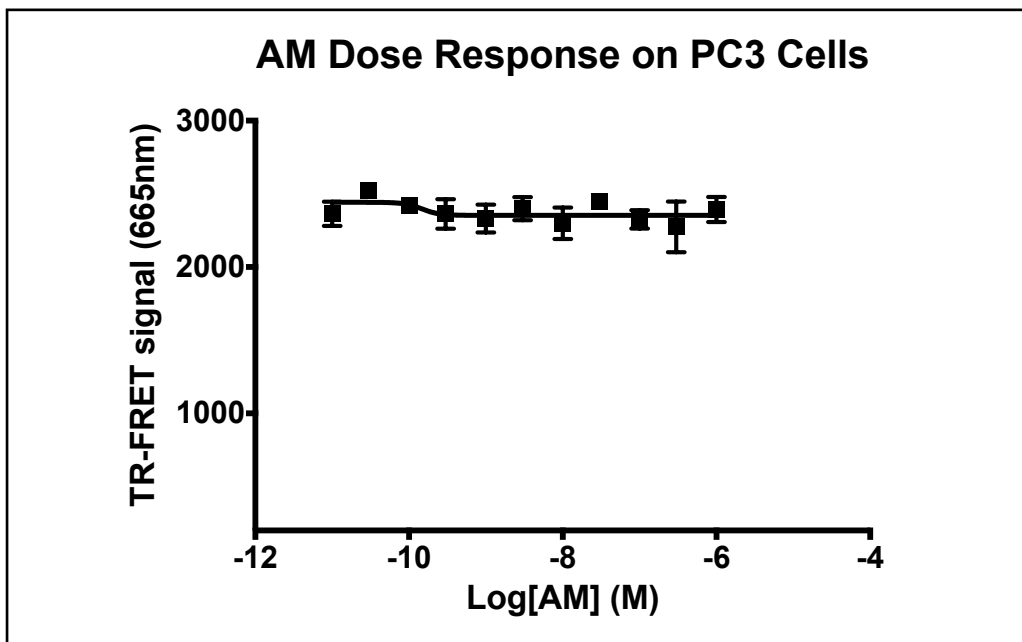


Figure 2.15 Dose response of AM stimulation on PC3 cells.

All values are mean \pm SEM, n=3.

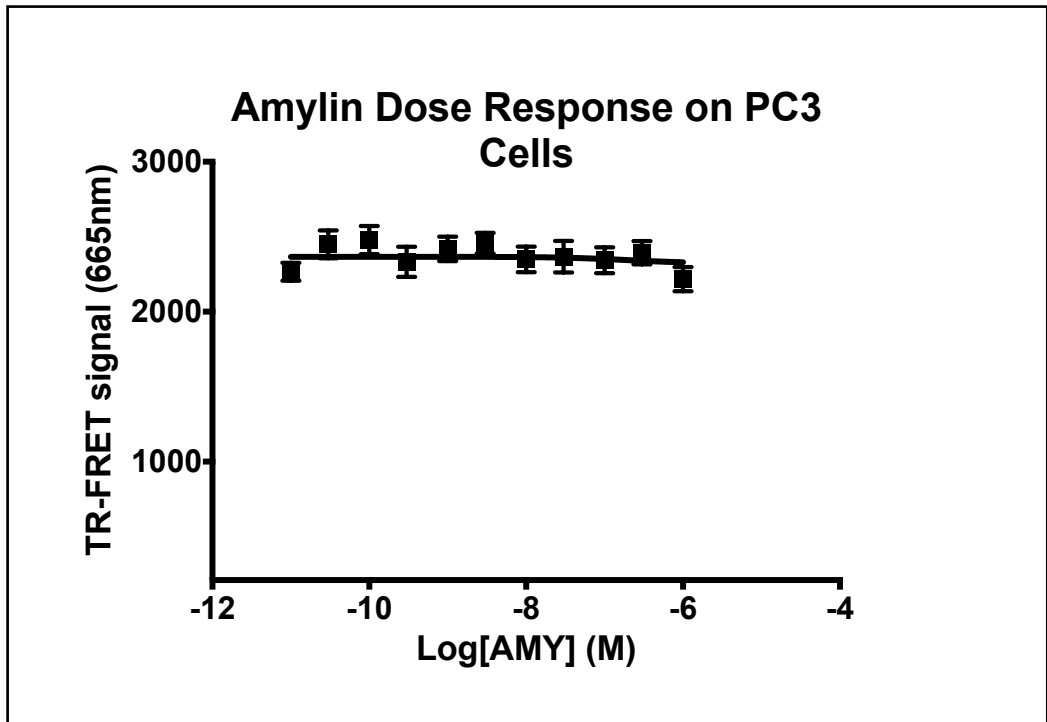


Figure 2.16 Dose response of Amylin stimulation on PC3 cells.

All values are mean \pm SEM, n=3.

2.6 Discussion

The PC3 cell line was chosen for this investigation as it a highly invasive cell line that mimics aggressive stages of prostate cancer both cellular and mouse models. When injected subcutaneously cells develop tumours in nude mice and can metastasise after intracardiac inoculation to tissue specific sites such as bone. This is a characteristic of prostate cancer that can significantly affect a patient's prognosis and therefore to understand the mechanisms behind in metastasis to bone, this cell line may be of consequential use. In order to study the effects of CGRP and AM in prostate cancer it was therefore important to first characterise this cell line and check for expression of both ligand and receptor components at an mRNA and protein level.

RNA was first extracted from PC3 cells and converted to cDNA to check expression of RAMPs 1-3, CLR and AM using RT-PCR. GAPDH housekeeping gene was first used as a control to check successful cDNA synthesis and lack of genomic DNA contamination. All targets were successfully amplified showing clear expression in varying intensities. RAMP1 was consistently expressed at a higher level in PC3 cells when compared with RAMP2 and RAMP3 but both CLR and AM were expressed at high levels across all experimental repeats (see Fig 2.9) All amplicons were sequenced using Sanger sequencing technique to show the correct target sequence was amplified (see Fig 2.10.) Sanger sequences were aligned with NCBI BLAST and all sequences showed at least 90% match with correct targets. This shows that components of both the CGRP and AM receptor are expressed at a mRNA level in PC3 cells.

To measure protein levels of RAMPs, CLR and AM, antibodies targeting these proteins were used for western blotting. The range of antibodies available for these targets is limited and those that are accessible often bind non-specifically or at unexpected molecular weights. It is therefore hard to draw solid conclusions from the results generated using these antibodies, without a high number of experimental

repeats. Results shown are examples of the most consistently observed. RAMPs 1-3 and CLR were measured at a protein level by Western blotting using PC3 cell lysate protein extracts. Antibodies targeting AM were not available to test expression with Western blotting. An antibody targeting vinculin housekeeping gene was used as a positive control for the technique and was found at the correct size (125kDa) All targets were found to be present when stained with the appropriate antibodies at the expected size (RAMP1 = 17kDa, RAMP2 = 20kDa, RAMP3 = 28kDa, CLR = 55kDa). RAMP3 has an actual weight of 17kDa however manufacturers suggest its monomer molecular weight is 28kDa, it therefore uncertain whether this antibody is targeting RAMP3. Nevertheless, western blot data suggests that all RAMPs and CLR are expressed at a protein level in PC3 cells (see Fig 2.11). Presence of CGRP in PC3 conditioned media was measured as not antibodies for western blotting could be optimised. Levels were found to be 35 pg/mL suggesting that PC3 cells do secrete CGRP (see Fig 2.12).

The effect of stimulation with CGRP or AM on PC3 cells was measured using LANCE Ultra cAMP assay to detect changes in intracellular cAMP. Forskolin produces direct stimulation of adenylyl cyclase and is used as a positive control for assay conditions. Stimulation with forskolin on PC3 cells consistently produced increases in intracellular cAMP in a dose dependent manner. This therefore shows that assay conditions were optimised correctly. However, when stimulated with CGRP or AM, doses ranging from 1×10^{-6} to 1×10^{-11} no changes in cAMP levels were seen in PC3 cells. Amylin is another member of the calcitonin peptide family that can signal through RAMP1 and CTR, it was therefore also used to stimulate PC3 cells however no effect was seen either. This may suggest that although PC3 cells express the different components of CGRP and AM receptors at both mRNA and protein level, they do not have functional receptors *in vitro*. Alternatively, these receptors may be functioning through a cAMP-independent mechanism as has been seen previously in the literature [83]. Prostate cancer cell lines have been found to respond to AM stimulation through alternative pathways such as the MAPK signalling pathway, most specifically activating ERK1/2. It may be therefore that alternative methods are required for validating the effect of CGRP and AM stimulation on PC3 cells.

It has therefore been shown that PC3 cells express all components of CGRP and AM receptors (RAMP1, RAMP2, RAMP3, CLR) at both an mRNA and protein level. To investigate the effect of these different receptor components in PC3 cells, a knockout cell line will be generated using CRISPR Cas9. The consequences of their deletion will then be measured *in vitro* and *in vivo*.

CHAPTER 3: GENERATION OF CRISPR/CAS9 KNOCKOUT IN PC3 CELLS

3.1 Introduction

In order to study the mechanistic role of CGRP and adrenomedullin in prostate cancer it is important to look at their individual receptor components: the calcitonin receptor (CLR) and three receptor activity modifying proteins (RAMPs 1-3). To determine the role of these proteins, we can observe any functional consequences of RAMP gene deletion in prostate cancer cell lines. Current techniques in gene editing can be categorized into either gene knockdown (reduced expression of a gene) or knockout (deletion of a gene). The former is often achieved using short hairpin or silencing RNA, known as RNA interference (RNAi) [141]. These short sequences target transcripts and cause destabilization, often resulting in a transient reduction of gene expression. Although a gene may only be expressed at low levels when targeted with RNAi it can often still have functional consequences within the cell. This leads to many disadvantages when using this technique especially when drawing conclusions on the role of the gene of interest. Nevertheless, deletion of essential genes can lead to lethality in both cellular and animal models. Therefore, RNAi reduction of gene expression has its advantages when aiding the investigation of particular targets.

An example of this has been recently documented when investigators found a possible role for a gene called MELK (Maternal Embryonic Leucine Zipper Kinase). RNAi studies suggested that the gene played an important role in cancer and this publication led to ongoing clinical trials testing a MELK inhibitor. However, after using a gene knockout technology (known as CRISPR/Cas9), to completely delete the MELK gene, it was found that cancer cells were not at all affected by the deletion. Further testing of the MELK inhibitor using MELK KO cell lines indicated that the inhibitor was acting on other cellular targets. RNAi techniques have a high chance of nonspecific targeting as short sequences are likely to occur elsewhere in the

genome. These findings led authors to suggest that in future knockout techniques should be used to better identify cancer-dependent genes or drug targets before clinical trials can begin [142].

To create a gene knockout, many technologies exploit cellular repair mechanisms. The first is non-homologous end joining (NHEJ) which occurs if no DNA template is provided and can lead to inactivating mutations. The second repair pathway is homology-directed repair (HDR) which uses template DNA to repair the cell. It has been reported that following endonuclease-generated double-stranded breaks (DSBs) in mammalian cell DNA, homology-directed repair will account for 30-50% of repair events [143]. This method of using cellular repair mechanisms and specific endonucleases enables precise editing by introducing point mutations at any given locus of the gene. An early example of gene knockout technology is the discovery of zinc finger nucleases (ZFNs) which were initially described in 1982 [144]. Zinc fingers (small protein motifs that require zinc ions for stable folding) are fused with FokI nucleases that recognise two adjacent sites and cleave single stranded DNA. Synthesis of ZFNs can be time consuming and identifying suitable pairs for specific loci is challenging.

Despite the disadvantages of ZFNs, this technology was a popular form of genetic editing for almost 30 years before another technique was discovered using endonuclease-induced DSBs. Transcription activator-like (TAL) effectors are proteins secreted by *Xanthomonas* bacteria which then enter the nucleus of plant cells to activate expression of specific genes [145, 146]. The modular design of TAL effectors, including DNA binding proteins has been exploited to create customizable gene targeting proteins, now known as TALENs (see Fig 3.1). These proteins, like ZFNs, are fused with a FokI endonuclease but unlike ZFNs, synthesis of TALENs can be achieved in much shorter times [147]. TALENs have therefore exceeded ZFN technology and have become a ubiquitous tool for genetic editing in both cellular and animal models.

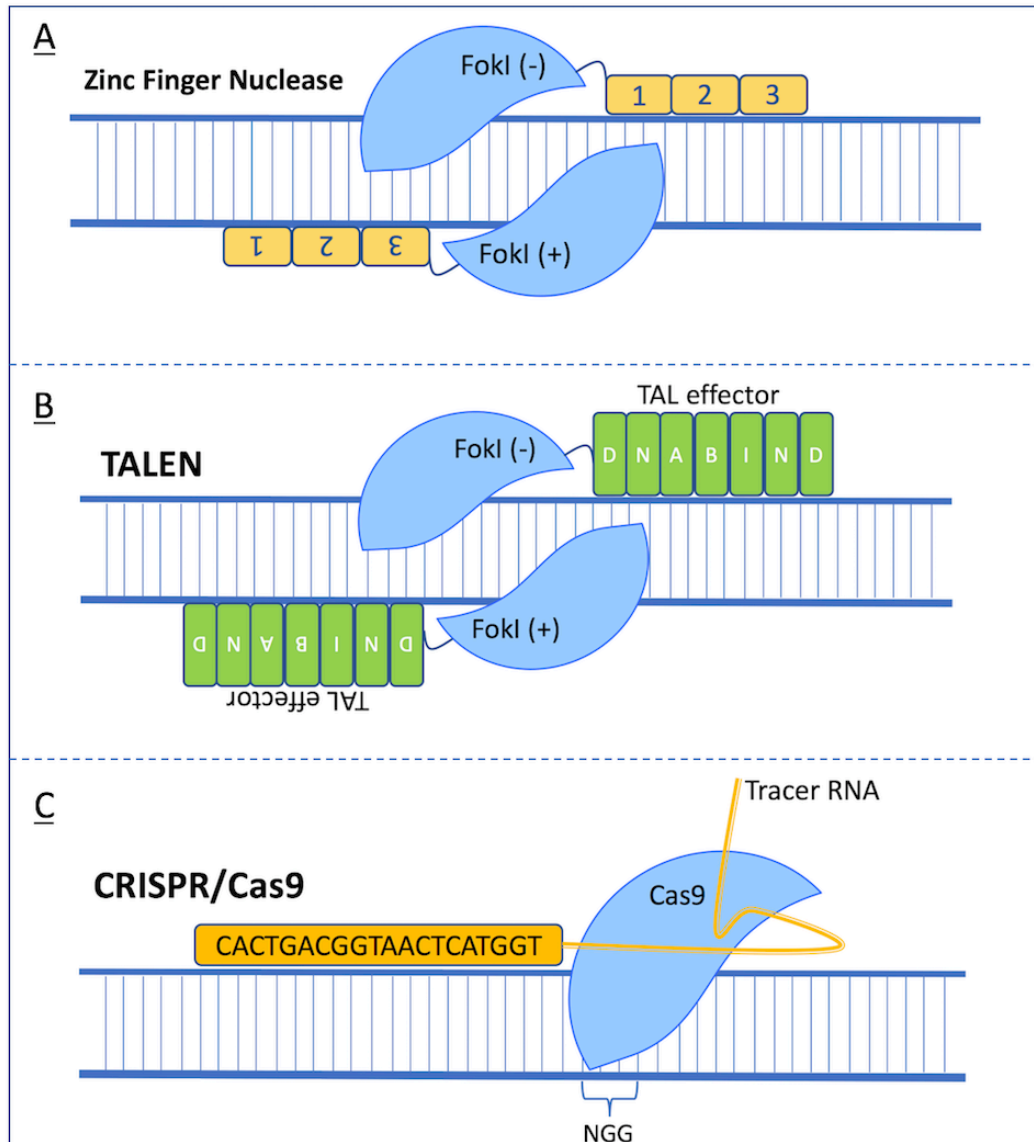


Figure 3.1 Diagrams of gene editing techniques

(A) Zinc finger nucleases consist of a zinc finger fused with a FokI endonuclease that cleave single strands of DNA at two different sites. (B) TALENs consist of a TAL effector and customizable DNA binding proteins also fused with a FokI endonuclease. (C) CRISPR-Cas9 consists of a guide RNA 20bp sequence with a tracer RNA to complex with a Cas9 endonuclease to induce double stranded DNA breaks.

The CRISPR (Clustered Regularly Interspaced Short Palindromic Repeats)/Cas9 system differs from these previous techniques as it uses a different endonuclease, known as Cas9. Cas9 complexes with a “guide” RNA (gRNA) sequence, homologous to the target locus. In the presence of the gRNA protospacer adjacent motif (PAM) site Cas9 is activated and induces a double stranded break in the DNA (see Fig 3.1). PAM sites always consist of an “NGG” sequence, which will occur often across the genome This makes the CRISPR/Cas9 system easy to customise as many different loci can be simultaneously targeted. CRISPR/Cas9, like ZFNs and TALENs, exploits cellular repair mechanisms but the use of gRNA sequences ensures more specific editing and reduces cost and time. It is therefore a valuable technique for genomic engineering, including high-throughput techniques as multiple loci may be targeted at once.

CRISPR sequences were first identified in 1982, when they were first identified in the *E. coli* genome [148]. The function of these sequences was not fully understood until 2007, when researchers hypothesised that CRISPR sequences and Cas (CRISPR associated) genes were used in prokaryotes as an adaptive immune system. It was found that Cas proteins cut foreign DNA sequences into smaller fragments and then incorporate them into the CRISPR sequence. Cas proteins can then express the CRISPR loci to recruit CRISPR RNAs (crRNAs) which guide Cas endonucleases to bind to the foreign DNA and cleave it, destroying the invasive material (see Fig 3.2) [149]. This discovery of an adaptive immune system was then used by Jinek et al. to exploit CRISPR/Cas9 targeted DNA cleavage *in vitro* [150]. The first articles published using CRISPR/Cas9 genome editing were in cell culture. This included using Cas9 to induce double stranded breaks which were then repaired by NHEJ, creating indel (insertion or deletion) mutations in the sequence. Alternatively, it was also shown that CRISPR/Cas9 could be used in combination with a “donor DNA” sequence, complementary to the site of interest. This donor DNA sequence could then be inserted into the breaks caused by Cas9 during homology-direct recombination (HDR). These insertions can be customised to include stop codons, expression cassettes, antibiotic resistance and even LoxP sites [151, 152].

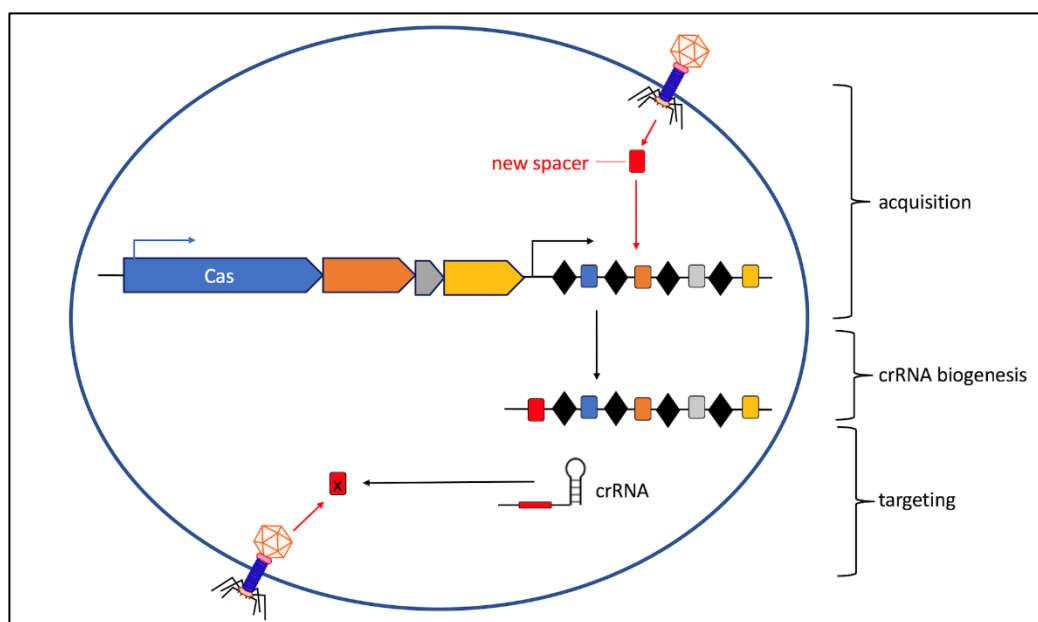


Figure 3.2 Prokaryote adaptive immunity.

CRISPR sequences and Cas proteins are targeted with CRISPR RNAs (crRNAs). Foreign material is first recognised and incorporated into CRISPR sequences. crRNAs are synthesised and are complimentary to the foreign DNA. crRNAs then complex with Cas proteins to target invading DNA sequences for cleaving.

CRISPR/Cas9 with homology directed repair (HDR) has many advantages over previous CRISPR/Cas9 systems. The use of short gRNA sequences alone, relies on Non-Homologous End Joining (NHEJ) which can give unexpected results. For example, any indel mutations that cause a frameshift in the genomic sequence have a 1 in 3 chance of still being in the correct frame and coding for the same amino acids. This technique therefore has a high failure rate of generating successful knockouts. Previous reports using Surveyor or T7 endonuclease assays have reported indel mutation rates of 20-30%. These endonucleases can detect edited DNA strands and cleave the fragments producing two smaller products whereas unedited DNA strands remain intact. After amplifying these products with PCR, it is possible to visualise with gel electrophoresis and determine rates of successful indel mutations. An additional drawback of this CRISPR method is that the gRNA sequence is likely to occur elsewhere in the genome apart from the target site. Consequently, off-target cutting of Cas9 can lead to unknown edits and so any functional changes

may not be due to the gene of interest but in fact a result of an off-target gene knockout. Off target effects can be minimised by designing “homology arm” sequences that are complimentary to the gene of interest and can include up to 1,000 nucleotides. These complimentary sequences are less likely to occur elsewhere from the target site, minimising the likelihood of off target effects. When Cas9 has induced a double stranded cut at the target site, cells will readily repair the DNA using homology arm sequences provided via the HDR process. This technique also has the advantage of customisable DNA donor templates that are inserted during HDR. For example, fluorescence markers and antibiotic resistance genes can be incorporated into the gene aiding validation of gene knockouts by antibiotic selection and fluorescence cell sorting (FACS). These insertions can also include stop codons to ensure transcription is halted at the target site.

There are currently no reports of knockouts generated in a cell line for either RAMP1, 2 or 3. Authors have reported a RAMP1 knockdown in PC3 cells, however only to link it as a target gene of a transcription factor named NKX3.1 [105]. A RAMP knockout cell line would therefore be an extremely useful tool for investigating the role of these proteins in prostate cancer. The CRISPR/Cas9 HDR system was selected as an appropriate technique to create knockouts for RAMPs 1-3 in PC3 cells, in order to investigate the role of these receptor subcomponents in prostate cancer. HDR plasmids were designed to target each gene with two “homology arms” located either upstream or downstream from the gRNA targeted sequence. These homology arms were around 800bp and were delivered into the cell in a plasmid. The HDR plasmid also contained a “donor” sequence for insertion into the double stranded break, containing an RFP marker, puromycin resistance and a stop codon. Large plasmids can be difficult to transfect, frequently having quite a low transfection efficiency. To accommodate this, three separate HDR plasmid with different gRNA locations were used simultaneously to increase the chances of a successful RAMP knockout. To validate the knockouts, cells were then selected with puromycin antibiotic to select positively transfected cells and then sorted using FACS into single cell colonies. Growing clonal colonies ensures that the entire cell population has a

RAMP gene knockout, as any wild type cells may outgrow the knockout cells and therefore increase RAMP expression of the cell population.

After sorting cells into clonal populations, they were then tested for successful deletion of the RAMP gene. This was first characterised using endpoint PCR as this is a robust method that will clearly show changes to mRNA sequences when comparing with wild type PC3 cells. Any successful RAMP knockouts found were then selected for further validation using qPCR to quantify RAMP expression levels. Analysis of protein extracts from knockout cells by Western blot should determine successful RAMP deletion. However, antibodies for these proteins are not often reliable, giving unexpected band sizes as described in the previous chapter.

3.2 Hypothesis:

1. CRISPR/Cas9 can be utilized to generate RAMP1-3 knockouts in a PC3 cell line.

3.3 Research Aims:

1. To determine the effectiveness of the CRISPR/Cas9 technique in creating RAMP1-3 knockouts in a PC3 cell line.
2. To validate successful CRISPR/Cas9 knockouts using PCR, Sanger sequencing and western blotting

3.4 Methods & Materials

3.4.1 Transfection of CRISPR Vectors into PC-3 Cells

PC3 cells were grown and seeded into 6 well plates as described previously (Chapter 2, Section 2.4.1-3) at a density of 1.5×10^5 in order to be 60% confluent on the day of transfection. After 24 hours cells were washed with PBS and 2mL PenStrep-free media was added with RS-1 (4-Bromo-*N*-(4-bromophenyl)-3-[[*(phenylmethyl)amino*]sulfonyl]benzamide) (Tocris Bioscience) at a concentration of 7.5 μ M. A mix containing 125 μ L OptiMEM media (Gibco) and 7.5 μ L Lipofectamine 3000 (Thermo Fisher) was added to a mix containing 125 μ L OptiMEM and 5 μ L P3000 and 2.5 μ g DNA. Mixtures were then incubated at room temperature for 10 mins before being added to the cells. Cells were co-transfected with a RAMP1/2/3 HDR plasmid and a RAMP1/2/3 CRISPR/Cas9 KO plasmid (Santa Cruz Biotechnology) (see Fig 3.3). Negative control cells were transfected with PBS alone. 24 hours after transfection, Scr7 pyrazine (Tocris Bioscience) was added at a concentration of 1 μ M in 10% RPMI media. 48 hours after transfection cells were selected with 2 μ g/mL puromycin for 5-7 days before being sorted into single cell colonies using FACS. This dose of puromycin has been previously reported when selecting clones in PC3 cells [153].

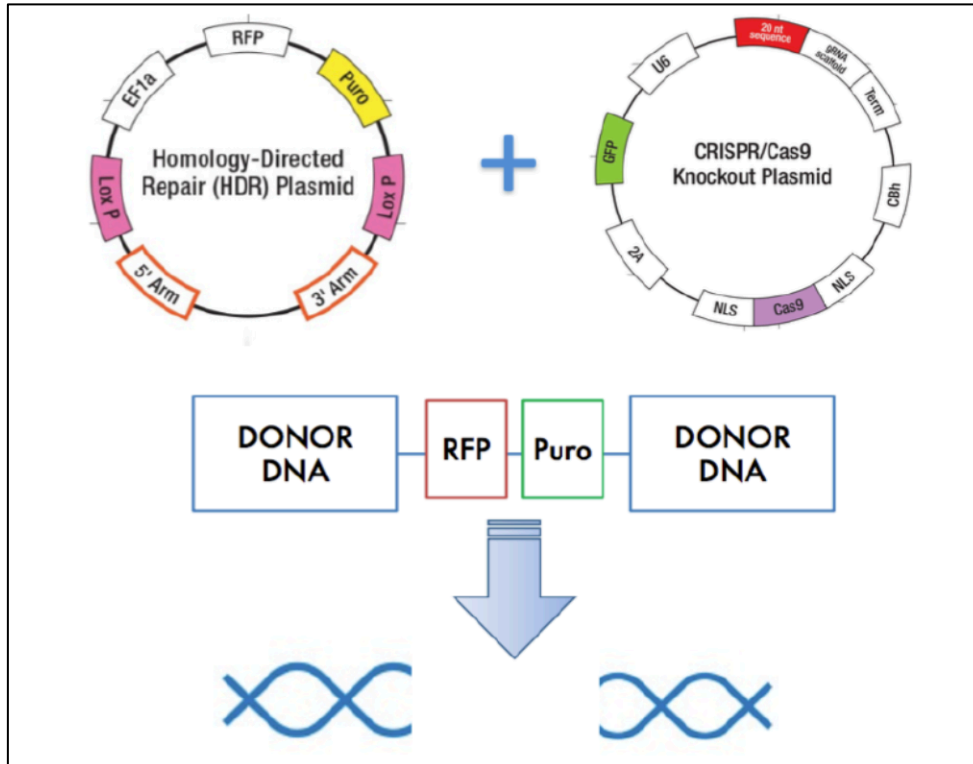


Figure 3.3 CRISPR/Cas9 HDR system.

Each HDR plasmid contained a 5' and 3' homology arm, complimentary DNA to the gene of interest. An expression cassette was also contained within this plasmid for insertion into the gene following double strand breaks caused by Cas9 endonuclease. This cassette contained an RFP marker, a puromycin resistance gene, a stop codon and LoxP sites. The CRISPR/Cas9 plasmid contained the gRNA situated in between each homology arm, the Cas9 endonuclease and a GFP marker.

3.4.2 Fluorescence-Activated Cell Sorting of CRISPR Cells

After transfection and selection of PC3 cells with CRISPR constructs targeting RAMPs 1-3, they were sorted into single cells using RFP fluorescence as a marker. All cell populations were grown in 6 well plates until 70% confluence and then detached and suspended in 10% RPMI media (see Chapter 2, Section 2.4.1-2). Cell samples were then processed by the Flow Cytometry Core Facility technician and sorted into 96 well plates using a FACS Aria IIu (BD Biosciences). Cells were collected in PC3 conditioned medium and grown into colonies for knockout screening. Single cells

were monitored by taking bright field images using Ensign plate reader (Perkin Elmer).

3.4.3 Endpoint Polymerase Chain Reaction

Endpoint PCR was completed using previously described Methods and Materials (see Chapter 2, Section 2.4.6). After validating successful CRISPR clones, primers were redesigned to span the full-length mRNA of RAMP1 for further confirmation (See Table 3.1.)

Target	Sense	Sequence 5' to 3'	Tm (°C)	Annealing Temperature (°C)	Amplicon Size (bp)
RAMP1	Forward	CCTCTTCATGACCACTGCCT	60	55	478
RAMP1	Reverse	CTGTCCAAGGCTCCAGAAG	60		

Table 3.1 Endpoint PCR primers for RAMP1 CRISPR validation.

3.4.4 Reverse Transcription for Quantitative Polymerase Chain Reaction (qPCR)

RNA was extracted from clonal colonies (see previously described Methods) and converted to cDNA using a Precision nanoScript™ 2 Reverse Transcription kit (PrimerDesign). Oligo-dT primers were used to bind to polyA tail of mRNA (see Table 3.2.) Annealing was completed at 65°C for 5 minutes and then samples were immediately cooled on ice.

Component	Volume
RNA Template (up to 2µg)	--
Oligo-dT RT primer	1µL
RNase/DNase free Water	--
Total	10µL

Table 3.2 cDNA synthesis primer annealing reaction.

10µL RT reactions were made up (see Table 3.3.) and added to 10µL samples on ice. Reverse transcription negative controls were run for each sample by excluding nanoScript2 enzyme from the reaction mix. Each sample was then briefly vortexed followed by a pulse spin and incubated at 42°C for 20 minutes followed by heat inactivation at 75°C for 10 minutes. Incubations were done using a ProFlex PCR thermocycler (Life Technologies). cDNA samples were stored at -20°C until use.

Component	Volume
nanoScript2 4X Buffer	5µL
dNTP mix 10mM	1µL
RNase/DNase free water	3µL
nanoScript2 enzyme	1µL
Total	10µL

Table 3.3 cDNA synthesis total reaction

3.4.5 Quantitative Polymerase Chain Reaction (qPCR)

Primers were designed to target RAMP1 mRNA by PrimerDesign (see Table 3.4) and mixed with DoubleDye hydrolysis probes labelled with a 6-carboxyfluorescein (FAM) reporter (PrimerDesign). Primer/probe mixes were then added to a PrecisionPLUS Mastermix (PrimerDesign) with a ROX reference dye (see Table 3.5.) A GENORM reference kit was used containing primer/probes targeting six different reference genes including: ACTB, B2M, UBC, YHWAZ, ATP5B and RPL13A.

Target	Sense	Sequence 5' to 3'	Tm (°C)	Amplicon Size (bp)
RAMP1	Forward	TCATTTTCAGCCCATCACCTCTTC	59	139
RAMP1	Reverse	TGCCCCAGTCACACCACA	58	

Table 3.4 qPCR primers designed to target RAMP1.

Component	Volume
PrecisionPLUS Mastermix with ROX	5µL
Primer/probe mix	0.5µL
DNA Template	--
RNase/DNase free water	2µL
Total	7.5µL

Table 3.5 qPCR Mastermix recipe.

cDNA samples were diluted with RNase/DNase free water to a concentration of 5ng/µL and 2.5µL of each sample was added to wells on a clear plastic 384 PCR plate in triplicates. Reverse transcription negative controls were tested using reference gene primers for genomic DNA contamination. 7.5µL of each master mix was then added to each well on top of cDNA samples. The PCR plate was then centrifuged at 1,000 x rpm for 1 minute and inserted into an Applied Biosystems

HT7900 thermocycler. Reactions were run using amplification protocols detailed in manufacturers guide (see Table 3.6). qPCR data was analysed using SDS 2.0 software and curves were plotted on a linear scale. Thresholds were set at the linear phase of the curve and ct values recorded for each sample. RAMP1 KO and PC3 samples were then compared using the $2^{-\Delta\Delta}$ ct method.

	Step	Time	Temperature
	Enzyme activation	2 minutes	95°C
	Denaturation	10 seconds	95°C
Cycling x40	Data Collection	60 seconds	60°C

Table 3.6 qPCR amplification protocol.

3.4.6 Genomic DNA Polymerase Chain Reaction

Primers were designed spanning from the EF1-alpha promoter of the HDR CRISPR construct to sequences complimentary to RAMP1 exon 2, upstream from the design homology arm (See Fig 3.4) to validate correct targeting of the construct.

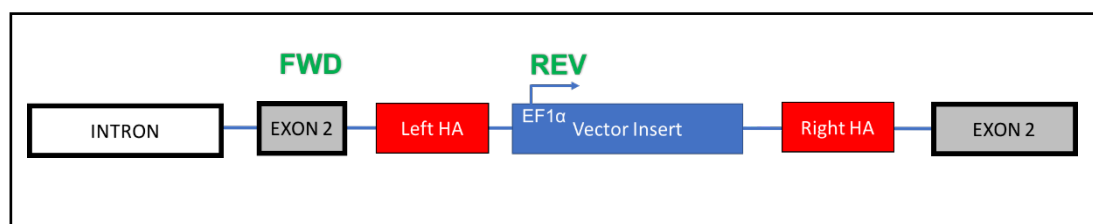


Figure 3.4 Genomic PCR primers.

Diagram illustrating positions of primers targeting RAMP1 DNA editing by CRISPR/Cas9 and insertion of expression vector into Exon 2.

3.4.7 Genomic DNA Extraction

Genomic DNA was extracted from wild type PC3 and RAMP1 knockout (KO) cells using methods previously described to count 5×10^4 cells suspended in 16 μ L PBS (See Chapter 2, Section 2.4.3). This cell suspension was then mixed with 4 μ L 5X microLYSIS-Plus buffer (Microzone) and samples were then extracted using a ProFlex PCR thermo cycler (Life Technologies) following the protocol detailed in the manufacturer's instructions (See Fig 3.5.)

Step	Temperature	Time
1	65°C	15 minutes
2	96°C	2 minutes
3	65°C	4 minutes
4	96°C	1 minute
5	65°C	1 minute
6	96°C	30 seconds
7	20°C	Hold

Figure 3.5 Thermal cycler protocol for genomic DNA extraction.

3.4.8 Genomic PCR Reaction

DNA extracts were then amplified using primers targeting RAMP1 exon 2 and the EF1-alpha promoter of the vector insert (see Fig 3.4) and positive control primers targeting RAMP2 (see Table 3.7) Positive controls primers validated successful genomic DNA extraction from cell samples. All PCR reactions were completed using a Phusion High-Fidelity polymerase, a polymerase more suited to amplifying GC-rich and large PCR products. The manufacturers PCR reaction recipe (see Table 3.8) was optimised for annealing temperatures and DMSO was added to reduce amplification

of non-specific targets. PCR products were then validated using Sanger sequencing as described previously (see Chapter 2, Section 2.4.8).

Target	Sense	Sequence 5' to 3'	T _m (°C)	Annealing Temperature (°C)	Amplicon Size (bp)
RAMP1	Forward	GCAAGGGGCAACTTGATGTC	60	64	1600
RAMP1	Reverse	ACTTCCCAGTTACCCCGC	60		
RAMP2 (positive control)	Forward	GGGGACGGTGAAGAACTATGA	59	63	300
RAMP2 (positive control)	Reverse	CCAGGTCAAACAACCTCTGCA	58		

Table 3.7 Genomic PCR primers

Primers were designed to target RAMP1 exon 2 upstream from designed homology arms and the EF1-alpha promoter of the vector expression cassette inserted into the CRISPR site.

Component	Volume
5X Phusion High-Fidelity Buffer	4µL
dNTP mix 10mM	1µL
Forward Primer	1µL
Reverse Primer	1µL
DNA template	1µL
Phusion DNA Polymerase	0.2µL
DMSO	0.6µL
DNase free water	11.2µL
Total	20µL

Table 3.8 Genomic PCR recipe

3.5 Results

3.5.1 Transfection of PC3 Cell Line with HDR CRISPR/Cas9 Constructs

PC3 cells were first transfected with a CRISPR/Cas9 construct which is transiently expressed and then a homology-direct repair (HDR) RAMP1/2/3 construct which contains donor DNA sequences complimentary to the target gene and an expression cassette with an RFP marker, puromycin resistance gene and stop codon. Transfected cells showed RFP positive colonies after 1 weeks of selection with 2 μ g/mL puromycin (see Fig 3.6) in RAMP1, 2 and 3 cells.

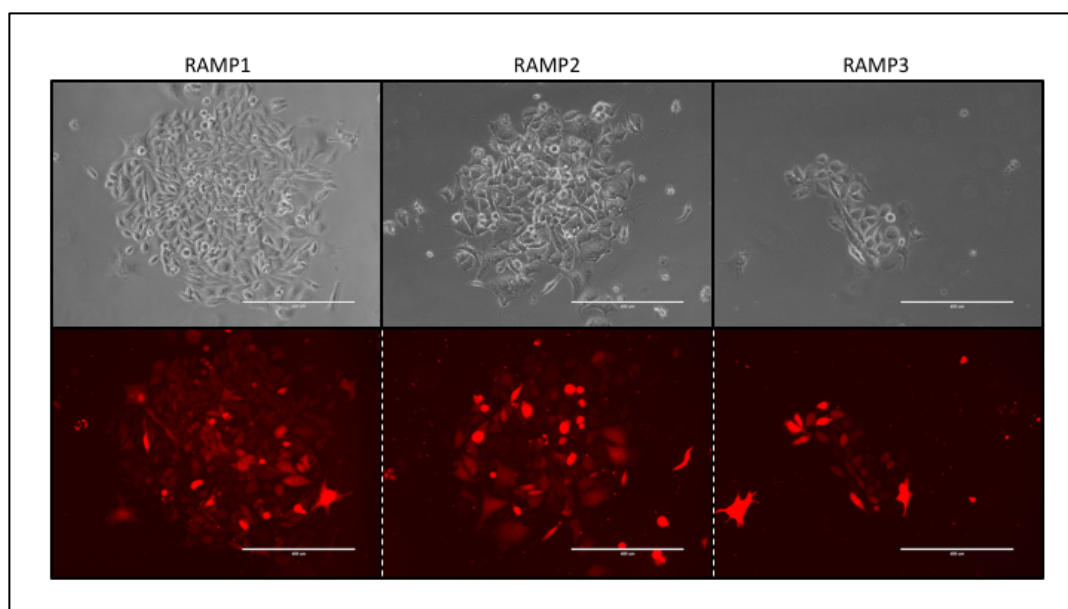


Figure 3.6 Transfection images.

Bright field and RFP images of cells transfected with CRISPR constructs targeting RAMP1, 2 and 3.

Transfected cells were then sorted into single cell clones using FACS targeting RFP positive cell populations. Unstained, non-transfected PC3 cells were used as a negative control to draw gates on RFP positive populations (see Fig 3.7). Cells were sorted into 96 well plates containing conditioned media and then monitored during growth to validate single cell colonies (see Fig 3.8-10.)

3.5.2 Fluorescent activated cell sorting of CRISPR transfected cells.

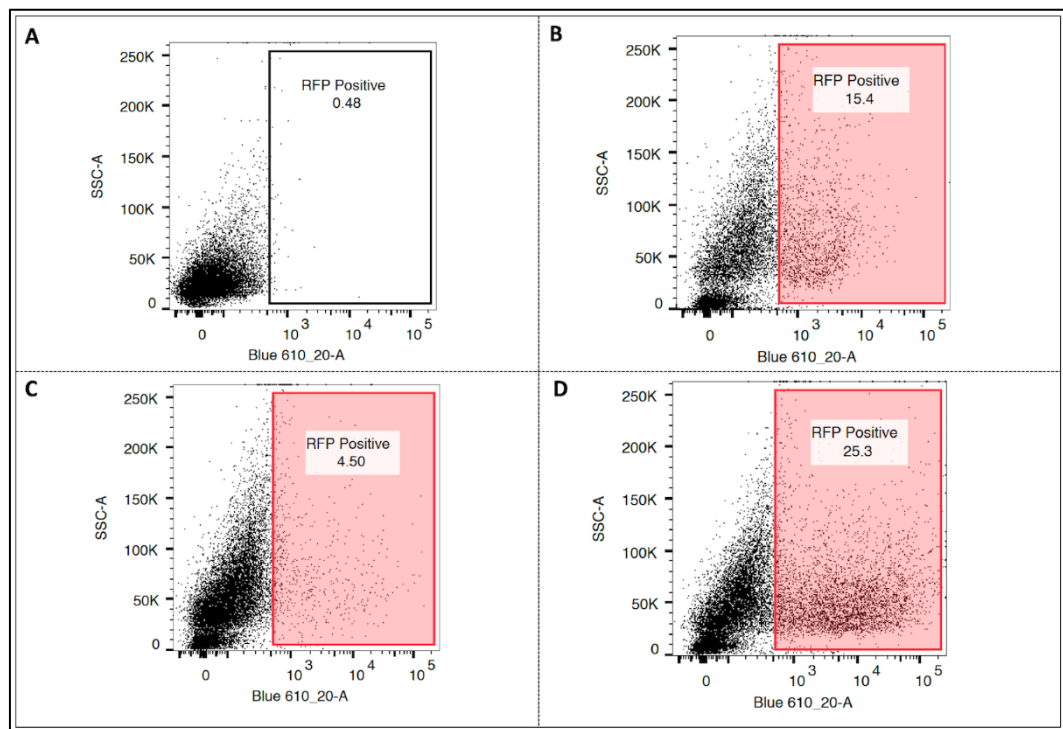


Figure 3.7 FlowJo analysis of cell sorting.

(A) Unstained PC3 wild type cells were used to draw RFP positive gates. (B) RAMP1 samples had 15.4% RFP positive cells. (C) RAMP2 samples had 4.5% RFP positive cells. (D) RAMP3 samples had 25.3% RFP positive cells.

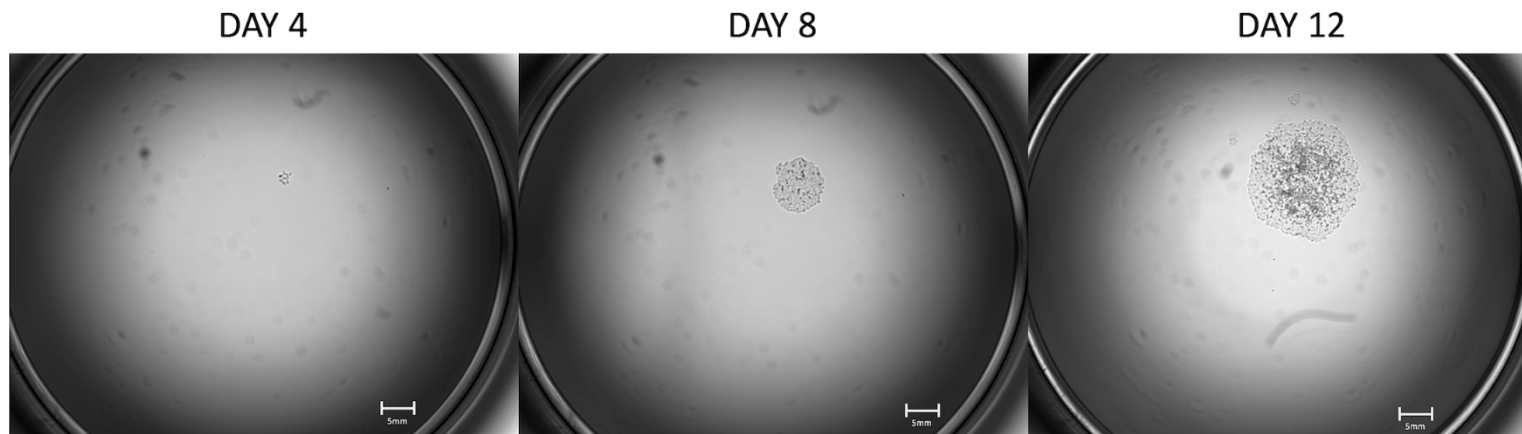


Figure 3.8 Bright field images of RAMP1 single cell colonies

RAMP1 single cell clonal colonies growing after sorted using FACS in PC3 conditioned media.

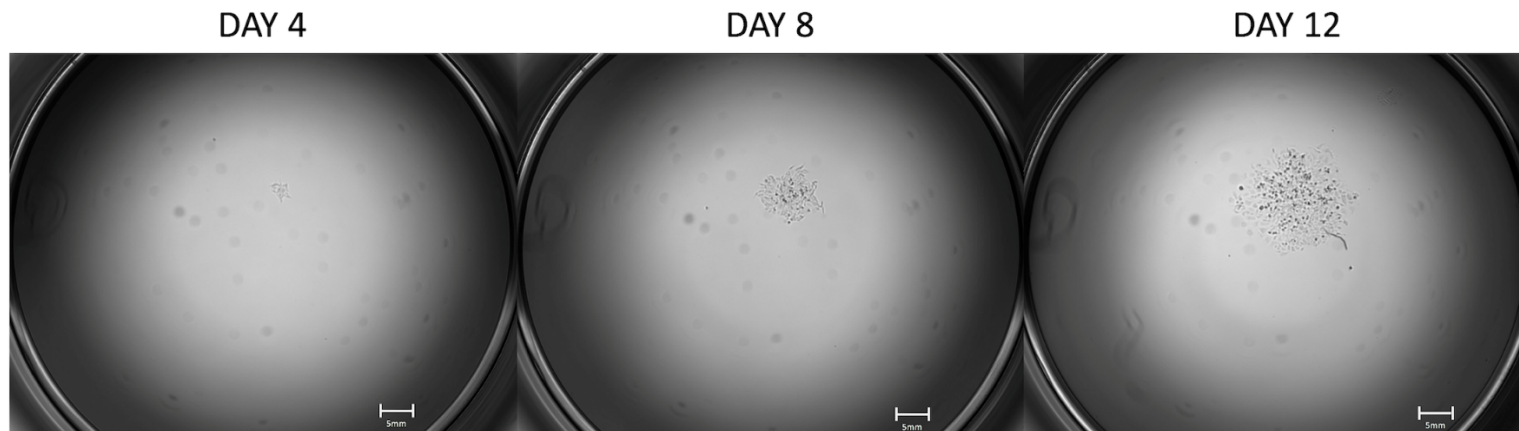


Figure 3.9 Bright field images of RAMP2 single cell colonies

RAMP2 single cell clonal colonies growing after sorted using FACS in PC3 conditioned media.

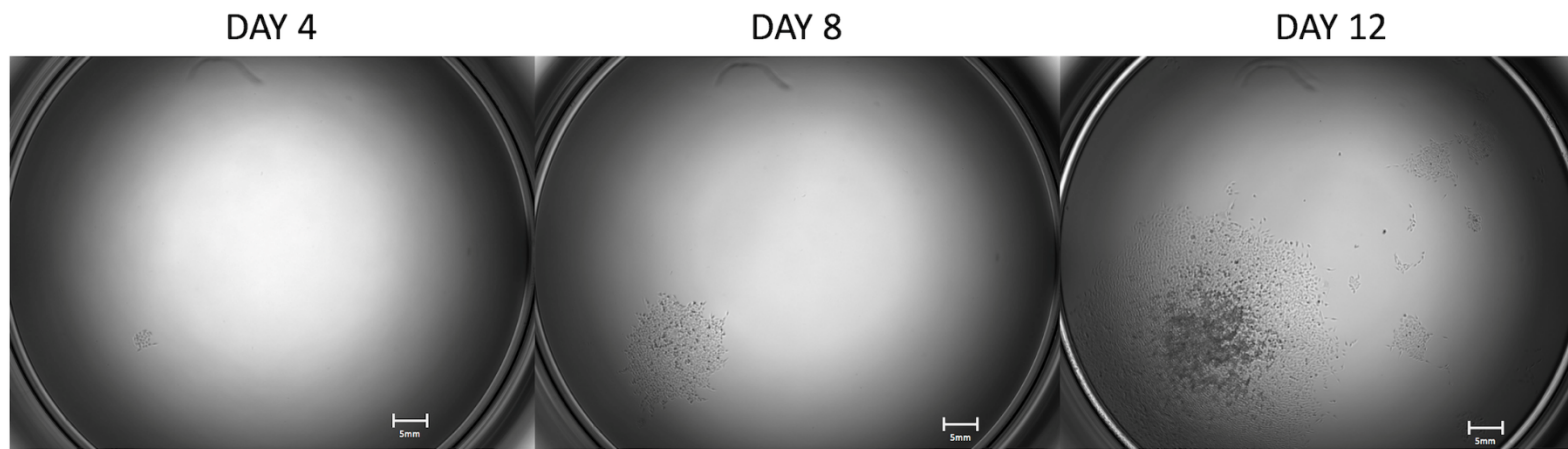


Figure 3.10 Bright field images of RAMP3 single cell colonies

RAMP3 single cell clonal colonies growing after sorted using FACS in PC3 conditioned media.

3.5.3 Validation of CRISPR Clones with Endpoint PCR

After clonal colonies were confluent, cells were split into another 96 well for RNA extraction and cDNA synthesis (see Chapter 2, Section 2.4.4). These samples were then validated using endpoint PCR for RAMP1,2 or 3 knockout using primers designed for previous characterisation of PC3 cells (see Chapter 2, Section 2.4.6). RAMP1 PCR showed bands at the correct height for RAMP1 for PC3 wild type samples and negative control cells (PBS only). Different clonal populations were tested for RAMP1 only two clones showed RAMP1 expression whereas up to 8 different clones showed no PCR band (see Fig 3.12). RAMP2 clones had reduced viability and only 2-3 clones were grown successfully to be validated with endpoint PCR. All clones showed a band at the correct height for RAMP2 compared with positive controls (see Fig 3.13). RAMP3 clones all showed to have PCR bands at the correct height for RAMP3 (see Fig 3.15).

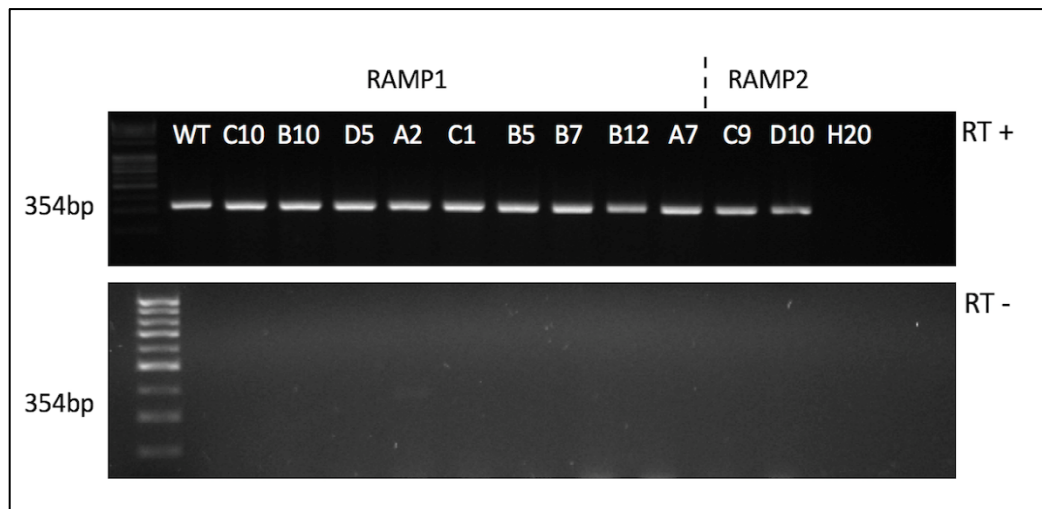


Figure 3.11 Endpoint PCR GAPDH for RAMP1 and RAMP2 CRISPR clones

PCR targeting GAPDH to validate reverse transcription negative controls for RAMP1 and RAMP2 clones are not contaminated with genomic DNA.

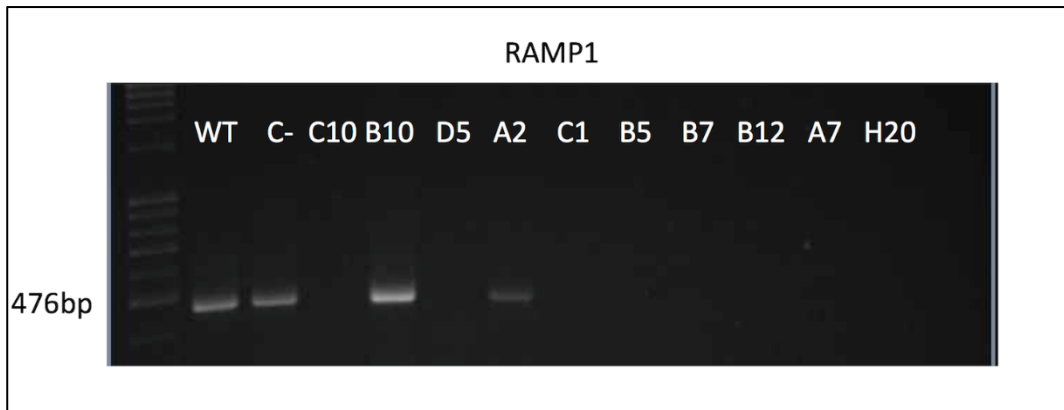


Figure 3.12 Endpoint PCR RAMP1

PCR targeting RAMP1 shows clear bands at the correct size (476bp) in wild type PC3, transfection negative controls and two clonal populations, B10 and A2. No band was detected in clonal populations C10, D5, C1, B5, B7, B12 and A7.

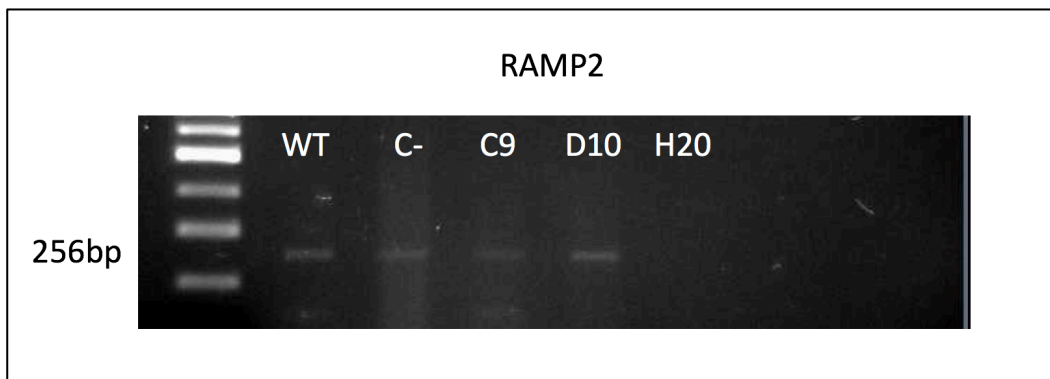


Figure 3.13 Endpoint PCR RAMP2

PCR targeting RAMP2 shows clear bands at the correct size (256bp) in wild type PC3, transfection negative controls and two clonal populations, D10 and C9.

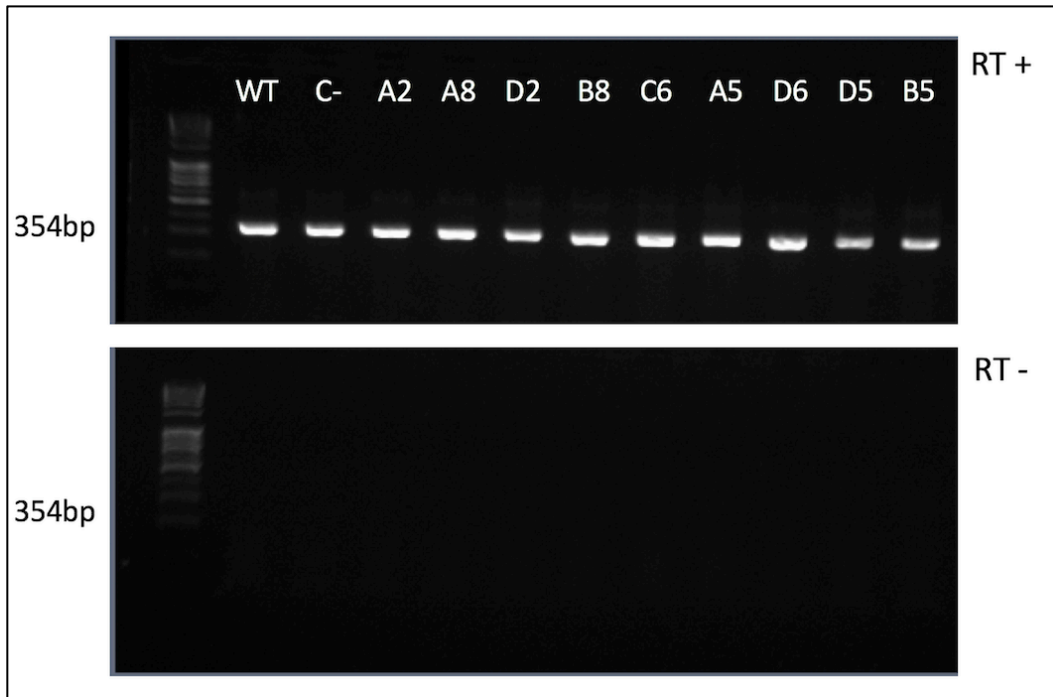


Figure 3.14 Endpoint PCR GAPDH for RAMP3 CRISPR clones

PCR targeting GAPDH to validate reverse transcription negative controls for RAMP3 clones are not contaminated with genomic DNA.

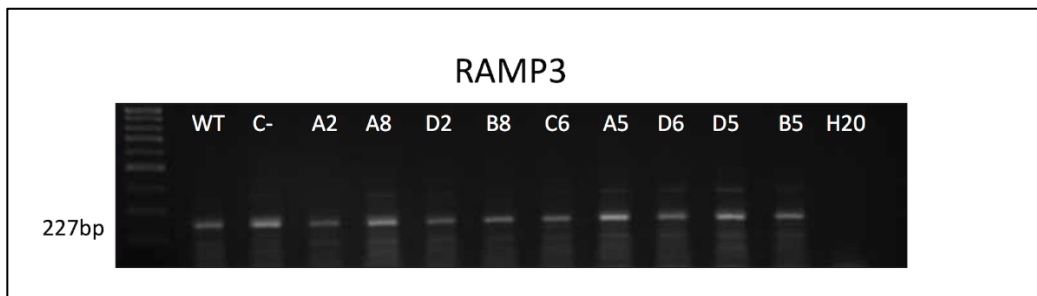


Figure 3.15 Endpoint PCR RAMP3

PCR targeting RAMP3 shows clear bands at the correct size (227bp) in wild type PC3, transfection negative controls and all clonal populations (A2, A8, D2, B8, C6, A5, D6, D5 and B5.)

3.5.4 Validation of CRISPR Clones with Genomic DNA and Endpoint PCR

Primers were designed targeting the HDR insert with a reverse primer and the RAMP1 gene (upstream from the homology arm) with a forward primer. PCR reactions with these primers were performed on PC3 wild type and RAMP1 CRISPR genomic DNA samples. After visualisation using gel electrophoresis, bands were only observed in CRISPR clones A7, C1 and B7. No bands were observed in the PC3 wild type reaction or the negative control (reaction without DNA template). To ensure that genomic DNA samples were viable, positive control primers targeting another gene (in this case, RAMP2) were used. These primers showed clear bands in all samples (see Fig 3.16).

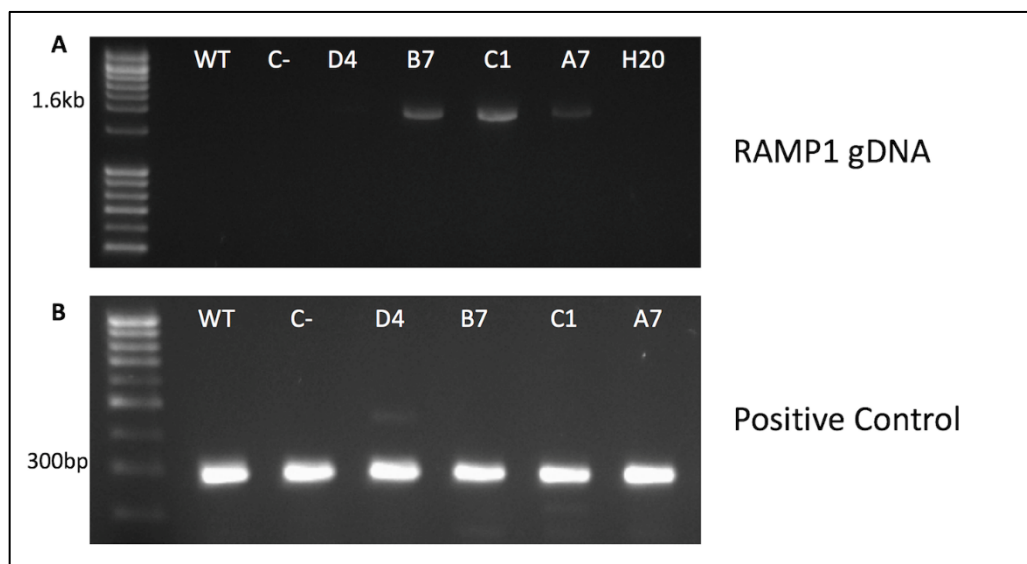


Figure 3.16 Endpoint PCR with RAMP1 genomic DNA

PCR using RAMP1 primers targeting the genomic region upstream from the left homology arm and the HDR insert. (A) Bands were observed only in CRISPR clones B7, C1 and A7. No bands were visible in the PC3 wildtype (WT) or negative control (H20). (B) Clear bands for all samples were observed when using positive control primers.

PCR products that were successfully amplified using RAMP1 genomic DNA primers were then analysed using Sanger sequencing as described previously (see Chapter 2, Section 2.4.8). The sequences were then aligned with the EF1-alpha

promoter sequence from the HDR insert, the RAMP1 homology arms that were designed for the CRISPR construct and also the RAMP1 gene upstream from this site (see Fig 3.17). Successful alignments determined that the CRISPR construct had targeted the RAMP1 gene correctly resulting in a large insertion that would effectively knockout the gene. For alignment and raw sanger sequencing data see Appendix.

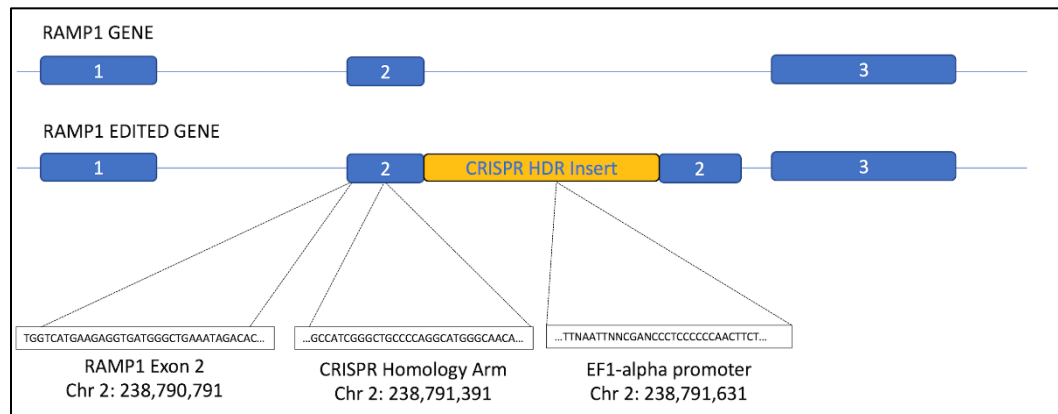


Figure 3.17 CRISPR edited RAMP1 gene.

Schematic diagram indicates site of CRISPR editing within exon 2 of RAMP1. Sequencing data alignment analysis shows RAMP1 Exon 2 with the targeting homology arm sequence and then an EF1-alpha promoter validating correct insertion of the HDR expression cassette.

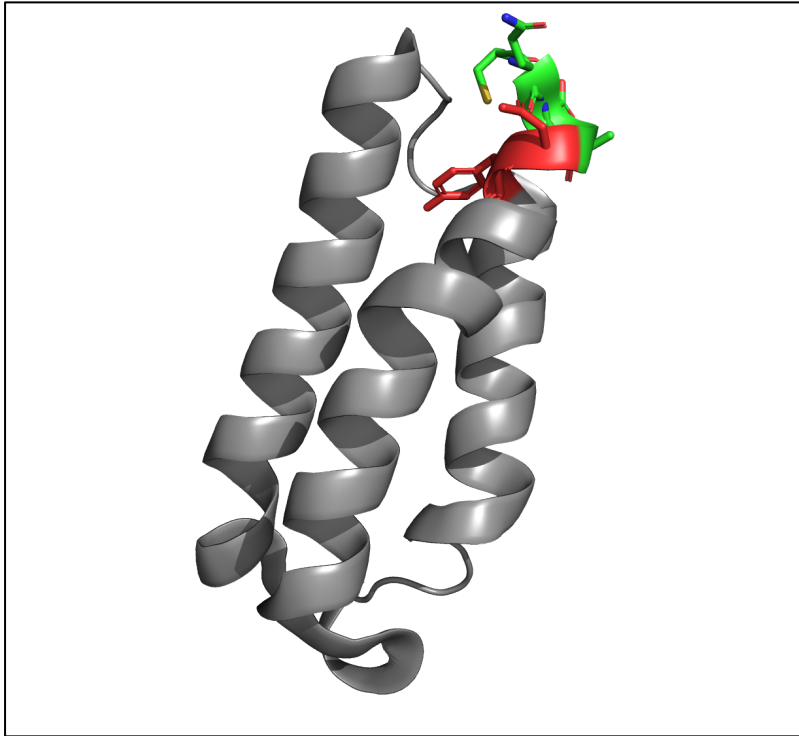


Figure 3.18 CRISPR edited RAMP1 crystal structure

Representation of the crystal structure of the RAMP1 extracellular domain shows unedited RAMP1 protein (highlighted green) and the site of CRISPR editing (red). RAMP1 protein sequence downstream of the CRISPR site (grey) may not be transcribed due to insertion of the HDR stop codon or mutational frameshifts.

3.5.5 Validation of CRISPR Clones with Quantitative PCR.

RAMP1 clones known as A7, C1, D5, B12, B5 and D4 were selected for further validation using quantitative PCR targeting RAMP1 mRNA. First many reference genes including beta-actin (ACTB), ubiquitin C (UBC) and beta-2 microglobulin (B2M), were measured for both wild type and CRISPR samples. ACTB was then chosen as the reference gene with least variation between all samples to be used for further investigations (see Figs 3.19 & 3.20.) Samples were then measured for both ACTB and RAMP1 expression and samples were compared using $\Delta\Delta$ CT analysis. Ct values for PC3 wildtype had an average of 30, whereas all clones were found to have ct values of 35+ (see Table 3.9.) Analysis of these samples was performed using $\Delta\Delta$ CT,

comparing CRISPR samples to PC3 wildtype samples and then the fold change was represented as a percentage of PC3 wild type expression (see Fig 3.21.) Clones A7, C1 and D5 were found to have expression levels of 5-10%, whereas clones B12, B5 and D4 had expression levels of 10-30% compared with PC3 wild type samples.

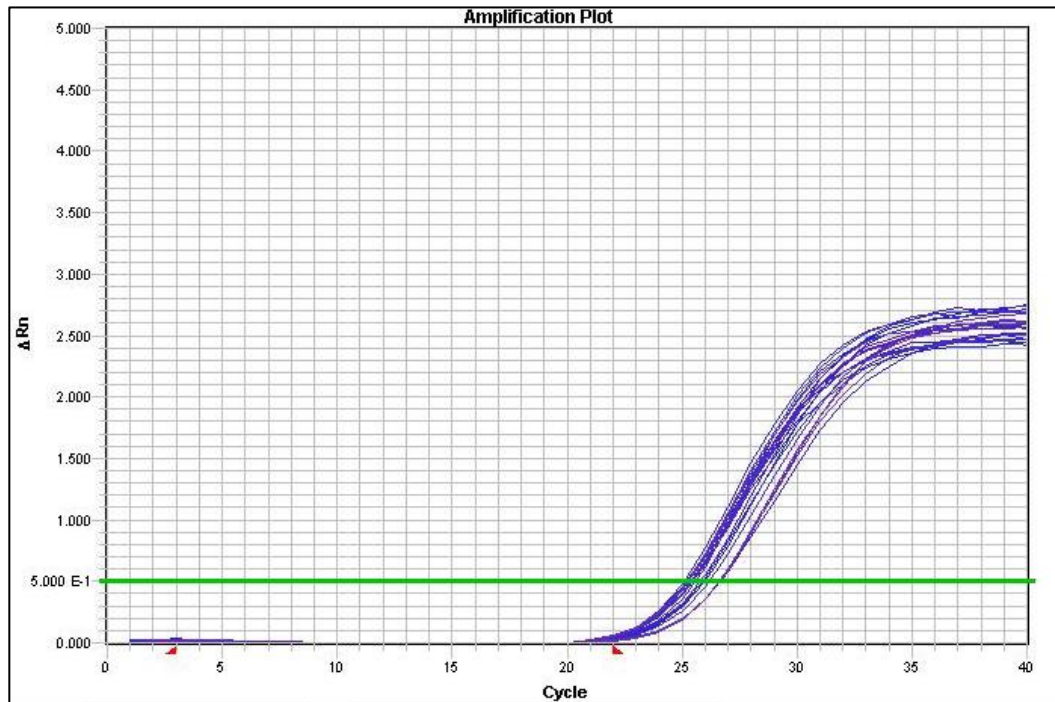


Figure 3.19 qPCR amplification plot for ACTB

Amplification plot of all samples, PC3 wild type and RAMP1 CRISPR knockouts, measuring ACTB expression. Ct values had an average of 26 and threshold was set at 0.5 ΔRn .

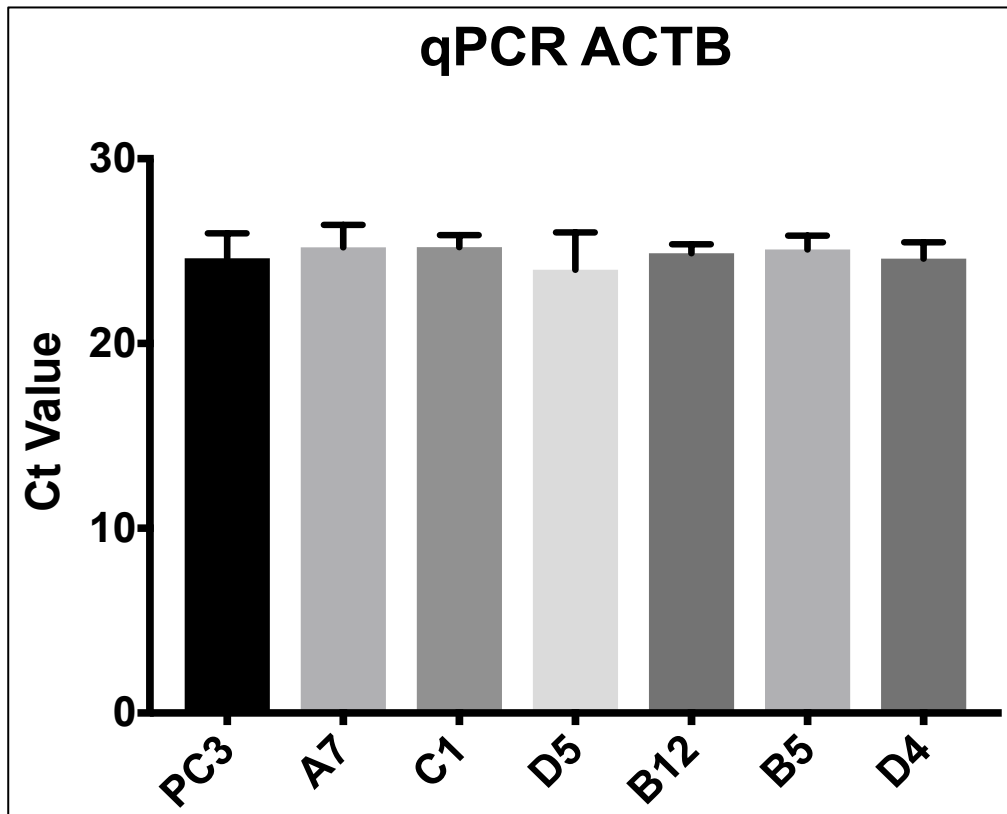


Figure 3.20 qPCR ACTB expression levels.

qPCR ACTB expression in PC3 wild type and CRISPR samples shows no significant differences in ct values (ANOVA $P = 0.2$) All values are mean \pm SEM, $n=3$. $P = 0.2$, (One-way ANOVA).

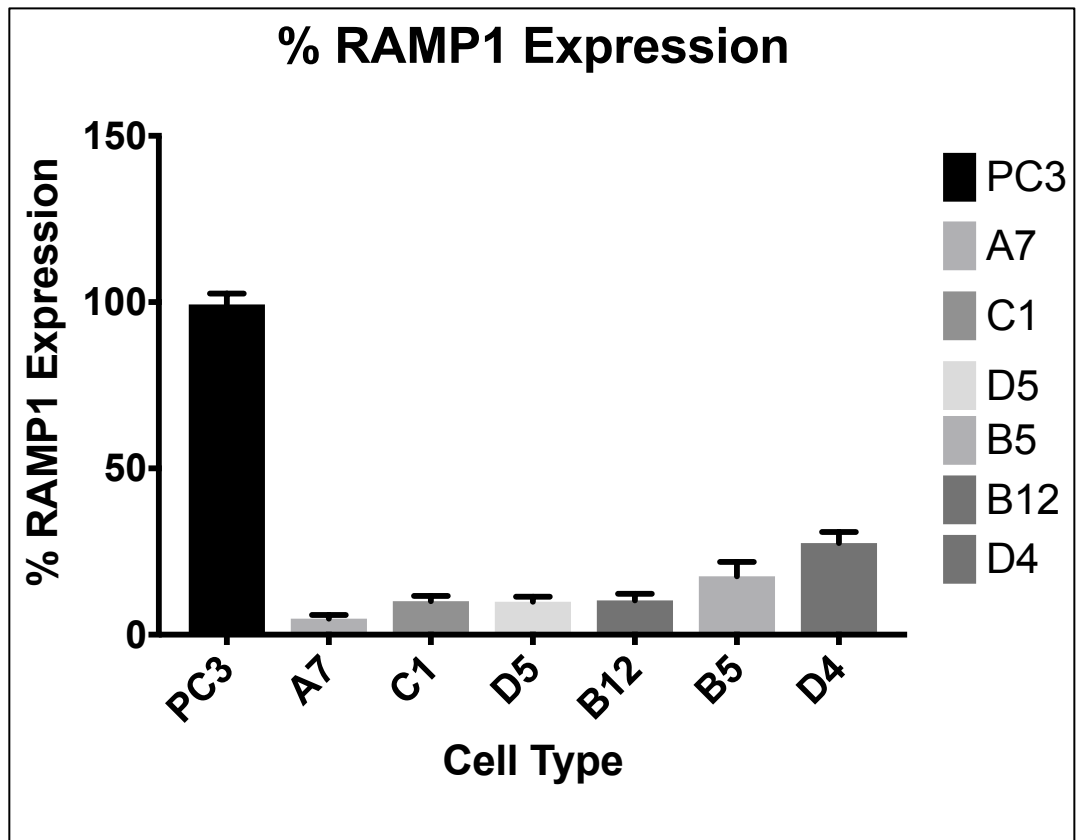


Figure 3.21 qPCR RAMP1 expression.

CRISPR samples were analysed using $\Delta\Delta CT$ and expressed as a percentage PC3 wild type RAMP1 expression. A7, C1 and D5 CRISPR samples had 5-10% RAMP1 expression whereas B12, B5 and D4 had levels of 10-30%. All values are mean \pm SEM, n=3. P-value = <0.0001, (Students unpaired t-test).

Sample	Ct Value
PC3 WT	30
A7	38
C1	37
D5	35
B12	37
B5	35
D4	38

Table 3.9 CT values for PC3 wild type and CRISPR samples.

3.5.6 Levels of RAMP2 and RAMP3 mRNA in RAMP1 CRISPR Clones Measured with Endpoint PCR.

The expression of RAMP2 and RAMP3 mRNA in RAMP1 knockout clones was analysed using semi-quantitative endpoint PCR (see Fig 3.22). Primers were designed as previously described (see Chapter 2, Section 2.4.6.) No differences were seen in levels of RAMP2 or RAMP3 compared with wild type PC3 positive controls. GAPDH reactions were used as loading controls for gel electrophoresis to ensure band density was not due to incorrect loading of products.

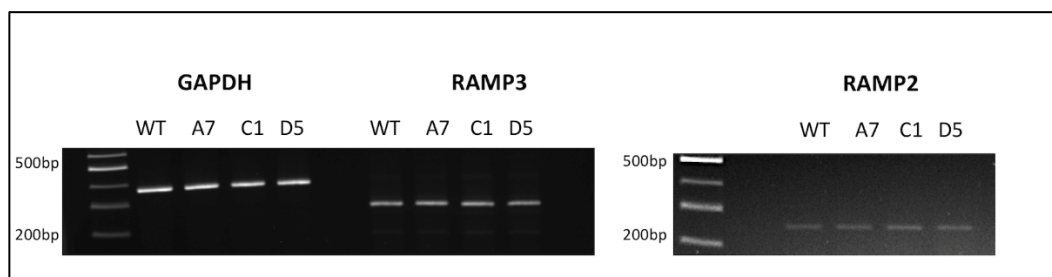


Figure 3.22 Endpoint PCR GAPDH, RAMP2 and RAMP3 on RAMP1 KO clones

Endpoint PCR targeting GAPDH (326bp), RAMP2 (256bp), RAMP3 (227bp). Samples include wild type PC3 as a positive control for RAMP2 and RAMP3 expression compared with RAMP1 KO clones A7, C1 and D5.

3.5.7 Validation of RAMP1 CRISPR Clones with Western Blotting

RAMP1 clones were then further validated for RAMP1 protein deletion by western blotting of extracts from each cell type. These were compared with wild type protein levels and normalised to a vinculin loading control. After three experimental repeats, results did not show any significant difference in RAMP1 KO and PC3 wild type protein expression.

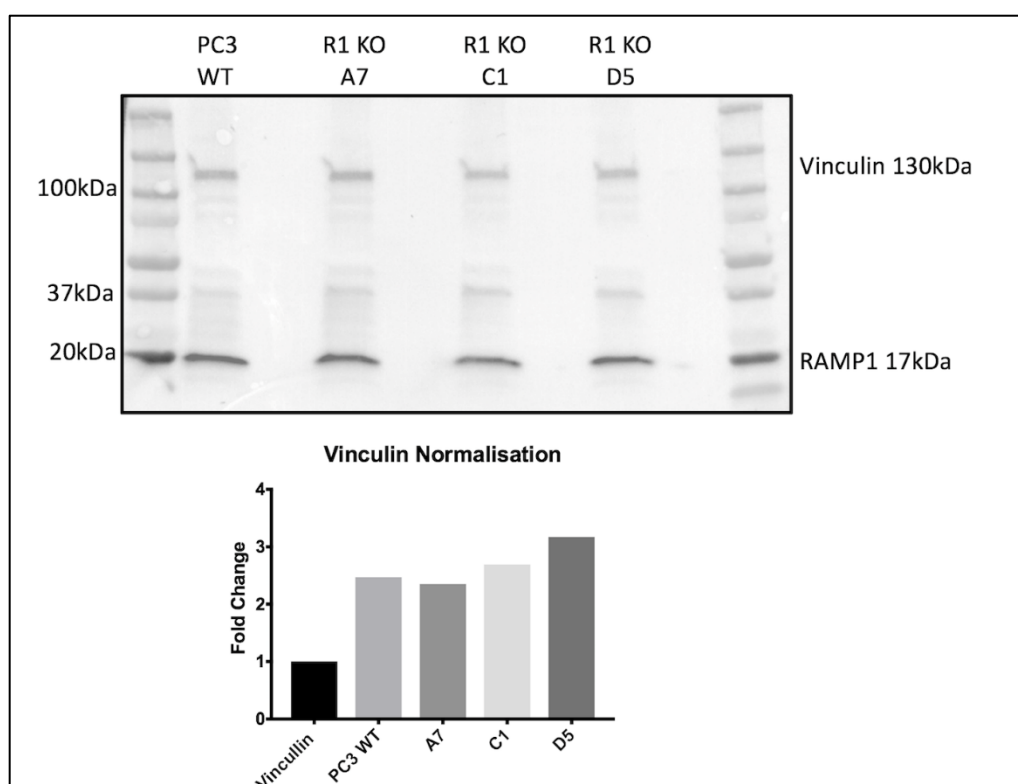


Figure 3.23 RAMP1 western blot for CRISPR knockouts.

Western blot for RAMP1 displayed bands for PC3 wild type and RAMP1 knockouts. Bands are also seen when overlaid with the protein standards at the same size as RAMP1 (17kDa). Analysis using densitometry normalised samples to vinculin and showed no significant differences between PC3 wild type and RAMP1 CRISPR samples.

3.6 Discussion

Homology arms were designed to target each of the three RAMPs and these were introduced via a plasmid. This plasmid also contained an expression cassette which was incorporated into the cut site during HDR. PC3 cells were co-transfected with a CRISPR/Cas9 plasmid (containing the gRNA sequence with Cas9) and HDR plasmid. To encourage homology directed repair (HDR) RS-1 was used as it is an activator of RAD51, which in turn activates homologous recombination. This has been found to enhance HDR up to 5 fold and increase CRISPR-mediated “knock in” efficiency both *in vitro* and *in vivo* [154]. After transfection, cells were treated with Scr7 pyrazine, an inhibitor of NHEJ which has been found to also enhance CRISPR-mediated HDR up to 19-fold *in vitro* [155].

After transfection, RFP labelled colonies were observed and it was noted that cells transfected with RAMP2 CRISPR constructs appeared unhealthy with a stressed morphology (see Fig 3.6 & 3.9). Transfection efficiencies were shown to be below 25% for all RAMP constructs. This was indicated by the presence of RFP positive cells detected during fluorescence-activated cell sorting (FACS). Large plasmids such as these CRISPR and HDR constructs (estimated 3-4kb) are notorious for yielding low transfection efficiencies [156, 157] and to alleviate this effect, three pairs of CRISPR and HDR constructs were used targeting three different target sites to increase the incidence of successful gene knockouts. All samples contained RFP negative cells which were assumed wild type or “unedited”. This creates a gene knockdown when taken together as entire population and it is likely that wild type cells will outgrow or dominate any CRISPR edited cells creating an overall “wild type” phenotype in the cell population.

To isolate knockout populations, RFP positive cells were sorted into single cell populations using FACS and then grown into clonal colonies. This ensures that any cells with a RAMP knockout grow into an entire population of gene knockouts. Cells were sorted into 48 single wells on a 96 well plate to increase chances of successful gene knockouts and to keep the number of colonies at a manageable

amount. As cells progressed from single cells to colonies they were imaged every 4 days to confirm single clonal populations (see Fig 3.8-10). It was observed that after cell transfection and sorting, few cells that had been transfected with RAMP2 targeting CRISPR constructs survived. Those that were sorted into single cells were also appeared unhealthy in their morphology and only 2-3 clones were able to be grown into larger populations for validation. This is an interesting observation as it has been reported in the literature that RAMP2 knockout mice die *in utero* [158]. This lethality *in vivo* was found to be due to abnormal vascular development, however this may not relate to cell cultures. Nevertheless, it was also found that when overexpressed in an endothelial cell line, RAMP2 can reduce permeability and cell barrier function [158]. It was found that RAMP2 is an important regulator of tight junction formation and therefore it could be hypothesised that its deletion would have harmful consequences on cell structure. It was also found that when subjected to H₂O₂– induced damage, RAMP2 overexpressing cells displayed increased viability compared to controls [158]. It could then be speculated that by effecting the structural integrity of the cell, RAMP2 deletion could also influence cell viability. This may explain why low numbers of RFP positive cells were found in the RAMP2 CRISPR population, if knockouts were present they may not have been viable cells.

Validation of successful CRISPR RAMP knockouts was primarily performed using endpoint PCR. RNA samples can be taken from as little as 1,000 cells using the Promega Reliaprep Mini Cell RNA Extraction kit (see Chapter 2, Section 2.4.4) and this was therefore an efficient way of screening clonal colonies as they grew into larger populations. The purpose of PCR experiments was to determine presence or absence of the RAMP gene, not levels of expression. Therefore, GAPDH was not used as a loading control but as a housekeeping gene to screen cDNA samples for contamination, including negative controls from reverse transcription reactions. Samples were taken from the CRISPR populations on three separate occasions and then tested for RAMP mRNA using endpoint PCR. The maximum concentration of cDNA was synthesised from RNA extracts (100ng/μL) in order to rigorously test for the presence of mRNA in CRISPR samples. Samples taken from RAMP1 CRISPR cells

included at least 7 clones that did not show a clear band after running PCR products on an agarose gel (see Fig 3.12). These were then selected for further validation as potential successful RAMP1 knockouts. Only two clones survived to be validated for RAMP2 knockouts and displayed clear bands at the correct size for RAMP2 (see Fig 3.13.) All clones tested for RAMP3 knockouts also displayed bands at the correct size, eliminating them as successful knockouts (see Fig 3.15).

It is unclear why no RAMP2 or RAMP3 knockouts were generated. RAMP2 knockouts may have had such reduced viability that no cells survived after transfection and therefore those sorted had a non-specific integration of the expression cassette. As was previously described, all CRISPR/Cas9 techniques carry a risk of non-specific targeting, leading to off target deletions [159-161]. The CRISPR-HDR method reduces this risk but does not eliminate it completely. However, it can be argued that if RAMP1 CRISPR constructs contain efficient gRNAs, then the presence of a double stranded cut will be most likely repaired with the HDR insert. Therefore, there is no obvious reason why, with an efficient gRNA, off target integration of the HDR insert should occur. It has been shown that off-target effects are often governed by the efficiency of gRNA and Cas9 activity [162]. Therefore, in the absence of an efficient gRNA, the expression cassette may be integrated non-specifically or into DNA breaks present in cells that are undergoing repair at the time of transfection. This integration would also be encouraged due to the presence of HDR enhancer RS-1 and NHEJ inhibitor Scr7 pyrazine. This is a possible explanation for the lack of successful RAMP2 and RAMP3 knockouts but despite these populations containing RFP positive cells post-transfection. Nevertheless, RAMP1 knockouts **were** successfully generated and these cells can be used as a research tool to learn more about the mechanism of RAMP1 (and its associated ligands e.g. CGRP) in prostate cancer.

As the presence of RFP labelled cells does not necessarily correlate with successful knockout, it was important to establish whether the CRISPR construct had targeted the RAMP1 gene specifically. To determine this, primers were placed

outside the RAMP1 homology arms in the RAMP1 gene and in the HDR insert or expression cassette that would be inserted into the gene (specifically the EF1-alpha promoter). It is possible that non-specific integration of the CRISPR construct made lead to the homology arms being inserted into the genome. Therefore, primers placed upstream of the homology arm in the RAMP1 gene, would only produce PCR products from a RAMP1 CRISPR edited gene. Wild type PC3 cells would not have the CRISPR HDR insert and therefore produce no PCR products. Primers targeting another genomic DNA site were used to determine that the genomic DNA samples were not degraded as this would also fail to produce PCR products (see Fig 3.16). The primers targeting RAMP1 revealed that three CRISPR clones had been successfully edited (B7, C1 and A7) and this was further validated using sanger sequencing (see Fig). Not all clones showed visible bands and it is possible that they were edited in different sites as the cells were transfected with three different CRISPR constructs. The primers designed span two of these gRNAs but if clones had only been edited at the third site, this would not be detected.

Quantitative PCR was used to measure RAMP1 expression in CRISPR samples when compared with wild type PC3 data using the $\Delta\Delta$ CT analysis method. For all clones tested, cycle threshold (Ct) values were above 35. This is often considered background/artefact as high ct values represent a very small amount of starting material. Nevertheless, when comparing these high ct values with $\Delta\Delta$ CT, expression levels of RAMP1 are less than 10% relative to wild type PC3 in 4 out of 6 CRISPR clones. qPCR primers were also designed targeting RAMP2 and RAMP3, however these did not yield any amplification of cDNA from wild type PC3 samples. Nevertheless, endpoint PCR does reveal positive results for RAMP2 and RAMP3 mRNA. To test whether deletion of RAMP1 by CRISPR/Cas9 had affected the expression of RAMP2 or RAMP3 in the knockout clones, endpoint PCR was performed. Using a housekeeping gene, GAPDH, as a loading control it was clear that there are no obvious differences in band density for RAMP2 or RAMP3 for any knockout clones when compared with PC3 wild type signal. It is therefore assumed that RAMP1 KO clones were not affected in RAMP2 or RAMP3 expression although

in the future, qPCR primers may be redesigned to confirm this result in a quantitative manner.

Further validation of the RAMP1 knockouts requires measurements of RAMP1 protein expression. Western blotting found no significant differences in protein levels between PC3 wild type and RAMP1 KO cells. A possible explanation for this may be that a truncated RAMP1 protein is being expressed, as the CRISPR editing occurs in early in the gene sequence (see Fig 3.18). Differences in the size of this truncated protein may not be detectable using western blot as already the RAMP1 protein has a small weight of 17kDa. However, the HDR insert does include a stop codon which should halt protein transcription. Therefore, alternative explanations for this result may point to reliability of the antibody used. RAMP1 antibodies are not easily found and can be difficult to optimise, often giving bands of the incorrect size. Only one anti-RAMP1 monoclonal antibody could be optimised producing bands at the correct size of 17kDa. However, it was also observed to bind to the protein standards of the ladder at the same size (see Fig 3.23). This questions the reliability and specificity of this antibody, especially when cells that express no RAMP1 mRNA display bands for the RAMP1 protein when probed with this antibody.

Taken together the findings of these experiments suggest that a RAMP1 knockout has been successfully generated in the PC3 cell line. Endpoint PCR results show no visible bands in multiple RAMP1 CRISPR clones, suggesting a lack of RAMP1 mRNA. This result was supported by qPCR data showing extremely high ct values in CRISPR clones, when compared to wild type PC3 samples with $\Delta\Delta$ CT analysis. Sanger sequencing data of PCR products using genomic DNA primers also validates the insertion of the CRISPR HDR construct into the site targeted by RAMP1 gRNA sequences. Sequencing data also reveals that the construct has targeted the RAMP1 gene specifically. Conflictingly, western blot results show RAMP1 antibody binding to both PC3 wild type and RAMP1 CRISPR protein samples. However, it has been found in these investigations that the antibody used also binds non-specifically and often at unpredicted sizes. Further investigation is therefore needed to determine

the protein expression of these RAMP1 CRISPR clones. The deletion of RAMP1 in PC3 cells will shed light on the role of this gene in prostate cancer and mechanisms affected downstream within the cell. RAMP1 knockout cells will be tested functionally *in vitro* at first, to determine the effect of RAMP1 on the tumorigenic potential of the cells.

CHAPTER 4: FUNCTIONAL EFFECTS OF RAMP1 DELETION IN PC3 CELLS *IN VITRO*.

4.1 Introduction

Increasing evidence has shown that patients diagnosed with fewer prostate cancer metastases have a better prognosis when compared with patients with advanced metastatic disease [163]. The process of primary tumours metastasising to secondary sites involves a series of interlinked and sequential steps [164]. These steps can also be defined as “hallmarks” of cancer and have been comprehensively reviewed by Weinberg, Hanahan & Roberts [5, 6]. In order to successfully determine the importance and role of RAMP1 in prostate cancer metastasis, the effect of its deletion can be measured in each of these important stages using cellular or *in vitro* experiments. A fundamental characteristic of cancer cells is their unique ability to sustain a hyper proliferative state without succumbing to cell death. To achieve this, cells undergo a variety of mutations that can alter both growth-promoting and pro-apoptotic pathways. These pathways exist to promote a homeostasis in cell number and aid the maintenance of tissue architecture and function [6]. Cancer cells can achieve this by either producing growth factors themselves or can influence their surrounding environment by stimulating stromal cells to produce growth-promoting factors [165, 166]. To date, no studies have shown a link between RAMP1 mutations and prostate cancer, however *in vitro* and *in vivo* studies have shown a correlation between RAMP1 and cell proliferation. After depletion of RAMP1 using shRNA in PC3 and LNCaP cells, proliferation was reduced by approximately 40% *in vitro* and xenograft studies using RAMP1 knockdown cells showed reduced tumour growth of 40% [105]. Subsequent immunohistological staining of RAMP1 knockdown tumours found reduction in Ki67 and pHH3. These are both markers of proliferation and have

been shown to be statistically relevant as prognostic markers of prostate cancer progression [167].

The method of counting cell proliferation *in vitro* has been established for more than 50 years, when the dye Trypan blue was first used to determine cell viability [168]. Cell viability can be defined as the health of cells and can be estimated by measuring cellular markers of activity. Cell viability assays are able to determine the ability of cells to respond to stress. By measuring the population of healthy/living cells overtime, the growth rate or proliferation of a population can also be deduced. By excluding non-viable or dead cells, the quantification of Trypan blue positive cells is achieved using a microscope and a haemocytometer. Although this method can often be accurate, it is time-consuming and more open to human error than other methods of counting cells [169]. Since then, new techniques have been developed to measure cellular metabolic activity (such as levels of tetrazolium salts or the corresponding reduction potential of the cells) producing high-throughput assays based on colorimetric, fluorimetric or luminescence readings [170]. These commonly used assays can be applied when testing the effect of RAMP1 deletion in PC3 cells on cell proliferation and viability. Studies have not yet elucidated the mechanism of RAMP1 in cell proliferation. This could be either by influencing pathways in the cancer cell directly or by targeting the surrounding stroma. This can be investigated by measuring the differences in downstream signalling pathways in RAMP1 KO PC3 cells compared with PC3 wild types.

Increased proliferation of cancer cells triggers pathways that activate programmed cell death or apoptosis. This is often due to increased proliferation causing DNA damage in the cells or mutations that lead to the upregulation of oncogenes [6]. Apoptosis is regulated by a number of different protein families, one of which is the caspase family. Caspases can be classed into upstream regulators (e.g. caspase 8) and downstream effector components (e.g. caspase 3/7). Apoptosis is mostly controlled by a balance of pro- and anti- apoptotic signals. Members of the Bcl-2 family are inhibitors of apoptosis which bind to proapoptotic signals such as

Bax and Bak, deactivating them [171, 172]. Cancer cells can often “hijack” these regulatory pathways in order to evade cell death. Previous reports have not linked RAMP1 with apoptosis regulation and no significant differences were seen in caspase 3 activity after RAMP1 depletion in PC3 cells [105]. However, independent from the context of cancer, the RAMP1/CLR complex has been reported to exert anti-apoptotic effects on cardiomyocytes under oxidative stress by increasing Bcl-2 expression [173]. Parallels may be drawn from these findings as cancer cells often need to adapt to hypoxic settings [6] and similar mechanisms would be useful under these conditions. The effect of RAMP1 KO on apoptotic pathways can be investigated using a caspase cleavage assay. The principle of such an experiment is to add a substrate directly onto cells in culture. The substrate will first lyse the cells and then also contains a luminogenic (or colorimetric/fluorimetric) substrate fused with a DEVD sequence. This sequence is a recognition site for caspases and any present will therefore cleave the substrate which then results in the release of luciferin and ultimately leading to a luminescence signal proportional to caspase activity [174, 175].

Subsequent to a primary tumour being formed after cancer cells have proliferated sufficiently, they may enter the “invasion-metastasis” cascade. This term describes the process whereby primary tumour cells undergo epithelial to mesenchymal transition (EMT) and begin to invade local tissues through the surrounding extracellular matrix (ECM). To do this, cells enter a migratory phenotype that can be described as the movement of a cell from one area to another. However, in order to penetrate the surrounding tissues, cells must also be capable of invasion [176]. EMT can cause pathways within the cell that regulate cell adherence and structure to either be activated or deactivated. In many prostate cancer cell lines such as PC3, DU145 and LNCaP it has been reported that treatment of 10^{-8} M CGRP can increase migration of cells by up to 30% across a gradient of fibronectin (an ECM protein) [104]. This is known as “haptotactic” migration where cells respond to a stimulus e.g. fibronectin which may trigger migration. Invasion of cells can be measured by using Matrigel-coated invasion chambers. Matrigel is a substance that

was first extracted from a tumour and contains all common ECM proteins such as laminin, collagen IV and heparan sulphates [177]. It has been reported that treatment with 10^{-7} M CGRP increases the invasive ability of PC3 and LNCaP cells by 30% [104, 178]. There are no current studies in the literature which show the importance of RAMP1 in migration and invasion of cancer cells of any type. However, it could be hypothesised that as RAMP1 is a component of the CGRP receptor, similar effects may be observed.

After cells have successfully located to the metastasis site, colonisation must occur. A proposed model of metastasis is the “seed and soil” hypothesis which states that only particular subset of cells (the “seeds”) that disseminate from the primary tumour landing in the optimal microenvironment (the “soil”) can successfully form secondary tumours [179]. In the context of prostate cancer, the “soil” is often the bone microenvironment. If only a small group of cells reach the bone microenvironment, the ability of these cells to form colonies and progress is paramount to tumour formation. Colony-forming assays have been developed to test the effect of anti-cancer treatments on the colony-forming ability of cancer cells. This can be achieved by sparsely plating cells on soft agar or standard cell culture plates and allowing the cells to growth for 2+ weeks to see how many individual cells form colonies of 50 cells or more [180]. It has been reported that depletion of RAMP1 resulted in a 55% reduction in the average number of colonies formed by PC3 cells [105]. This indicates RAMP1 is an important factor in the ability of single cells to divide into larger populations and therefore may reflect its role in metastatic tumour progression. Cancer cells must also lose their adhesive properties when dissociating from the stroma in order to intravasate into the circulation. However, after the metastasis site has been reached, cancer cells must reverse this effect in order to anchor themselves in the bone microenvironment [181]. This requires the switching on or off of different adhesion-associated pathways. In prostate cancer, annexin II has been found to be produced in endothelial and osteoblast cells and can promote adhesion of cancer cells expressing the annexin II receptor [182]. The effect of RAMP1 depletion was not reported on adhesion of PC3 cells, however previous

reports show when stimulated with CGRP, no effect on PC3 cell adhesion was observed [178].

It is vital that future investigations find therapeutic targets that are involved in the metastasis of prostate cancer. RAMP1 has been shown to be upregulated in prostate cancer patients [140] and genome-wide studies find it to be the significantly upregulated in prostate cancer when compared with other solid tumours e.g. breast, lung and liver [105]. RAMP1 is therefore a candidate for playing a key role in prostate cancer metastasis. By generating successful RAMP1 knockouts in a PC3 cell line, we can now test this hypothesis. *In vitro* assays have been previously reported in the literature as useful tools for determining changes in a cell line's metastatic potential. These will be used to compare RAMP1 KO and wild type PC3 cells for their ability to proliferate, migrate and invade, adhere and colonise and finally to evade apoptosis. It is also important to investigate whether the CGRP (RAMP1:CLR) receptor is responsible for the tumorigenic effects seen in wild type PC3 cells. Therefore, by using CGRP and CGRP antagonist treatments in *in vitro* experiments, it can be determined whether the CGRP receptor is important for PC3 cell growth and other metastatic processes.

4.2 Hypotheses

1. Deletion of RAMP1 in PC3 cells will affect:
 - a. Cell survival
 - b. Processes of metastasis
 - c. Downstream signalling pathways
2. The effect of RAMP1 on PC3 cells is mediated by CGRP.

4.3 Research Aims

1. To determine the effect of RAMP1 deletion on cell survival and processes of metastasis using *in vitro* assays.

2. To determine the effect of RAMP1 deletion on downstream signalling pathways using a multiplex magnetic bead assay

3. To determine the cause of RAMP1's effect using CGRP stimulation and CGRP antagonists *in vitro*.

4.4 Materials and Methods

4.4.1 Viability Assays

Cell viability was measured using the RealTime-Glo™ MT Cell Viability kit (Promega). This is a non-lytic bioluminescent method for measuring viability in real time. The number of viable cells in culture is determined by measuring the reducing potential and metabolism (MT) of the cells (see Fig 4.1). A 1,000X NanoLuc cell-permeable substrate was added to cells in culture in combination with a 1,000X NanoLuc enzyme (luciferase) to final concentration of 1X. Viable cells then reduced the proprietary substrate to generate a second substrate (luciferin) for the NanoLuc enzyme (luciferase) which in turn produces a luminescent signal which was then read using an Enight plate reader (Perkin Elmer) using the settings described in Table 4.1.

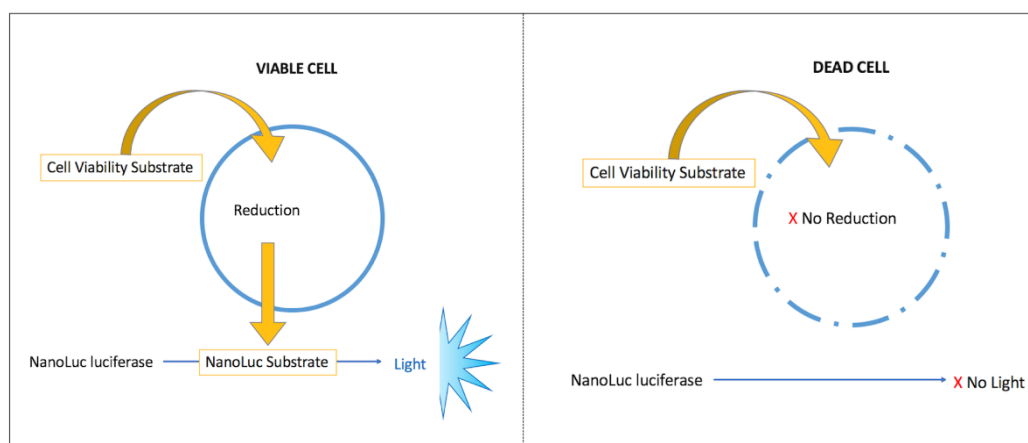


Figure 4.1 Principle of cell viability assay.

This assay relies on reduction of the viability substrate by viable cells to produce a luciferin substrate for the luciferase enzyme. This produces a luminescent signal proportional to the number of viable cells in culture.

A continuous-read format allows the luminescent signal to be monitored over an extended period of time, allowing measurements of cell viability in real time. Viability assays were typically run for 3 days. PC3 wild type cells were first used to optimise cell density for this viability assay (see Fig 4.2). It was found that a seeding of 2,000 cells per well produced very dramatic increases in viable cells, due to an

increased growth rate. This creates a narrow window of time to perform the experiment, limiting the time for any effects on viability to be measured. Cells seeded at 1,000 cells per well displayed a continuing linear phase after 72 hours and therefore were chosen as the optimal cell density for performing viability experiments. Cells were cultured as previously described (see Chapter 2, Section 2.4.1-3) and seeded at 500 cells per well showed similar linear growth rates but were also slow to begin growth and were therefore not selected as the optimal density. PC3 wild type and RAMP1 CRISPR cells were seeded at the optimal density of 1,000 cells per well for all viability experiments. Measurements were taken every 24 hours for a total of 3 days. In some cases, cells were treated daily with either calcitonin gene related peptide (CGRP) (Sigma) or Telcagepant/MK0974 (MedChem Express). Ligand or antagonists were made to concentrations of 1, 3 or 5 μ M and were diluted in PBS to a 50X concentration in a 2 μ L volume to be added to each well containing 100 μ L media.

Condition	Setting
Plate Distance	0.1mm
Measurement Time	0.5 seconds
No. of columns	5
No. of rows	5
Distance between points	0.5mm

Table 4.1 Plate reader settings for viability assays.

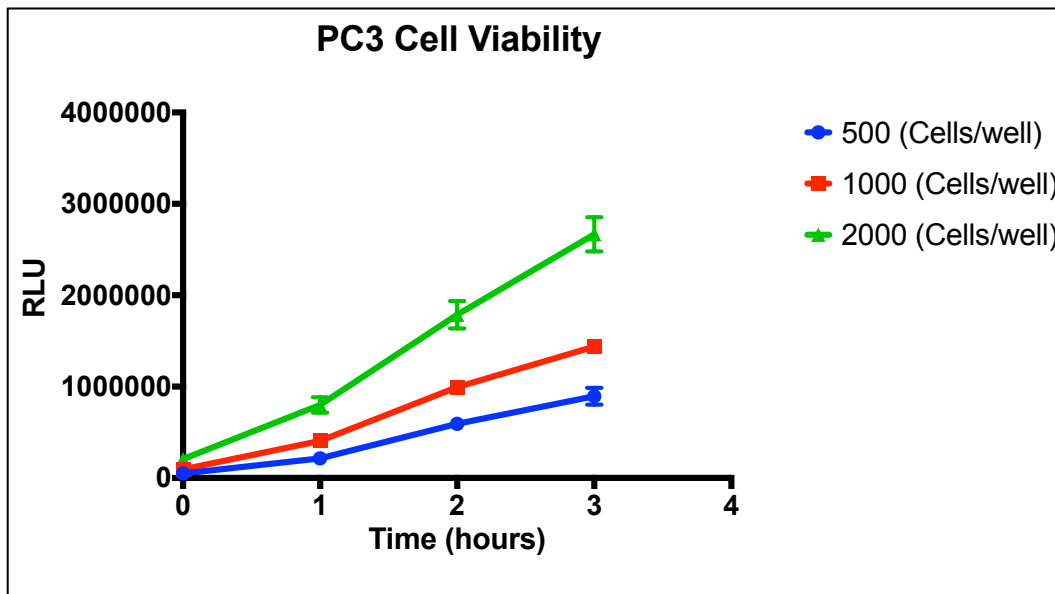


Figure 4.2 Cell density optimisation for viability assay.

Optimisation of PC3 cell density for viability assays. 1,000 cells per well (red) was selected as the optimal cell density. All values are mean \pm SEM, n=3.

4.4.2 Apoptosis Caspase 3/7 Assays

To measure rates of apoptosis in PC3 wild type and RAMP1 KO cells, the Caspase-Glo 3/7 assay kit (Promega) was used. This is a homogenous, luminescent assay that measures caspase 3 and caspase 7 activity. These are renowned members of the cysteine aspartic acid-specific protease (caspase) family and play key roles in apoptosis in mammalian cells [183]. Cells were cultured using previously described methods (see Chapter 2, Section 2.4.1-3) and then seeded 1,000 cells per well in a white opaque 96 well plate and incubated at 37°C for 24 hours. Cells were then serum-starved to induce apoptosis and the incubation times were optimised for PC3 cells. Cells were compared with “unstressed” conditions (complete media) to find the most significant difference between stressed and unstressed. After incubation with serum-free media 50 μ L of a luminogenic caspase 3/7 substrate reconstituted in 2.5mL Caspase-Glo® 3/7 Buffer was added to each well. This resulted in cell lysis and

cleavage of the substrate by caspase3/7, leading to the release of aminoluciferin and causing a reaction with luciferase and production of light (see Fig 4.3). It was found that 48 hours of serum starvation yielded the biggest difference in caspase 3/7 activity between stressed and unstressed conditions (see Fig 4.4). This increases the opportunity to see an effect in caspase 3/7 activity between PC3 wild type and RAMP1 KO cells. All experiments comparing PC3 wild type and RAMP1 KO cells used a serum starvation incubation time of 48 hours.

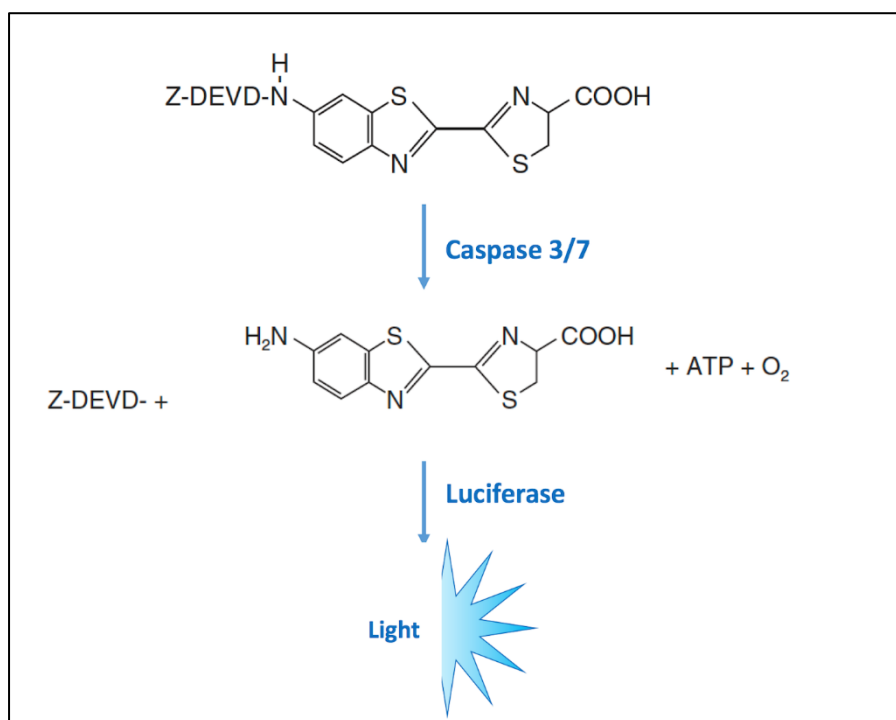


Figure 4.3 Caspase 3/7 assay principle.

Cleavage of luminogenic substrate by caspase 3/7 results in release of aminoluciferin and reaction with luciferase leads to production of light.

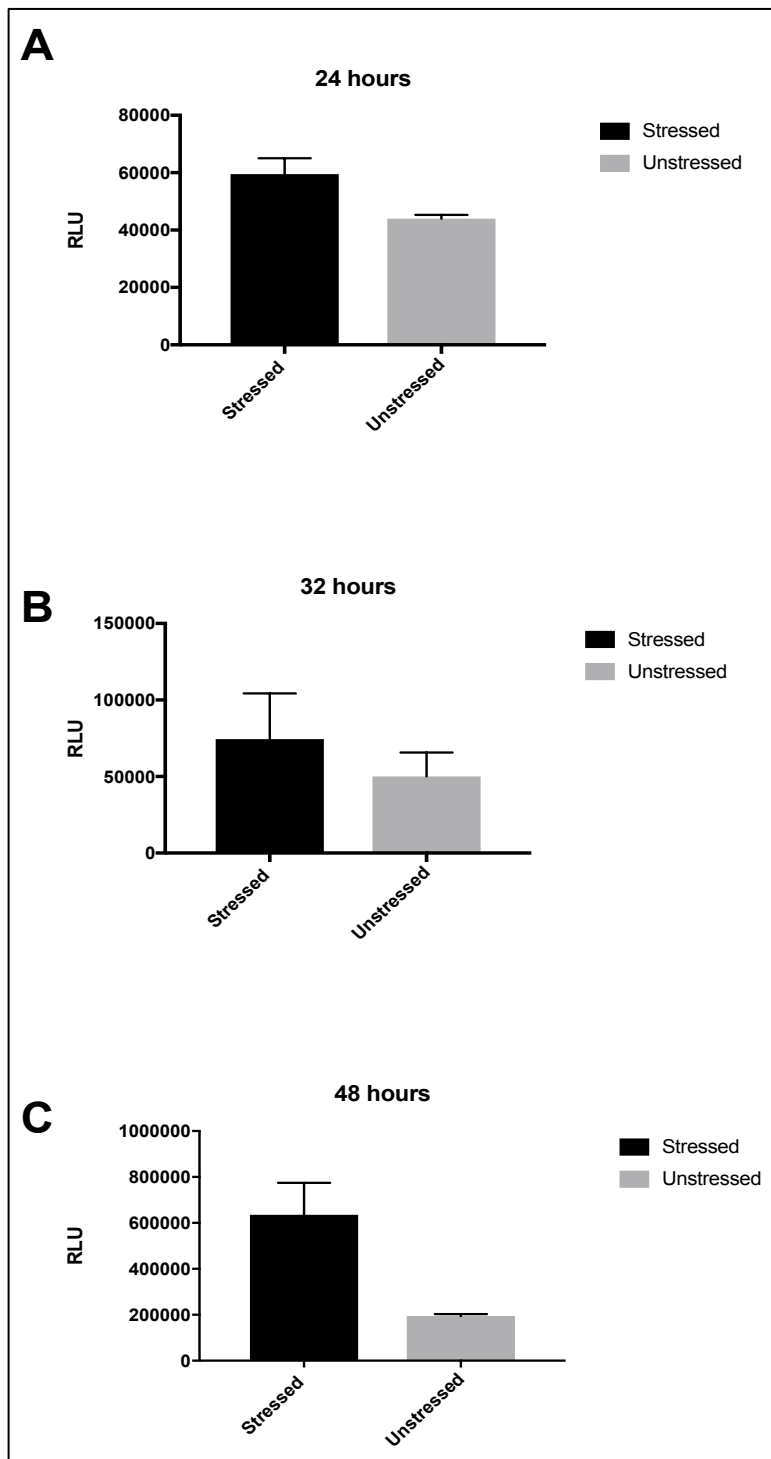


Figure 4.4 Optimisation of incubation time for caspase 3/7 assay.

(A) 24 hours incubation showed a 26% increase in caspase 3/7 activity compared with unstressed conditions. (B) 32 hours incubation showed a 33% increase in caspase 3/7 activity. (C) 48 hours showed a 69% increase in caspase 3/7 activity. All values are mean ± SEM, n=4. P<0.05, (Students unpaired t-test).

4.4.3 Migration “Scratch” Assays

To measure migration in PC3 wild type and RAMP1 KO populations, cells were cultured as previously described (see Chapter 2, Section 2.4.1-3). 3×10^5 cells were seeded in 6 well plates (in triplicates) and were 90% confluent 24 hours later. All cells were then treated with $0.5\mu\text{M}$ Mitomycin C for 2 hours as this has been shown to suppress PC3 cell proliferation without causing harmful toxicity [184]. After treatment, scratches were made in the cell monolayer using a $200\mu\text{L}$ pipette tip. Cells that became unattached after scratching were removed by washing with $500\mu\text{L}$ PBS three times. Complete media was then added to all wells and images were taken at three different regions of interest (ROIs) for each scratch using an EVOS FL Auto Imaging System (Thermo Fisher Scientific). Cells were incubated overnight and then imaged again at the same ROIs. Closure of the scratch or “wound” was quantified using the MRI Wound Healing Tool macro for Image J.

(http://dev.mri.cnrs.fr/projects/imagej-macros/wiki/Wound_Healing_Tool)

4.4.4 Transwell Invasion Assays

Invasion and migration of PC3 wild type and RAMP1 CRISPR cells was measured using a BD BioCoat™ Matrigel™ Invasion Chamber (Corning). Cell density was first optimised using PC3 wild type cells which were cultured as previously described (see Chapter 2, Section 2.4.1-3) and seeded at 1×10^5 , 5×10^5 and 1×10^6 cells in Matrigel-coated and control inserts. Prior to seeding cells were incubated in serum-free medium for 24 hours. $750\mu\text{L}$ complete RPMI medium was added to the wells beneath the inserts and cell suspensions were made in serum-free media. After being seeded in either control or Matrigel inserts, cells were incubated for 24 hours at 37°C . Non-invasive cells were removed from the upper surface of the membrane by scrubbing with a cotton swab moistened with serum-free RPMI media. Invasive cells on the lower surface of the membrane were then fixed in $500\mu\text{L}$ methanol for

2 minutes and then stained with 1% Toluidine Blue in 1% borax solution (Sigma) for another 2 minutes. Inserts were then air dried and image using an EVOS FL Auto Imaging System (Thermo Fisher Scientific). Analysis was performed by taking six different regions of interest in the well and counting cells manually. It was found that 1×10^6 PC3 cells was the optimal density for both control and Matrigel coated membranes (see Fig 4.5). Experiments comparing RAMP1 KO and PC3 wild type cells were performed using 1×10^6 cells for both control and Matrigel inserts. Percentage of invaded cells was calculated using the following formula as suggested in the manufacturer's protocol:

$$\% \text{ Invasion} = \frac{\text{Mean number of cells through Matrigel insert membrane}}{\text{Mean number of cells through control insert membrane}} \times 100$$

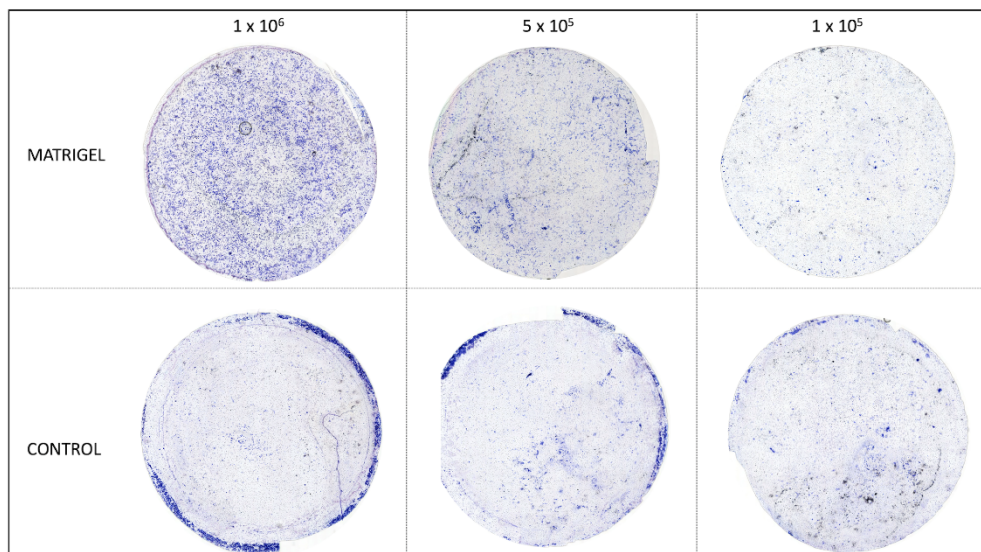


Figure 4.5 Transwell control and Matrigel-coated membranes

Different densities of PC3 cells were seeded. Cells were fixed with 100% methanol and then stained with 1% toluidine blue in 1% borax solution for visualisation and analysis.

4.4.5 Colony Formation Assays

To measure the ability of PC3 wild type and RAMP1 KO cells to form colonies in culture, colony formation assays were performed. PC3 and RAMP1 KO cells were cultured as previously described (see Chapter 2, Section 2.4.1-3) and cell density was first optimised for colony formation by seeding 25, 50 and 100 cells in single wells of a 6 well plate. This was performed in triplicates using RAMP1 CRISPR clone “D5” and PC3 wild type cells to determine the optimal density to form colonies that could be visualised. (see Fig 4.6). After cells were seeded, plates were incubated at 37°C for 14 days and the media was changed on all wells every 3 days. The media was then removed and the cells were fixed with ice cold 100% methanol for 15 minutes. Cells were then stained with 0.25g crystal violet diluted with 25% methanol-PBS for 10 minutes. The stain was then removed with distilled water and

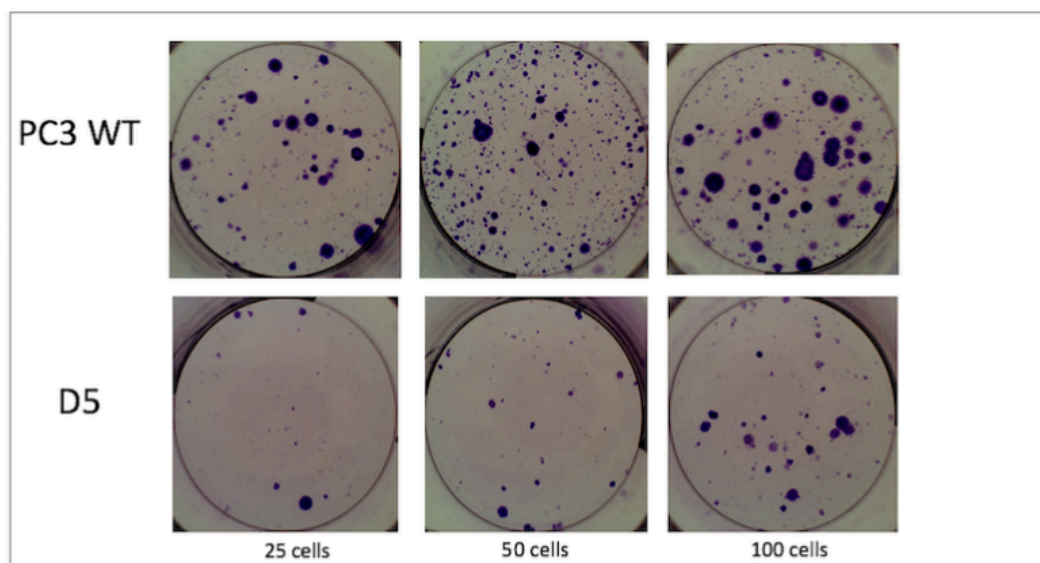


Figure 4.6 Optimisation of cell density for colony formation assay.

Density was optimised using both PC3 wild type and RAMP1 KO clone “D5” cells. The optimal density was determined as 100 cells as this yielded quantifiable colonies after 14 days of growth.

plates were air dried before imaging with a Pixera Professional High-Resolution Digital Camera (Pixera). Colonies were then quantified using GeneTools 4.01

software (SynGene). It was determined that seeding of 100 cells was the optimal density for colony formation and subsequent analysis. Subsequent experiments were performed by seeding 100 cells in each well of all cell types.

4.4.6 Adhesion Assays

To measure the ability of PC3 wild type and RAMP1 KO cells to adhere to extracellular matrix proteins, adhesion assays were performed. Cells were cultured as previously described (see Chapter 2, Section 2.4.1-3). Cells were counted and then resuspended at 2×10^5 /mL in serum-free media and stained with 1 μ M Calcein AM for 30 minutes at 37°C. Cell suspensions were then washed twice with 1mL serum-free medium and centrifuged at 1,000 x G. Cells were finally suspended in 1mL complete media and 100 μ L was added per well to BioCoat™ 3-5 μ g/cm² Fibronectin-coated 96 well plates (Corning). Cells were left to adhere at 37°C for 30 minutes and then selected wells were washed three times with 100 μ L PBS and then 200 μ L PBS was added to the wells. Washed wells were chosen to represent “adherent cells” whereas unwashed cells represented the “total population of cells”. Adherence was then calculated as the percentage of adherent cells to the total population of cells. This calculation was account for any differences in seeding. Fluorescence intensity of each well was then measured using an Enight plate reader (Perkin Elmer) at an emission/excitation wavelength of 485/ 520nm.

4.4.7 Multiplex Magnetic Bead Assay

A multi-pathway 9-plex magnetic bead kit (Merck) was used to detect phosphorylated proteins from different signaling pathways in PC3 wild type and RAMP1 KO cell lysates. This assay is an immunoassay combined with magnetic beads and the principle is very similar to a sandwich ELISA (see Fig 4.6). Capture antibodies specific to a protein of interest are covalently bound to the beads. The coupled beads react with proteins within the cell lysate sample, and a Bio-Plex Pro™ Wash Station (BioRad) was then used to remove unbound protein. A biotinylated detection antibody was then added to create a sandwich complex. A final complex was then

formed with a streptavidin-phycoerythrin (SA-PE) conjugate and a fluorescent signal was then read using a Luminex MAGPIX Instrument (Biorad). Magnetic beads contain internal specific fluorescent dyes allowing multiplexing of different beads and antibodies targeting different proteins within the same sample.

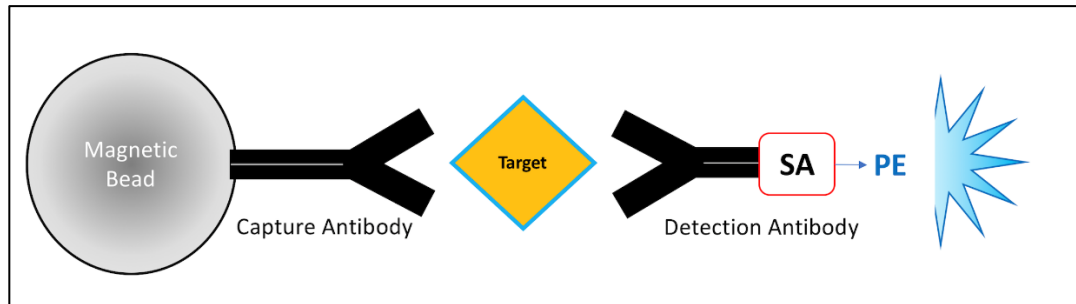


Figure 4.7 Schematic diagram of multiplex magnetic bead immunoassay.

Magnetic beads are bound to antibodies specific to a protein of interest. Biotinylated detection antibody is also specific to protein of interest and conjugated to a streptavidin-phycoerythrin (SA-PE) complex which acts as a fluorescent reporter.

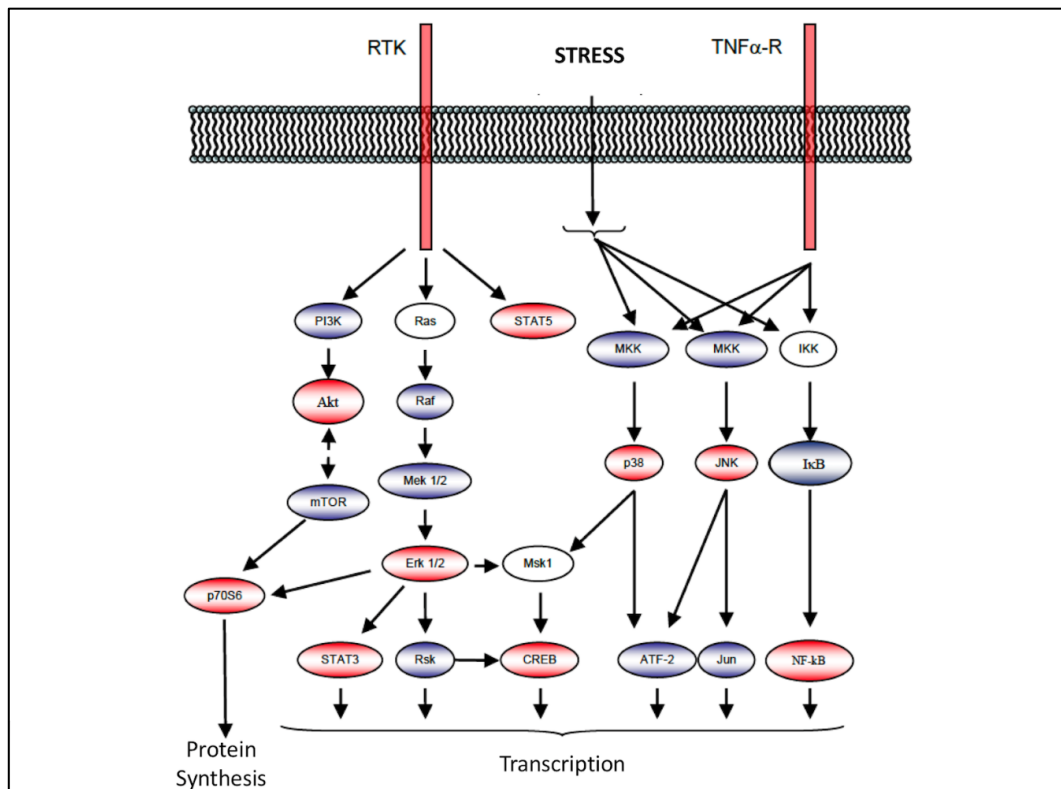


Figure 4.8 Schematic diagram of multiple pathways targeted in multiplex bead assay.

Phosphorylated proteins from different interacting signaling pathways (highlighted red) were targeted by magnetic beads bound to specific antibodies.

4.4.7.1 Preparation of Cell Lysates

PC3 and RAMP1 KO cells were cultured as previously described (see Chapter 2, Section 2.4.1-3). 2×10^5 wild type PC3 or RAMP1 KO cells were then seeded in 6 well plates and incubated at 37°C overnight in complete media. Cells were then washed once with PBS and then 1% RPMI media was added and cells were incubated at 37°C overnight. Cells were washed with 500 μ L ice cold PBS and then 500 μ L ice cold 1X MILLPLEX[®] lysis buffer with protease inhibitor cocktail set III (Calbiochem) diluted 1:200 was added to the cells. A cell scraper was used to remove adherent cells and the cell suspension was transferred to a 1.5mL Eppendorf tube. Samples were then gently rocked for 15 minutes at 4°C. Samples were then transferred to a 0.5mL filter column (Merck) and centrifuged for 4 minutes at 4°C. Samples were then

aliquoted and stored at -80°C . Quantification of protein concentration was performed using a BCA assay as previously described (see Chapter 2, Section 2.4.10).

4.4.7.2 *Immunoassay Protocol*

An opaque black 96 well plate was used for multiplex magnetic bead assays and all wells were first washed with $50\mu\text{L}$ assay buffer (Merck). $25\mu\text{L}$ magnetic beads were added to all wells and $25\mu\text{L}$ assay buffer was added to blank negative controls. Samples and positive controls were added at $25\mu\text{L}$ in triplicate wells. Positive controls included cell lysates provided in the kit and included a HeLa cell lysate (unstimulated), a A431 cell lysate (EGF stimulated), a MCF7 cell lysate (IGF-1 stimulated) and a HeLa cell lysate ($\text{TNF}\alpha$ /Calyculin A stimulated). PC3 wild type and RAMP1 KO cell lysates were added at a concentration of $0.5\text{mg}/\text{mL}$ and positive controls were added at a concentration of $0.8\text{mg}/\text{mL}$. All incubation steps were performed on a plate shaker at 800 rpm. All samples and magnetic beads were left to incubate overnight in the dark at 4°C . The plate was then placed on a magnetic block for 1 minute to allow beads to settle and washed with $100\mu\text{L}$ assay buffer twice. $25\mu\text{L}$ detection antibody was added to each well and the plate was incubated in the dark at room temperature for 1 hour. The detection antibody was then removed by placing the plate on a magnetic block and removing the detection antibody by pipetting. $25\mu\text{L}$ streptavidin-PE was added to each well and the plate was incubated in the dark at room temperature for 15 minutes. The SA-PE was not removed and $25\mu\text{L}$ amplification buffer was added to each well. The plate was then incubated in the dark at room temperature for 15 minutes. All liquid was removed from each well using the magnetic block and beads were then suspended in $150\mu\text{L}$ assay buffer before the plate was read using a Luminex MAGPIX instrument (BioRad). Fluorescent signal for blank wells was subtracted from sample values and positive controls were checked as a quality control for the assay.

4.4.8 Statistical Analysis

All data are expressed as mean \pm SEM. Statistical significance was tested for (unless otherwise stated) using an unpaired Student's t-test and F-test with Prism 7 software (GraphPad). $P < 0.05$ was considered significant.

4.5 Results

4.5.1 Viability Assays

RAMP1 KO cells were tested for differences in cell viability compared with PC3 wild type cells. Measurements were taken every 24 hours for a total of 3 days. All clones that were validated with qPCR were selected for viability experiments. After four experimental repeats, it was found that three clones (A7, C1 and D5) showed significant reductions in viability compared with PC3 wild type cells on days 1-3. A7 showed a 32% reduction, C1 a 31% reduction and D5 displayed reduced viability by 41% compared with PC3 wild type cells. CRISPR clones B5, D4 and B12 did not show significant differences in viability on days 1 and 2. B5 and D4 showed reduced viability by 20% and 23% respectively on day 3, but B12 did not show any significant differences from days 1-3 (see Fig 4.9).

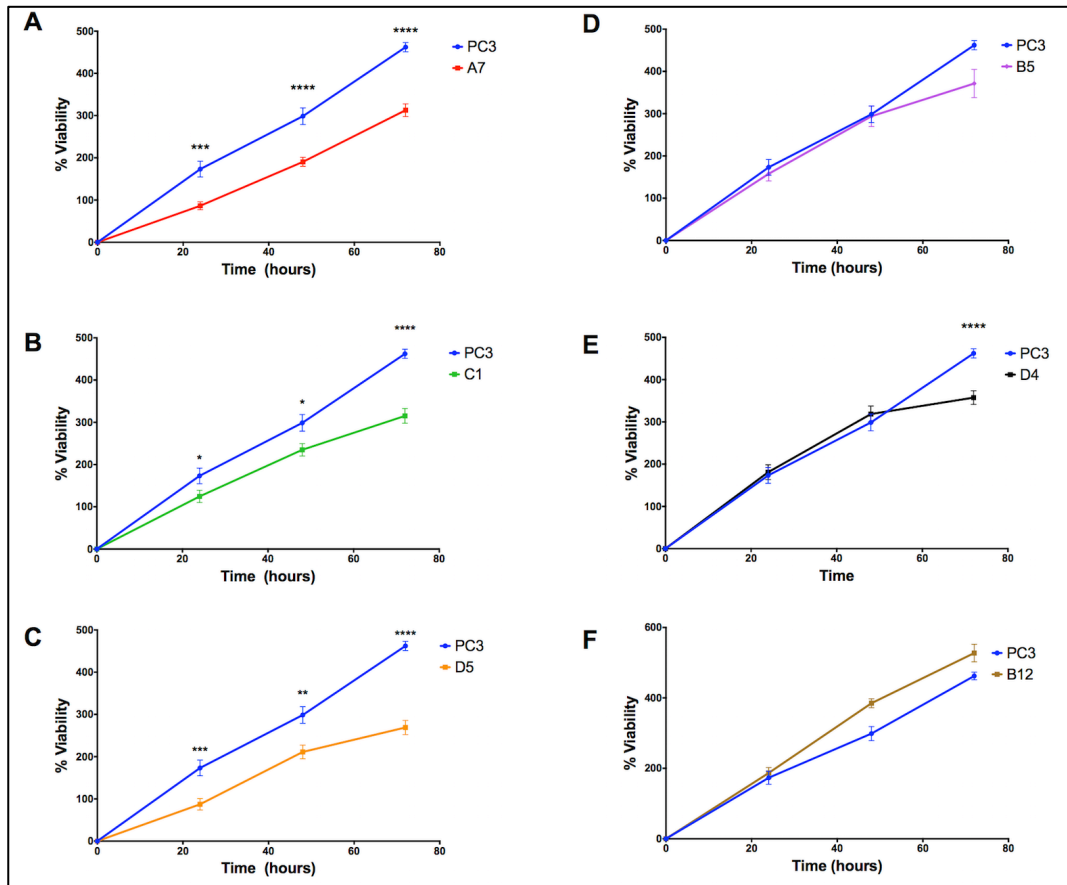


Figure 4.9 Viability assays comparing PC3 wild type and RAMP1 KO cells.

Measurements were taken every 24 hours for 3 days. A) A7 showed 32% reduced viability compared with PC3 controls after 3 days growth ($P = 0.0001$). (B) C1 showed 31% reduced viability ($P = <0.0001$.) (C) D5 showed 41% reduced viability ($P = <0.0001$). (D) B5 showed 20% reduced viability ($P = 0.834$). (E) D4 showed 23% reduced viability ($P = <0.0001$). (F) B12 showed no significant difference in viability compared with PC3 wild type controls. All values are mean \pm SEM, $n=4$. (Students unpaired t -test).

CRISPR Clone	Percentage Difference with PC3 Wild Type
A7	↓32%
C1	↓31%
D5	↓41%
B5	↓20%
D4	↓23%
B12	0%

Table 4.2 Percentage differences in cell viability.

Reductions in viability at Day 3 of different CRISPR clones compared with PC3 wild type cells.

Viability assays were performed on wild type PC3 cells in combination with treatment of 1, 3 or 5 μ M CGRP or Telcagepant (a CGRP antagonist). Viability assays were continued for 5 days and repeated three times resulting in no significant differences in viability between untreated cells and those treated with CGRP or Telcagepant (see Fig 4.10).

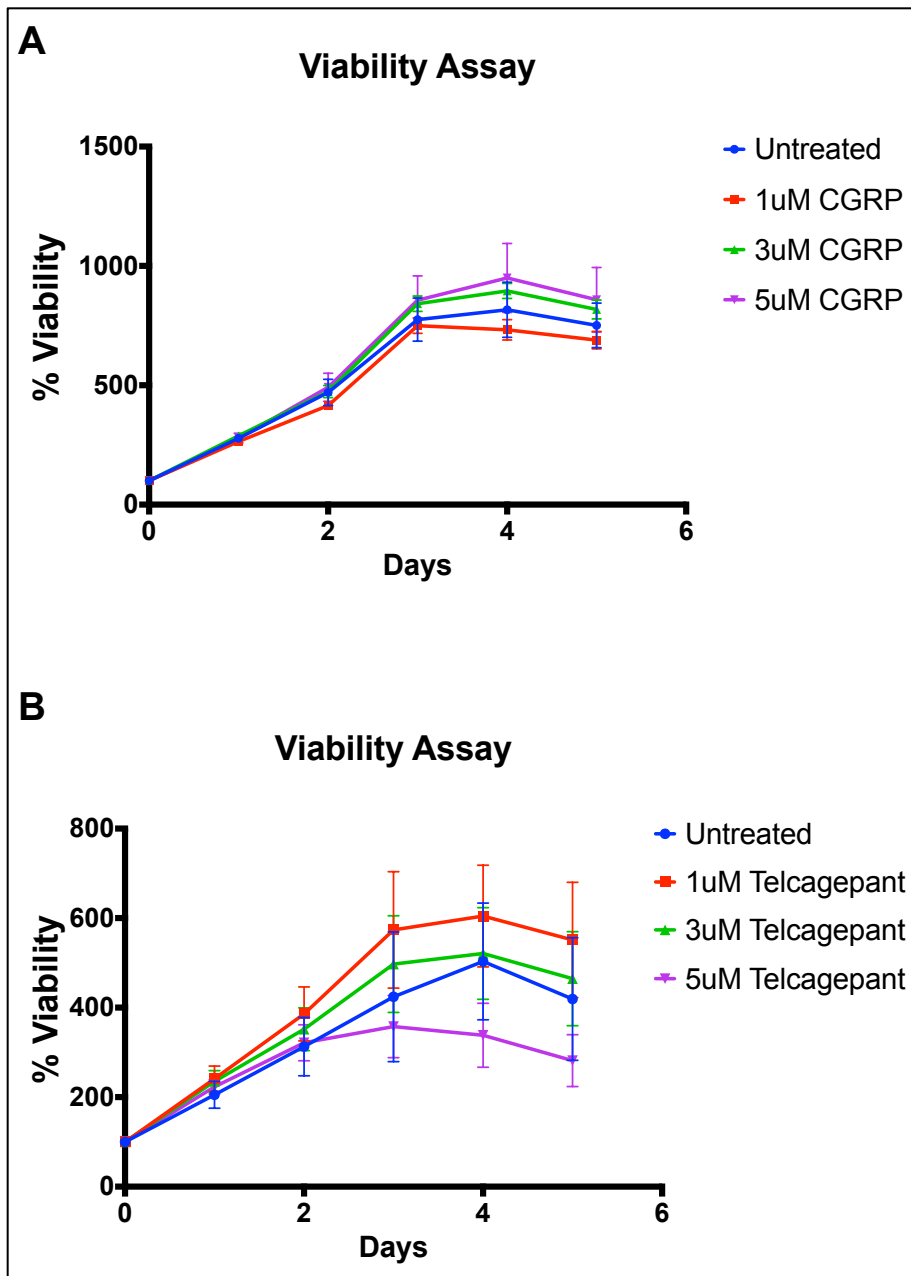


Figure 4.10 CGRP and antagonist cell viability.

Viability assays performed using wild type PC3 cells. Treatment of CGRP or Telcagepant had no significant effect on PC3 cell viability at any time point. All values are mean \pm SEM, n=3. $P > 0.05$, (Students unpaired t-test).

4.5.2 Migration “Scratch” Assays

The ability of RAMP1 KO cells compared with PC3 wild type cells to migrate in culture was measured using a migration “scratch” or “wound healing” assay. All cells were plated in 6 well plates and treated with Mitomycin C for 2 hours to halt proliferation. Scratches were made in the cell monolayer and then images taken at 0 hr and 22 hr time points. These images were analysed using ImageJ MRI Wound Healing tool to calculate the percentage of wound closure in each cell type (see Fig 4.12). After three experimental repeats, it was found that RAMP1 KO clones A7 and C1 appeared to migrate 94% and 54% faster than PC3 wild type cells however RAMP1 KO clone D5 showed no significant difference (see Fig 4.11).

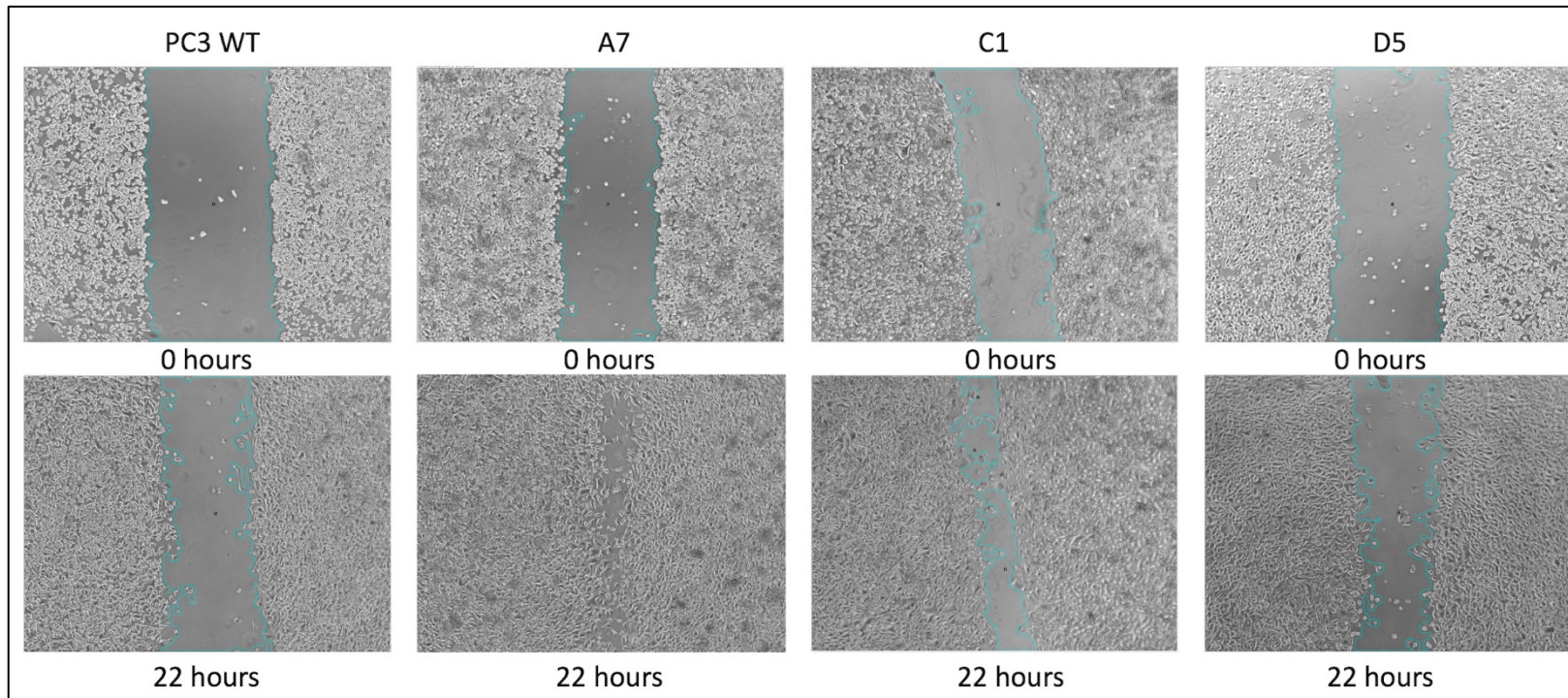


Figure 4.11 Migration (scratch) assay.

Images were taken of "scratches" for PC3 wild type cells and RAMP1 KO clones A7, C1 and D5 at 0 hour and 22 hour time points.

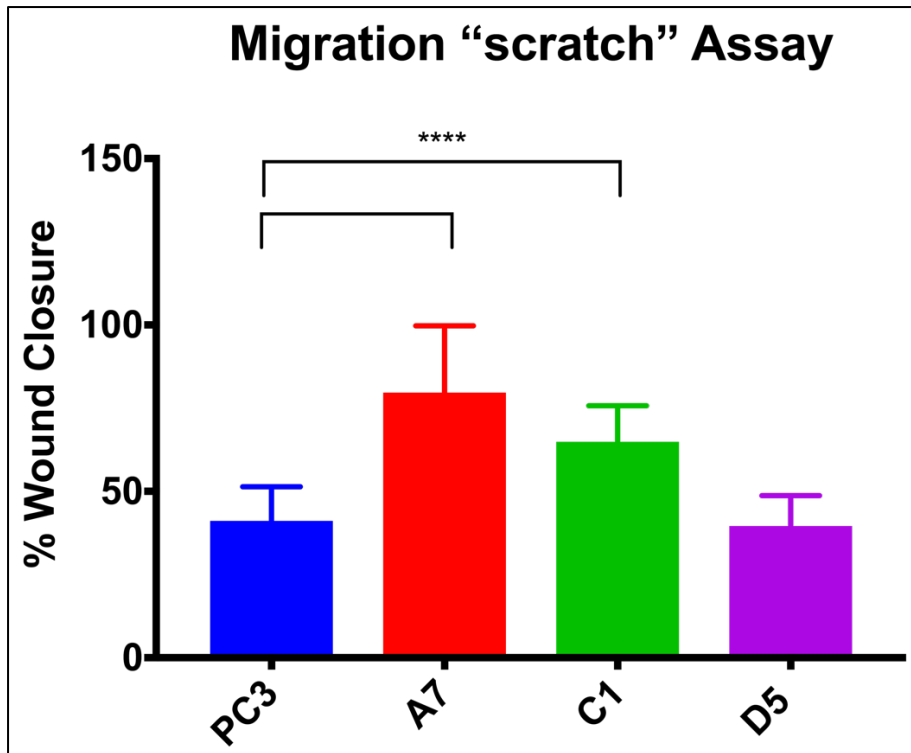


Figure 4.12 ImageJ analysis of migration assay.

ImageJ analysis using MRI Wound Healing software indicates that both RAMP1 KO clones A7 and C1 have an increased rate of wound closure of 94% and 58% respectively compared with PC3 wild type cells ($P = <0.0001$). All values are mean \pm SEM, $n=3$. $P<0.05$, (Students unpaired t-test).

CRISPR Clone	Percentage Difference with PC3 Wild Type
A7	↑94%
C1	↑58%
D5	0%

Table 4.3 Percentage differences in migration.

Percentage of increased migration of different CRISPR clones compared with PC3 wild type cells.

4.5.3 Transwell Invasion Assays

The invasive potential of RAMP1 KO cells was compared with PC3 wild type cells using a Transwell invasion assay. Cells were seeded in Transwell inserts coated with or without Matrigel. Control inserts had no coating and represented the migration of cells over a period of 24 hours. After three experimental repeats, it was found that migration was higher in RAMP1 KO cells when compared with PC3 wild type cells. RAMP1 clones A7, C1 and D5 showed an increase in 4-fold or more in the number of migrated cells compared with PC3 wild type cells (see Fig 4.13). The percentage of invaded cells was calculated from the number of migrated cells through the control insert membrane. This indicated a decrease in invasion in RAMP1 KO cell clones A7, C1 and D5 of 51%, 83% and 83% respectively (see Fig 4.14)

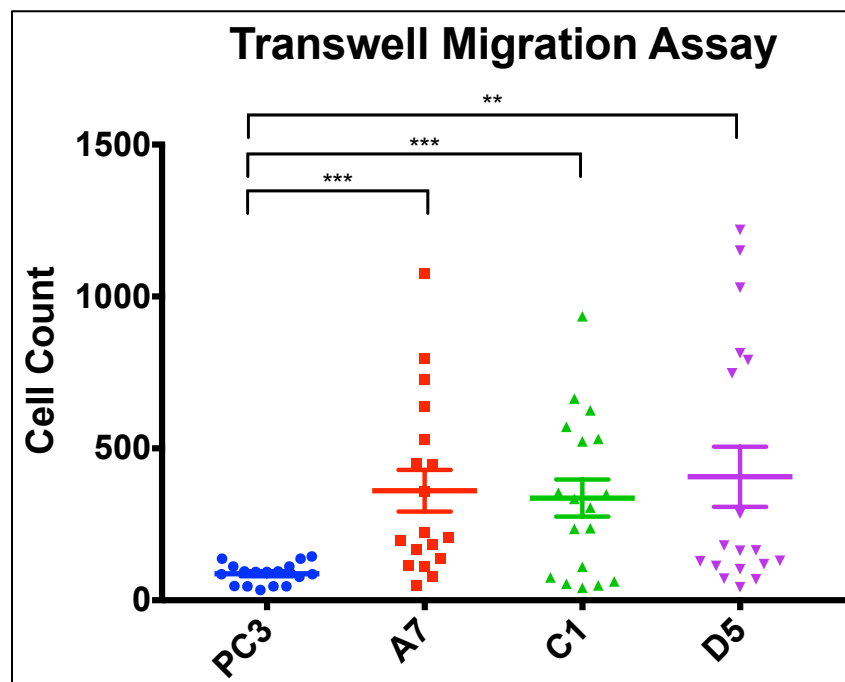


Figure 4.13 Transwell migration assay.

Analysis of number of cells migrating through control Transwell insert membrane shows a four-fold increase in RAMP1 KO clone A7 ($P = 0.003$), a four-fold increase in C1 ($P = 0.03$) and a five-fold increase in clone D5 compared with PC3 wild type cells ($P = 0.009$). All values are mean \pm SEM, $n=3$. (Students unpaired t-test).

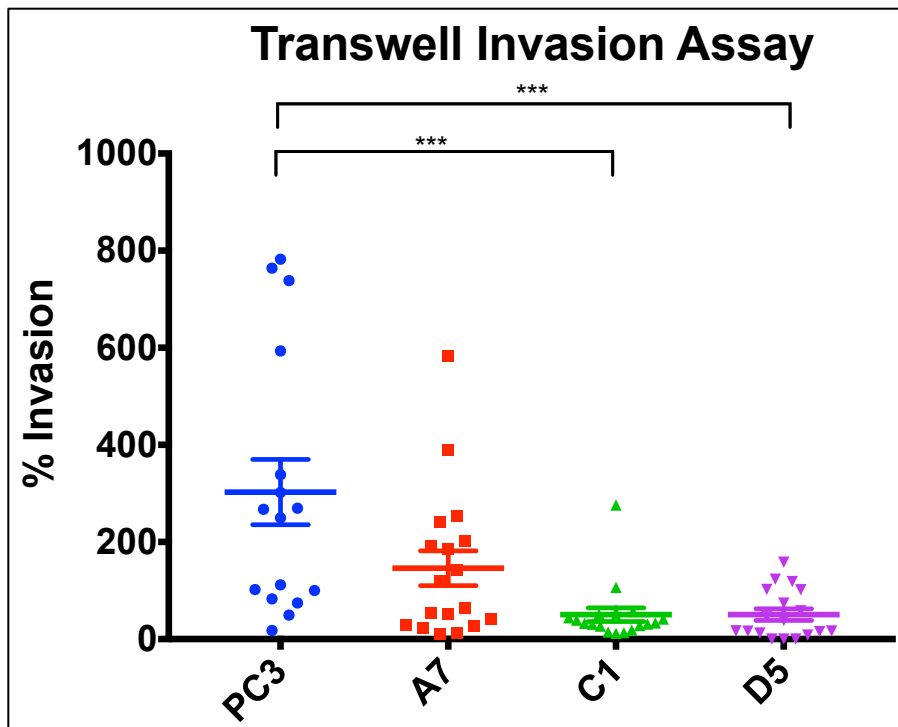


Figure 4.14 Transwell invasion assay.

Percentage of invaded cells was calculated by comparing with number of migrated cells. RAMP1 KO clone A7 showed a 51% decrease in invasion compared with PC3 wild type cells ($P = 0.09$). C1 showed an 83% decrease ($P < 0.0001$) and D5 a 83% decrease compared with PC3 wild type cells ($P = 0.015$). All values are mean \pm SEM, $n=3$. (Mann-Whitney test).

CRISPR Clone	Percentage Difference with PC3 Wild Type	
	Migration	Invasion
A7	↑413%	↓51%
C1	↑385%	↓83%
D5	↑465%	↓83%

Table 4.4 Percentage differences in migration and invasion.

Percentage increases in migration and decreases in invasion of different CRISPR clones compared with PC3 wild type cells.

4.5.4 Colony Formation Assays

The ability of RAMP1 KO cells to form colonies in culture was compared with PC3 wild type cells. Cells were plated in 6 well plates and left to form colonies for 14 days. After fixation and staining (see Fig 4.15) the number of colonies was counted. In case the software miscounted or ignored small colonies the percentage of total area that was positively stained was also calculated. RAMP1 CRISPR clones that showed reduced viability (A7, C1 and D5) were selected for colony formation experiments. After three experimental repeats, it was found that the number of colonies was reduced 44% for A7, 89% for C1 and a 54% reduction was seen in D5 (see Fig 4.16). These reductions were also reflected when measuring the percentage of total area that was positively stained compared with the total area of the well (70% for A7, 96% C1 and D5 78%) (see Fig 4.17).

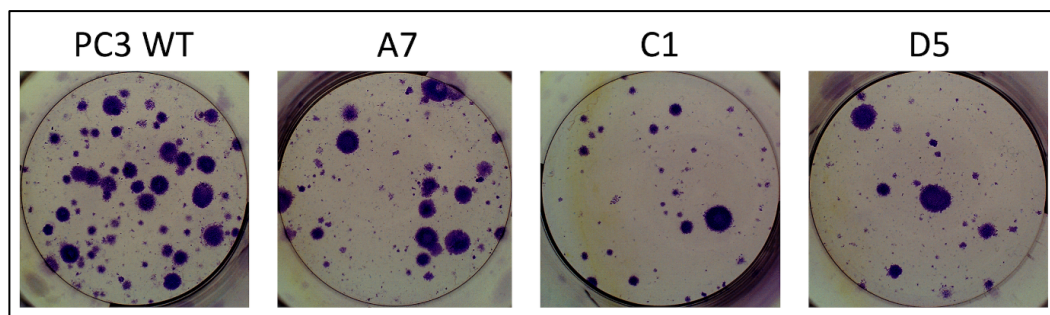


Figure 4.15 Colony formation images

Scanned images of cells stained with crystal violet to show visible differences in colony formation in RAMP1 KO clones (A7, C1, D5) and PC3 wild type cells.

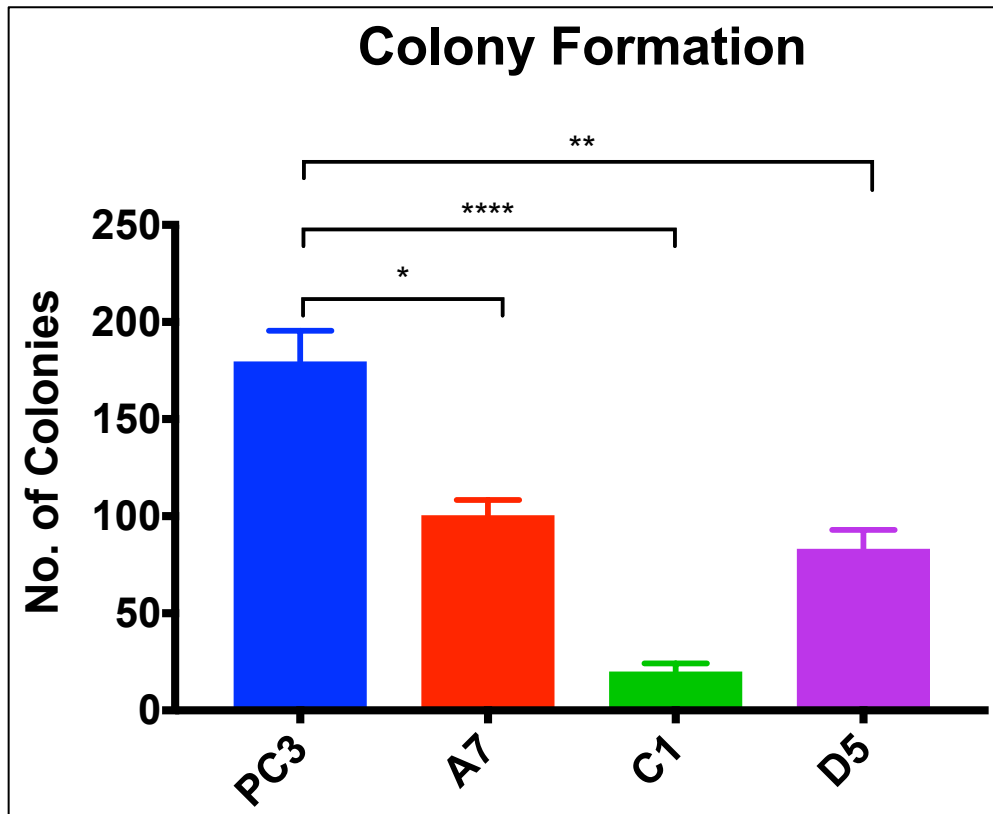


Figure 4.16 Number of colonies in colony formation assay.

Quantification of the total number of colonies indicates that RAMP1 KO clone A7 showed a 44% reduction compared with PC3 wild type cells ($P = 0.02$). 89% reduction was seen in C1 ($P < 0.0001$) and 54% reduction in D5 ($P = 0.015$). All values are mean \pm SEM, $n=3$. (Students unpaired t-test).

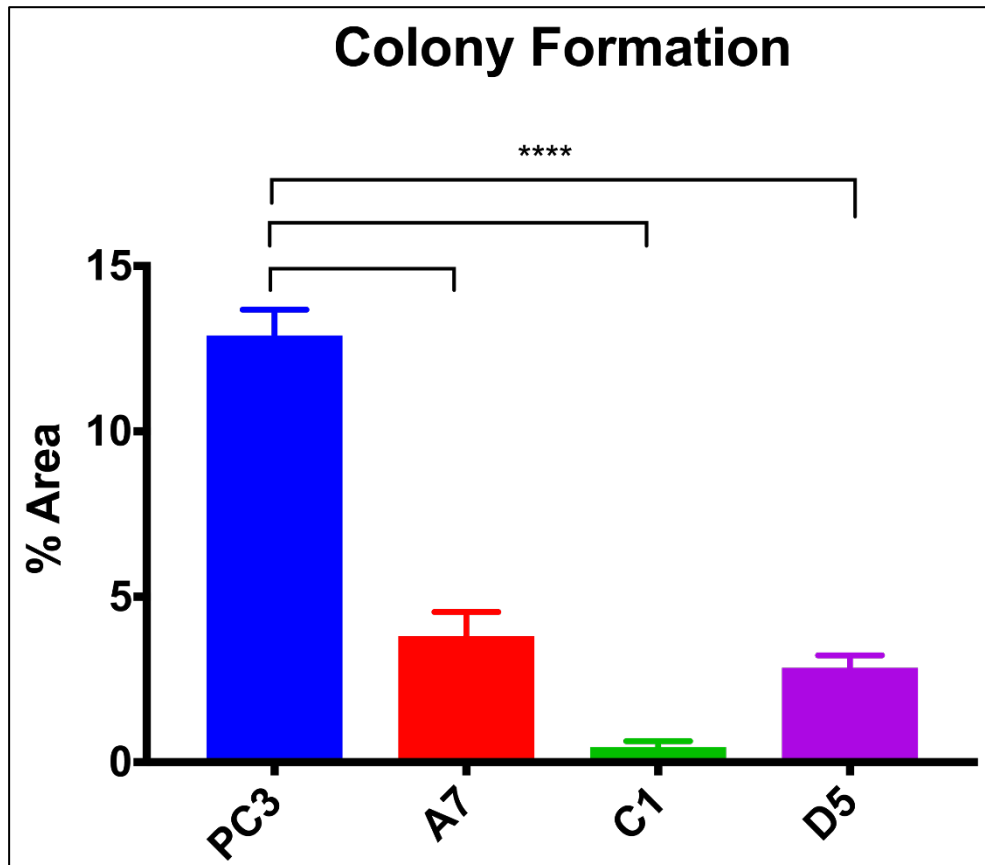


Figure 4.17 Percentage area of colonies in colony formation assay.

Percentage of total area that was positively stained indicates a 70% reduction in A7, a 96% reduction in C1 and a 78% reduction in D5 compared with PC3 wild type cells ($P = <0.0001$). All values are mean \pm SEM, $n=3$. (Students unpaired t-test).

CRISPR Clone	Percentage Difference with PC3 Wild Type	
	Total Number of Colonies	Percentage Total Area
A7	↓44%	↓70%
C1	↓89%	↓96%
D5	↓54%	↓78%

Table 4.5 Percentage differences in colony formation.

Reduction in number of colonies and percentage of total area covered by colonies of different CRISPR clones compared with PC3 wild type cells.

4.5.5 Adhesion Assays

To measure the ability of RAMP1 KO cells to adhere in culture compared with PC3 wild type cells, adhesion assays were performed using fibronectin-coated 96 well plates. Cells were stained with calcein AM prior to adhering. After allowing cells to adhere for 30 minutes, fluorescence was measured. For analysis, wells containing cells that were washed three times (adherent population) were then compared with wells that were not washed (total population) to calculate percentage of adherent cells from the total amount seeded. After three experimental repeats, it was found that there was a 33% reduction in the percentage of adherent cells in RAMP1 CRISPR clone A7 compared with PC3 wild type cells. A 75% reduction was seen in C1 and 40% in D5 (see Fig 4.18).

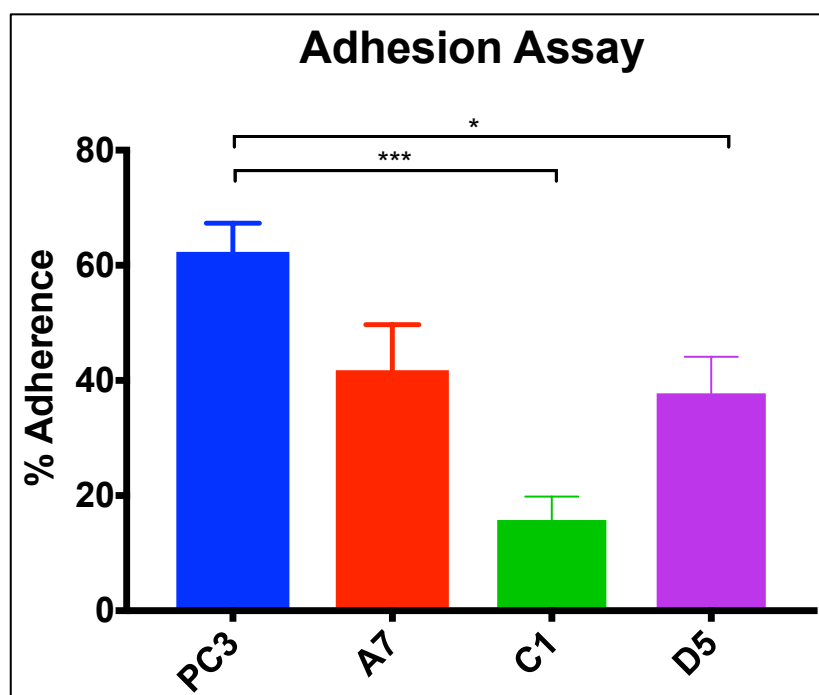


Figure 4.18 Adhesion assay.

Adhesion assay was performed using 3-5 $\mu\text{g}/\text{cm}^2$ fibronectin-coated 96 well plates. A 33% reduction in percentage of adherent cells was seen in RAMP1 CRISPR clone A7 compared with PC3 wild type ($P = 0.117$). A 75% reduction was seen in C1 ($P = 0.0015$)

and a 40% reduction was seen in D5 ($P = 0.02$). All values are mean \pm SEM, $n=3$. (Students unpaired t -test).

CRISPR Clone	Percentage Difference with PC3 Wild Type
A7	↓33%
C1	↓75%
D5	↓40%

Table 4.6 Percentage differences in adhesion.

Reductions in adhesion to fibronectin-coated culture plates of different CRISPR clones compared with PC3 wild type cells.

4.5.6 Apoptosis Assays

To determine apoptosis activity in RAMP1 KO cells compared with PC3 wild type cells, caspase 3/7 activity was measured. To induce apoptosis, cells were serum starved for 48 hours and then caspase 3/7 activity was measured. This was compared with measurements from cells in “unstressed” conditions, grown in complete media. After three experimental repeats, PC3 wild type cells displayed a 70% increase in caspase 3/7 activity after serum starvation. However, no increases in caspase 3/7 activity were seen in RAMP1 KO cells after serum starvation (see Fig 4.19). In unstressed conditions, RAMP1 KO clones A7 and D5 showed increased caspase 3/7 activity of 83% and 88% respectively compared with PC3 wild type cells. RAMP1 KO clone C1 did not show any increases in caspase 3/7 activity in both unstressed and stressed conditions (see Fig 4.19).

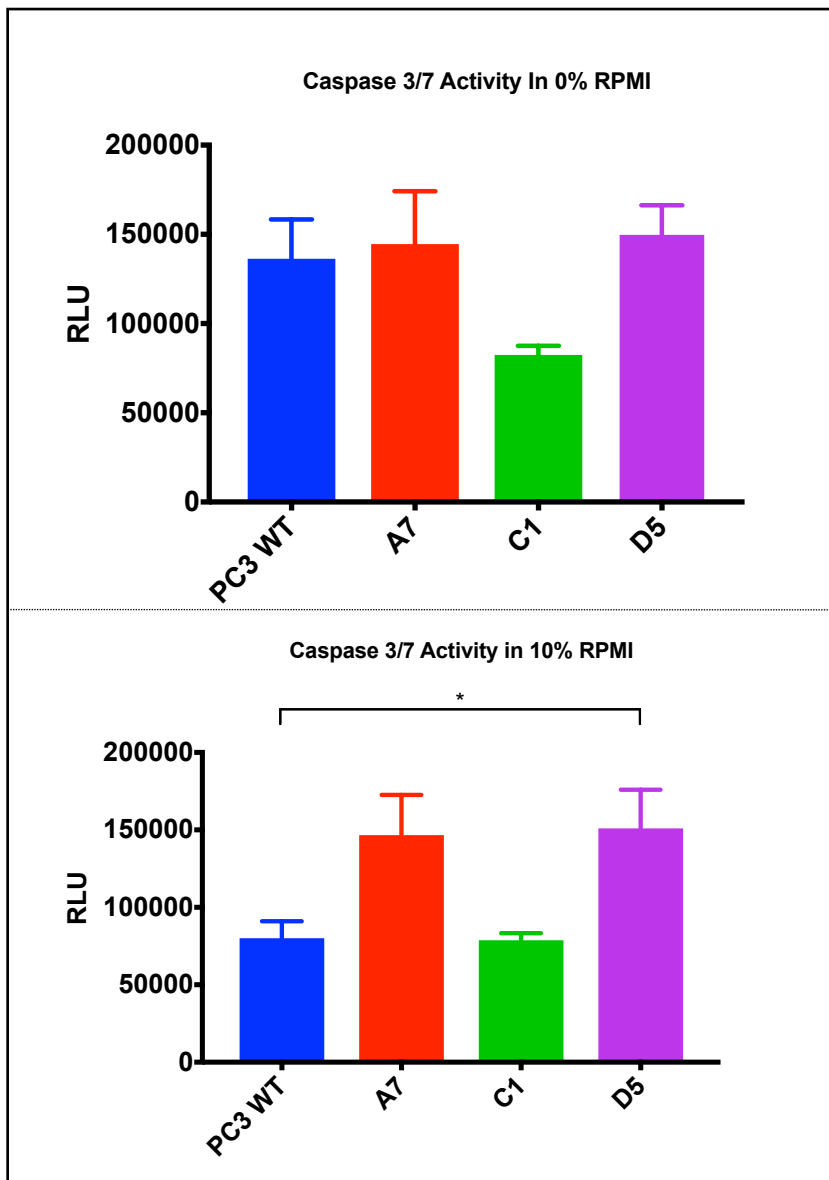


Figure 4.19 Caspase 3/7 activity.

Caspase 3/7 activity in PC3 wild type cells showed a 70% increase after 48 serum starvation ($P = 0.09$). RAMP1 KO clones A7, C1 and D5 showed no difference in activity after serum starvation. In unstressed conditions RAMP1 KO clone A7 showed an 83% increase ($P = 0.06$) and D5 an 88% increase ($P = 0.03$) compared with PC3 wild type controls. CRISPR KO clone C1 showed no significant difference in caspase activity with PC3 wild type cells in unstressed conditions and did not show any increases after serum starvation. All values are mean \pm SEM, $n=3$. (Students unpaired t -test).

CRISPR Clone	Percentage Difference with PC3 Wild Type	
	10% RPMI	0% RPMI
A7	↑83%	0%
C1	↑88%	↓39%
D5	↑88%	0%

Table 4.7 Percentage differences in caspase 3/7 activity.

Percentage differences in caspase activity in both unstressed (10% RPMI) and stressed (serum starvation, 0% RPMI) conditions in different CRISPR clones compared with PC3 wild type cells.

4.5.7 Multiplex Magnetic Bead Assay: Multi-Pathway 9 Plex

Cell lysates for both PC3 wild type and RAMP1 KO clone D5 were tested for the presence of phosphorylated proteins from different signaling ERK1/2 (Thr185/Tyr187), Akt (Ser473), STAT3 (Ser727), JNK (Thr183/Tyr185), p70 S6 kinase (Thr412), NF- κ B (Ser536), STAT5A/B (Tyr694/699), CREB (Ser133), and p38 (Thr180/Tyr182). In all experiments, positive control lysates (unstimulated or stimulated) were used as a quality control for the assay. Three separate protein extractions were performed on each cell type and assayed in triplicate. Significant differences were found in the amount of phosphorylated Akt which was increased in PC3 wild type cell lysates compared to RAMP1 KO (see Fig 4.20.A) ($P = 0.003$). A significant reduction in phosphorylated STAT3 was also found in RAMP1 KO samples compared with PC3 wild type ($P = 0.03$) (see Fig 4.20.B). No significant differences were found in the remaining targets (see Fig 4.21.C-I).

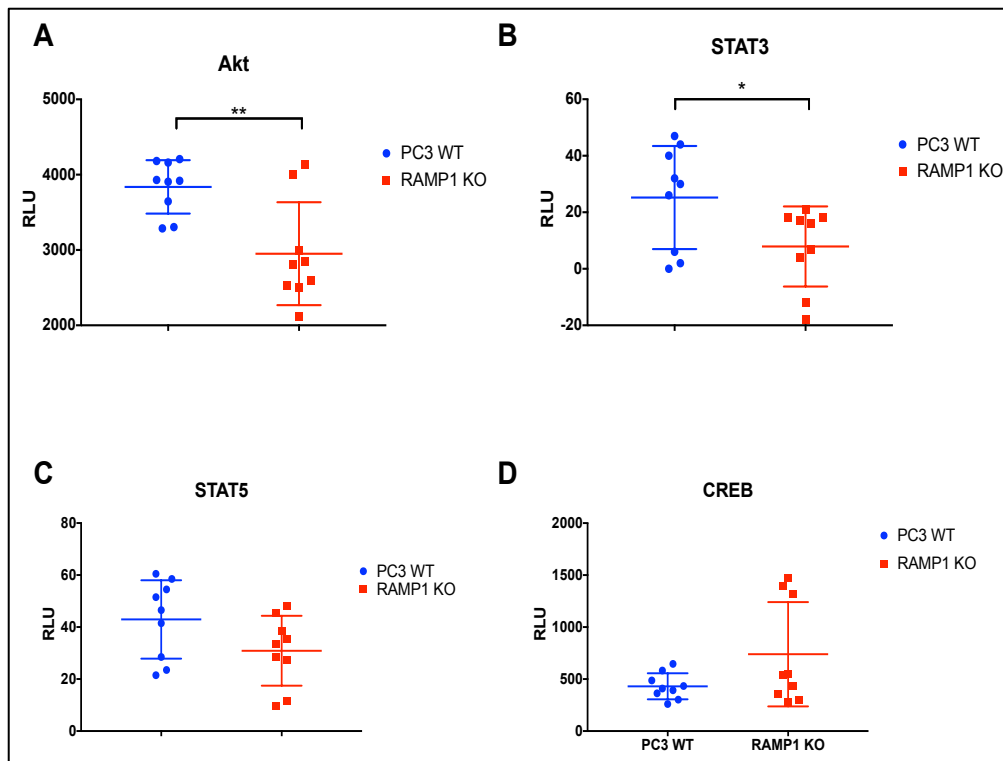


Figure 4.20 Multiplex multi-pathway magnetic bead assay A-D

Multiplex multi-pathway magnetic bead assay. PC3 wild type and RAMP1 KO (clone D5) cell lysates were assayed for different phosphorylated proteins (A) Akt was found to be significantly downregulated in RAMP1 KO samples (P = 0.003). (B) STAT3 was also found to be significantly downregulated in RAMP1 KO samples (P = 0.03). All values are mean ± SEM, n=3. (Students unpaired t-test).

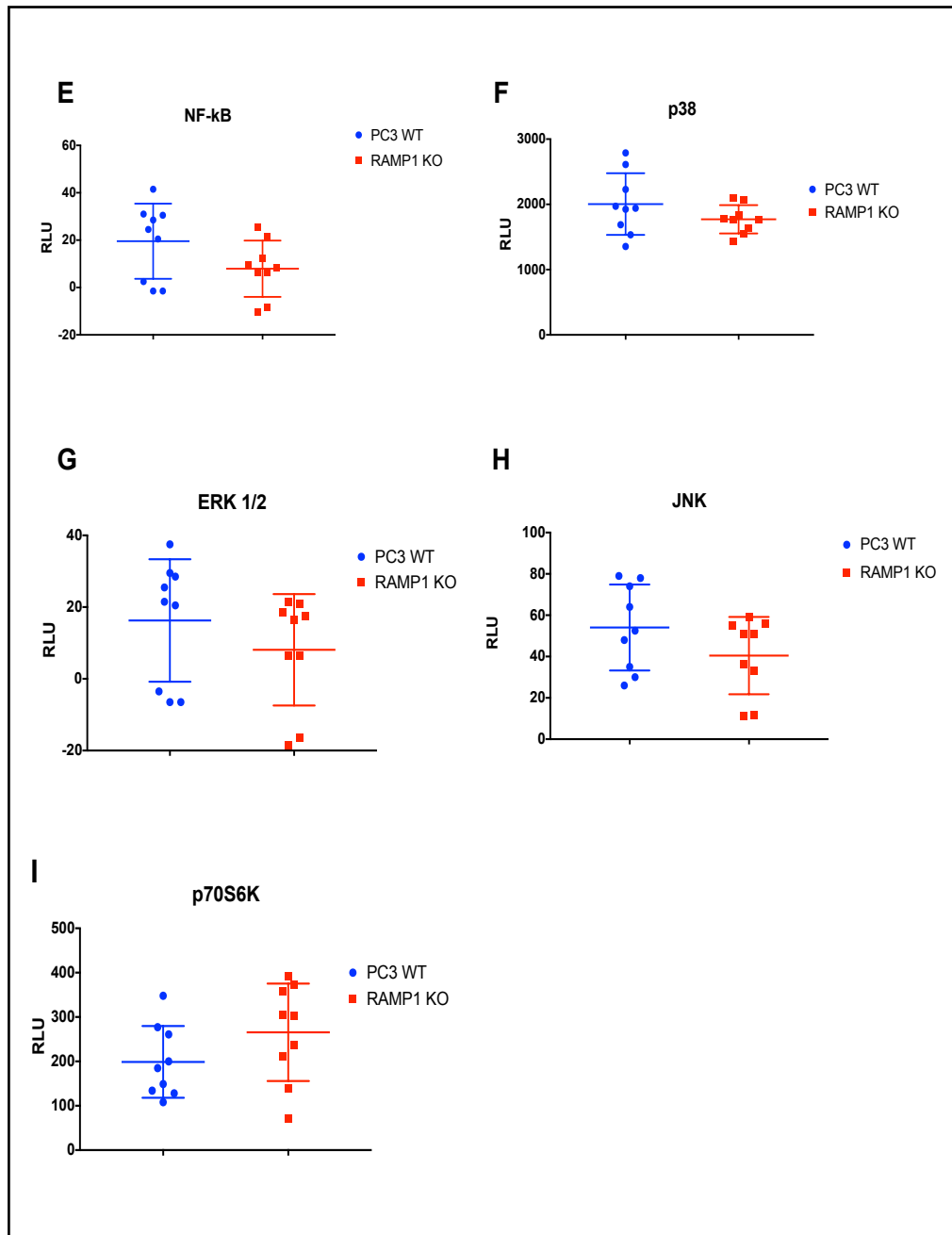


Figure 4.21 Multiplex multi-pathway magnetic bead assay (E-I).

Multiplex multi-pathway magnetic bead assay. PC3 wild type and RAMP1 KO (clone D5) cell lysates were assayed for different phosphorylated proteins (C-I) STAT5, CREB, NF-κB, p38, ERK1/2, JNK and p70S6K were not found to significantly different. All values are mean \pm SEM, n=3. (Students unpaired t-test).

4.6 Discussion

On the whole, the results of these *in vitro* experiments implicate RAMP1 as an important factor in many processes of prostate cancer metastasis including, cell viability/proliferation, evasion of apoptosis, invasion across the ECM and cell colonisation. To assess cell growth and viability, RAMP1 KO and PC3 wild type cells were grown for 3 days and the number of viable cells was counted every 24 hours. RAMP1 deletion appears to affect PC3 cell viability and consequently reduced cell growth over 3 days when compared with wild type cells. The RealTime-Glo™ MT Cell Viability assay allows real-time luminescent measurements of cell viability. This has advantages over standard endpoint proliferation assays which can be time consuming requiring numerous cell counts which can often lead to human error and inaccurate results. Nevertheless, this assay measures the reducing potential of cells which represents the metabolism of the cell. Cellular metabolism has been found to be quite varied and this is therefore a limiting factor of this particular viability assay [185].

Optimisation of the cell viability assay was achieved using PC3 wild type cells as this was also a positive control cell line to compare RAMP1 KO cell viability. All clones tested for cell viability had been previously validated for RAMP1 KO using endpoint and qPCR. Measurements indicated exponential cell growth over three days however, when comparing results of PC3 wild type cells with each RAMP1 KO clone, it was found that three clones showed reduced viability on all time points across days 1-3. This reflected a decreased growth rate in RAMP1 KO clones A7, C1 and D5. RAMP1 KO clones B5, D4 and B12 did not show any significant differences in cell viability apart from B5 and D4 on Day 3. RAMP1 KO clone B12 did not show any significant differences in viability throughout the experiment.

A possible explanation for the differences in viability between these clones could be the editing that has occurred. Editing events may not be identical in each cell and therefore this could lead to differences in cell viability. Efforts were made to investigate differences in gene editing between each clone using Sanger sequencing,

however this technique has a capacity of less than 1,000 base pairs and therefore sequencing the entire RAMP1 gene was impossible. PCR primers were designed to amplify a region targeted by 2 of the 3 guide RNA sequences and these products were sequenced (See previous chapter). The last guide RNA sequence was targeted by PCR primers but these could not be optimised possible due to the GC-rich amplicons. Next generation sequencing has the capacity to sequence entire genes however this is an expensive technique but may be used in the future for further investigations. qPCR analysis showed that B5, D4 and B12 had slightly higher relative expression of 10-30% compared with other CRISPR clones, even though CT values were consistently >35 (see Chapter 3, Section 3.5.5, Table 3.9). This may mean that a RAMP1 expression has been reduced but not completely deleted and therefore cells may retain viability through a knockdown phenotype. Reports of RAMP1 knockdown in both PC3 and LNCaP cells show that cell proliferation was not reduced significantly until day 6 [105]. Experiments could have been run for longer and may have revealed differences in these CRISPR clones at a later time point.

An alternative explanation for the variance seen between different CRISPR clones is that these are simply different cells. Many genetic changes occur in cancer cells and this leads to heterogeneity in tumours which are often described as polyclonal in nature. This means that one population of tumour cells may have different genetic changes compared with host cells and also other cancer cells within the same tumour. This intratumour plasticity is why single biopsies in the clinic can often neglect to reveal the complete tumour heterogeneity and this failure to detect all variants can often lead to drug-resistant populations of cancer cells [186]. It may therefore be argued that *in vitro* study of single cells isolated from a cancer cell line has equal disadvantages when investigating the role of RAMP1 deletion in prostate cancer. This is why multiple CRISPR clones were selected for functional testing in order to eliminate the possibility of “clonal” effects disguising the true effect of RAMP1 deletion. The selected CRISPR clones may not harbour the heterogeneity of a PC3 cell line but single cell analysis has become a popular technique in cancer research due to the interest in “cancer stem” or “tumour-initiating” cells. Prostate cancer tumours can often derive from single cell clones that have reached secondary

sites of metastasis as stated in the “seed and soil” hypothesis [179]. There is further evidence of prostate tumours originating from a small number of “tumour-initiating” stem-like cells [187]. It has been hypothesised that these clones give rise to cancer cells that undergo further genetic mutations ultimately forming a heterogenetic tumour population [188]. Although cancer cell lines are often described as poor models of cancer as they fail to represent the true characteristics of an *in vivo* tumour, they are nonetheless an important tool in identifying key targets in a disease. Heterogeneity is also seen in prostate cancer cell lines and this may also explain the differences in viability seen in different clonal populations. In conclusion, CRISPR clones A7, C1 and D5 all had below 10% expression after qPCR analysis and consistently showed reduced viability. These were selected as RAMP1 KO clones to be further tested for the effect of RAMP1 deletion *in vitro*.

RAMP1 deletion appears to affect PC3 cell viability and also the growth rate of cells over a period of three days however the mechanism by which RAMP1 may be acting remains unknown. In attempt to determine this, wild type PC3 cells were assayed for viability over a course of five days and were treated with either CGRP or Telcagepant (a CGRP antagonist). Previous reports have claimed treatment of CGRP to influence PC3 cell growth at 1 μ M concentrations however this effect was very slight [103]. Experiments here show no significant effect of either CGRP or Telcagepant on PC3 cell viability on any time point measured. This may indicate that CGRP is not responsible for the effect seen in RAMP1 KO cells and their viability.

After a primary tumour has been established, the first step in metastasis will be migration of the cells. In the case of prostate cancer, this is often towards the bone microenvironment and this is reflected in prostate cancer patients where around 90% have incurable bone metastases [189]. To test the effect of RAMP1 deletion on the migratory capacity of PC3 cells, wound healing or “scratch” assays were performed. Interestingly, results show that two different RAMP1 KO clones were migrating (up to 94%) faster than PC3 wild types, whereas one clone showed no significant differences. When migration was measured using a Transwell migration chamber, all RAMP1 KO clones showed faster migration rates when

compared with PC3 wild type cells. It is unclear why deletion of RAMP1 results in increased migration rates however previous studies have found a relationship between RAMP1 and NF- κ B in vascular smooth muscle cell (VSMC) migration. It was found that RAMP1 inhibits migration of these cells through NF- κ B signal pathways [190]. It could be hypothesised that deletion of RAMP1 would remove this inhibitory effect leading to increases in migration in VSMCs and possibly also in PC3 cells but this has not been investigated. Cells are pre-treated with Mitomycin C, a DNA cross-linker which stops cell proliferation and ensures only migration is measured during *in vitro* assays. The dose of mitomycin C was taken from the literature from studies on PC3 cells [184], however it is possible that RAMP1 KO cells were not responsive to this dose and so the proliferation of these cells has been mistaken as migration.

The process of prostate cancer cells migrating away from the primary tumour also requires their invasion into the stroma. Triggering of signalling pathways that control cytoskeletal dynamics allows invading tumour cells to penetrate basement membranes and endothelial walls of vessels to enter the blood stream and metastasise to distant sites [191]. To determine the effect of RAMP1 deletion on PC3 cell invasion, Transwell Matrigel-coated invasion chambers were used *in vitro*. Basement membranes contain extracellular matrix which is composed structural proteins such as laminin, collagen IV and heparin sulphate proteoglycan [177]. Matrigel is an extract taken from a tumour found to contain all of these components and can be used to culture cells and to test the invasive potential of cells [192]. Invasion data was expressed as a percentage of cells invading through the Matrigel-coated membrane relative to cells migrating through the control membrane. Using this recommended calculation, it was found that RAMP1 KO cells had 70-90% reduced invasion compared with PC3 wild type cells. This is an interesting result as migration was not found to be reduced, a process that is often associated with invasion. In order to acquire this ability of invasion, cancer cells must enter epithelial-to-mesenchymal transition (EMT). In many cases this increase in invasion has been coupled with increased migration [193], however recent findings have suggested that migration is not always a characteristic of EMT and that migration and invasion can act separately in EMT-cancer cells *in vitro* and *in vivo* [176].

The next step in metastasis for prostate cancer cells is to colonise distant sites to form secondary tumours. RAMP1 KO cells were tested for the ability of single cells to proliferate into colonies using clonogenic or colony formation assays [194]. Results showed decreases in both number of colonies and the average size of colonies. The latter result may not be surprising as these cells had already shown reduced viability and growth rates. However, RAMP1 KO clearly resulted in fewer cells growing successfully into colonies. This *in vitro* study suggests that the colonisation of PC3 cells is altered by the deletion of RAMP1. An important property of cancer cells during colonisation of secondary sites, is the ability to adhere to extracellular matrix. It was important to also test the adherence of RAMP1 KO cells to more accurately measure the ability of the KO cells to colonise during metastasis. Fibronectin is an extracellular matrix protein that plays a major role in the adhesion of many different cell types [195]. Adhesion was measured by counting the amount of PC3 wild type and RAMP1 KO cells that could adhere to fibronectin-coated culture plates. The percentage of adherent cells was found to be significantly reduced in RAMP1 KO cells by up to 75%. This indicates RAMP1 as an important factor in PC3 cell adherence and colonisation.

Once cancer cells have successfully metastasised and formed secondary tumours they must evade apoptosis. This is described as the third hallmark of cancer [5] and is a characteristic of cancer cells that permits uncontrollable division by “hijacking” cell growth pathways and evade cell death by loss-of-function mutations, most commonly in p53 a prominent regulator of cell death [196] or by upregulating anti-apoptosis proteins such as Bcl-2 and downregulating pro-apoptosis proteins such as Bax and Bak [197]. Caspases are regulators of the apoptosis pathway and often execute cell death. These regulatory factors are often indicative of levels of apoptosis within a cell population [172]. Caspase 3/7 are part of the downstream caspase pathway and are known as effectors or “executioners”. The caspase 3/7 activity was measured in RAMP1 KO cells to see the effect of RAMP1 deletion on cell death. Interestingly, it was found in PC3 wild type cells that caspase 3/7 activity was relatively low until apoptosis was “induced” with a period of serum starvation. This

effect however was not seen in RAMP1 KO cells. In normal conditions, RAMP1 KO clones A7 and D5 showed high caspase levels indicating the number of cells undergoing apoptosis is always relatively high compared with PC3 wild type cells. This high amount of activity did not further increase after a period of serum starvation. A possible explanation is that cells had produced the maximum amount of caspase 3/7 possible during normal conditions as an effect of RAMP1 deletion. RAMP1 KO clone C1, did not show significant differences in caspase 3/7 activity between PC3 wild types in normal conditions, nor any increases in caspase activity after serum starvation. It is unclear why this was found, however if apoptosis is occurring but at an earlier stage, the activity of different caspases may increase (such as caspase 8.) Experiments were attempted to measure early caspase “apoptosis initiators” levels but could not be successfully optimised. Future work may determine the activity of these markers in RAMP1 KO and PC3 wild type cells.

These findings are typically concomitant with the current literature. Studies have used RAMP1 shRNA knockdown to show this decreases proliferation in prostate cancer cells and disrupts the ability of cells to form colonies *in vitro*. However, knockdown of RAMP1 did not, in this case, influence caspase 3 activity [105]. It is therefore possible that complete deletion of RAMP1 is required to alter pro-apoptotic factors in prostate cancer cell lines such as PC3. CGRP has been used to treat prostate cancer cells and increases in migration and invasion have been reported [178, 198]. This sets a precedent for reduced migration or invasion after RAMP1 deletion, however only reductions in invasion were observed in PC3 cells. The increased migration in RAMP1 KO cells confounds previous reports on CGRP as RAMP1 is a key receptor component of CGRP. However, the same studies found no significant effect of CGRP treatment of prostate cancer cell adherence. Therefore, it is possible that RAMP1 may be acting separately from CGRP or through another ligand. In cardiomyocytes, RAMP1 has been reported to exert anti-apoptotic effects during oxidative stress by increasing expression of Bcl-2 [173]. This mechanism was contributed to a CLR-RAMP1 complex and therefore attributed to CGRP. Another hallmark of cancer is the resistance of cancer cells to hypoxia, a condition that can trigger oxidative stress [5]. It is therefore interesting that RAMP1 should be

implicated in inhibiting apoptosis during oxidative stress and the understanding of this role may benefit from further investigations into the effect of RAMP1 in hypoxic conditions.

It is also important to consider the effect of RAMP1 deletion on downstream signalling in prostate cancer cells. Magnetic bead assays have been developed to allow the targeting of multiple analytes within cell lysates. A multi-pathway 9-plex assay was used to investigate which signalling pathways may be regulated by RAMP1. Results showed significant downregulation in Akt and STAT3 phosphorylation in RAMP1 KO samples compared with PC3 wild type. Akt promotes cell survival and is often mutated in cancers, prostate cancer included. PTEN, a negative regulator of Akt signalling is mutated in 60% prostate cancer patients and the PI3K/Akt pathway is associated with androgen signalling too [199, 200]. Previous studies have also shown that depletion of RAMP1 results in downregulation of IL-6 signalling which is known to activate Akt in LNCaP cells [105, 201]. Interestingly, IL-6 is expressed predominantly in androgen insensitive cell lines such as DU145 and PC3 suggesting a link with androgen independence. LNCaP cells do not express IL-6 but do possess IL-6 receptor. Transfection of IL-6 into LNCaP cells results in increased proliferation ($P = <0.05$) and activates STAT3 binding [202]. Results showing that RAMP1 KO in a PC3 cell line cause downregulation of Akt and STAT3 may therefore be due to IL-6 downregulation in RAMP1 KO cells. This should be further investigated as it is clinically relevant to advanced prostate cancer patients. Serum levels of IL-6 are found to be higher in patients with bone metastasis compared with those without [203]. Although no significant differences were found in levels of other phosphorylated protein the data was observed to be slightly different between each extraction of cell lysates. Therefore, further repeats may reveal smaller changes in protein levels between PC3 wild type and RAMP1 KO cells that are not currently significant.

Taken together these findings implicate RAMP1 as an important factor in prostate cancer metastasis at each sequential step, including downstream molecular interactions. Results show that in PC3 cells RAMP1 is required for proliferation and

viability, invasion into the ECM, adhering to the surrounding stroma and promoting the colonisation of individual cells. These findings will be tested *in vivo* to determine the role of RAMP1 in the growth of xenograft tumours and metastatic tumours in the bone microenvironment.

CHAPTER 5: FUNCTIONAL EFFECT OF RAMP1 DELETION *IN VIVO*.

5.1 Introduction

Despite continuing advances in the field of prostate cancer research, this disease remains the most common cancer to affect men in the western world [204]. In the UK, 1 in 8 men will be diagnosed with prostate cancer at some point in their lifetime and 54% of those patients will be aged 70 or over [1]. Although prostate cancer is often considered an age-related disease due to these statistics, over 10% of new cases in the US occur in men aged 55 or less [205]. This early onset of prostate cancer is also often associated with a poorer prognosis compared with older patients [206].

Further investigation into the progression of prostate cancer in both young and old patients relies on realistic models of the disease. There is a limited availability of prostate cancer cell lines that have been successfully immortalised to allow *in vitro* studies of the intracellular mechanisms promoting tumorigenesis [207]. Unfortunately, *in vitro* studies may not reveal useful information on the effect prostate cancer cells have on the tumour microenvironment. To study this mechanism, *in vivo* prostate cancer models are required. Models must have both pathological and physiological relevance to the human disease studied, presenting a challenge in prostate cancer as this disease does not naturally occur in mice (the most frequently used animals for *in vivo* studies) [125]. A tractable method that utilises prostate cancer cell lines in an *in vivo* environment, is the subcutaneous xenograft mouse model. Over 25 years ago this model was developed to use immortalised human cancer cell lines that can be injected subcutaneously into athymic (and therefore immunocompromised) mice. These cells, when injected in combination with reconstituted basement membrane matrix (also known as

Matrigel), can quickly establish subcutaneous tumours that often result in rapid proliferation [208].

Cell lines named LNCaP, PC3 and DU145 have all been previously used for prostate xenograft models, but the PC3 cell line has been described to have a higher metastatic potential than the DU145 and is androgen-independent, unlike LNCaP cells [126, 209]. PC3 cells may therefore best represent the most aggressive stages of prostate cancer where cells lose their androgen dependence and become metastatic [210]. Subcutaneous xenograft models may not mimic prostate cancer in humans very accurately, but they have been previously described as a “first port-of-call” for initial studies that may lead to more advanced *in vivo* models which often have longer time frames and higher costs [138]. Recent uses of subcutaneous PC3 xenograft models have led to important findings, for example treatment with simvastatin has been found to reduce tumour growth and to decrease Akt activity and prostate serum antigen (PSA) levels [211]. This groundwork allows for more in-depth studies into a treatment as a potential therapy in prostate cancer. In addition, a comprehensive review of this technique found that xenograft models can be highly predictive of drug efficacy and activity in humans. Therefore they are important tools for screening cytotoxic chemotherapeutic drugs and can often reveal information regarding pharmacokinetics or drug doses that are clinically relevant [212].

The most common site for xenograft in prostate cancer is a subcutaneous site, usually on the flank. The advantage of this is that injected cancer cells are grown in a site containing nutrients and other circulating factors which are physiologically relevant. Tumour cells are therefore given the opportunity to influence their local environment by acting on host stromal cells and tissue to promote tumour growth. An example of this is the cells ability to promote the production of new blood vessels at the site of injection. Tumours in this location are easy to measure/monitor and the method is generally very reproducible [138]. Nevertheless a key disadvantage of subcutaneous xenograft is that this does not represent the true prostate microenvironment and metastasis is rarely observed, even with highly aggressive cell lines such as PC3 [212]. Nonetheless, prostate cancer is a metastatic disease which

has the capacity to metastasise to bone in more than 80% of prostate cancer cases [213]. Therefore, understanding of disease progression is limited without models that mimic that characteristic *in vivo*.

Orthotopic xenografts of human prostate cancer cell lines such as LNCaP and PC3 result in lymph node, lung and bone metastases when tested in male athymic (nude) mice [135, 136]. This not only permits the study of metastasis of cells from the prostate to distant sites, but also may reveal the behaviour of these cells in a new metastatic niche. A limitation of orthotopic models of prostate cancer metastasis is that the mouse prostate gland differs from human both in structure and composition. The mouse prostate is composed of four distinct lobes unlike the human which is described as having central, peripheral and transitional “zones” which are not clearly demarcated [214]. Mouse prostate glands also have differences in the proportion of basal and neuroendocrine cells with reduced fibromuscular stromal populations [215]. These variations also reflect differing genetic backgrounds of the prostate gland compared with humans and require that care is taken in interpretation of data from mouse orthotopic studies. Orthotopic models are also predominantly relevant to advanced/late stages of human disease therefore restricting what can be learned about prostate cancer as a progressive disease [216].

Alternative mouse models have been developed in attempts to overcome the limitations of xenograft experiments and to improve understanding of mechanisms of metastasis in prostate cancer. Injection of prostate cancer cell lines into the left ventricle of the heart allows cells to circulate with oxygen-rich blood around the body. Targeting the left ventricle, minimises the risk of cells clumping in the lung capillary bed. Intracardiac injection models mimic the later stages of metastasis when tumour cells have left the primary site and are circulating to distant sites to form secondary tumours. The cells can also be labelled with luminescent markers such as luciferase, allowing detection of metastasis in real time compared with previous results solely based on endpoint microdissection of distant metastases [217, 218]. Following intracardiac injection of luciferase-labelled PC3 cells, skeletal metastases can be observed after 1 week and using bioluminescent imaging

techniques, hind limb and craniofacial metastases can be seen to develop progressively [218, 219]. Information potential therapeutic treatments can be achieved by treating at the time of intracardiac injection. This will show how effective the treatment may be at preventing cells from homing to the site of metastasis. Alternatively, treatments that are started after 1 week may show the effect on metastatic growth and the ability of cells to contribute to the metastatic niche.

Results of such experiments are both highly informative and clinically relevant. The intracardiac xenograft model allows the study of prostate cancer cells and their interaction with the bone microenvironment. This complicated relationship can therefore be more deeply explored when compared with *in vitro* studies or modest subcutaneous and orthotopic xenografts. To recapitulate human prostate cancer in a mouse model, transgenic mice can be genetically engineered to present with prostate cancer in the later stages of life. For example, the disruption of target genes such as Nkx3.1 or PTEN results in transgenic mice developing defects that resemble prostate intra-epithelial neoplasia [220, 221]. These mice can then be studied for specific changes or deregulation of genetic pathways that may also be key to prostate cancer progression in humans. Transgenic models still only represent a single mutation contrasting with the true disease which will harbour many different genetic alterations. Practically, this method can also be time-consuming and costly and therefore can be described as a more high-end, complex and involved *in vivo* model.

In an attempt to better represent the genetic landscape of prostate cancer, patient derived xenograft (PDX) are considered a good preclinical model highlighting histological compatibility and harbouring similar gene expression and variants found in prostate tumours [222-224]. Practically, PDX models can be difficult to successfully establish as implantation of patient derived tissues can often be hard to do, especially when orthotopic. The site of implantation must ensure a good vascular supply and production of cytokines or growth factors required for tumour growth [225, 226]. Aggressive tumours are more likely to be engrafted successfully, limiting

PDX models to investigations of late stage disease rather than the early development of prostate cancer [222, 224]. Recent studies have also found that when generating human prostate cancer xenograft models, only 2% of biopsies result in a stable cell line that resembles prostate cancer. The remaining xenografts were found to be B cell lymphomas due to injection of xenografts inadvertently infected with the Epstein Barr virus (EBV) into immunocompromised mice [227]. EBV infects over 90% of humans often lying dormant and asymptomatic in immunocompetent individuals in their B-lymphocytes population. Therefore, care must be taken when selecting patient samples for PDX models.

Recent research into the role of RAMP1 in prostate tumour progression using *in vivo* models is limited but there have been studies using subcutaneous xenografts and the PC3 cell line. Knockdown of RAMP1 was achieved using shRNA in a PC3 cell line and these cells were then injected into male athymic (nude) mice. RAMP1 knockdown tumours were then compared with PC3 cells transfected with a control shRNA which were also injected subcutaneously. After 25 days of tumour growth, reductions of 20-30% in growth were seen in RAMP1 knockdown tumours and after the mice were sacrificed, this reduction was also seen in final tumour weight and size. Subsequent immunohistological staining of the tumour tissues found Ki67 and pHH3 to be decreased in the RAMP1 knockdown tumours [105]. These are markers of proliferation and have been argued to be clinically relevant prognostic markers [167].

There is a gap in the literature with regards to the mechanism by which RAMP1 may promote prostate cancer. RAMP1 is a subcomponent of G protein-coupled receptors for different ligands, one of which is the calcitonin gene-related peptide (CGRP). CGRP has been previously found to be elevated in the sera of prostate cancer patients and can promote migration/invasion of prostate cancer cell lines including PC3 *in vitro* [101, 103]. It would therefore be beneficial to investigate the possible recruitment of CGRP by RAMP1 in the effort of promoting prostate tumour growth *in vivo*. This can be achieved by the use of CGRP antagonists such as Telcagepant (MK-0974) which have been incidentally clinically approved to treat

migraine [228, 229]. Reports have used the crystal structure of the RAMP1/CLR complex to show how Telcagepant can block access to the peptide-binding cleft at the CLR and RAMP1 interface [230]. Although there is a lack of data regarding telcagepant treatment in mice, a dose response of the antagonist will be tested on a mouse cell line to determine whether Telcagepant (or other available CGRP antagonists such as MK-3027 and Olcegepant) are potent on mouse CGRP receptors. This can be achieved using cAMP TR-FRET assays and will also indicate IC50 of the antagonist when inhibiting CGRP, also demonstrating appropriate doses to use for treatments *in vivo*.

If a link exists between CGRP and RAMP1 in prostate tumour growth *in vivo*, then the treatment of Telcagepant may reduce growth of subcutaneous tumours in PC3 wild type xenografts. Subcutaneous xenograft of RAMP1 KO cells will answer the null hypothesis that RAMP1 is not involved in the growth of prostate tumours *in vivo*. RAMP1 KO cells will therefore be subcutaneously injected with Matrigel into male athymic (nude) mice and compared with PC3 wild type xenografts. Treatment with Telcagepant will also aid to elucidate the mechanism by which RAMP1 is affecting tumour growth. Results of this *in vivo* experiment will either validate or repute previous *in vitro* findings.

Histological analysis of tumour sections can be undertaken after the experiment to determine any changes in the expression of proliferative markers. Ki67 is a proliferative marker than can be targeted with immunohistochemistry and will reveal any differences in the number of proliferating cells in tumours from the different experimental groups. CD31 staining can also be used to measure differences in the number of blood vessels as this is an endothelial cell marker.

5.2 Hypothesis:

1. Deletion of RAMP1 in a PC3 cell line reduces subcutaneous tumour growth in male athymic (nude) mice.

2. CGRP is signalling through the RAMP1:CLR complex to promote prostate tumour growth

5.3 Research Aims:

1. To determine if RAMP1 knockout in a PC3 cell line results in reduced tumour growth in a subcutaneous xenograft model.
2. To determine if CGRP is promoting prostate tumour growth *in vivo* via the RAMP1:CLR complex by treating mice with CGRP antagonist Telcagepant (MK-0974) and observing the effects of tumour growth compared with vehicle treated mice.

5.4 Methods and Materials

5.4.1 Mice

Xenograft subcutaneous studies were performed using 6-week-old male BALB/c immunocompromised (athymic nude) mice (Envigo). All procedures complied with the UK Animals (Scientific Procedures) Act 1986 and were reviewed and approved by local Research Ethics Committees of the University of Sheffield under Home Office project licence PF61050A3.

5.4.2 CGRP Antagonist Preparation

Telcagepant (MK-0974) was purchased from MedChem Express. The compound was reconstituted to 10mM in 1mL DMSO and then further diluted with Kolliphor® HS 15: Kollisolv® PEG E 400: dH₂O=1:3:6. 10mg/kg of Telcagepant was used to treat each mouse in 100uL Kolliphor® HS 15: Kollisolv® PEG E 400: dH₂O=1:3:6.

5.4.3 Preparation of Cells for Subcutaneous Injection

PC3 wild type and RAMP1 KO (clone D5) cells were grown in triple layered cell culture flasks (Thermo Fisher) as previously described (see Chapter 2, Section 2.4.1-3). When cells had been grown to 70% confluence, all cells were washed with 100mL PBS (Gibco) per flask once. 10mL TrypLE (Thermo Fisher) was diluted with 10mL PBS and added to each flask, cells were then incubated at 37°C for 5-10 minutes. Cell detachment was then confirmed using an inverted microscope (model?). 20mL PBS was then added to wash cells and the total cell suspension was transferred to a 50mL Falcon tube. Cells were then centrifuged at 1,000 x pm for 5 minutes. Cell pellets were resuspended in 2mL PBS and combined together for cell counting using methods previously described (See Chapter 2, Section 2.4.3). Twice the needed number of cells were resuspended in 50% PBS – 50% Matrigel solution to account for human error. Matrigel solution (Corning) was thawed on ice at 4°C overnight before being used to resuspend cells.

5.4.4 Subcutaneous Injection of Cells

1.5×10^8 PC3 wild type or RAMP1 KO cells were suspended in 50% PBS and 50% Matrigel and kept on ice in 1.5mL eppendorf tubes. 40 mice were divided into four groups. The experimental group contained 20 mice subcutaneously injected with 100 μ L of either PC3 wildtype or RAMP1 KO cell suspension. These two groups of mice were then treated daily with intraperitoneal injections of 10mg/kg 100 μ L Telcagepant (in Kolliphor[®] HS 15: Kollisolv[®] PEG E 400: dH₂O=1:3:6). The vehicle control group contained 20 mice that were also subcutaneously injected with 100 μ L of either PC3 wildtype or RAMP1 KO cell suspensions (5×10^6 in 50% PBS and 50% Matrigel) and these mice were treated daily with intraperitoneal injections of 100 μ L Kolliphor[®] HS 15: Kollisolv[®] PEG E 400: dH₂O=1:3:6.

5.4.5 Measurement of Tumour Growth

After cells had been subcutaneously injected into the mice, tumour growth was monitored twice a week by measuring with vernier callipers (LOUISWARE). Length and width of each tumour was recorded and then volume was calculated as a cylinder using the following formula based upon the assumption that they are cylindrical:

$$V = h\pi(r^2)$$

V = Volume

r = width of tumour ÷ 2

h = length of tumour

Weights were also recorded for each mouse twice a week and monitored for any weight loss of >10%.

5.4.6 Experiment Endpoint

After 2 weeks, the mice were euthanased using Schedule 1 method of concussion and cervical dislocation and then blood was collected. Collection of subcutaneous tumours, liver, spleen, kidneys, heart and lungs was performed and these organs were then weighed and stored in 100% formalin for histological processing by the Skeletal Analysis Laboratory (University of Sheffield.)

5.4.7 Immunohistochemistry Staining of Tumour Tissues

Tumour tissues were sectioned and embedded in paraffin wax and then select slides were stained for haematoxylin and eosin by Mark Kinch from the Skeletal Analysis Laboratory (University of Sheffield).

5.4.8 Ki67 Immunohistochemistry Staining

Slides were first dewaxed by immersion in xylene for 5 minutes twice and then rehydrated for two minutes through a gradient of concentrated ethanol (from 100% to 70%) before being left to rest in distilled water for a minimum of 5 minutes. Antigen retrieval was performed by incubating slides in TE (10mM Tris, 1mM EDTA, PBS pH 8.0) buffer with 0.05% Tween-20 (Fisher Scientific) for 25 minutes in a food steamer (Tesco). Slides were left to cool to room temperature for 20 minutes and were then washed once with TE buffer quickly and then twice for 10 minutes on a plate shaker at 650rpm. Sections were then blocked using 15% goat serum (Vector Laboratories) in TBS-T (50mM Tris, 150mM NaCl, 0.05% Tween-20, PBS, pH 7.6) buffer for 1 hour at room temperature in an immunotray. Slides were then incubated with Ki67 anti-human rabbit monoclonal antibody (AbCam) diluted in blocking buffer 1:250 for one hour at room temperature in an immunotray.

Slides were then washed three times in TBS buffer for 5 minutes each on a plate shaker at 650rpm. Slides were next incubated with a goat anti-rabbit IgG HRP conjugated secondary antibody (Dako) diluted in blocking serum 1:150 for 30 minutes at room temperature in an immunotray. Slides were then washed in TBS buffer three times for 5 minutes each on a plate shaker at 650rpm. Slides were then incubated in an avidin-biotin substrate diluted in TBS buffer (Vector Laboratories) for 30 minutes at room temperature in an immunotray. Slides were then washed three times in TBS buffer for 5 minutes each on a plate shaker at 650rpm. Slides were then incubated with a DAB solution (Vector Laboratories) for 2 minutes each and then DAB was inactivated by washing the slides with distilled water. Slides were continually rinsed in distilled water for a minimum of 5 minutes and then counterstained with haematoxylin for 20 seconds. Slides were dehydrated through increasing concentrations of ethanol (from 70% to 100%) for 2 minutes and then incubated in xylene twice for 5 minutes. Slides were then mounted with coverslips using DPX mounting medium. Slides were scanned using a Panoramic 250 Flash III

slide scanning system (3DHISTECH) and percentage of positively stained cells was calculated and analysed using QuPath v0.1.2 software [231].

5.4.9 CD31 Immunohistochemistry Staining

Slides were first dewaxed by immersion in xylene for 5 minutes twice and then rehydrated for 30 seconds through a gradient of concentrated ethanol (from 100% to 70%) before being left to rest in distilled water for a minimum of 5 minutes. Antigen retrieval was achieved by heating 1X citrate buffer (AbCam) pH 6.0 to 80°C in a PT module (Thermo Scientific). Slides were then added to the citrate buffer and incubated for 25 minutes at 95°C. After cooling slides were rinsed in distilled water for a minimum of five minutes. Slides were then blocked for endogenous peroxidases using 3% hydrogen peroxidase in distilled water (Sigma) for 20 minutes. Slides were then rinsed with distilled water for five minutes on a shaker at 550 rpm. Sections were outlined using a PAP pen and blocked with 15% rabbit serum in T-BST (Vector Laboratories) for 30 minutes at room temperature in an immunotray. A monoclonal rat anti-mouse CD31 primary antibody (Strattech) was diluted 1:50 in TBS and slides were incubated overnight at 4°C in an immunotray.

Slides were then washed three times on a shaker at 550 rpm in TBS-T before being incubated with a biotinylated anti-rat secondary antibody diluted 1:400 in block for 30 minutes at room temperature in an immunotray. Slides were then washed for 10 minutes in PBS on a shaker at 550 rpm and then incubated with an avidin-biotin substrate (Vector Laboratories) diluted in TBS for 30 minutes at room temperature in an immunotray. Slides were then washed again in PBS for 5 minutes on a shaker at 550 rpm. Impact DAB Eq (Vector Laboratories) was then added to the slides and incubated at room temperature for 10 minutes in the dark. Slides were then washed twice in PBS for 5 minutes on a shaker at 550 rpm. Slides were counterstained with haematoxylin for 30 seconds and rinsed with distilled water. Slides were dehydrated through increasing concentrations of ethanol (from 70% to 100%) for 2 minutes and then incubated in xylene twice for 5 minutes. Slides were then mounted with coverslips using DPX mounting medium. Slides were scanned

using a Panoramic 250 Flash III slide scanning system (3DHISTECH) and analysed using ImageJ software.

5.4.10 ImageJ Analysis of CD31 Staining

Slide images were opened in QuPath v0.1.2 software and regions of interest (ROIs) were chosen at random for each tumour at a magnification of 3.5x. Due to large differences in tumour size only one or two ROIs were required for RAMP1 KO tumours to include the entire section. Six different ROIs were drawn for larger wild type PC3 tumours. These were then exported as TIFF files to ImageJ for analysis. Colour thresholds were set to exclude all blue (haematoxylin staining) sections and highlight brown staining. Thresholds were adjusted to exclude non-specific staining using a section with the highest amount of background and then these thresholds were used for all tumours sections (see Fig 5.2). Images were then converted to 8-bit and the Analyse Particles function was used with the following settings (see Fig 5.1.) to generate “masks” of areas of staining.

Mask images were then saved for all ROIs for each tumour and compressed into a stack of images for analysis. All slides in the stack were then measured for area fraction, giving a percentage value for the area of positive staining for each ROI. These values were then compiled using Graphpad Prism.

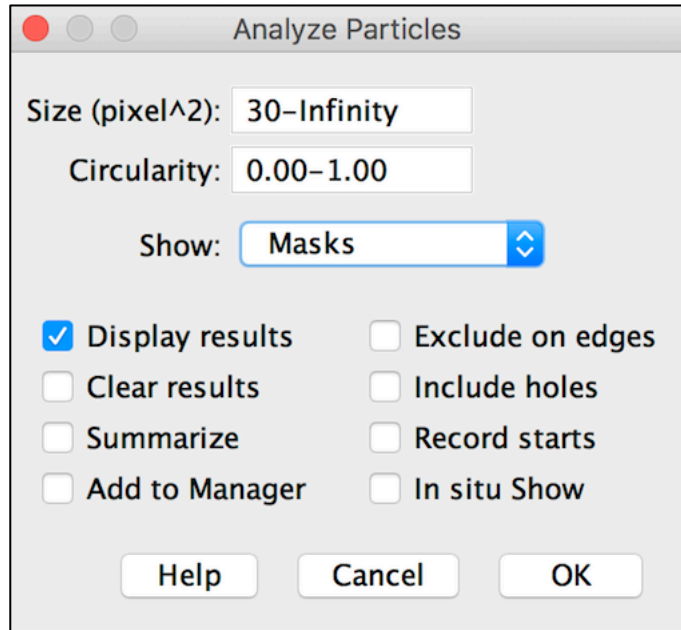


Figure 5.1 ImageJ analysis settings

Screenshot of settings used to analyse particles. Pixel size was increased to 30 to exclude small particles resulting from background non-specific staining.

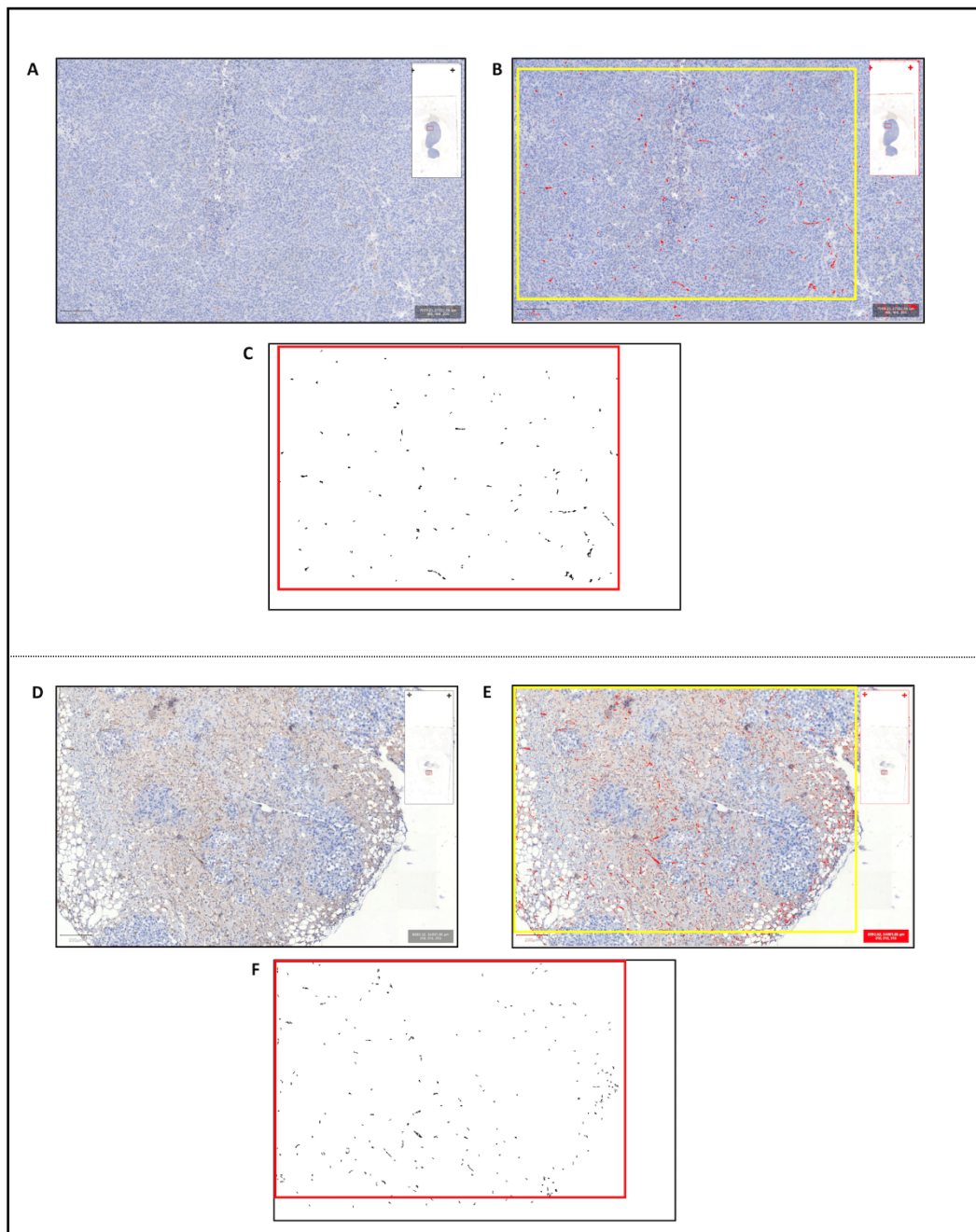


Figure 5.2 ImageJ analysis for CD31 IHC staining.

ImageJ analysis of CD31 positive staining. TIFF files of ROI were exported to Image J for wild type PC3 (A-C) and RAMP1 KO (D-E). Colour thresholds were set and a region for analysis was drawn to exclude scale bars (B & E). 8-bit images were then analysed for particles larger than 30 pixels and these images were measured for percentage area of staining.

5.4.11 cAMP LANCE TR-FRET Assays

Measurements of cAMP activity were performed using methods as previously described (see Chapter 2, Section 2.4.15). Forskolin dose response curves were generated to optimize cell density of cell lines. Panc02 cells were found to result in the largest linear range when adding 500 cells to each well (see Fig 5.3). A dose response of CGRP was then performed (see Fig 5.4) to calculate the IC50 and this dose was used for assays testing the inhibitory effect of CGRP antagonists: Telcagepant, MK-3207 and Olcegepant. CGRP antagonist dose responses were performed using concentrations ranging from 10 μ M to 10pM at every log. Data was plotted using Graphpad Prism 7 software in a non-linear four parametric curve.

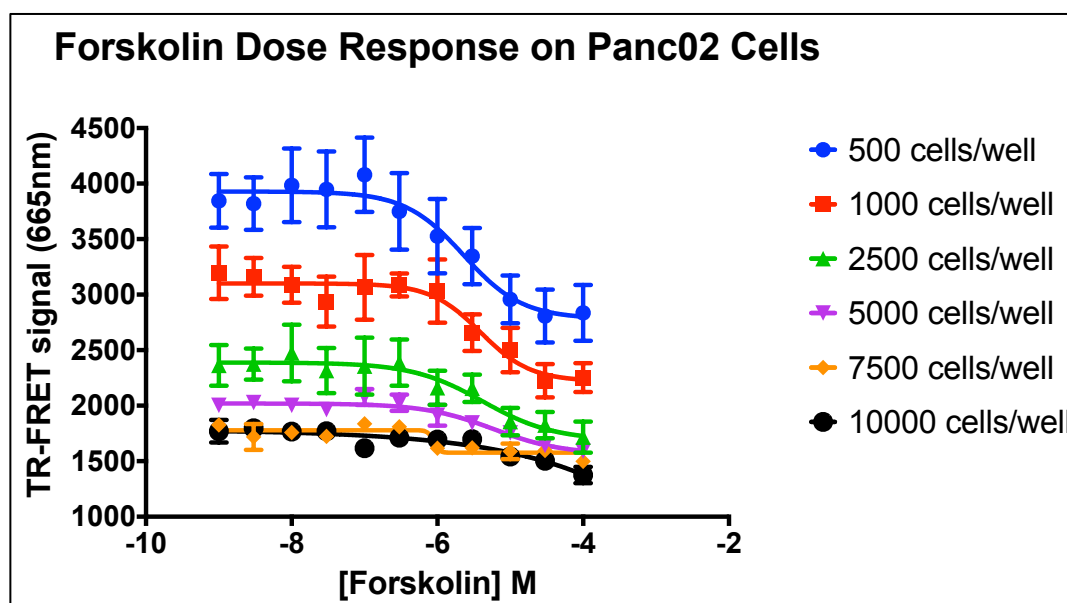


Figure 5.3 Forskolin dose response on Panc02 cells.

Dose response of forskolin using different densities of Panc02 cells. 500 cells per well (blue) was chosen as the optimal density giving the widest linear range. All values are mean \pm SEM, n=3.

Best Fit Values	500 cells	1000 cells	2500 cells	5000 cells	7500 cells	10,000 cells
Bottom	2783	2220	1687	1561	1576	-
Top	3929	3101	2389	2020	1779	1784
Log IC50	-5.64	-5.408	-5.376	-5.233	-	-
Hill Slope	-1.077	-1.263	-0.8908	-0.9111	-	-0.2931
IC50	2.29e-06	3.91e-06	4.20e-06	5.84e-06	-	-
Span	1146	880.8	701.5	458.2	202.9	-

Table 5.1 Best fit values for forskolin curves.

Best fit values for each cell density show that 500 cells per well gives that highest “span” compared to other cell densities and therefore the widest linear range.

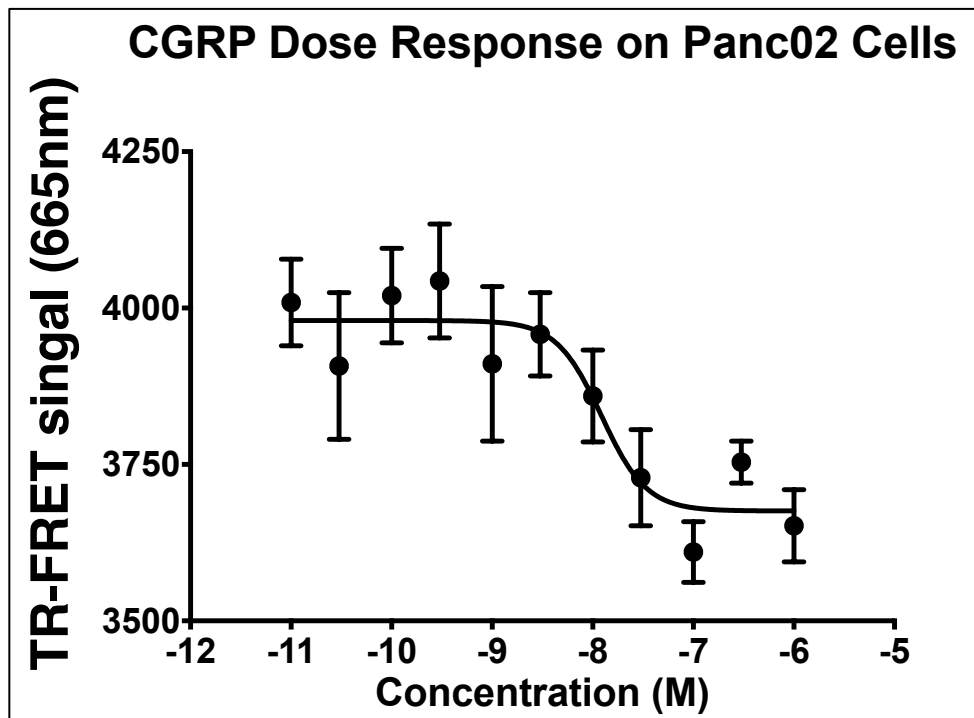


Figure 5.4 CGRP dose response on Panc02 cells

Dose response of CGRP on Panc02 cells shows a dose-dependent production of cAMP.

All values are mean \pm SEM, n=3.

Best Fit Values	CGRP
Bottom	3676
Top	3980
Log IC50	-7.913
Hill Slope	-1.938
IC50	1.22e-08
Span	304.4

Table 5.2 Best fit values for CGRP curve.

Best fit values for CGRP dose response shows a low linear range compared with forskolin dose responses and an IC50 of 12nM.

5.4.12 Statistical Analysis

All data are expressed as mean \pm SEM. Statistical significance was tested for (unless otherwise stated) using an unpaired Student's t-test and F-test with Prism 7 software (GraphPad). P <0.05 was considered significant. Values of best fit were generated for dose response curves (see Tables 5.1 & 5.2).

5.5 Results

5.5.1 Tumour Development

Measurements of tumour volume were performed twice weekly using callipers and were then plotted for each time point to see the growth of tumours from 72 hours post-injection (to allow tumours time to establish and Matrigel to dissolve) until the last day of measurement before the. RAMP1 KO tumours were found to be significantly smaller than PC3 wild type tumours at all time points (see Fig 5.5.) This result was also reflected in tumour mass, measured at the end of the experiment. There were significant reductions in the size and weight of the RAMP1 KO tumours compared with PC3 wild type (see Fig 5.6).

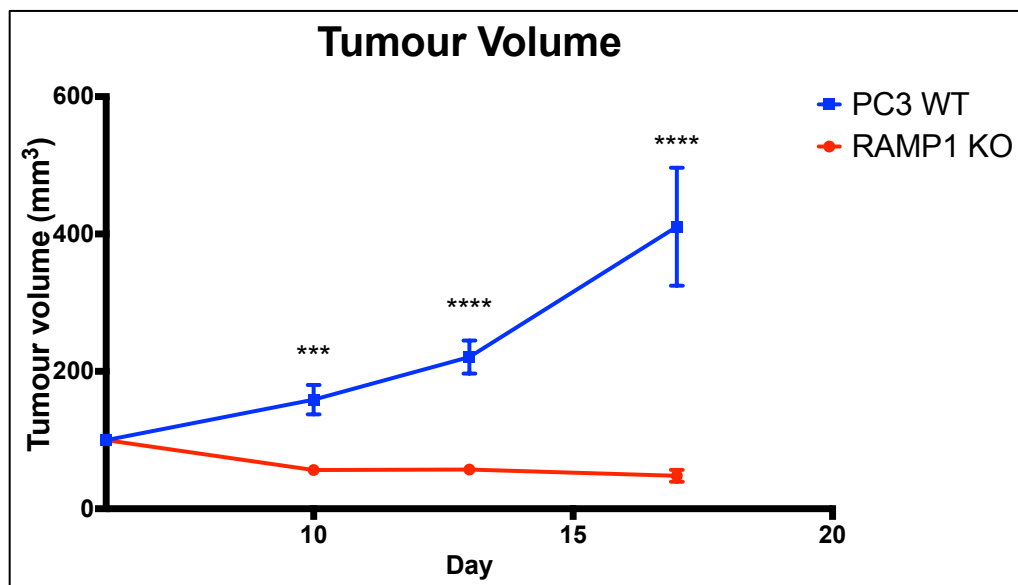


Figure 5.5 Tumour volume measurements.

Tumour volume of PC3 wild type and RAMP1 KO tumours. RAMP1 KO tumours showed significant decreases in tumour volume across all time points ($P = <0.0001$). All values are mean \pm SEM, WT $n=8$, KO $n=10$. (Students unpaired t-test).

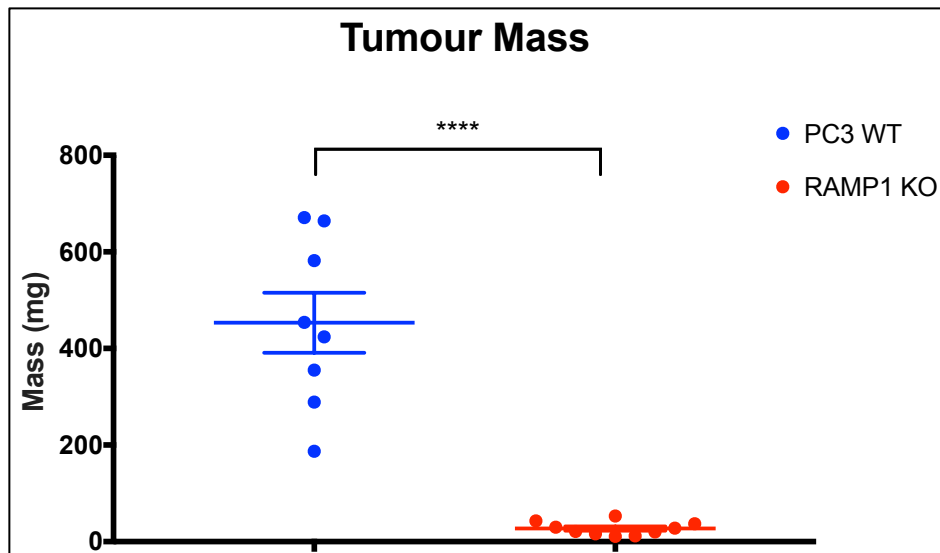


Figure 5.6 Tumour mass measurements.

Tumour mass was calculated after dissection of tumours at the end of the experiment. A significant reduction in tumour mass was seen in RAMP1 KO tumours compared with PC3 wild type. All values are mean \pm SEM, WT n=8, KO n=10. (Students unpaired t-test).

Comparison of tumour volumes between groups treated with 10mg/kg Telcagepant and groups treated with a vehicle control showed no significant differences in both PC3 wild type and RAMP1 KO tumours (see Fig 5.7). However, on Day 17, a slight separation of tumour growth could be observed between PC3 wild type treatment and vehicle control groups. This was also reflected in tumour mass which was calculated after dissection of tumours at the end of the experiment (see Fig 5.8). Endpoint liver mass was also measured in all groups and was seen to be significantly decreased in both treatment and control PC3 wild type groups compared with treatment and control RAMP1 KO groups (see Fig 5.9). However, differences in liver mass were also reflected in the total weight of the mice (see Fig 5.10).

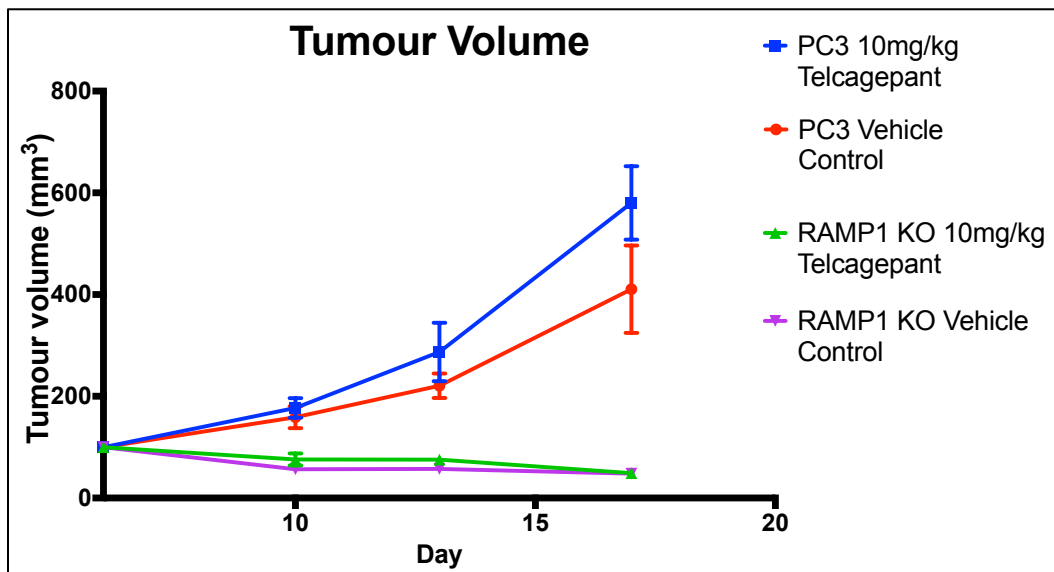


Figure 5.7 Tumour volume measurements for all experimental groups.

Tumour volume of treatment and vehicle control groups for both PC3 wild type and RAMP1 KO tumours. No significant differences were found in tumour volume between treatment and control groups for either PC3 wild type or RAMP1 KO. A slight separation of PC3 treated and control groups was observed on Day 17. All values are mean \pm SEM, WT control n=8, KO control n=10 WT treatment n=8, KO treatment n=9. (Students unpaired t-test).

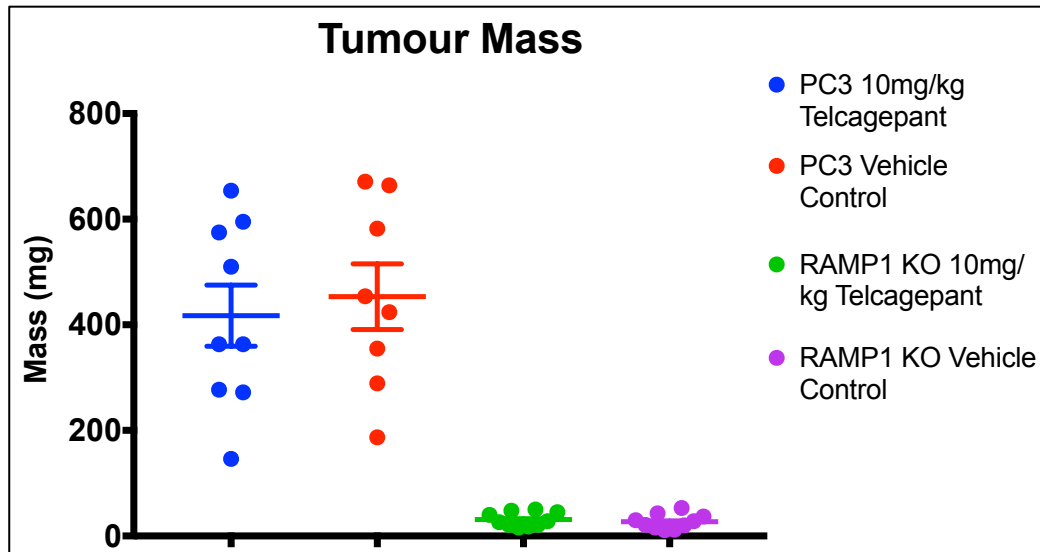


Figure 5.8 Tumour mass measurements for all experimental groups.

Tumour mass of treatment and vehicle control groups for both PC3 wild type and RAMP1 KO tumours. No significant differences were found in tumour mass between treatment and control groups for either PC3 wild type or RAMP1 KO.

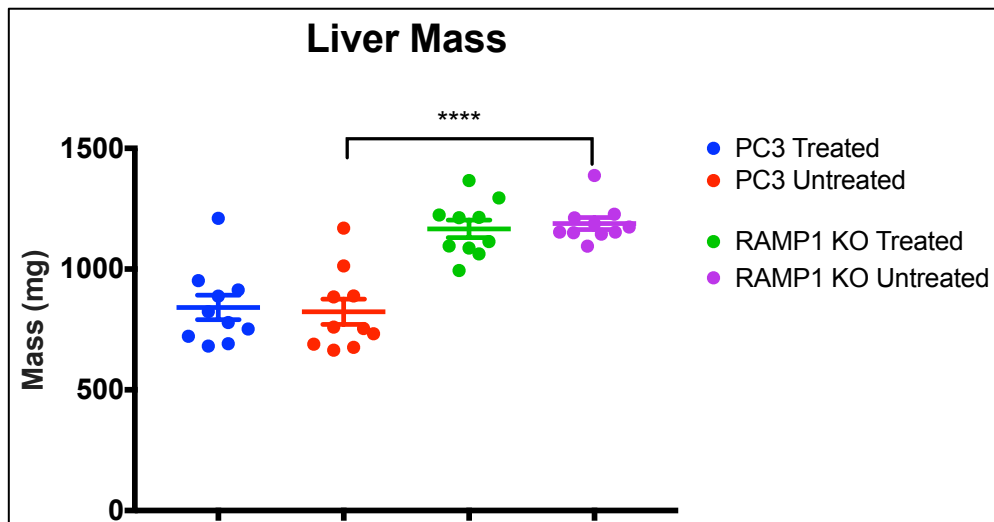


Figure 5.9 Endpoint liver mass measurements for all experimental groups.

Liver mass for treatment and vehicle control groups for both PC3 wild type and RAMP1 KO tumours. Significant decreases in liver mass was seen for PC3 wild type tumours (both treatment and control groups) when compared with RAMP1 KO ($P < 0.0001$). All values are mean \pm SEM, WT control $n=8$, KO control $n=10$ WT treatment $n=8$, KO treatment $n=9$. (Students unpaired t -test).

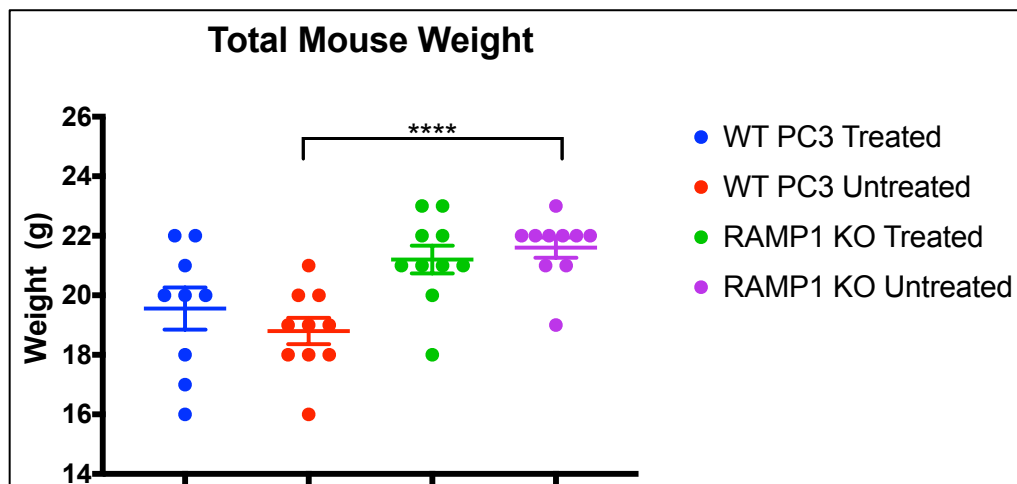


Figure 5.10 Endpoint total mice weights for all experimental groups

Total mouse weights for treatment and vehicle control groups for both mice injected with PC3 wild type and RAMP1 KO cells. Significant decreases in weight were seen between PC3 wild type and RAMP1 KO groups ($P < 0.0001$). All values are mean \pm SEM, WT control $n=8$, KO control $n=10$ WT treatment $n=8$, KO treatment $n=9$. (Students unpaired t -test).

5.5.2 Immunohistochemistry

Staining of tumour sections with haematoxylin and eosin resulted in observed differences in structure between PC3 wild type and RAMP1 KO tumours. PC3 wild type tumours were much larger than RAMP1 KO and showed evidence of necrotic lesions in the largest tumours (see Fig 5.11 & 5.12.) These lesions were not found in any RAMP1 KO tumours, which appeared much less dense in structure and sections showed variation in tissue types including fat and muscle whereas PC3 wild type tumours were much more homogenous. Many PC3 wild type tumours showed increased development of blood vessels both within the tumour tissue and towards the surface of the dermis. Blood vessels were also observed in RAMP1 KO tumours but not as often and in lower numbers (see Fig 5.13), however quantification with CD31 marker showed this not to be the case. Tumour sections were also stained to target Ki67, a proliferative marker (see Fig 5.14). No significant differences in the positivity of Ki67 stained cells were observed between PC3 wild type and RAMP1 KO tumours (see Fig 5.15).

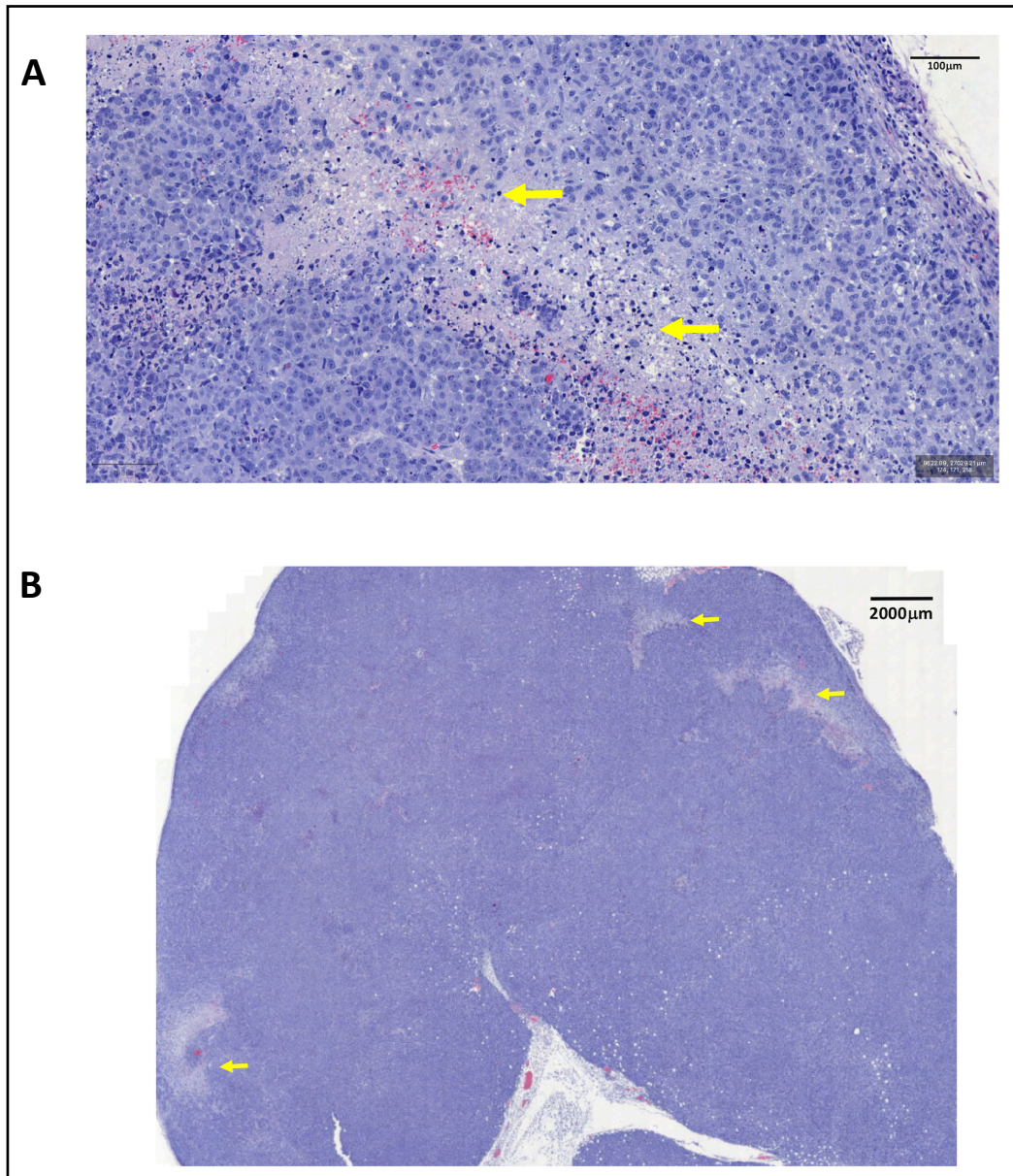


Figure 5.11 Images of H&E staining of PC3 WT tumour.

Haematoxylin and eosin staining of a wild type PC3 tumour. Multiple PC3 wild type tumours showed necrotic lesions (yellow arrows) identified by the damaged cell structure and an increased presence of extracellular matrix.

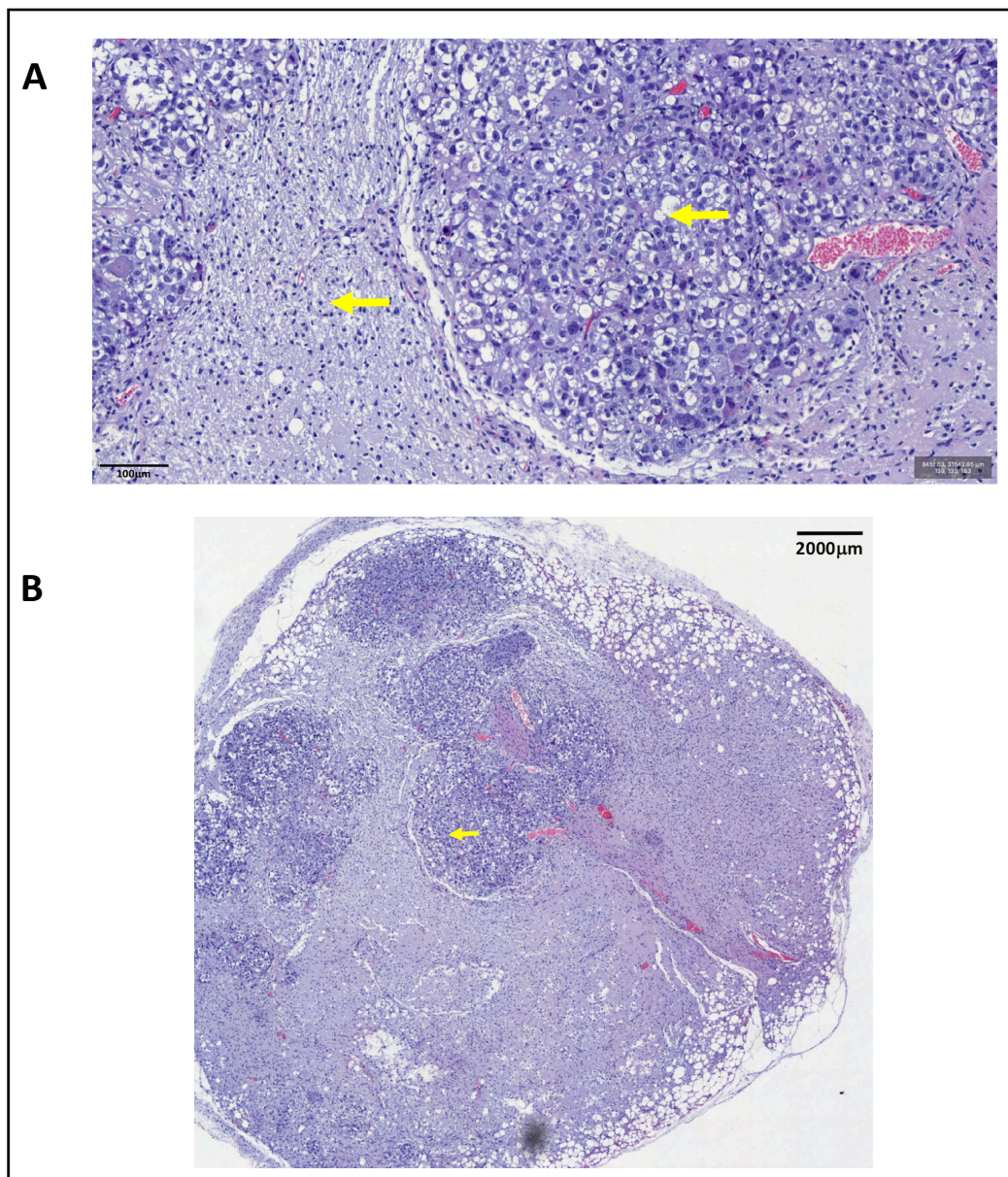


Figure 5.12 Image of H&E staining for RAMP1 KO tumour.

Haematoxylin and eosin staining of RAMP1 KO tumour. Structural differences were observed in RAMP1 KO tumours compared with PC3 wild type including reduced density of the tumour tissue and more variation in cell types (yellow arrows) .

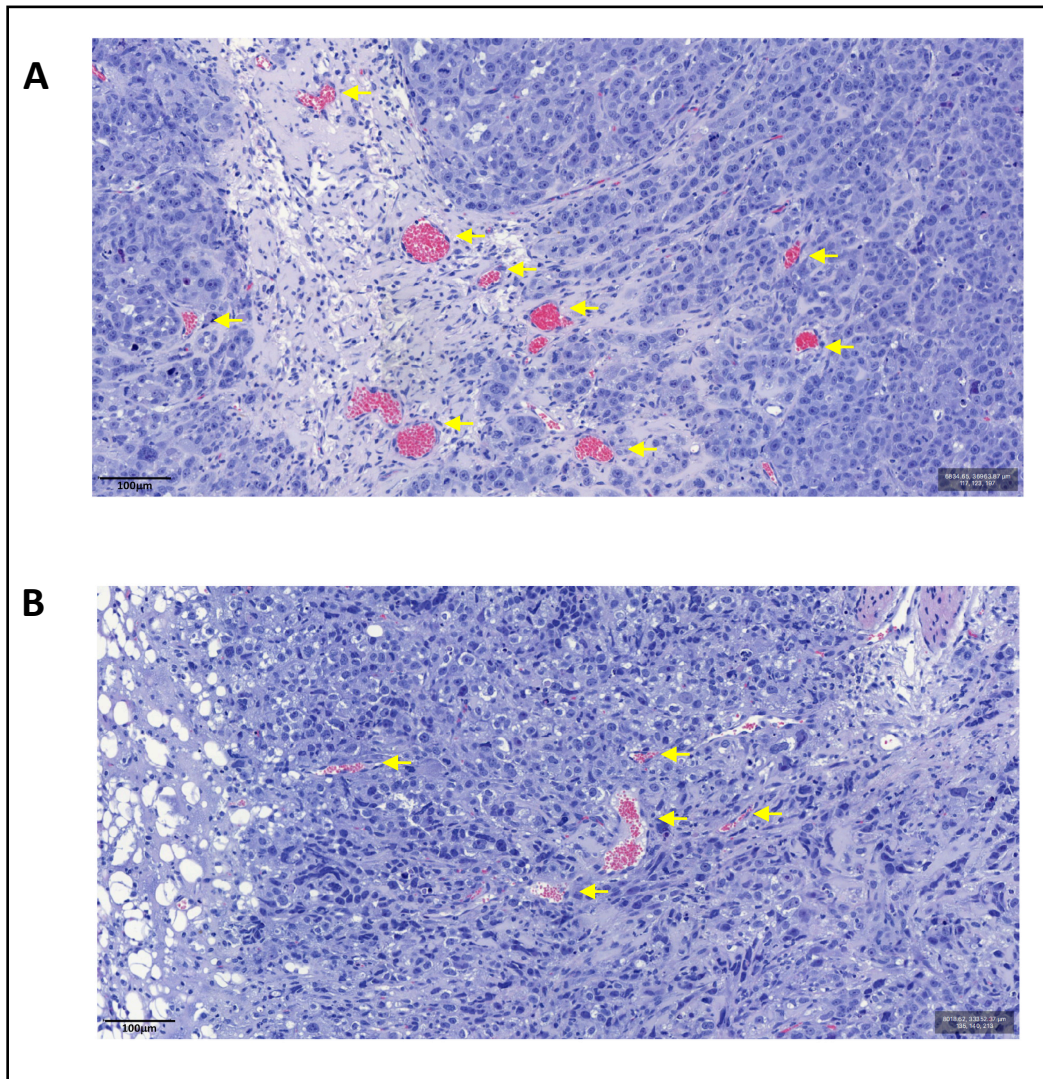


Figure 5.13 Images of H&E staining for wild type and RAMP1 KO PC3 tumours.

Haematoxylin and eosin staining of PC3 wild type and RAMP1 KO tumour tissue. An increased number of blood vessels (yellow arrows) were observed in PC3 wild type (A) tumours when compared with RAMP1 KO (B). This was quantified using CD31 IHC (see Fig 5.17.)

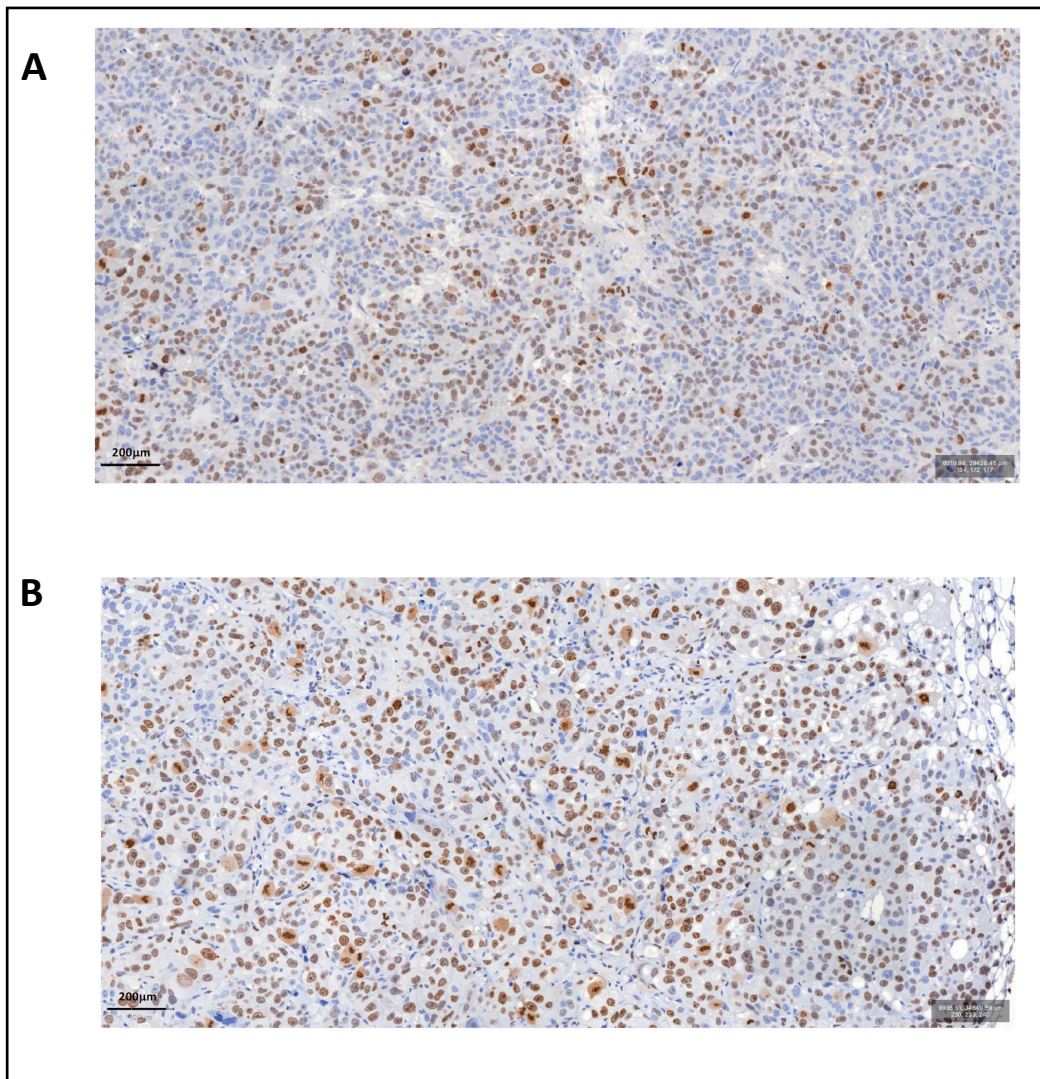


Figure 5.14 Image of Ki67 staining for wild type and RAMP1 KO PC3 tumours.

Immunohistochemistry staining for Ki67 (brown) in PC3 wild type (A) and RAMP1 KO (B) tumour sections. No obvious differences were observed between wild type and knockout sections. Intensity of staining (brown) appears slightly more pronounced in RAMP1 KO tumours.

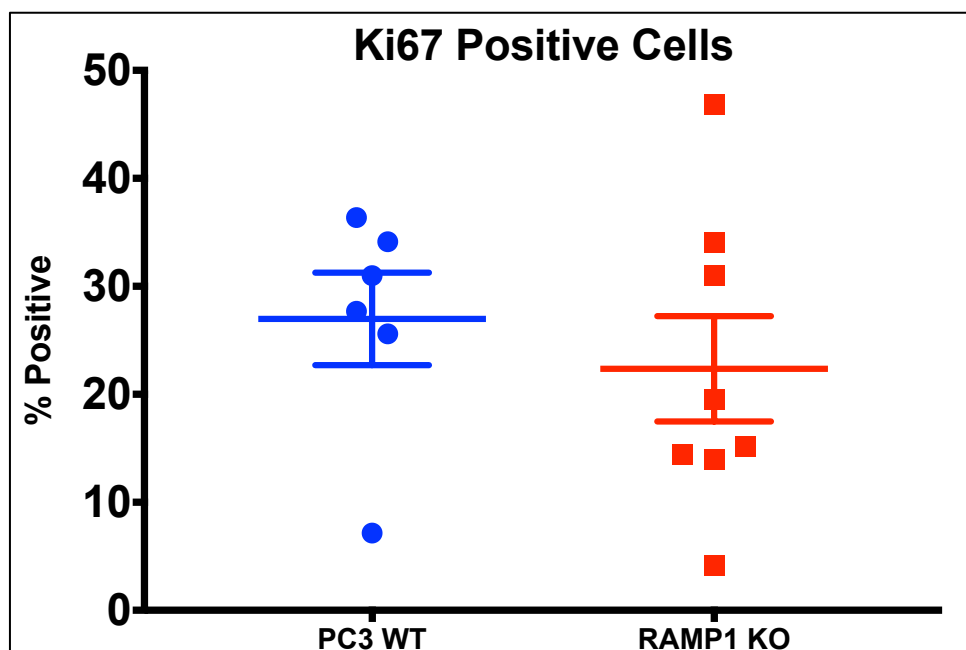


Figure 5.15 Analysis of Ki67 positive cells.

No significant differences were seen in the number of positive cells stained for Ki67 between PC3 wild type and RAMP1 KO tumours. All values are mean \pm SEM, WT n=6, KO n=8. (Students unpaired t-test).

CD31 staining was also performed on both PC3 wild type and RAMP1 KO control tumour sections. In wild type tumours, staining was very specific and highlighted endothelial cells situated in small blood vessels through the tumour structure and collections of larger vessels were often found near the surface of tumours (see Fig 5.15). CD31 staining in RAMP1 KO tumours had a very different appearance. Staining appeared more non-specific in areas of the tumour with a less dense structure and in the presence of stroma. These results are also reflected when observing haematoxylin and eosin staining which shows clear differences in tumour structure in RAMP1 KO and PC3 wild type groups. Some RAMP1 KO tumours had a more similar and dense tumour structure compared with PC3 wild types with blood vessels appearing through the tumour. Quantitative found that RAMP1 KO tumours had a higher percentage of tumour area stained positive ($P = 0.001$), indicating that

these tumours had an increased number of blood vessels compared with PC3 wild type tumours (see Fig 5.16).

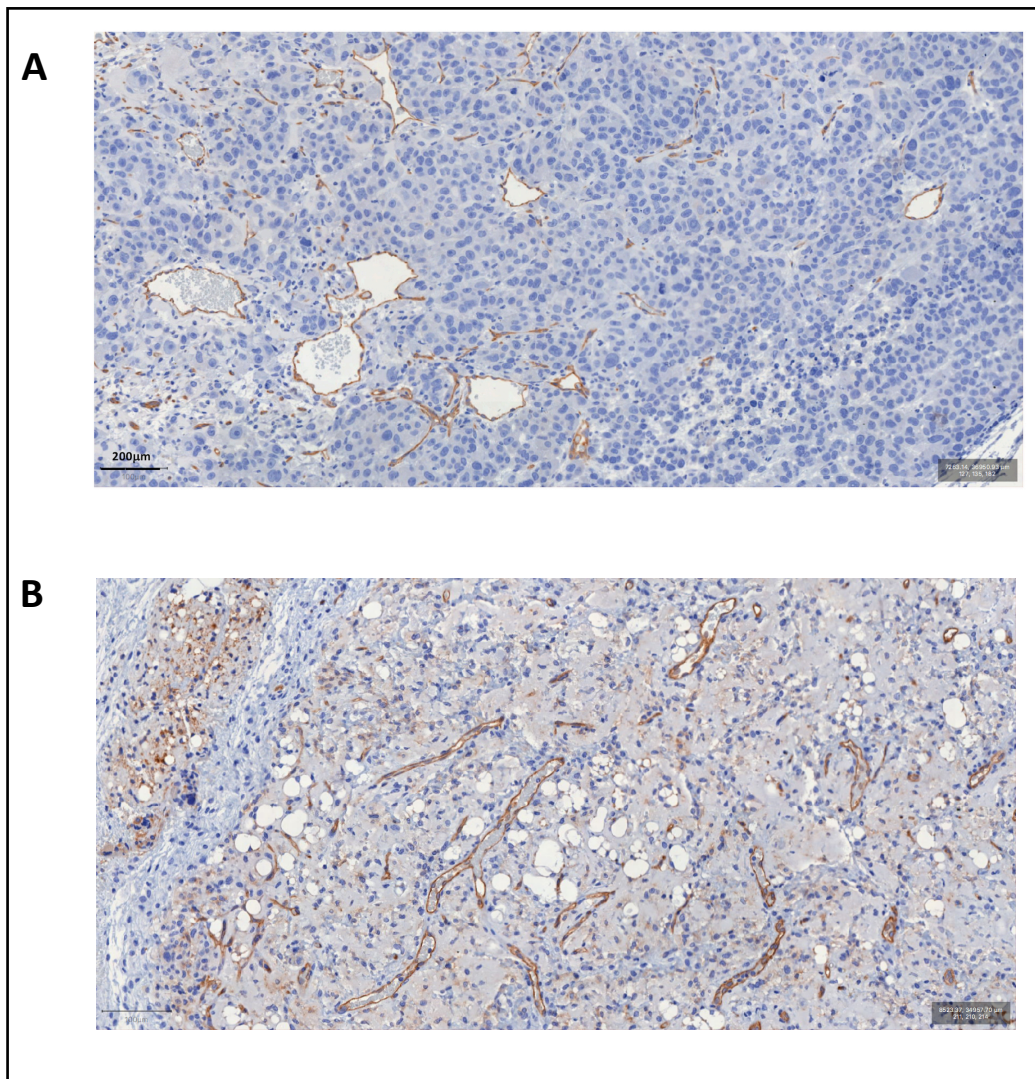


Figure 5.16 Images of CD31 staining of wild type and RAMP1 KO PC3 tumours.

CD31 immunohistological staining (brown) of PC3 wild type (A) and RAMP1 KO (B) tumour sections from untreated control groups. (A) CD31 positive staining in PC3 wild type tumours indicates small blood vessels are situated throughout the dense tumours structure and collections of larger vessels can be found at the tumour surface. (B) RAMP1 KO tumours show more non-specific staining compared with PC3 wild type tumours however small blood vessels can be identified throughout the tumour.

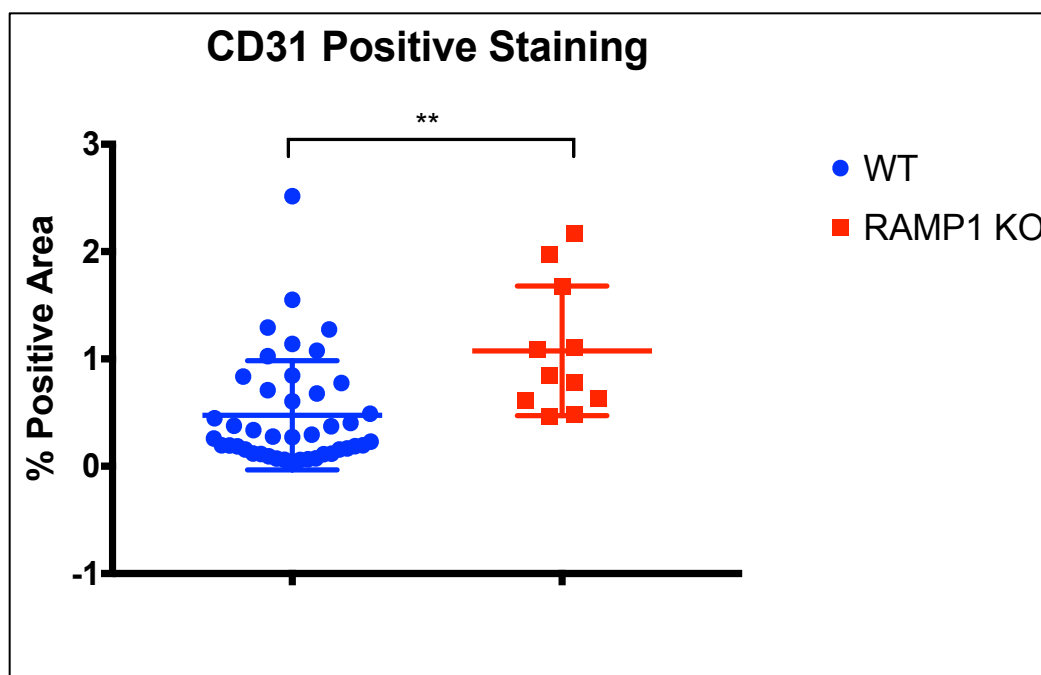


Figure 5.17 Quantification of CD31 analysis.

Quantification of CD31 analysis was achieved using ImageJ software and analysing the percentage of CD31 positive staining for each region of interest (ROI). A significant increase in the amount of CD31 staining was found in RAMP1 KO tumours when compared with wild type PC3 ($P = 0.001$), indicating a higher prevalence of blood vessels.

5.5.3 cAMP LANCE TR-FRET

Dose responses of Telcagepant and other CGRP antagonists such as MK-3207 and Olcegepant were performed on a mouse Panc02 cell line using a cAMP LANCE TR-FRET assay. Using a 25nM dose of CGRP, inhibitory effects of CGRP antagonists were seen in higher doses (see Fig 5.18). Olcegepant was observed to have the most potent effect with an IC₅₀ of 771nM and MK-3207 was much less potent with an IC₅₀ of 22nM. Although Telcagepant was the least potent of the CGRP antagonists tested it showed an IC₁₅₀ of 1.2µM and maintained an inhibitory effect at a 10µM dose (see Table 5.3) The span of the Telcagepant dose response curve was the highest of the three CGRP antagonist indicating that at higher doses, the inhibitory effect was greater than MK-3207 and Olcegepant.

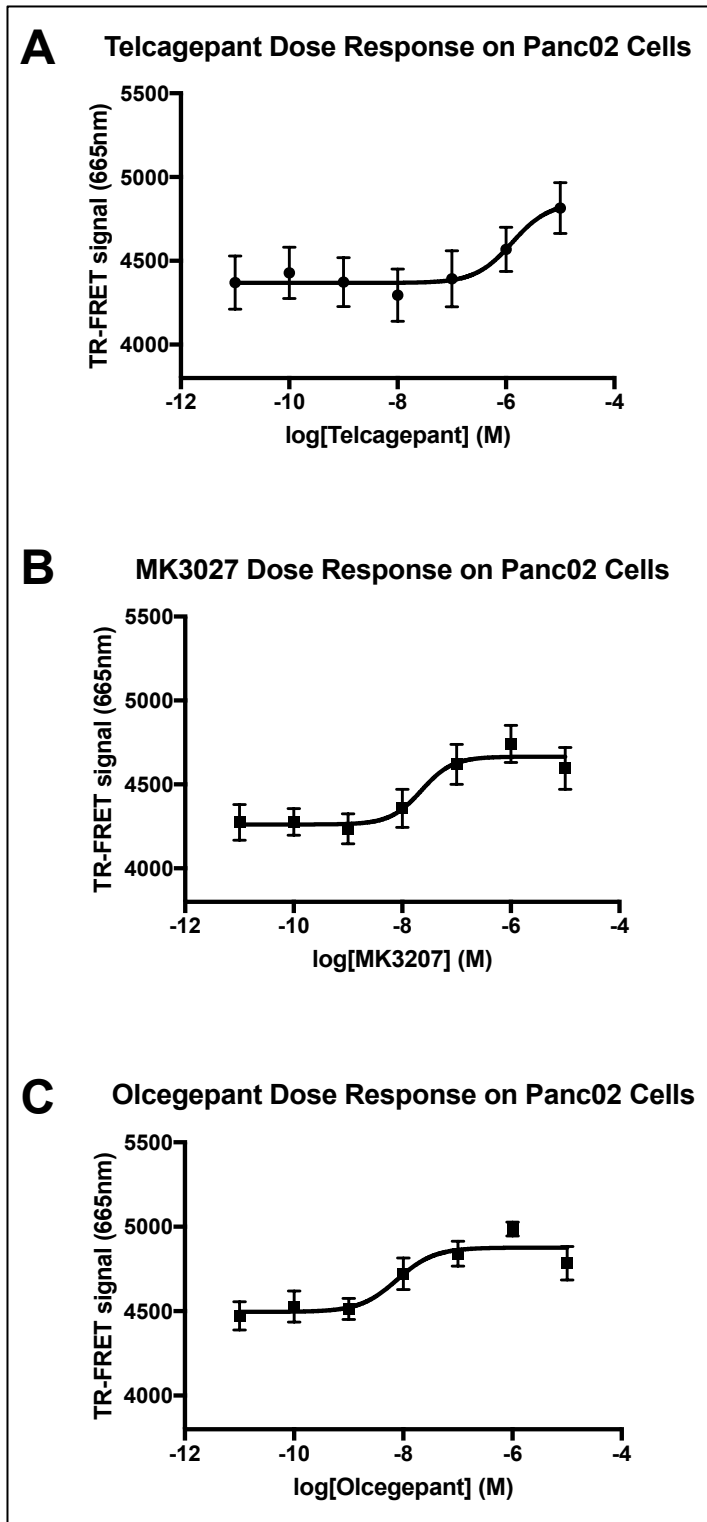


Figure 5.18 cAMP dose response curves for CGRP antagonists.

Dose response of CGRP antagonists (A) Telcagepant, (B) MK-3207 and (C) Olcegepant on Panc02 cells stimulated with 25nM CGRP. All values are mean \pm SEM, n=3.

Best Fit Values	Telcagepant	MK3207	Olcegepant
Bottom	4368	4261	4496
Top	4848	4665	4876
Log IC50	-5.889	-7.649	-8.113
Hill Slope	1.285	1.516	1.275
IC50	1.29e-06	2.24e-08	7.71e-09
Span	479.6	403.9	380.6

Table 5.3 Best fit values for CGRP antagonist curves.

Best fit values for dose response curves generated for CGRP antagonists Telcagepant, MK-3207 and Olcegepant.

5.6 Discussion

This *in vivo* study demonstrates that PC3 cells lacking RAMP1 expression have a gross reduction in their ability to form tumours in a subcutaneous xenograft model. Results show that RAMP1 KO tumours were significantly reduced in tumour growth across all time point measurements. In fact, it appears that after tumours were established they did not increase in size at all (see Fig 5.5). *In vitro* data shows that the RAMP1 KO clone D5 has 41% decreased viability after three days of growth compared with PC3 wild type cells. This clone was selected for *in vivo* study as it shared typical characteristics with other RAMP1 KO clones (for example A7 and C1) (see Chapter 4, Section 4.5.1). It was therefore expected that tumour growth would also be reduced, however the complete cessation of tumour development in RAMP1 KO tumours was unprecedented. Endpoint analysis of dissected tumour also revealed reduced tumour mass in RAMP1 KO tumours compared with PC3 wild type (see Fig 5.6). In many cases, dissection of RAMP1 KO tumours was difficult as they were so small that they were hard to locate. In these cases, sections of skin were taken at the injection site to be analysed after histological staining for the presence of tumour cells. Interestingly, differences in liver mass were significant between PC3

wild type and RAMP1 KO tumours. Liver mass was decreased in PC3 wild type tumours (in both treatment and control groups) which were incidentally much larger in both tumour volume and size. This therefore may be an effect of tumour burden in the mouse, the strain of subcutaneous xenograft may focus physiological processes and reduce energy spent on other vital organs. It is also possible that PC3 wild type tumours are secreting factors that cause liver shrinkage and that deletion of RAMP1 results in deregulation of these factors. Further analysis is required to test this hypothesis however a lack of difference between treatment and control groups suggest that this reduction in liver mass is not treatment-related. No other side effects were seen in any of the treatment or control groups.

No significant differences were found in tumour volume or mass between treatment and control groups for both PC3 wild type and RAMP1 KO tumours. However, a slight separation was observed in tumour volume on Day 17 between PC3 wild type treatment and vehicle control groups. Although this was not a significant difference it could be the continuation of the experiment may have revealed a Telcagepant effect. Due to the aggressiveness of the PC3 cell line, this experiment had to be finished to abide by Home Office laws as tumours may not be grown about 1cm³. Telcagepant has been previously reported to have been used in humans and rats [228, 232]. However, there is no current literature on the use of Telcagepant in mouse models. It is possible therefore that the absence of effect on tumour growth in treated mice was due to incorrect dosing of Telcagepant. The dose for Telcagepant to be administered in mice was calculated from current successful doses in humans. Administration of 400mg in humans results in potent effects of Telcagepant with a half-life of 6 hours, this would translate approximately to 5mg per kilogram (mg/kg) [233]. To increase the half-life and allow daily treatments to be successfully potent, this drug was administered to mice at 10mg/kg via daily subcutaneous injections. Telcagepant was prepared in Kolliphor® HS 15: Kollisolv® PEG E 400: dH₂O=1:3:6, as it is not very soluble in more aqueous solutions such as PBS or water.

The effect of Telcagepant was tested on a mouse cell line *in vitro* using cAMP LANCE TR-FRET assays. When activated, GPCRs can often stimulate the production of cAMP and therefore the effect of ligands or antagonists can be measured as a proportional differences in cAMP production [234]. Other CGRP antagonists were also tested for their effect to determine if Telcagepant stocks were inactive. Results show that all CGRP antagonists have an inhibitory effect on CGRP-stimulated Panc02 mouse cells, with Olcegepant having the highest affinity. This is concurrent with the literature which ranks Olcegepant higher in potency compared with Telcagepant in humans and rats [235]. Telcagepant was administered at a dose of 10mg/kg which is equal to approximately 3mM. This can be considered a very high dose of Telcagepant and therefore, according to cAMP data should have an inhibitory effect on CGRP in mouse cells.

Panc02 cells are derived from C57/B6 mice and originate from pancreatic adenocarcinomas. These cells may be genetically different from a Balb/c nude mouse and are also cancerous. Future experiments may identify the effect of Telcagepant on primary mouse cells derived from a Balb/c nude strain. Nevertheless, it is possible that Telcagepant had no effect in treatment groups because subcutaneous tumours were not driven by CGRP but another factor may be responsible. RAMP1 has been reported to traffic other receptors to the cell surface including the calcium sensing receptor (CaSR) [58] and also GPRC6A [60]. These peptide hormones have also been implicated in prostate cancer and therefore the deletion of RAMP1 may be also affecting these GPCRs which can now no longer traffic to the surface of PC3 cells, thereby removing their tumorigenic potential [107, 236]. This hypothesis can be explored in the future by measuring the expression levels of CaSR and GPRC6A in both wild type and RAMP1 KO PC3 cells.

Haematoxylin and eosin (H&E) staining of tumour sections was performed to investigate possible differences in structure and histological architecture between tumours. Observations of histological staining reflected results seen in tumour development, no differences were seen between treatment and control groups in both PC3 and RAMP1 KO tumours. The first observation that was made when

comparing tumours types was the presence of necrotic lesions (see Fig 5.10 & 5.11) in PC3 wild type sections. This is characterised by a lack of cell structure and an increased presence of extracellular matrix. Necrotic lesions can often occur in subcutaneous tumours that are so large, the tumour cells situated in the centre of the tumour are “cut off” from nutrients and blood supply feeding the tumour. These cells are outcompeted by the surrounding tumour and this ultimately leads to death. Necrotic lesions were not found in any RAMP1 KO tumours, which were much smaller in size and had a far less dense structure with more variation in tissue type e.g. tumour, fat, muscle.

Analysis of H&E staining also revealed a high number of blood vessels in PC3 wild type tumours when compared with RAMP1 KO. However, after staining with CD31 quantitative analysis did not confirm this observation. CD31 staining of RAMP1 KO control tumours was significantly increased after ImageJ analysis compared with PC3 wild type tumours. However, it was observed that staining on RAMP1 KO tumours appeared to have increased amounts of non-specific staining and this may have effected quantification of positive staining. General observation of the stained slides did not show clear differences in the RAMP1 KO and PC3 wild type tumours. This suggests that the number of blood vessels which are composed of endothelial cells expressing CD31 is not affected by deletion of RAMP1. It also indicates that the difference in tumour growth and size is not due to a lack of blood supply or angiogenesis. Immunohistochemistry results therefore show that aside from proliferation and angiogenesis/vascular structure, alternative factors are responsible for the reduction in tumour growth in the absence of RAMP1

Histological staining for Ki67, a proliferative marker, showed no differences in the percentage of positive cells when comparing PC3 wild type and RAMP1 KO (treatment and control) tumours. It was observed that staining in the RAMP1 KO tumour sections had a higher intensity but this is most likely due to the differences in the size of tumours that are stained with the same amount of anti-Ki67 antibody and DAB. Ki67 has been described as a prognostic marker for prostate cancer and is often used to label tumour cells which are commonly hyper proliferative [167]. Previous studies using RAMP1 knockdown subcutaneous xenografts have reported

a reduction in the number of Ki67 positive cells in RAMP1 knockdown tumours [105]. Differences seen are not highly significant ($P = <0.05$) and quantification was achieved by selected just five regions of interest (ROI) per section at a high-power magnification and manually counting positively stained cells. Tumour sizes in wild type PC3 cells were reported at up to 650mm³ and therefore five high-power ROIs may not be sufficient for such large sections. Quantification of Ki67 staining in this study was achieved using QuPath software, allowing quantification of entire tumour sections and minimising the risk of bias ROI selection. The lack of difference may suggest that the deletion of RAMP1 does not merely reduce proliferation in PC3 cells but also affects other processes that are vital for prostate tumour development. Further histological analysis for alternative markers of tumour development may provide key insights into the mechanisms behind the reduced growth of subcutaneous xenografts in RAMP1 KO cells.

These results suggest a very important role for RAMP1 in prostate tumour development. The effect seen in this *in vivo* study is much greater than previously published data (Logan et al.) Knockdown of RAMP1 only results in significant reductions of tumour growth after 25 days [105]. This may be a consequence of using knockdown of RAMP1 instead of complete gene knockout. The authors also do not mention injection of cells with Matrigel in their methods and materials. This may explain why the first measurement of tumour volume takes place on Day 14. Mixing of cell suspensions with reconstituted basement membrane proteins such as Matrigel has been shown to promote the establishments of subcutaneous tumours *in vivo* and may therefore have yielded a larger window of measurements to see the effect of RAMP1 depletion in more detail [208]. Nevertheless, the finding that complete deletion of RAMP1 using gene knockout can result in more pronounced reductions in tumour growth is important. The complete cessation of tumour growth in RAMP1 KO PC3 xenografts is compelling evidence for the implication of RAMP1 in the progression of aggressive prostate cancer.

Although the lack of effect of Telcagepant treated mice may suggest this antagonist is not appropriate for use in mouse models it is also possible that the

RAMP1 KO effect on tumour growth is not related to CGRP. Either of these hypotheses could yield interesting research questions that may be further investigated in future and could reveal whether clinically available CGRP antagonists such as Telcagepant should be used as a therapeutic intervention in prostate cancer patients. Further investigations may also explore the role of RAMP1 in the bone metastatic niche. Prostate cancer metastasis occurs in bone in 80% of cases and it is therefore imperative that the effect of RAMP1 deletion is investigated in the bone microenvironment. This can be achieved *in vitro* using co-culture experiments but *in vivo* models are key to exploring the true value of RAMP1 in prostate cancer metastasis.

CHAPTER 6: GENERAL DISCUSSION

This study has successfully used CRISPR/Cas9 to delete RAMP1 in a PC3 cell line and enabled the role of RAMP1 to be more fully elucidated in prostate cancer. Deletion of RAMP1 not only results in a 40% reduction in cell viability but protects against apoptosis induced by serum starvation. This implicates RAMP1 as an important regulator of prostate cancer cell survival and further *in vitro* testing has shown that it has a strong influence in processes of metastasis such as invasion, colony formation and adhesion. These results were reflected when using *in vivo* models of prostate tumour growth, where the deletion of RAMP1 led to the complete cessation of subcutaneous tumour growth. RAMP1 KO cells also showed reduced levels of phosphorylated proteins associated with the progression of prostate cancer from an androgen sensitive disease to an aggressive and metastatic cancer. These unprecedented findings provide compelling evidence that RAMP1 is not only a key player in the mechanisms behind advanced prostate cancer but also that it should be considered as a therapeutic target for the treatment of high risk prostate cancer patients.

Although PC3 cells express both components of the CGRP receptor, and secrete CGRP itself, evidence suggests that RAMP1 is promoting prostate cancer through a CGRP-independent mechanism. This study aimed to generate CRISPR/Cas9 knockouts for RAMPs 1-3 in the hope of identifying if the CGRP or adrenomedullin receptors are involved in prostate cancer progression. Despite only generating successful knockouts for RAMP1, this has led to novel findings that dispute CGRP as the relevant peptide in promoting prostate cancer through RAMP1. The viability of PC3 cells was found to be unaffected by CGRP peptide or CGRP antagonists *in vitro*. In addition, treatment with Telcagepant, a CGRP antagonist had no effect on subcutaneous tumour growth in Balb/c nude mice, despite inhibitory effects found on mouse cancer cell lines *in vitro*. This leads to the conclusion that RAMP1 may be trafficking other GPCRs to promote prostate cancer. RAMP1 can traffic other receptors to the cell surface apart from CLR, such as the calcium sensing

receptor and GPRC6A, both of which have been linked with prostate cancer progression [58, 60, 107, 236]. Future work will be required to answer this hypothesis but for now it can be undisputed that findings from this study warrant further investigations into RAMP1 and its role in prostate cancer.

This study was conducted with a two-fold objective:

- To knockout RAMPs 1-3 individually in a prostate cancer cell line and measure the effect of this deletion on function both *in vitro* and *in vivo*
- To determine if the effect of RAMP1 deletion is due to CGRP or other RAMP-associated peptides.

The CRISPR/Cas9 technique was chosen to delete RAMPs 1-3 in a prostate cancer cell line and in the hope of providing insight into the role of the individual CGRP or AM receptors. Previous reports using gene knockout are limited to the use of knockout mice to investigate the individual receptor components of CGRP and AM receptors. Findings have shown that RAMPs can have distinct physiological and pathological roles. Homozygous deletion of the AM, CLR or RAMP2 in mice leads to lethality *in utero* during mid-gestation [158, 237-239]. This provides evidence that the CLR:RAMP2 heterodimer that forms the AM2 receptor is essential for development, however RAMP3 knockout mice appear to be unaffected until they reach old age whereupon they begin to experience weight loss [237]. RAMP1 knockout mice have no abnormalities other than increased blood pressure but have normal heart rates. These mice also have elevated serum levels of CGRP, showing that RAMP1 is an essential component of the CGRP receptor [240]. The effect of the deletion of the AM1 and AM2 receptors has not been previously studied in the context of prostate cancer. Deletion of RAMPs 1-3 *in vitro* may therefore provide useful information on which receptor components are responsible for the effect of CGRP and AM in prostate cancer.

RAMP knockouts were generated in a PC3 cell line, this is a highly invasive prostate cancer cell line that represents advanced stages of the disease. By selecting an aggressive cell line, it can be determined whether RAMPs and their appropriate GPCRs play an important role in advanced prostate cancer which is currently an unmet clinical need. However, future investigations may include RAMP1 deletion in other prostate cancer cell lines, such as LNCaP as this would provide insight into the role of RAMP1 in an androgen dependent environment. It is important to understand the mechanisms involved during the transition from low risk androgen sensitive prostate cancer to a resistant and metastatic disease. Previous studies have confirmed the expression of AM, CLR, RAMP1 and RAMP2 mRNA transcripts in PC3 cells, although RAMP3 expression was not found [241]. While the authors did not find RAMP3 expression in PC3 cells, they found it to be upregulated in prostate carcinomas more significantly when compared with prostate hyperplasia. Alternative studies have found all components of the AM receptors, including RAMP3 to be expressed at an mRNA level in PC3 cells [85]. These results are further evidence of discrepancies between immortalised cell lines and primary cells and tissues. PC3 cells like many other cell lines are genetically different to their origin tissue as they have undergone a series of passages causing genotypic and phenotypic changes over an extended period of time. It is therefore advised that care be taken when using cell lines and key findings should always be confirmed in primary cells or *in vivo* if possible [242].

In this study, protein expression was first investigated using antibodies targeting RAMPs 1-3 and CLR. Western blotting revealed positive results for RAMPs 1-3 and CLR in PC3 cell protein samples, however no AM antibody could be optimised to determine AM protein levels. The reliability of these antibodies should be questioned as manufacturers of the monoclonal RAMP1 antibody (AbCam) have since stated that on retesting of the antibody it was found to have incorrect subcellular staining. They maintain that the antibody is still appropriate for western blotting but later analysis using RAMP1 CRISPR clones with no mRNA RAMP1 expression showed false positive staining. Nevertheless, this study has found expression of AM, CLR and RAMPs 1-3 in PC3 cells at an mRNA level (see Fig 2.9).

This finding led to targeting the RAMPs for deletion using the CRISPR/Cas9 gene editing technique to effectively remove both CGRP and AM receptors in a PC3 cell line.

The use of CRISPR/Cas9 has allowed complete gene deletion in a prostate cancer cell line in order to explore the potential role of the target gene in promoting prostate cancer progression. Previous studies using knockdown techniques in cancer cell lines have led to false conclusions that have since been validated using gene knockout and therefore the decision to use CRISPR/Cas9 avoids this risk [142]. When studying the role of AM in prostate cancer, previous studies have used different techniques including treatment with AM in prostate cancer cell lines or inducing overexpression of the AM gene (which is often a transient effect). Often, treatment with AM to cells in culture can be hampered by AM that is secreted by the cells naturally. An example of this is ambiguous effects seen in the proliferation of prostate cancer cell lines after treatment with AM, which authors have attributed to maximal proliferative effects already being achieved due to AM secretion [80]. Prostate cancer cell lines can be transiently transfected with gene overexpression constructs which may be useful in determining the possible role of AM but can often have unforeseen consequences. Increasing the expression of a gene from its native level within a cell can put pressure on downstream factors which then becoming limited. It has also been argued that overproduction of a single protein that networks with other proteins (as many regulatory proteins do) can lead to misfolding and inactive subcomplexes that alter biological activity [243].

These *in vitro* techniques also fail to investigate the AM receptors individually and their role in prostate cancer. Studies blocking AM using an antibody cocktail show significant effects on prostate cancer cell growth *in vitro* and in xenograft tumours but it is unknown which of the AM receptors is responsible for this effect as CLR, RAMP2 and RAMP3 have been targeted simultaneously [85]. The same issue is present when linking CGRP and prostate cancer, clinical investigations show a correlation between serum levels in prostate cancer patients and staging but no studies have investigated the mechanism behind this effect [102, 244]. Although, the

role of RAMP1 in prostate cancer cell lines has been explored using shRNA knockdown in PC3 and LNCaP cells, the effects seen are minimal but significant. In RAMP1 knockdown cells, reductions in proliferation *in vitro* are only seen after 6 days of growth and significant differences in xenograft tumour volume is also only present at late stages of growth [105]. It would therefore be apt to completely delete the RAMP1 gene in prostate cancer cells and see if these effects are seen and if they are more pronounced when compared with gene depletion.

Gene knockout is a useful tool for determining if AM, CGRP and their corresponding receptor components are important for the progression of prostate cancer. However, gene knockouts cannot be considered a realistic view of the physiology of primary cells and tissues. It is important to highlight that the use of CRISPR/Cas9 is a research tool that allows pinpointing of relevant genes. Like all gene expression techniques, CRISPR/Cas9 has limitations, such as off target effects. Care has been taken to avoid off target effects by choosing a CRISPR/Cas9 system that is highly specific. Incorporating CRISPR constructs using homology directed repair (HDR) not only reduces off target effects but allows insertion of an expression cassette which then aids the validation process when confirming successful gene knockouts. Unfortunately, CRISPR constructs targeting RAMP2 and RAMP3 were not successful, nevertheless this may be an interesting find in itself. RAMP2 knockout mice are known to not survive mid-gestation and this is also relevant in cell culture [237]. RAMP2 has been found to be essential for cell barrier regulation in endothelial cells and also regulates permeability, suggesting it's deletion could have consequences on cell structure [158]. It may be that in future, when determining the role of RAMP2 in prostate cancer, knockdown techniques must be used to ensure cell survival.

Nevertheless, RAMP1 knockouts were successfully generated in a PC3 cell line and gene deletion was confirmed at an mRNA level using quantitative PCR (see Fig 3.21). Despite repeated experiments using heavily concentrated cDNA samples that indicated a lack of RAMP1 mRNA, western blotting still produced positive results for RAMP1 protein expression. Recent retesting of this antibody by the

manufacturers has led to a doubt in its reliability. For these reasons, this result was regarded as a false positive result as probing with the RAMP1 antibody also displays bands at correct size of 17kDa on the protein standards ladder (see Fig 3.23). In order to ensure a population of knockout cells, CRISPR targeted PC3 cells were sorted using a fluorescence marker present in the expression cassette that is incorporated into the gene when targeted for knockout. Cells were sorted into single cells to ensure a complete knockout population, as incorporation of the expression cassette may occur without gene knockout in a small subset of cells. These cells would be essentially wild type in both genotype and phenotype, leading to a “mixed” population and effectively a gene knockdown instead of knockout. This technique of isolating CRISPR cell clones has been previously used in different investigations in the hope identifying the role of regulatory genes in cancers including breast, colon and lung (in both mouse and human cell lines) [245-247]. The use of single cell clones has obvious limitations as this does not represent the heterogeneous population seen in real prostate tumours and therefore care must be taken when drawing conclusions from such studies. To alleviate this multiple CRISPR clones that were validated as successful RAMP1 knockouts were used for all functional testing *in vitro* in order to determine whether observations were a RAMP1 or “clonal” effect.

Three different CRISPR clones had RAMP1 mRNA deletion when validated using qPCR and reduced viability when cultured for 3 days and compared with PC3 wild type cells (see Fig 3.21 & 4.9). These clones were then selected for all functional testing *in vitro* to ensure results were not based on a single clone effect. PC3 wild type cells were used as positive controls for all *in vitro* and *in vivo* experiments as no scrambled CRISPR construct could be provided by the manufacturer. Interestingly, variation was seen in viability results between other CRISPR clones (see Fig 4.9). These clones did not show reduced viability until towards the end of the experiments which is concomitant with previous studies using RAMP1 knockdown in PC3 cells [105]. Interestingly the clones in question also showed slightly higher expression levels of RAMP1 mRNA expression (<10%) after $\Delta\Delta$ CT analysis and could therefore be heterozygous edits and considered RAMP1 knockdown cells instead of complete knockouts. This would explain the similarity in findings compared with Logan et al.

The overall finding that RAMP1 deletion results in reduced viability of PC3 cells and decreases their rate of growth is clinically significant. Prostate cancer enters its most advanced stages after becoming androgen independent. Studies have found that pro-proliferative factors such as aldoketoreductase (AKR1C3) influence the transition of prostate cancer cells to androgen independence also promote proliferation [248]. This therefore results in relapsing patients who have increasing growth of once benign tumours that have since gained androgen independence. It is yet unknown what mechanism RAMP1 is utilising in promoting the viability and proliferation of prostate cancer cells but it is irrefutably an important pathway and further understanding will benefit advanced prostate cancer patients. RAMP1 KO in alternative prostate cancer cell lines, for example androgen sensitive LNCaP may provide interesting and clinically relevant insight into the role of this protein in prostate cancer relapse and the triggering of metastasis.

A crucial step in the metastasis of prostate cancer involves the ability of cells to leave the primary site, invade through the surrounding extracellular matrix and migrate to distant sites. It has been suggested that these functional processes are key to detecting the transition from low risk disease to advanced metastatic prostate cancer which significantly lowers a patients prognosis [249]. The deletion of RAMP1 in PC3 cells did not reduce migration when tested *in vitro*. In fact, it was observed that multiple RAMP1 clones migrated faster compared with PC3 wild type controls (see Fig 4.12). This may represent a limitation of *in vitro* assays which fail to recapitulate the true physiological conditions that prostate cancer cells face when migrating across the body. There are currently no published studies testing the effect of RAMP1 on the migration of cancer cells specifically, however treatment of CGRP does seem to affect the migratory capacity of several prostate cancer cell lines [104, 178]. This may suggest that results seen in RAMP1 KO cells are not a “CGRP effect”. Nevertheless, RAMP1 has been found to regulate migratory patterns of vascular smooth muscle cells via inhibition of the NF- κ B pathway [190]. It has also been found to interact with tubulin, an important component of the cell cytoskeleton and essential for migration of prostate cancer cells [250]. In fact, tubulin has also been implicated in the promotion of androgen independence and it has been suggested

that targeting of the cytoskeleton itself may have value in future prostate cancer treatments [251, 252]. The role of RAMP1 in migration can be investigated further by exploring its effect on downstream signalling pathways associated with this process, rather than relying on simplistic *in vitro* assays.

It is interesting that RAMP1 KO cells did show an increased invasive phenotype compared with PC3 wild type controls, despite the absence of a pro-migratory effect (see Fig 4.14). It has however been suggested that these two mechanisms do not necessarily occur simultaneously and that migration is not always characterised by an epithelial-to-mesenchymal transition (EMT) of the cancer cells [176]. The ability of prostate cancer cells to invade the surrounding stroma does require EMT and this is often characterised as a switch in the expression of cadherin markers. In prostate cancer specifically, an increase in N-cadherin and decrease in E-cadherin expression is not only a marker of EMT in prostate cells but also correlates with higher Gleason scores [253].

Although there are no current findings associating RAMP1 with cadherin expression, others RAMPs such as RAMP3 have been found to promote a mesenchymal phenotype in breast cancer by regulating E-cadherin expression [254]. Although this is an unpublished thesis study, it is interesting that this family of receptor components could be influencing such specific pathways of cancer metastasis. Another important factor to consider is that the invasion of prostate cancer cells requires degradation of the surrounding extracellular matrix. This is achieved through the action of matrix metalloproteinases (MMPs) and serine proteases such as urokinase-type plasminogen activator (uPA) [255]. It has been shown that uPA acts on PC3 and DU145 cells and results in an invasive phenotype with increased proliferation [256]. It may therefore be important to investigate the possible role of RAMP1 in uPA and other MMPs in promoting prostate cancer invasion as these factors also correlate with clinical outcomes in patients [257].

The adhesive properties of prostate cancer cells undergo pronounced changes to initiate the process of metastasis. First, cells must lose their ability to

adhere to each other and the surrounding stroma. This is described as cell-cell or cell-ECM adhesion. When a cell has metastatic potential it has been suggested that its interactions with the ECM changes [249]. This represents the colonisation of cancer cells at the distant site through adhesion to the ECM. The ability of RAMP1 KO PC3 cells to adhere to fibronectin, an extracellular matrix protein was tested *in vitro*. It was found that these cells had a reduction in adhesion to ECM compared with PC3 cells (see Fig 4.18). It was also found that the ability of RAMP1 KO cells to form colonies in cultures was decreased in both number and size of colonies (see Fig 4.16 & 4.17). These processes are key to the progression of advanced prostate cancer [195, 249]. It is therefore essential to investigate the mechanisms RAMP1 may be regulating to influence both adhesion and colonisation in metastasis. An important factor in cell adhesion is focal adhesion kinase and levels of expression are correlated with a greater metastatic potential in different prostate cancer cell lines and also staging and progression of prostate adenocarcinomas [258, 259]. Although there is no current evidence of RAMP1 regulating FAK, or other adhesion factors, CGRP has been shown to enhance vascular tube formation in human umbilical vein endothelial cells (HUVECs) through the upregulation of FAK and VEGF receptors [260]. Further investigation into the role of RAMP1 is required to determine whether the effect of its deletion is due to a lack of CGRP effect or other receptors are responsible.

In vitro studies are indicative of RAMP1 being an important factor in PC3 cells and therefore could also be in the advanced aggressive stages of prostate cancer. However, cell lines do not efficiently represent the true pathology of the disease studied and it is important to always validate results found *in vitro* using *in vivo* models. Subcutaneous xenografts of RAMP1 KO PC3 cells resulted in a dramatic difference in the volume and mass of subcutaneous tumours compared with wild type PC3 (see Fig 5.5 & 5.6). In fact, it appeared that RAMP1 KO tumours failed to grow at all and many could not be located during dissection. This result could be expected due to the clear differences in cell viability and growth rates *in vitro*, however after histological analysis it was found that the presence of Ki67 positive cells was not different between RAMP1 KO and PC3 wild type tumours (see Fig 5.14).

This therefore suggests that alternative mechanisms are being influenced by RAMP1 during the promotion of prostate tumour growth. CD31 staining was also found to be significantly higher in RAMP1 KO tumours, suggesting a higher prevalence of endothelial cells leading to the assumption that more blood vessels were present in these tumours (see Fig 5.16). However, CD31 staining was observed to be highly non-specific in RAMP1 KO tumours due to different tissue structure compared with PC3 wild type tumours. RAMP1 KO tumours appeared to be composed of more extracellular matrix and showed traces of collagen, whereas PC3 wild type tumours were more densely packed with tumour tissue alone (see Fig 5.15). Quantitative analysis was hindered by the increased background in tumours with more extracellular matrix and collagen fibres. Nevertheless, this finding does not provide evidence that the reduction in tumour growth seen in RAMP1 KO cells can be attributed to a lack of vascular supply.

It was also found in subcutaneous xenograft experiments that treatment of a CGRP antagonist, Telcagepant, had no effect on tumour growth (see Fig 5.7). Telcagepant has been heavily reported in the field of migraine research and is a clinically approved compound for the treatment of migraine [228, 229, 233]. Therefore, if the effect seen in RAMP1 KO cells in prostate cancer is a CGRP effect, it could be hypothesised that the treatment of an approved CGRP antagonist such as Telcagepant could be beneficial to advanced prostate cancer patients. Previous studies have used rat or human dosing of Telcagepant and so dosing for mice was calculated by scaling down these doses to 5mg/kg [233]. Telcagepant has a short half-life of 6 hours and so mice were treated with 10mg/kg daily to counter this effect. Previous studies have shown that Telcagepant has a 1000-fold lower affinity for the CGRP receptor in rats and dogs, leading to most preclinical work being done in rhesus monkeys [261]. The lack of effect seen in treated mice could be a result of incorrect dosing or reflect the reduced potency of the antagonist in rodent species. Another possible explanation is that RAMP1 is acting in a CGRP-independent manner in prostate cancer. *In vitro* testing of PC3 wild type cells showed that treatment with CGRP has no effect on cell growth (see Fig 4.10). Experiments have shown using immunoassays that CGRP is secreted into the media from PC3 cells in culture (see

Fig 2.12). It could be argued that treatment may have no effect as the cells already display maximum proliferation. However, it was also found that treatment with Telcagepant at varying doses also had no effect to viability or cell growth (see Fig 4.10). This evidence suggests that PC3 cells are not driven by CGRP and that RAMP1 may be acting through alternative mechanisms. Although human PC3 cells were the source of subcutaneous tumours, the surrounding stroma and tumour environment was mouse. It was therefore important to investigate the effect of Telcagepant on a mouse cell line. Stimulation with CGRP results in a dose response of cAMP production which was measured using a LANCE TR-FRET assay (see Fig 5.4). It was then found that Telcagepant only had inhibitory effects at high doses of $<1\mu\text{M}$ (see Fig 5.17). Other CGRP antagonists were tested such as MK-3207 and Olcegepant and these also were inhibitory at very high doses (see Fig 5.17). Treatment of mice with 10mg/kg Telcagepant approximately equates to a daily treatment of 3mM.

Although it is unknown how efficiently Telcagepant is absorbed this can still be considered a very high dose and therefore it could be concluded that the lack of effect seen in treatment groups is not due to a lack of Telcagepant efficacy but most likely tumour growth is not driven by CGRP. This possibility must be further investigated in future studies as it is important to establish the true mechanism pertaining to the role of RAMP1 in prostate cancer. RAMP1 is important in CGRP signalling as it traffics the calcitonin-like receptor (CLR) to the cell surface and therefore without the RAMP1:CLR complex, CGRP cannot exert any cellular functions. Other receptors have been found to be trafficked by RAMP1 and co-localise on the cell surface.

Results of the subcutaneous xenograft experiment show a clear role for RAMP1 in the growth of PC3 cells in a more physiologically relevant setting. However, this model is far from similar to the environment of prostate tumours *in situ* and also does not investigate the effect of RAMP1 deletion in metastasis. Orthotopic models represent clinical stages of prostate cancer most accurately as cells are faced with a native host environment [262]. However there has been a lack of standardisation over the number of injected tumour cells in orthotopic models

and are often used to study effects in localised prostate tumour environments [263]. Prostate cancer is a disease that is lethal after metastasis, in which over 80% of cases are skeletal [189]. It is therefore imperative to recapitulate this in a mouse model of prostate cancer. This will also reveal the role of RAMP1 in promoting metastasis of prostate cancer cells and their development within the bone environment. To understand the effect of RAMP1 deletion on bone metastasis a model of cell colonisation in bone using intracardiac injection of RAMP1 PC3 cells could be performed in the future [264]. Before injection cells can be stained with fluorescent lipophilic membrane dyes (e.g. DiD or Dil). After cells have travelled through circulation and metastasised to the bone they can be quantified using two-photon microscopy. When the cells divide they will not retain the dye and so only colonising cells will be quantified therefore showing whether the number of RAMP1 KO cells to successfully metastasise to bone is different from PC3 wild type cells.

It is also important to measure the ability of RAMP1 KO PC3 cells to grow within the bone environment. It is possible that the deletion of RAMP1 may have downstream consequences that affect the metastatic niche and this could reveal a novel role for RAMP1 in the tumour microenvironment. Tagging of wild type and KO cells with luciferase can allow the real-time measurement of bone metastasis growth following intracardiac injection [216-218, 265]. Bones can then be dissected and analysed using microCT and histological staining to investigate the effect of RAMP1 on the bone environment. Size and number of metastatic sites will reveal the effect of RAMP1 on tumour growth in the bone. This is very relevant to prostate cancer patients who have a significantly low prognosis after bone metastasis. Currently, there is a lack of agreed treatment for these advanced patients and their best hope is to enter a clinical trial [37]. Therefore, understanding what important factors and mechanisms are acting on metastatic tumours is vital for developing new therapeutic treatments.

In an effort to develop new therapies for advanced prostate cancer patients, it is vital to examine the molecular mechanisms behind the transition from androgen dependence to independence that leads to relapsing patients with aggressive

metastatic disease and a poor prognosis. The effect of RAMP1 deletion was investigated with regards to downstream signalling pathways in PC3 cells. Using a magnetic bead assay targeting multiple phosphorylated proteins from different signalling pathways it was found that RAMP1 KO cells show reduced levels of phosphorylated Akt and STAT3 compared with PC3 cells (see Fig 4.20). Akt is an important member of the P13K cell survival pathway and is often mutated in cancer cells [266]. In fact, in prostate cancer it has been found to be activated by IL-6 to promote cell survival by inhibiting apoptosis [201, 267].

Previous studies have also implicated RAMP1 in the regulation of IL-6 expression in prostate cancer cells [105]. Interestingly, IL-6 can promote growth in androgen independent cell lines such as PC3 and DU145 by increasing STAT3 binding activity and its expression has been linked with promoting androgen independence in LNCaP cells [202, 268]. This association between IL-6 and STAT3 has led to preclinical models using inhibitors of upstream STAT3 effectors, JAK1 and JAK2. Overexpression of IL-6 in DU145 cells results in a seven-fold increase in lung metastases in nude mice, however this effect was almost completely abolished after daily treatments of AZD1480, a JAK1/2 inhibitor. This effect was also achieved using shRNA knockdown of STAT3 [269]. This has led to recent reviews questioning the relevance of STAT3 inhibitors in the treatment of prostate cancer [270, 271]. Nevertheless, limitations with drug potency in phase I clinical trials have led to reviewers calling for further investigation into the STAT3 molecular pathway in cancer. Results showing that RAMP1 may be important for STAT3 signalling are therefore highly clinically relevant and further investigation of RAMP1 deletion on IL-6 in both advanced and androgen sensitive cell lines may provide interestingly results.

Upstream mechanisms acting with RAMP1 remain unclear, however evidence from this study suggests that CGRP may not be responsible for the effect seen in RAMP1 KO PC3 cells. It is therefore apposite to look to other RAMP1 associated GPCRs. The calcium sensing receptor (CaSR) should first be considered as a potential mechanism by which RAMP1 can promote prostate cancer. Previous

work in this group has found that in thyroid human carcinoma cells, RAMP1 (and RAMP3) are able to chaperone CaSR to the cell surface and that knockdown of RAMP1 using siRNA results in a 50% reduction in CaSR signalling in response to known CaSR-associated ligands [58]. Expression of this receptor correlates with risk of developing advanced prostate cancer and it has also been suggested to be involved in the process of bone metastasis in both breast and prostate cancer [272, 273]. Knockdown of CaSR results in decreased proliferation in PC3 cells in both *in vivo* and *in vitro* [274]. It could therefore be hypothesised that the effect of RAMP1 deletion in PC3 cells is the result of CaSR no longer being trafficked to the cell surface efficiently.

Unpublished work in this group has also found that RAMP1 may traffic the G protein-coupled receptor family C group 6 member A (GPC6A) to the cell surface of thyroid human carcinoma cells [60]. Knockdown of this receptor not only effects PC3 cell proliferation but also reduced ERK activity. These effects could then be reversed after treatment with GPC6A-associated ligands (e.g. extracellular calcium, osteocalcin, testosterone)[59, 107]. As previously mentioned it is vital to confirm *in vitro* results with appropriate *in vivo* models. This was achieved by crossing GPC6A *-/-* mice onto the transgenic adenocarcinoma of the mouse prostate (TRAMP) model. Traditionally, TRAMP mice displayed evidence of hyperplasia of the prostate after 30 weeks [275]. However, GPC6A *-/-* mice had reduced hyperplasia and an increased survival rate of 23% [107]. RAMP1 KO cells should be tested for CaSR and GPC6A expression and signalling as this could provide information on signalling mechanisms important for advanced prostate cancer progression.

To continue the investigation of RAMP1 in prostate cancer, other GPCRs must be considered and explored. Both the CaSR and GPC6A have been shown to be highly associated with prostate cancer both *in vitro* and *in vivo*. Our group has shown that these receptors rely on RAMP1 for cell surface trafficking and therefore they may be responsible for the effect seen in RAMP1 KO PC3 cells. Future studies must investigate the signalling of these receptors in PC3 WT and PC3 RAMP1 KO cells to discriminate which (if not both) is required for promoting prostate cancer

progression. The crystal structure of the CaSR has enabled the development of potent antagonists which are clinically available and have been used in clinical trials for diseases such as osteoporosis [276]. In cancer, CaSR compounds have been shown to be tumour suppressive in colorectal cancer [277].

The structure of GPRC6A has not been fully described however its similarities with other Class C GPCRs has allowed the development of low micromolar range antagonists that show 9-fold selectivity for GPRC6A over other GPCRs [278]. If future work attributes the effect of RAMP1 deletion in prostate cancer to one of these receptors, it will provide further evidence for a new therapeutic treatment for men with aggressive prostate cancer. Studies specifically looking at the signalling of RAMP1 and its relevant GPCR may provide insight into mechanisms that promote cancer progression and it is possible that these mechanisms may be conserved across many solid cancers. RAMP1 has been found to regulate downstream pathways linked with hormone refractory prostate cancer. RAMP1 should therefore also be investigated in the process of androgen resistance, by testing its role in androgen sensitive cell lines such as LNCaP. This may provide useful insights into the mechanisms behind androgen resistance in prostate cancer and explain why relapsing patients experience this process.

6.1 Future Work

Further investigations can be done to precede this PhD project, including further validation and characterisation of the RAMP1 KO PC3 cells and the continuation of testing functional effects of RAMP1 deletion both *in vitro* and *in vivo*. If antibodies targeting RAMP1 can be optimised in the future, this will be useful for determining if RAMP1 is present at the cell surface of RAMP1 KO PC3 cells. Further characterisation of both wild type and RAMP1 KO PC3 cells could also investigate the presence of CGRP, CaSR and GPRC6A at an mRNA and protein level. To determine if the effects of PC3 cells are regulated by the CGRP receptor, treatment with CGRP and its antagonists can be implemented in *in vitro* assays modelling prostate cancer cell growth and metastasis. Alternatively, the effect of RAMP1 deletion can be

investigated in downstream signaling pathways associated with mechanisms such as invasion and adhesion. This can be achieved by looking at expression levels of important factors such as $\alpha 5\beta 1$ -integrin or focal adhesion kinases which have been previously implicated in many solid cancers [279, 280]. Similarly, additional downstream targets associated with apoptosis can also be investigated to validate effects seen in caspase 3/7 levels after RAMP1 deletion. These downstream investigations could also be expanded by using RNAseq technology to determine any significant differences in mRNA targets between wild type and RAMP1 KO PC3 cells.

To test hypotheses that CaSR or GPRC6A may be signaling through RAMP1 in PC3 cells, further *in vitro* assays could be used. Evidence for CaSR or GPRC6A involvement can be gathered by stimulating both wild type and RAMP1 KO PC3 cells with known agonists or antagonists and measuring downstream responses. Cinacalcet is a known agonist of the CaSR and intracellular calcium levels can be measured using cell permeant, calcium indicator fluorescent dyes. Alternatively, CaSR antagonists have been developed and are also available such as NPS 2143. GPRC6A can be stimulated by multiple endogenous ligands such as testosterone, osteocalcin and amino acids such as L-arginine. However, these ligands are not selective for the GPRC6A receptor and therefore changes in levels of phosphorylated ERK, cAMP or intracellular calcium may not provide conclusive evidence. Fortunately, recent work using computational models has identified selective agonists for the GPRC6A receptor and these could be used in the future to provide further evidence on the possible involvement of this receptor [281].

Further investigation using *in vivo* studies will also provide more information about the role of RAMP1 in metastatic disease. Intracardiac mouse models can be used in the future to determine the effect of RAMP1 deletion on PC3 growth in a bone environment. Testing of CGRP antagonists also found Olcegepant to be more potent on mouse cancer cells compared with Telcagepant, therefore subcutaneous xenograft studies could also be repeated with this antagonist to further test the role of CGRP in prostate tumour growth. By generating RAMP1 knock outs in other prostate cancer cell lines, more can be learned about its role in other prostate cancer

phenotypes. RAMP1 was found to regulate downstream pathways linked with hormone refractory prostate cancer. RAMP1 should therefore also be investigated in the process of androgen resistance, by testing its role in androgen sensitive cell lines such as LNCaP. This may provide useful insights into the mechanisms behind androgen resistance in prostate cancer and explain why relapsing patients experience this process. Alternatively, more aggressive cell lines such as C42B (derived from LNCaP osseous tumours grown in castrated mice) could also be used to generate RAMP1 knock outs to examine the role of RAMP1 in prostate cancer bone metastasis.

6.2 Conclusion

Together, the results of this study have highlighted RAMP1 as an important player in advanced prostate cancer both *in vitro* and *in vivo*. This protein not only promotes cell survival in an aggressive prostate cancer cell line but is also involved in key processes of metastasis. RAMP1 has been found to be essential for invasion, adhesion and colony formation of PC3 cells and its deletion leads to the dysregulation of signalling pathways known to be important in prostate cancer, specifically the development of androgen independent, aggressive tumours that lead to metastasis. RAMP1 is also vital for the growth of tumours in a prostate cancer *in vivo* model, where its deletion causes complete inhibition of tumour growth. This pronounced effect on an aggressive metastatic prostate cell line shows great promise for relapsing patients who after initial treatment transition to an increasingly poor prognosis and limited treatment options. This study provides compelling evidence that RAMP1 should be further considered for therapeutic targeting in advanced prostate cancer and that additional investigations may yield interesting information about the molecular mechanisms behind this protein target.

CHAPTER 7: APPENDIX

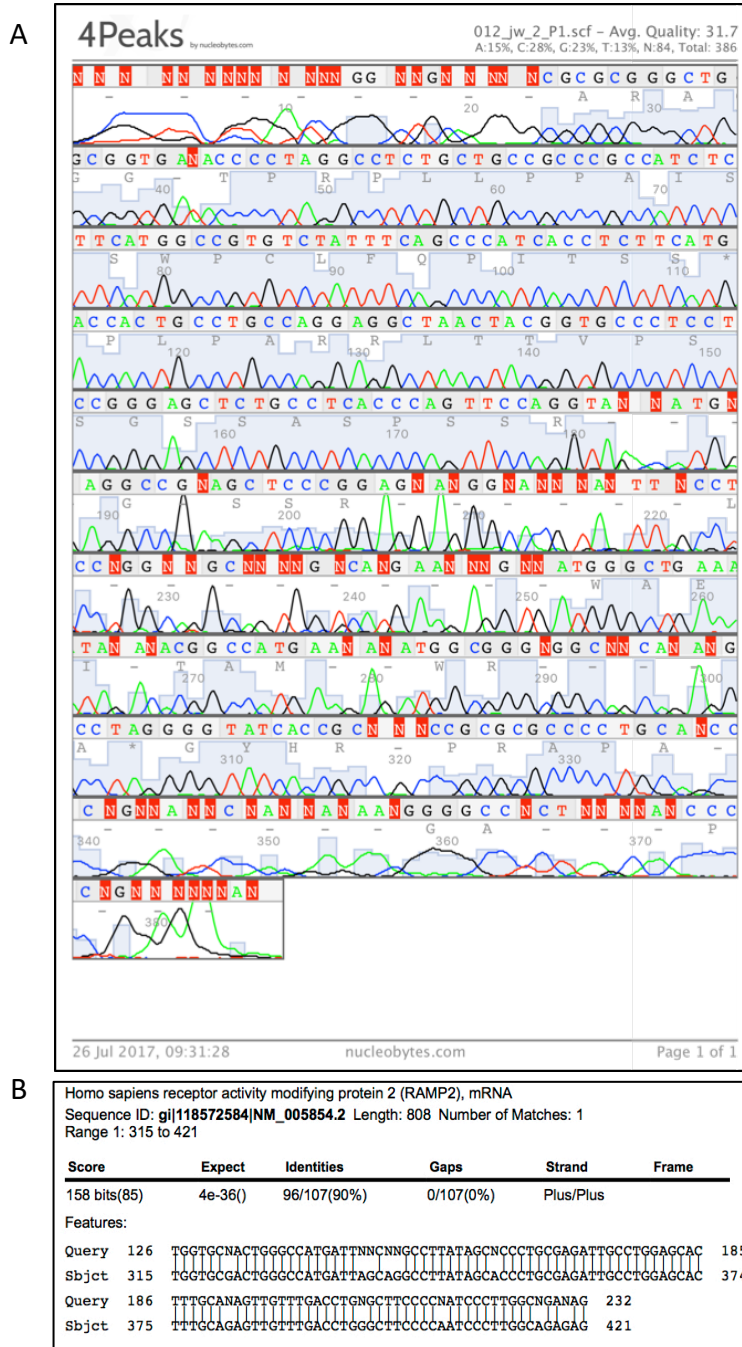


Figure 0.1 Sanger sequencing PC3 WT and RAMP1

Sanger sequence for wild type PC3 targeting RAMP1 analysed using 4Peaks software shows 67% accurate base calling. Background noise found 1-40bp, target size = 256bp. Screenshot of Sanger sequence for RAMP2 aligned with NCBI NM_005854.2 RAMP2 mRNA sequence. 90% identity match was found.



B

Homo sapiens receptor (G protein-coupled) activity modifying protein 3 (RAMP3), mRNA
Sequence ID: [gi|118572586|NM_005856.2](#) Length: 1376 Number of Matches: 1
Range 1: 259 to 435

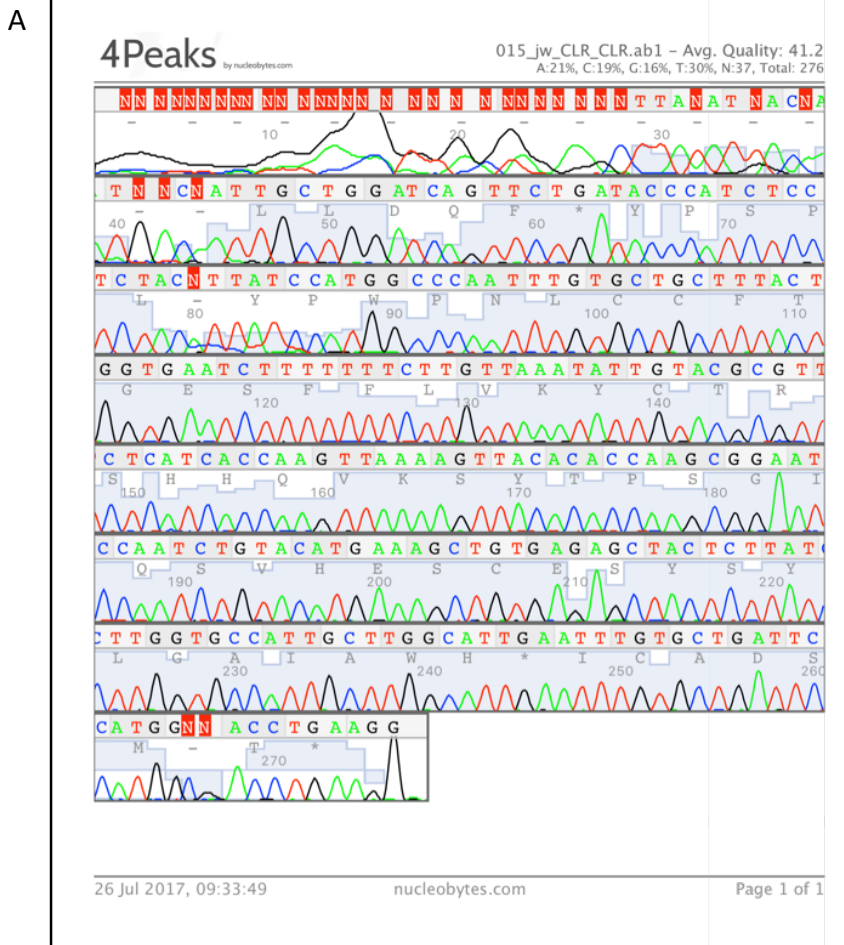
Score	Expect	Identities	Gaps	Strand	Frame
316 bits(171)	5e-84()	174/177(98%)	0/177(0%)	Plus/Plus	

Features:

Query	24	TGANAGTTTCNCCNACTGCACCGAGATGGAGGCCAATGTCGTGGGCTGCTACTGGCCCAA	83
Sbjct	259	TGAGAGTTTCACCAACTGCACCGAGATGGAGGCCAATGTCGTGGGCTGCTACTGGCCCAA	318
Query	84	CCCCCTGGCCCAGGGCTTCATCACCGGCATCCACAGGCAGTTCTTCTCCAACATGCACCGT	143
Sbjct	319	CCCCCTGGCCCAGGGCTTCATCACCGGCATCCACAGGCAGTTCTTCTCCAACATGCACCGT	378
Query	144	GGACAGGGTCCACTTGGAGGACCCCCAGACGAGGTTCTCATCCCGCTGATCGTTAT	200
Sbjct	379	GGACAGGGTCCACTTGGAGGACCCCCAGACGAGGTTCTCATCCCGCTGATCGTTAT	435

Figure 0.2 Sanger sequencing PC3 and RAMP3

Sanger sequence for wild type PC3 targeting RAMP3 analysed using 4Peaks software shows 87% accurate base calling. Background noise found 1-20bp, target size = 227bp. Screenshot of Sanger sequence for RAMP3 aligned with NCBI NM_005856.2 RAMP3 mRNA sequence. 98% identity match was found.



B

Homo sapiens calcitonin receptor-like (CALCRL), transcript variant 2, mRNA
Sequence ID: gij414144893|NM_001271751.1 Length: 5990 Number of Matches: 1
Range 1: 1209 to 1457

Score	Expect	Identities	Gaps	Strand	Frame
443 bits(490)	7e-122()	247/249(99%)	0/249(0%)	Plus/Plus	

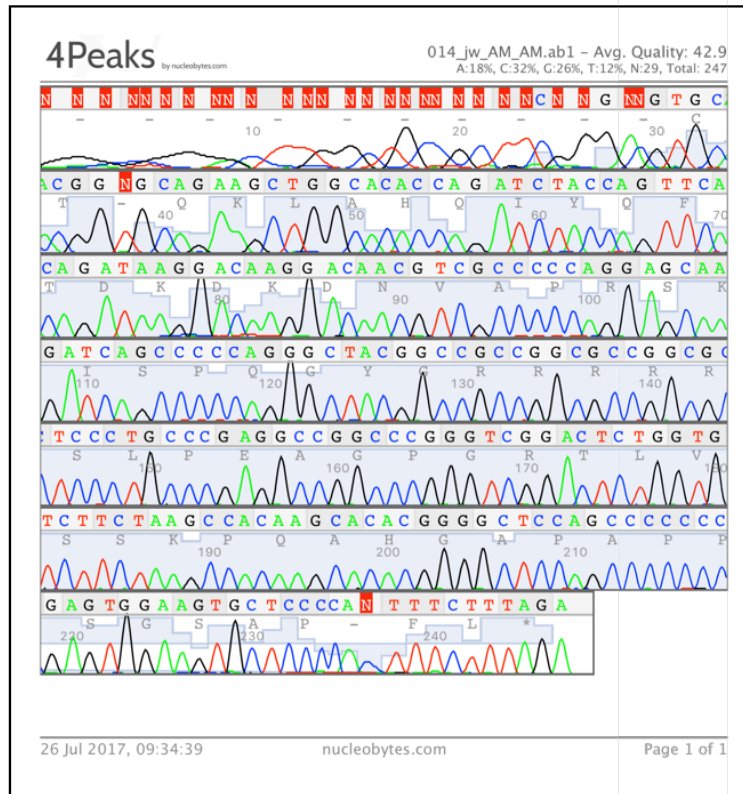
Features:

Query	29	TTATATNACAATNACAATTGCTGGATCAGTTC	TGATACCCATCTCCTCTACATTATCCAT	88
Sbjct	1209	TTATATTACAATGACAATTGCTGGATCAGTTC	TGATACCCATCTCCTCTACATTATCCAT	1268
Query	89	GGCCCAATTTGTGCTGCTTTACTGGTGAATC	tttttttCTTGTAAATATTGTACGCGTT	148
Sbjct	1269	GGCCCAATTTGTGCTGCTTTACTGGTGAATC	TTTTTTCTTGTAAATATTGTACGCGTT	1328
Query	149	CTCATCACCAAGTTAAAAGTTACACCAACG	CGGAATCCAATCTGTACATGAAAGCTGTG	208
Sbjct	1329	CTCATCACCAAGTTAAAAGTTACACCAACG	CGGAATCCAATCTGTACATGAAAGCTGTG	1388
Query	209	AGAGCTACTCTTATCTTGGTGCATTGCTT	GGCATTGAATTTGTGCTGATCCATGGCGA	268
Sbjct	1389	AGAGCTACTCTTATCTTGGTGCATTGCTT	GGCATTGAATTTGTGCTGATCCATGGCGA	1448
Query	269	CTGAAGGA	277	
Sbjct	1449	CTGAAGGA	1457	

Figure 0.3 Sanger sequencing PC3 and CLR

(A) Sanger sequence for wild type PC3 targeting CLR analysed using 4Peaks software shows 87% accurate base calling. Background noise found 1-40bp, target size = 302bp. **(B)** Screenshot of Sanger sequence for CLR aligned with NCBI NM_001271751.1 CLR mRNA sequence. 99% identity match was found.

A



B

Homo sapiens adrenomedullin (ADM), mRNA
Sequence ID: [gi|675022745|NM_001124.2](#) Length: 1606 Number of Matches: 1
Range 1: 605 to 829

Score	Expect	Identities	Gaps	Strand	Frame
396 bits(438)	8e-108()	222/225(99%)	0/225(0%)	Plus/Plus	

Features:

Query	22	TTCNNGANGTGCACGGTGCAGAAGCTGGCACACCAGATCTACCAGTTACAGATAAGGAC	81
Sbjct	605	TTCGGACGTGCACGGTGCAGAAGCTGGCACACCAGATCTACCAGTTACAGATAAGGAC	664
Query	82	AAGGACAACGTGCGCCCCAGGAGCAAGATCAGCCCCAGGGCTACGGCCGCGCGCCGG	141
Sbjct	665	AAGGACAACGTGCGCCCCAGGAGCAAGATCAGCCCCAGGGCTACGGCCGCGCGCCGG	724
Query	142	CGCTCCCTGCCCGAGGCCCGCCCGGCTCGGACTTGGTGTCTTCTAAGCCACAAGCACAC	201
Sbjct	725	CGCTCCCTGCCCGAGGCCCGCCCGGCTCGGACTTGGTGTCTTCTAAGCCACAAGCACAC	784
Query	202	GGGGCTCCAGcccccccGAGTGGAAAGTCTCCCCACTTTCTTTAG	246
Sbjct	785	GGGGCTCCAGCCCCCGAGTGGAAAGTCTCCCCACTTTCTTTAG	829

Figure 0.4 Sanger sequencing PC3 and AM

Sanger sequence for wild type PC3 targeting AM analysed using 4Peaks software shows 88% accurate base calling. Background noise found 1-40bp, target size = 3276bp. Screenshot of Sanger sequence for AM aligned with NCBI NM_001124.2 AM mRNA sequence. 99% identity match was found.

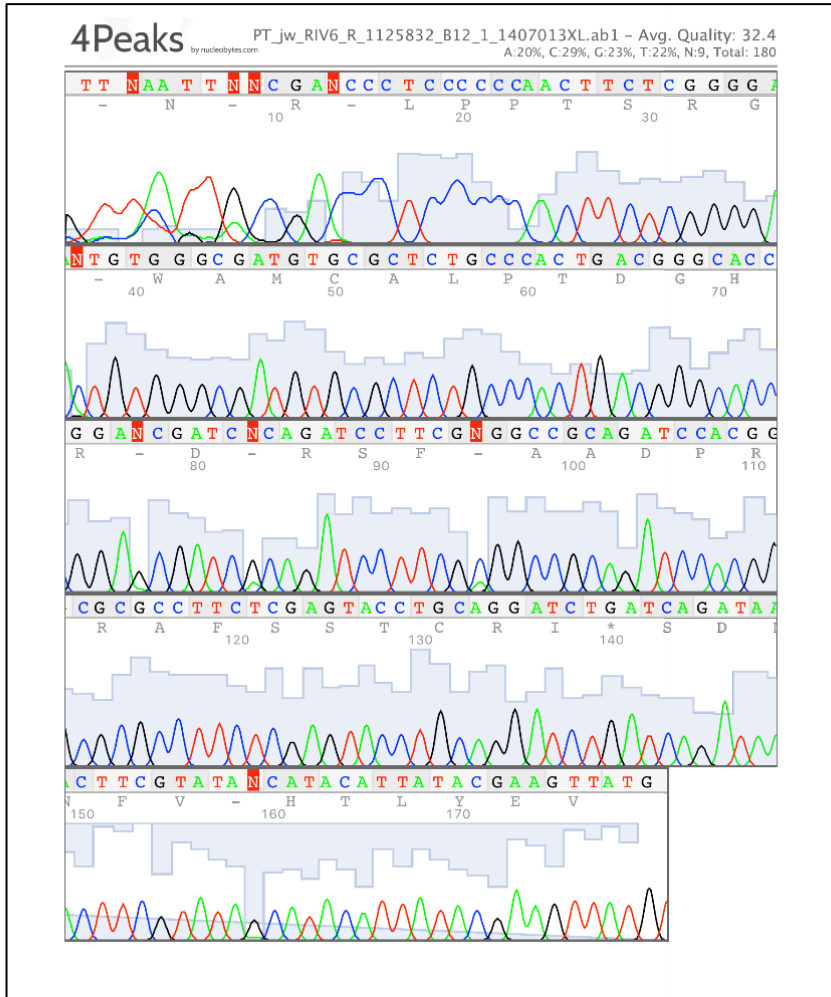


Figure 0.5 Sanger sequencing of CRISPR clone A7 and EF1-alpha promoter region

Sanger sequencing results of CRISPR clone “A7” matches with the EF1-alpha promoter from the CRISPR HDR expression cassette. This demonstrates that the HDR cassette has been inserted into the RAMP1 gene.

Sequence ID: Query_227181 Length: 2730 Number of Matches: 1
Range 1: 1 to 178

Score	Expect	Identities	Gaps	Strand	Frame
291 bits(157)	1e-82()	169/179(94%)	1/179(0%)	Plus/Minus	

Features:

Query	1	TTNAATTNCGANCCCTCCCCCAACTTCTCGGGGANTGTGGGCGATGTGCGCTCTGCC	60
Sbjct	178	TTCAATTGCCGACCCCTCCCCCAACTTCTCGGGGACTGTGGGCGATGTGCGCTCTGCC	119
Query	61	ACTGACGGGCACCGGANCATCNCAGATCCTTCGNGGCCGCAGATCCACGGCGCGCCTTC	120
Sbjct	118	ACTGACGGGCACCGGAGCGATCGCAGATCCTT-GCGGCCGCAGATCCACGGCGCGCCTTC	60
Query	121	TCGAGTACCTGCAGGATCTGATCAGATAACTTCGTATANCATACATTATACGAAGTTAT	179
Sbjct	59	TCGAGTACCTGCAGGATCTGATCAGATAACTTCGTATAGCATAACATTATACGAAGTTAT	1

Figure 0.6 BLAST alignment for CRISPR clone A7

BLAST alignment of RAMP1 CRISPR clone "A7" matches sequence of the EF1-alpha promoter in the CRISPR HDR insert. This demonstrates that the HDR cassette has been inserted into the RAMP1 gene.

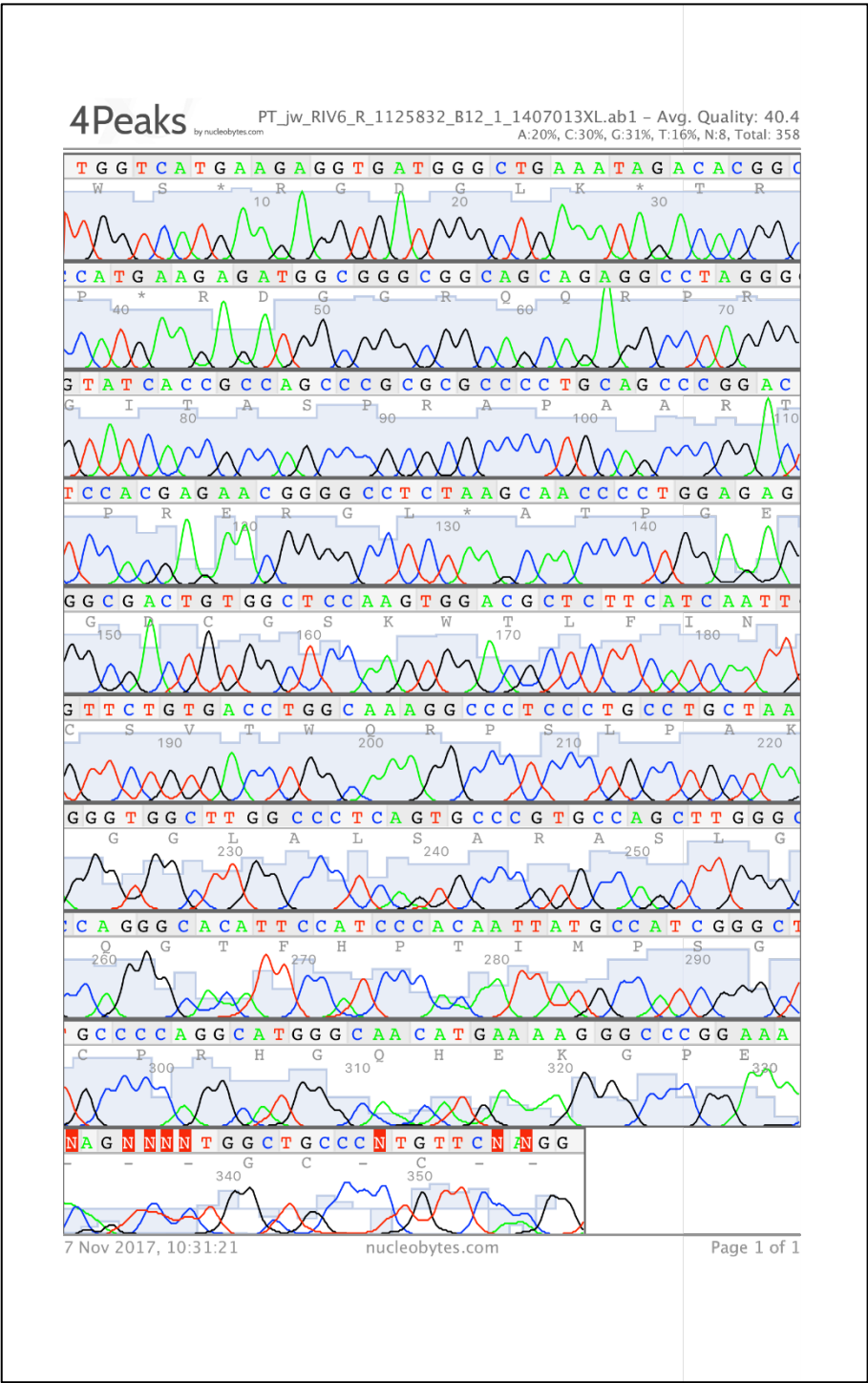


Figure 0.7 Sanger sequencing for CRISPR clone A7 and left homology arm

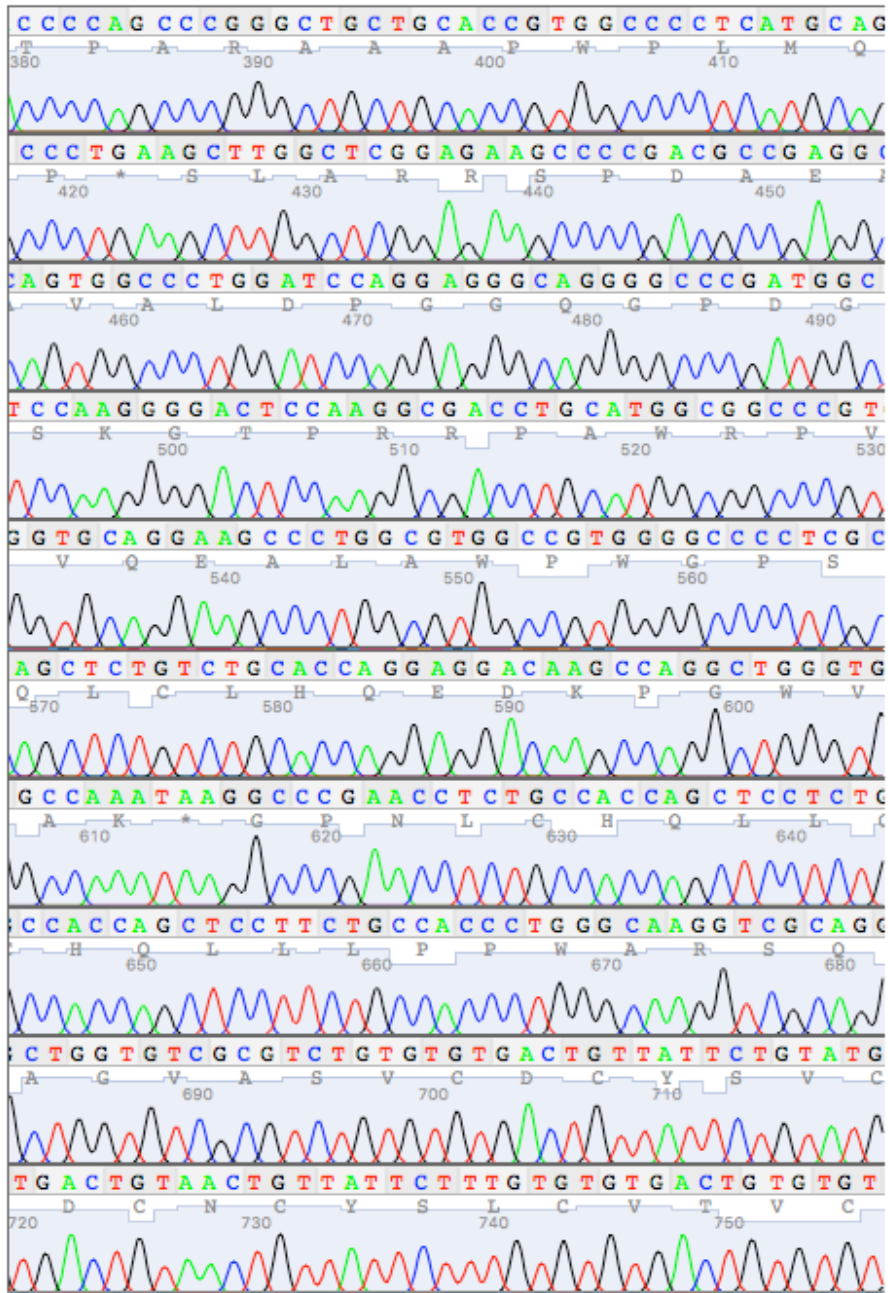
Sanger sequencing results of CRISPR clone “A7” match with the left homology arm from the CRISPR HDR construct and also the RAMP1 gene upstream from the homology arm. This demonstrates that the CRISPR construct has correctly targeted the RAMP1 gene.

Sequence ID: Query_205659 Length: 1439 Number of Matches: 1
Range 1: 1079 to 1431

Score	Expect	Identities	Gaps	Strand	Frame
608 bits(329)	3e-178()	343/353(97%)	0/353(0%)	Plus/Minus	
Features:					
Query 1		TGGTCATGAAGAGGTGATGGGCTGAAATAGACACGGCCATGAAGAGATGGCGGGCGGCAG			60
Sbjct 1431		TGGTCATGAAGAGGTGATGGGCTGAAATAGACACGGCCATGAAGAGATGGCGGGCGGCAG			1372
Query 61		CAGAGGCCTAGGGGTATCACCGCCAGCCCGCGCCCTGCAGCCCGACTCCACGAGAA			120
Sbjct 1371		CAGAGGCCTAGGGGTATCACCGCCAGCCCGCGCCCTGCAGCCCGACTCCACGAGAA			1312
Query 121		CGGGGCTCTAAGCAACCCCTGGAGAGGGCGACTGTGGCTCCAAGTGGACGCTCTTCATC			180
Sbjct 1311		CGGGGCTCTAAGCAACCCCTGGAGAGGGCGACTGTGGCTCCAAGTGGACGCTCTTCATC			1252
Query 181		AATTGTCTGTGACCTGGCAAAGGCCCTCCCTGCCTGCTAAGGGTGGCTTGGCCCTCAGT			240
Sbjct 1251		AATTGTCTGTGACCTGGCAAAGGCCCTCCCTGCCTGCTAAGGGTGGCTTGGCCCTCAGT			1192
Query 241		GCCCGTGCCAGCTTGGGCCAGGGCACATTCATCCACAATTATGCCATCGGGCTGCCCC			300
Sbjct 1191		GCCCGTGCCAGCTTGGGCCAGGGCACATTCATCCACAATTATGCCATCGGGCTGCCCC			1132
Query 301		AGGCATGGGCAACATGAAAAGGGCCCGGAAANAGNNNNTGGCTGCCNTGTTC			353
Sbjct 1131		AGGCATGGGCAACATGAGAGGGGCCCGGAGACAGTCTCTGGCTGCCCTGTTC			1079

Figure 0.8 BLAST alignment of RAMP1 CRISPR clone A7 and left homology arm.

BLAST alignment of RAMP1 CRISPR clone “A7” matches homology arm sequence (highlighted yellow) designed for the CRISPR construct and also the RAMP1 gene upstream from the homology arm (unhighlighted). This demonstrates that the CRISPR construct has correctly targeted the RAMP1 gene.



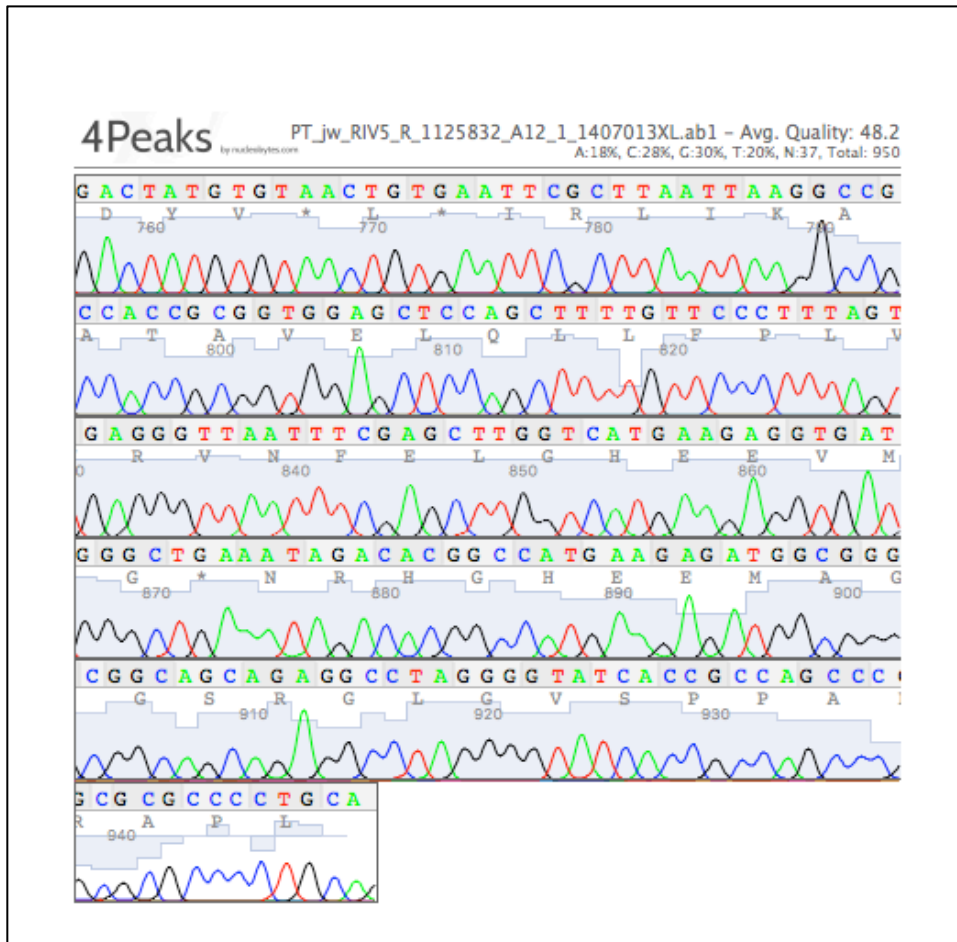


Figure 0.9 Sanger sequencing of CRISPR clone C1 and left homology arm.

Sanger sequencing results of CRISPR clone “C1” match with the left homology arm from the CRISPR HDR construct and also the RAMP1 gene upstream from the homology arm. This demonstrates that the CRISPR construct has correctly targeted the RAMP1 gene.

Sequence ID: Query_95331 Length: 235 Number of Matches: 5
 Range 1: 44 to 201

Score	Expect	Identities	Gaps	Strand	Frame
277 bits(306)	2e-78()	157/158(99%)	1/158(0%)	Plus/Minus	
Features:					
Query	1	ATAACTTCGTATAATGTATGCTATACGAAGTTATCTGATCAGATCCTGCAGGTACTCGAG			60
Sbjct	201	ATAACTTCGTATAATGTATGCTATACGAAGTTATCTGATCAGATCCTGCAGGTACTCGAG			142
Query	61	AAGGCGCGCCGTGGATCTGCGGCCGC-AAGGATCTGCGATCGCTCCGGTGCCCGTCAGTG			119
Sbjct	141	AAGGCGCGCCGTGGATCTGCGGCCGC-AAGGATCTGCGATCGCTCCGGTGCCCGTCAGTG			82
Query	120	GGCAGAGCGCACATCGCCACAGTCCCGAGAAAGTTGG		157	
Sbjct	81	GGCAGAGCGCACATCGCCACAGTCCCGAGAAAGTTGG		44	

Figure 0.10 BLAST alignment of CRISPR clone C1 and EF1-alpha promoter

BLAST alignment of RAMP1 CRISPR clone “C1” matches sequence of the EF1-alpha promoter in the CRISPR HDR insert. This demonstrates that the HDR cassette has been inserted into the RAMP1 gene.

Homo sapiens chromosome 2, alternate assembly CHM1_1.1
Sequence ID: **gij528476665|NC_018913.2** Length: 243205335 Number of Matches: 1
Range 1: 238790791 to 238791674

Score	Expect	Identities	Gaps	Strand	Frame
1110 bits(601)	0.0()	744/884(84%)	0/884(0%)	Plus/Plus	

Features:
receptor activity-modifying protein 1 isoform 1 precursor
receptor activity-modifying protein 1 isoform 2

Query	53	GTCTCCNANGGCAGCTCTGGCCTC	NNANTGNCAAGCTCCTTCCANGAATTTNAAANGGNN	112
Sbjct	238790791	GTCTCCCAGGGCAGCTCTGGCCT	CCCAGTGCCAAGCTCCTTCCAGGAATTTGAAAGGGCC	238790850
Query	113	ANGCCGNTANGGGTGGGGCTGGG	NGTCCCCCTGGGNANANGATGTGNNCTGNNNGGAAA	172
Sbjct	238790851	AGGCCGGTAGGGGTGGGGCTGGG	GTCCCCCTGGGCAGAGGATGTGGCTGGGGGAAA	238790910
Query	173	ANGANGNNANNTGNNGANANTG	NNAGNCCANGANCCANNCTTAAANAGGNAATGCAA	232
Sbjct	238790911	AGGAGGGGACCTGGGGACAGTGG	GAGGCCAGGAGCCAAGCCCTAAACAGGGAATGCAA	238790970
Query	233	AGCTTCTGCCCCAGCTGNCTAC	NANGTGNCCAANAANANANGCTCAGNNTGAGGAGG	292
Sbjct	238790971	AGCTTCTGCCCCAGCTGCCCTAC	GAGGTGGCCAAGAAAGAGAGGCTCAGCCTGAGGAGG	238791030
Query	293	AANAAGAAGCCTGGTGGGTGGGG	GANCAAGGCCATGCTCTCCCCGCCACNCCCGCCCC	352
Sbjct	238791031	AAGAAGAAGCCTGGTGGGTGGGG	GACCAAGGCCATGCTCTCCCCGCCACCCCGCCCC	238791090
Query	353	ANCCAGCCAGCAGTGAAGTACG	GGNNGAAATTAGTCAATCCTGATTTCTGTGCGGGNATCG	412
Sbjct	238791091	ACCCAGCCAGCAGTGAAGTACG	GGGAAATTAGTCAATCCTGATTTCTGTGCGGGCATCG	238791150
Query	413	CTGGNCANGTNACTGTNCTCTN	TGTATGGCTNGAGGCAGGANGAGGAGCACANTTCA	472
Sbjct	238791151	CTGGCAGGTCACTGTGTCTGTG	TATGGCTCAGGCAGGAGGAGGAGCACAGTTCA	238791210
Query	473	TGCTTCCNTTGTTCAGCTCGTT	CATAGCCCGCAAATAGTCAGACAGGANATGTGCCTGC	532
Sbjct	238791211	TGCTTCCGTTGTTCAGCTCGTT	CATAGCCCGCAGATAGTCAGACAGGAGATGTGCCTGC	238791270
Query	533	AGCTCCTGGGCTGGGNGNACAN	CCANCCANNCNATCNCNCANGTANNCGTGAACANG	592
Sbjct	238791271	AGCTCCTGGGCTGGGGGACAG	CCAGCCAGCCCATCCCCAGGTACCCGTGAACAGG	238791330
Query	593	GGNAGCNAGANACTGTCTNCN	GGNCCCTCTNATGCTGCCNATGCNTGGNGCAGCNCGATG	652
Sbjct	238791331	GGCAGCCAGAGACTGTCTCCG	GGCCCTCTCATGCTGCCATGCCTGGGGCAGCCCGATG	238791390
Query	653	GCATAATTGTGGGATGGAATGT	GCNNTGGNCCAAGCTGGNACGGGCANTGANNGNNAANN	712
Sbjct	238791391	GCATAATTGTGGGATGGAATGT	GCCTTGGCCCAAGCTGGCACGGGCACAGGGCCAAGA	238791450
Query	713	NANCCTTANCAGGCANGNAGG	GCCTTTGNAGGTACAGAACAAATGATGAAGAGCGTCC	772
Sbjct	238791451	CACCCCTAGCAGGCAGGGAGG	GCCTTTGCCAGGTACAGAACAAATGATGAAGAGCGTCC	238791510
Query	773	ACTTNGAGCCACAGTCGCCCT	TCCAGNGNTTGCTTANAGGCNCCGTTCTCGTNGAGTCC	832
Sbjct	238791511	ACTTGGAGCCACAGTCGCCCT	TCCAGGGGTTGCTTAGAGGCCCCGTTCTCGTGGAGTCC	238791570
Query	833	NGNCTGNACGGGCNCNNGNCT	TGGNGATGATANNNCTAGGNCCTTGCTGNCNNCNGNNAT	892
Sbjct	238791571	GGGCTGCAGGGGCGCGGGCT	TGGCGGTGATACCCCTAGGCCTCTGCTGCCGCCGCCAT	238791630
Query	893	CTCTTCATGGCCGTGTCTATTT	CAGCCATCACCTCTTCATGAC	936
Sbjct	238791631	CTCTTCATGGCCGTGTCTATTT	CAGCCATCACCTCTTCATGAC	238791674

Figure 0.11 BLAST alignment of CRISPR clone C1 and left homology arm.

BLAST alignment of RAMP1 CRISPR clone “C1” matches homology arm sequence (highlighted yellow) designed for the CRISPR construct and also the RAMP1 gene upstream from the homology arm (unhighlighted). This demonstrates that the CRISPR construct has targeted the RAMP1 gene correctly.

Homo sapiens receptor activity modifying protein 2 (RAMP2), mRNA
Sequence ID: [gi|118572584|NM_005854.2](#) Length: 808 Number of Matches: 1
Range 1: 315 to 421

Score	Expect	Identities	Gaps	Strand	Frame
158 bits(85)	4e-36()	96/107(90%)	0/107(0%)	Plus/Plus	

Features:

```

Query 126 TGGTGCNACTGGGCCATGATTNNCNGCCTTATAGCNCCCTGCGAGATTGCCTGGAGCAC 185
Sbjct 315 TGGTGCGACTGGGCCATGATTAGCAGGCCTTATAGCACCCCTGCGAGATTGCCTGGAGCAC 374
Query 186 TTTGCANAGTTGTTTGACCTGNGCTTCCCNATCCCTTGGCNGANAG 232
Sbjct 375 TTTGCAGAGTTGTTTGACCTGGGCTTCCCAATCCCTTGGCAGAGAG 421

```

Figure 0.13 BLAST alignment of PC3 for RAMP2

BLAST alignment of wild type PC3 with NCBI sequence for RAMP2 (NM_005854) results in a 90% sequence match.

Sequence ID: Query_180129 Length: 233 Number of Matches: 1
Range 1: 47 to 184

Score	Expect	Identities	Gaps	Strand	Frame
113 bits(124)	4e-30()	103/139(74%)	2/139(1%)	Plus/Minus	

Features:

```

Query 14 TGCTCCAGGCA-TCTCGCAGGGTGTATAAGGCCTGCTAATCATGGCCCAGTCGCACCAA 72
Sbjct 184 TGCTCCAGGCAATCTCGCAGGGNGCTATAAGGCNNGNNAATCATGGCCCAGTNGCACC-A 126
Query 73 TCCTTTTCGATAGGATCCATTGATCCTTATAATGATTCCAGCAAAATGGACAGCTGTC 132
Sbjct 125 NNCNNNNNGATAGGANCCATNNGATCNNNATAANGANNCCANCAAAAANNGGACANNNGTN 66
Query 133 TCATAGTTCTTACCGTCC 151
Sbjct 65 TNATAGTTNNNCACCN TCC 47

```

Figure 0.14 BLAST alignment of CRISPR clone A7 and PC3 wild type

BLAST alignment of RAMP1 KO clone "A7" with wild type PC3 sanger sequences results in a 74% match.

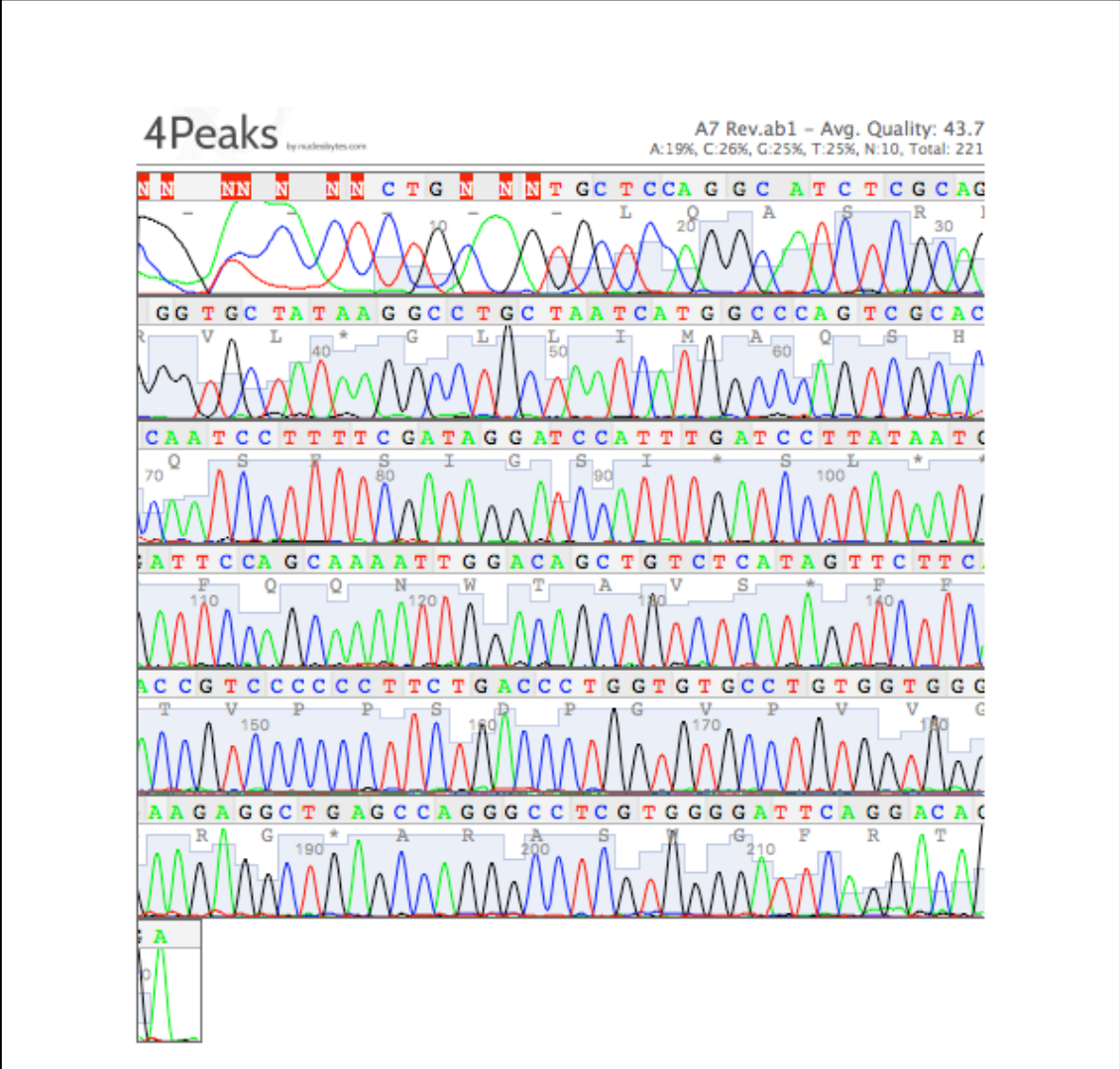


Figure 0.15 Sanger sequencing for CRISPR clone A7 and RAMP2

Homo sapiens receptor activity modifying protein 2 (RAMP2), mRNA
Sequence ID: **gi|118572584|NM_005854.2** Length: 808 Number of Matches: 1
Range 1: 315 to 421

Score	Expect	Identities	Gaps	Strand	Frame
158 bits(85)	9e-35()	96/107(90%)	0/107(0%)	Plus/Plus	

Features:

Query	126	TGGTGCNACTGGGCCATGATTNNCNGCCTTATAGCNCCTGCGAGATTGCCTGGAGCAC	185
Sbjct	315	TGGTGCGACTGGGCCATGATTAGCAGGCCTTATAGCACCTGCGAGATTGCCTGGAGCAC	374
Query	186	TTTGCANAGTTGTTTGACCTGNGCTTCCCCNATCCCTTGGCNGANAG	232
Sbjct	375	TTTGCAGAGTTGTTTGACCTGGGCTTCCCAATCCCTTGGCAGAGAG	421

Figure 0.16 BLAST alignment for CRISPR clone A7 and RAMP2

BLAST search of RAMP1 KO clone "A7" sequence results in a 90% sequence match with NCBI RAMP2 sequence (NM_005854).

Sequence ID: Query_206255 Length: 233 Number of Matches: 1
Range 1: 59 to 233

Score	Expect	Identities	Gaps	Strand	Frame
161 bits(178)	9e-45()	144/176(82%)	1/176(0%)	Plus/Plus	

Features:

Query	49	ACTATNNNACAGNTGTCNAWTTTTCGNGNNATCNTTATNNGGATCNNATGNATCCTATCG	108
Sbjct	59	ACTATNANACNNNTGTCNNNTTGTGNTGGNNTCNTTATNNGATCNNATGGNTCCTATCN	118
Query	109	AAAAGGATTGGTGGCGACTGGGCCATGATTAGCAGGCCTTATAGCACCTGCGAGATTGCC	168
Sbjct	119	NNNNGNNT-GGTGCNACTGGGCCATGATTNNCNGCCTTATAGCNCCTGCGAGATTGCC	177
Query	169	TGGAGCACTTTGCAGAGTTGTTTGACCTGGGCTTCCCCAATCCCTTGGCANANAGA	224
Sbjct	178	TGGAGCACTTTGCANAGTTGTTTGACCTGNGCTTCCCNATCCCTTGGCNGANAGA	233

Figure 0.18 BLAST alignment of CRISPR clone C1 and PC3 wild type

BLAST alignment of RAMP1 KO clone “C1” and wild type PC3 Sanger sequences result in an 82% match.

Homo sapiens mRNA encoding RAMP2
Sequence ID: [gi|3171911|AJ001015.1](#) Length: 780 Number of Matches: 1
Range 1: 213 to 416

Score	Expect	Identities	Gaps	Strand	Frame
303 bits(164)	1e-78()	184/204(90%)	0/204(0%)	Plus/Plus	

Features:

Query	15	GGCNCNCAGGGTCAGAAGGGGGNANGTGAAGNACTATNNNACAGNTGTCNAWTTTTCG	74
Sbjct	213	GGCACACCAGGGTCAGAAGGGGGACGGTGAAGAATATGAGACAGCTGTCCAATTTTCG	272
Query	75	NGNNATCNTTATNNGGATCNNATGNATCCTATCGAAAAGGATTGGTGGCGACTGGGCCATG	134
Sbjct	273	TGGAATCATATAAGGATCAAATGGATCCTATCGAAAAGGATTGGTGGCGACTGGGCCATG	332
Query	135	ATTAGCAGGCCTTATAGCACCTGCGAGATTGCCTGGAGCACTTTGCAGAGTTGTTTGAC	194
Sbjct	333	ATTAGCAGGCCTTATAGCACCTGCGAGATTGCCTGGAGCACTTTGCAGAGTTGTTTGAC	392
Query	195	CTGGGCTTCCCCAATCCCTTGGCA	218
Sbjct	393	CTGGGCTTCCCCAATCCCTTGGCA	416

Figure 0.19 BLAST alignment of CRISPR clone C1 and RAMP2

BLAST search of RAMP1 KO clone “C1” results in a 90% match with NCBI RAMP2 sequence (NM_005854).

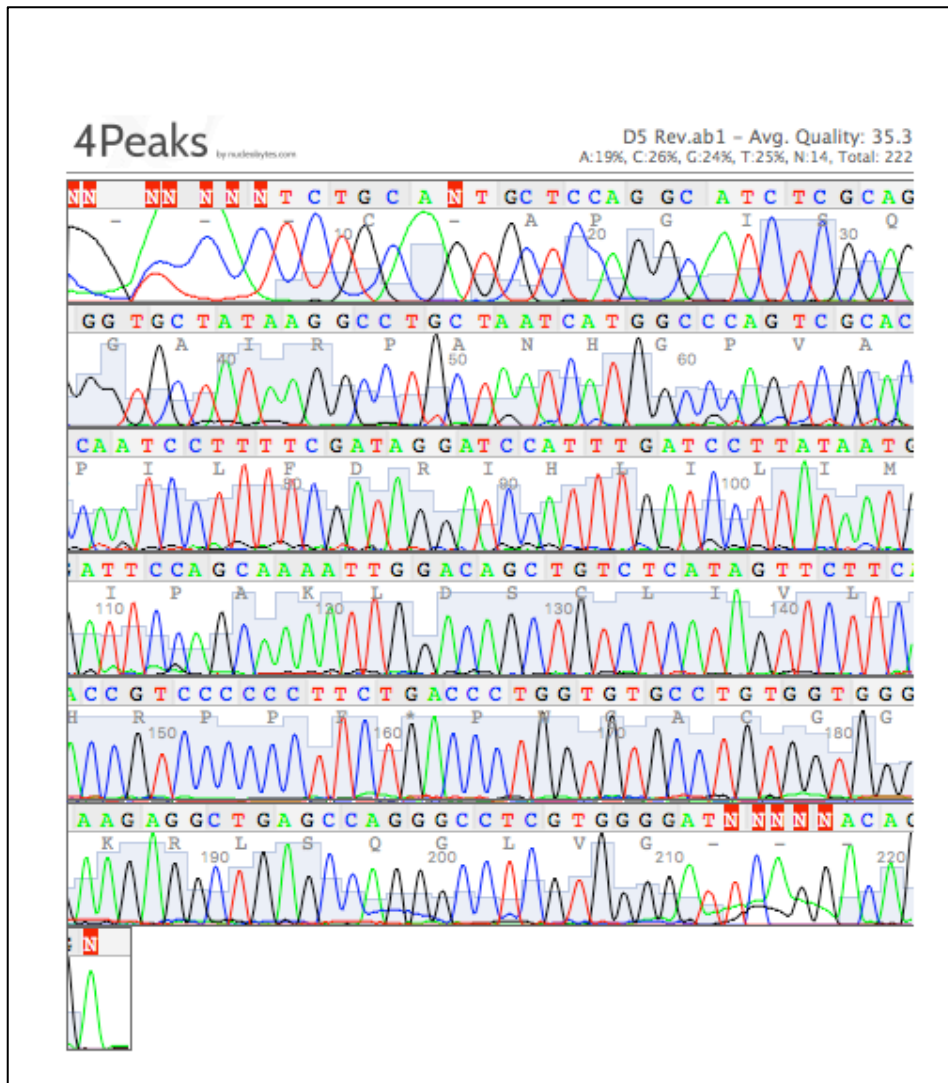


Figure 0.20 Sanger sequencing for CRISPR clone D5 and RAMP2

Sequence ID: Query_58867 Length: 233 Number of Matches: 1
Range 1: 47 to 184

Score	Expect	Identities	Gaps	Strand	Frame
113 bits(124)	4e-30()	103/139(74%)	2/139(1%)	Plus/Minus	

Features:

```

Query 15  TGCTCCAGGCA-TCTCGCAGGGTGCTATAAGGCCTGCTAATCATGGCCCAGTCGCACCAA 73
Sbjct 184 TGCTCCAGGCAATCTCGCAGGGNGCTATAAGGCNNGNNAATCATGGCCCAGTNGCACC-A 126
Query 74  TCCTTTTCGATAGGATCCATTTGATCCTTATAATGATTCCAGCAAAAATTGGACAGCTGTC 133
Sbjct 125  NNCNNNNNGATAGGANCCATNNGATCNNNATAANGANNCCANCAAAAANNGGACANNNGTN 66
Query 134 TCATAGTTC TTCACCGTCC 152
Sbjct 65  TNATAGTTNNNCACCNTCC 47

```

Figure 0.21 BLAST alignment of CRISPR clone D5 and PC3 wild type

BLAST alignment of RAMP1 KO clone “D5” and wild type PC3 sequences results in a 74% match.

Homo sapiens receptor activity modifying protein 2 (RAMP2), mRNA
Sequence ID: [gi|118572584|NM_005854.2](#) Length: 808 Number of Matches: 1
Range 1: 175 to 373

Score	Expect	Identities	Gaps	Strand	Frame
361 bits(195)	6e-96()	198/199(99%)	1/199(0%)	Plus/Minus	

Features:

```

Query 15  TGCTCCAGGC-ATCTCGCAGGGTGCTATAAGGCCTGCTAATCATGGCCCAGTCGCACCAA 73
Sbjct 373  TGCTCCAGGCAATCTCGCAGGGTGCTATAAGGCCTGCTAATCATGGCCCAGTCGCACCAA 314
Query 74  TCCTTTTCGATAGGATCCATTTGATCCTTATAATGATTCCAGCAAAAATTGGACAGCTGTC 133
Sbjct 313  TCCTTTTCGATAGGATCCATTTGATCCTTATAATGATTCCAGCAAAAATTGGACAGCTGTC 254
Query 134 TCATAGTTC TTCACCGTCCCCCTTC TGACCTGGTGTGCCTGTGGTGGGAAGAGGCTGA 193
Sbjct 253  TCATAGTTC TTCACCGTCCCCCTTC TGACCTGGTGTGCCTGTGGTGGGAAGAGGCTGA 194
Query 194 GCCAGGGCCTCGTGGGGAT 212
Sbjct 193  GCCAGGGCCTCGTGGGGAT 175

```

Figure 0.22 BLAST alignment of CRISPR clone D5 and RAMP2

BLAST search of RAMP1 KO clone “D5” sequence results in a 99% match with NCBI RAMP2 sequence (NM_005854).

Table 0.1 List of manufacturers and reagents

Reagent	Company, Product No.
Cell Culture	
RPMI 1640, GlutaMAX	Thermo Fisher, 61870
Fetal Bovine Serum	Sigma-Aldrich, F7524
Penicillin-Streptomycin (P/S)	Thermo Fisher, 15140
Dulbecco's Phosphate-Buffered Saline (PBS)	Thermo Fisher, 14040
TrypLE Express Enzyme	Thermo Fisher, 12605
Trypan Blue Solution, 0.4%	Thermo Fisher, 15250
Polymerase Chain Reaction (Endpoint and Quantitative)	
Reliaprep Cell Miniprep System	Promega, TM370
High-Capacity RNA-to-cDNA™ Kit	Thermo Fisher, 4387406
GoTaq® G2 Flexi DNA Polymerase	Promega, M7801
5X GoTaq G2 Green Buffer	Thermo Fisher, AM9780
MgCl ₂	Promega, M7481
dNTP mix	Promega U1511
PCR Primer Oligonucleotides	Eurofins
microLYSIS-Plus	Microzone
Phusion High-Fidelity DNA Polymerase	Thermo Scientific, F530S
Gel Electrophoresis	
Agarose	Fisher Scientific, BP1356
Tris Acetate EDTA (TAE)	National Diagnostics, EC861
Ethidium Bromide	Sigma Aldrich, E1385
FullRanger 100bp DNA Ladder	GeneFlow, L3-0014
Western Blot	
Tergitol (NP40)	Sigma-Aldrich, NP40S
Sodium Chloride	Fisher Scientific, S/3120/63
Tris Base	Fisher Scientific, BP152-1
Halt™ Protease and Phosphatase Inhibitor Cocktail (100x)	Thermo Fisher, 78440
DC Protein Assay Kit II	Bio-Rad, 5000002
4x Laemmli Buffer	Bio-Rad, 1610747
Dithiothreitol (DTT)	Fisher Scientific, R0861
10x Tris/Glycine/SDS (TGS)	Bio-Rad, 1610772

Precision Plus Protein WesternC Standards	Bio-Rad, 16103796
4-20% Mini-PROTEAN® Precast Protein Gels	Bio-Rad, 4561094
Trans-Blot® Turbo™ Mini PVDF Transfer Packs	Bio-Rad, 1704156
SuperSignal™ West Dura Extended Duration Substrate	Thermo Fisher, 34075
ELISA	
Human CGRP fluorescent enzyme immunoassay (EIA)	Phoenix Pharmaceuticals, FEK-015-02
cAMP Assay	
LANCE cAMP 384 Kit	PerkinElmer, AD0264
384-well Optiplates	PerkinElmer, 6007299
Hank's Buffered Saline Solution (HBSS)	Thermo Scientific, 24020
Hank's Buffered Saline Solution (no Ca ²⁺ , no Mg ²⁺)	Thermo Scientific, 14170
Stabilizer, 7.5% (DTPA-purified BSA)	PerkinElmer, CR84
3-isobutyl-1-methylxanthine	Sigma-Aldrich, I5879
HEPES	Fisher Scientific, BP310-1
Forskolin	Sigma-Aldrich, F3917
Human adrenomedullin	Anaspec, AS-60447
Human calcitonin gene-related peptide	Sigma-Aldrich, SCP0060
Rat amylin	Bachem, H-9475
Telcagepant	MedChem Express, HY-32709
MK3207	MedChem Express, HY-10302
Olcegepant	MedChem Express, HY-10095A
CRISPR Transfections	
RS-1	TOCRIS Bioscience, 5810
Scr7 Pyrazine	TOCRIS Bioscience, 53410
OptiMEM Reduced Serum Media	Gibco, 31985062
Lipofectamine 3000	Thermo Scientific, L3000001
RAMP1 HDR + Cas9 Plasmids	Santa Cruz Biotechnology, sc-424560
RAMP2 HDR + Cas9 Plasmids	Santa Cruz Biotechnology, sc-424864

RAMP3 HDR + Cas9 Plasmids	Santa Cruz Biotechnology, sc- 425003
Control CRISPR/Cas9 Plasmid	Santa Cruz, sc-418922
Viability Assay	
RealTime-Glo™ MT Cell Viability Assay	Promega, G9712
Corning™ Costar™ 96-Well White Clear-Bottom Plates	Corning, 3610
Apoptosis Assays	
Caspase-Glo™ 3/7 Apoptosis Assay	Promega, G8093
Migration/Invasion/Adhesion/CFU	
Mitomycin C	Sigma, M4287
Toluidine Blue	Sigma, T3260
Sodium Tetraborate	Sigma, 221732
BD Biocoat™ Matrigel™ Transwell Chambers	Corning, 354481
Crystal Violet	Sigma, 61135
Calcein AM	Thermo Scientific, C1430
Fibronectin-coated 96 well plates	Corning, 354409
Multiplex Bead Assay	
MILLIPLEX Map Multi-Pathway Magnetic Bead 9- plex – Cell Signalling Multiplex Assay Kit	Merck, 48-680MAG
Protease Inhibitor Cocktail Set III	Merck, 539134
Ultrafree-MC VV Centrifugal Filter	Merck, UFC30VV25
Subcutaneous In Vivo Study	
Telcagepant	MedChem Express, HY- 32709
Kolliphor® HS 15	Sigma-Aldrich, 42966
Kollisolv® PEG E 400	Sigma-Aldrich, 06855
PBS	Thermo Fisher, 10010
Dimethyl Sulfoxide (DMSO)	Sigma-Aldrich, D8418
Corning® Matrigel® Basement Matrix	Corning, 354234

Immunohistochemistry	
Rat anti-mouse CD31 mAb (Clone SZ31)	Dianova, DIA-310
Rabbit anti-human Ki67 pAb	Abcam, ab15580
VECTASTAIN® ABC-HRP Kit (Peroxidase, Rat IgG)	Vector Laboratories, PK-4004
VECTASTAIN® ABC-HRP Kit (Peroxidase, Rabbit IgG)	Vector Laboratories, PK-4001
ImmPACT DAB EqV Peroxidase (HRP) Substrate	Vector Laboratories, SK-4103
100x Citrate Buffer pH 6.0	Abcam, ab93678
Tris Base	Fisher Scientific, BP337-500
Sodium chloride	Fisher Scientific, 5/3120/63
PBS Tablets	Thermo Fisher, BR0014G
Tween-20	Fisher Scientific, BP337-500
UltraPure EDTA	Thermo Fisher, 15575020
30% Hydrogen Peroxide Solution	Sigma-Aldrich, 31642
ImmEdge Hydrophobic Barrier PAP Pen	Vector Laboratories, H-4000
DPX Mountant	Sigma-Aldrich, 06522
Gill's Haematoxylin	Merck, 105174

BIBLIOGRAPHY

1. *Cancer Research UK*. [cited 2017 30th December]; Available from: <http://www.cancerresearchuk.org/health-professional/cancer-statistics/statistics-by-cancer-type/prostate-cancer#heading-Zero>.
2. Finkel, T., M. Serrano, and M.A. Blasco, *The common biology of cancer and ageing*. *Nature*, 2007. **448**(7155): p. 767-74.
3. Wang, M., J. Zhao, L. Zhang, F. Wei, Y. Lian, Y. Wu, Z. Gong, S. Zhang, J. Zhou, K. Cao, X. Li, W. Xiong, G. Li, Z. Zeng, and C. Guo, *Role of tumor microenvironment in tumorigenesis*. *Journal of Cancer*, 2017. **8**(5): p. 761-773.
4. Bissell, M.J. and D. Radisky, *Putting tumours in context*. *Nat Rev Cancer*, 2001. **1**(1): p. 46-54.
5. Hanahan, D. and R.A. Weinberg, *The hallmarks of cancer*. *Cell*, 2000. **100**(1): p. 57-70.
6. Hanahan, D. and Robert A. Weinberg, *Hallmarks of Cancer: The Next Generation*. *Cell*, 2011. **144**(5): p. 646-674.
7. Seisen, T., M. Roupret, A. Faix, and S. Droupy, *[The prostate gland: a crossroad between the urinary and the seminal tracts]*. *Prog Urol*, 2012. **22 Suppl 1**: p. S2-6.
8. Aumuller, G., H.W. Goebel, M. Bacher, W. Eicheler, and U. Rausch, *[Current aspects on morphology and functions of the prostate]*. *Verh Dtsch Ges Pathol*, 1993. **77**: p. 1-18.
9. Vinjamoori, A.H., J.P. Jagannathan, A.B. Shinagare, M.E. Taplin, W.K. Oh, A.D. Van den Abbeele, and N.H. Ramaiya, *Atypical metastases from prostate cancer: 10-year experience at a single institution*. *AJR Am J Roentgenol*, 2012. **199**(2): p. 367-72.
10. Attard, G., C. Parker, R.A. Eeles, F. Schroder, S.A. Tomlins, I. Tannock, C.G. Drake, and J.S. de Bono, *Prostate cancer*. *Lancet*, 2016. **387**(10013): p. 70-82.

11. Daniyal, M., Z.A. Siddiqui, M. Akram, H.M. Asif, S. Sultana, and A. Khan, *Epidemiology, etiology, diagnosis and treatment of prostate cancer*. Asian Pac J Cancer Prev, 2014. **15**(22): p. 9575-8.
12. Heidenreich, A., P.J. Bastian, J. Bellmunt, M. Bolla, S. Joniau, T. van der Kwast, M. Mason, V. Matveev, T. Wiegand, F. Zattoni, and N. Mottet, *EAU Guidelines on Prostate Cancer. Part 1: Screening, Diagnosis, and Local Treatment with Curative Intent*; Update 2013. European Urology, 2014. **65**(1): p. 124-137.
13. Carvalhal, G.F., D.S. Smith, D.E. Mager, C. Ramos, and W.J. Catalona, *Digital rectal examination for detecting prostate cancer at prostate specific antigen levels of 4 ng./ml. or less*. J Urol, 1999. **161**(3): p. 835-9.
14. Wang, T.Y. and T.P. Kawaguchi, *Preliminary evaluation of measurement of serum prostate-specific antigen level in detection of prostate cancer*. Ann Clin Lab Sci, 1986. **16**(6): p. 461-6.
15. Balk, S.P., Y.J. Ko, and G.J. Bubley, *Biology of prostate-specific antigen*. J Clin Oncol, 2003. **21**(2): p. 383-91.
16. Lilja, H., D. Ulmert, and A.J. Vickers, *Prostate-specific antigen and prostate cancer: prediction, detection and monitoring*. Nat Rev Cancer, 2008. **8**(4): p. 268-78.
17. Verim, L., A. Yildirim, E.K. Basok, E. Peltekoglu, E.S. Pelit, E. Zemheri, and R. Tokuc, *Impact of PSA and DRE on histologic findings at prostate biopsy in Turkish men over 75 years of age*. Asian Pac J Cancer Prev, 2013. **14**(10): p. 6085-8.
18. Prensner, J.R., M.A. Rubin, J.T. Wei, and A.M. Chinnaiyan, *Beyond PSA: The next generation of prostate cancer biomarkers*. Science translational medicine, 2012. **4**(127): p. 127rv3-127rv3.
19. Bussemakers, M.J., A. van Bokhoven, G.W. Verhaegh, F.P. Smit, H.F. Karthaus, J.A. Schalken, F.M. Debruyne, N. Ru, and W.B. Isaacs, *DD3: a new prostate-specific gene, highly overexpressed in prostate cancer*. Cancer Res, 1999. **59**(23): p. 5975-9.
20. de Kok, J.B., G.W. Verhaegh, R.W. Roelofs, D. Hessels, L.A. Kiemeny, T.W. Aalders, D.W. Swinkels, and J.A. Schalken, *DD3(PCA3), a very sensitive and*

- specific marker to detect prostate tumors. Cancer Res, 2002. 62(9): p. 2695-8.*
21. Hessels, D., F.P. Smit, G.W. Verhaegh, J.A. Witjes, E.B. Cornel, and J.A. Schalken, *Detection of TMPRSS2-ERG fusion transcripts and prostate cancer antigen 3 in urinary sediments may improve diagnosis of prostate cancer. Clin Cancer Res, 2007. 13(17): p. 5103-8.*
 22. Rubin, M.A., M. Zhou, S.M. Dhanasekaran, S. Varambally, T.R. Barrette, M.G. Sanda, K.J. Pienta, D. Ghosh, and A.M. Chinnaiyan, *alpha-Methylacyl coenzyme A racemase as a tissue biomarker for prostate cancer. Jama, 2002. 287(13): p. 1662-70.*
 23. Gleason, D.F. and G.T. Mellinger, *Prediction of prognosis for prostatic adenocarcinoma by combined histological grading and clinical staging. J Urol, 1974. 111(1): p. 58-64.*
 24. Gordetsky, J. and J. Epstein, *Grading of prostatic adenocarcinoma: current state and prognostic implications. Diagnostic Pathology, 2016. 11: p. 25.*
 25. Albertsen, P.C., J.A. Hanley, D.F. Gleason, and M.J. Barry, *Competing risk analysis of men aged 55 to 74 years at diagnosis managed conservatively for clinically localized prostate cancer. Jama, 1998. 280(11): p. 975-80.*
 26. Chodak, G.W., R.A. Thisted, G.S. Gerber, J.E. Johansson, J. Adolfsson, G.W. Jones, G.D. Chisholm, B. Moskovitz, P.M. Livne, and J. Warner, *Results of conservative management of clinically localized prostate cancer. N Engl J Med, 1994. 330(4): p. 242-8.*
 27. Holmberg, L., A. Bill-Axelson, G. Steineck, H. Garmo, J. Palmgren, E. Johansson, H.O. Adami, and J.E. Johansson, *Results from the Scandinavian Prostate Cancer Group Trial Number 4: a randomized controlled trial of radical prostatectomy versus watchful waiting. J Natl Cancer Inst Monogr, 2012. 2012(45): p. 230-3.*
 28. Wilt, T.J., M.K. Brawer, K.M. Jones, M.J. Barry, W.J. Aronson, S. Fox, J.R. Gingrich, J.T. Wei, P. Gilhooly, B.M. Grob, I. Nsouli, P. Iyer, R. Cartagena, G. Snider, C. Roehrborn, R. Sharifi, W. Blank, P. Pandya, G.L. Andriole, D. Culkin, and T. Wheeler, *Radical prostatectomy versus observation for localized prostate cancer. N Engl J Med, 2012. 367(3): p. 203-13.*

29. Novara, G., V. Ficarra, R.C. Rosen, W. Artibani, A. Costello, J.A. Eastham, M. Graefen, G. Guazzoni, S.F. Shariat, J.U. Stolzenburg, H. Van Poppel, F. Zattoni, F. Montorsi, A. Mottrie, and T.G. Wilson, *Systematic review and meta-analysis of perioperative outcomes and complications after robot-assisted radical prostatectomy*. Eur Urol, 2012. **62**(3): p. 431-52.
30. Dearnaley, D.P., V.S. Khoo, A.R. Norman, L. Meyer, A. Nahum, D. Tait, J. Yarnold, and A. Horwich, *Comparison of radiation side-effects of conformal and conventional radiotherapy in prostate cancer: a randomised trial*. Lancet, 1999. **353**(9149): p. 267-72.
31. Zelefsky, M.J., E.J. Levin, M. Hunt, Y. Yamada, A.M. Shippey, A. Jackson, and H.I. Amols, *Incidence of late rectal and urinary toxicities after three-dimensional conformal radiotherapy and intensity-modulated radiotherapy for localized prostate cancer*. Int J Radiat Oncol Biol Phys, 2008. **70**(4): p. 1124-9.
32. J, T., *Hormonal management of stage D carcinoma of the prostate*. Problems in urology, 1993. **7**: p. 215-25.
33. Huggins, C. and C.V. Hodges, *Studies on prostatic cancer II: the effects of castration on advanced carcinoma of the prostate gland*. Arch Surg, 1941. **43**: p. 209-23.
34. Clark, J.A., N.P. Wray, and C.M. Ashton, *Living with treatment decisions: regrets and quality of life among men treated for metastatic prostate cancer*. J Clin Oncol, 2001. **19**(1): p. 72-80.
35. Seidenfeld, J., D.J. Samson, V. Hasselblad, N. Aronson, P.C. Albertsen, C.L. Bennett, and T.J. Wilt, *Single-therapy androgen suppression in men with advanced prostate cancer: a systematic review and meta-analysis*. Ann Intern Med, 2000. **132**(7): p. 566-77.
36. Barmoshe, S. and A.R. Zlotta, *Pharmacotherapy for prostate cancer, with emphasis on hormonal treatments*. Expert Opin Pharmacother, 2006. **7**(13): p. 1685-99.
37. Heidenreich, A., P.J. Bastian, J. Bellmunt, M. Bolla, S. Joniau, T. van der Kwast, M. Mason, V. Matveev, T. Wiegand, F. Zattoni, and N. Mottet, *EAU*

- guidelines on prostate cancer. Part II: Treatment of advanced, relapsing, and castration-resistant prostate cancer.* Eur Urol, 2014. **65**(2): p. 467-79.
38. van Poppel, H. and S. Nilsson, *Testosterone surge: rationale for gonadotropin-releasing hormone blockers?* Urology, 2008. **71**(6): p. 1001-6.
39. Isbarn, H., L. Boccon-Gibod, P.R. Carroll, F. Montorsi, C. Schulman, M.R. Smith, C.N. Sternberg, and U.E. Studer, *Androgen deprivation therapy for the treatment of prostate cancer: consider both benefits and risks.* Eur Urol, 2009. **55**(1): p. 62-75.
40. Saad, F. and S.J. Hotte, *Guidelines for the management of castrate-resistant prostate cancer.* Can Urol Assoc J, 2010. **4**(6): p. 380-4.
41. Cookson, M.S., B.J. Roth, P. Dahm, C. Engstrom, S.J. Freedland, M. Hussain, D.W. Lin, W.T. Lowrance, M.H. Murad, W.K. Oh, D.F. Penson, and A.S. Kibel, *Castration-resistant prostate cancer: AUA Guideline.* J Urol, 2013. **190**(2): p. 429-38.
42. Tan, J., Y. Sharief, K.G. Hamil, C.W. Gregory, D.Y. Zang, M. Sar, P.H. Gumerlock, R.W. deVere White, T.G. Pretlow, S.E. Harris, E.M. Wilson, J.L. Mohler, and F.S. French, *Dehydroepiandrosterone activates mutant androgen receptors expressed in the androgen-dependent human prostate cancer xenograft CWR22 and LNCaP cells.* Mol Endocrinol, 1997. **11**(4): p. 450-9.
43. DiGiovanni, J., K. Kiguchi, A. Frijhoff, E. Wilker, D.K. Bol, L. Beltrán, S. Moats, A. Ramirez, J. Jorcano, and C. Conti, *Deregulated expression of insulin-like growth factor 1 in prostate epithelium leads to neoplasia in transgenic mice.* Proceedings of the National Academy of Sciences of the United States of America, 2000. **97**(7): p. 3455-3460.
44. Grossmann, M.E., H. Huang, and D.J. Tindall, *Androgen receptor signaling in androgen-refractory prostate cancer.* J Natl Cancer Inst, 2001. **93**(22): p. 1687-97.
45. Diaz, M., M. Abdul, and N. Hoosein, *Modulation of neuroendocrine differentiation in prostate cancer by interleukin-1 and -2.* Prostate Suppl, 1998. **8**: p. 32-6.

46. Iwamura, M., P.A. Abrahamsson, K.A. Foss, G. Wu, A.T. Cockett, and L.J. Deftos, *Parathyroid hormone-related protein: a potential autocrine growth regulator in human prostate cancer cell lines*. *Urology*, 1994. **43**(5): p. 675-9.
47. Jemal, A., T. Murray, A. Samuels, A. Ghafoor, E. Ward, and M.J. Thun, *Cancer statistics, 2003*. *CA Cancer J Clin*, 2003. **53**(1): p. 5-26.
48. Petrylak, D.P., *Docetaxel for the Treatment of Hormone-Refractory Prostate Cancer*. *Reviews in Urology*, 2003. **5**(Suppl 2): p. S14-S21.
49. Saad, F., D.M. Gleason, R. Murray, S. Tchekmedyian, P. Venner, L. Lacombe, J.L. Chin, J.J. Vinholes, J.A. Goas, and M. Zheng, *Long-term efficacy of zoledronic acid for the prevention of skeletal complications in patients with metastatic hormone-refractory prostate cancer*. *J Natl Cancer Inst*, 2004. **96**(11): p. 879-82.
50. Parker, C., S. Nilsson, D. Heinrich, S.I. Helle, J.M. O'Sullivan, S.D. Fossa, A. Chodacki, P. Wiechno, J. Logue, M. Seke, A. Widmark, D.C. Johannessen, P. Hoskin, D. Bottomley, N.D. James, A. Solberg, I. Syndikus, J. Kliment, S. Wedel, S. Boehmer, M. Dall'Oglio, L. Franzen, R. Coleman, N.J. Vogelzang, C.G. O'Bryan-Tear, K. Staudacher, J. Garcia-Vargas, M. Shan, O.S. Bruland, and O. Sartor, *Alpha emitter radium-223 and survival in metastatic prostate cancer*. *N Engl J Med*, 2013. **369**(3): p. 213-23.
51. Bellmunt, J., *Tackling the bone with alpha emitters in metastatic castration-resistant prostate cancer patients*. *Eur Urol*, 2013. **63**(2): p. 198-200.
52. Serpa Neto, A., M. Tobias-Machado, R. Kaliks, M.L. Wroclawski, A.C. Pompeo, and A. Del Giglio, *Ten years of docetaxel-based therapies in prostate adenocarcinoma: a systematic review and meta-analysis of 2244 patients in 12 randomized clinical trials*. *Clin Genitourin Cancer*, 2011. **9**(2): p. 115-23.
53. O'Neill, A.J., M. Prencipe, C. Dowling, Y. Fan, L. Mulrane, W.M. Gallagher, D. O'Connor, R. O'Connor, A. Devery, C. Corcoran, S. Rani, L. O'Driscoll, J.M. Fitzpatrick, and R.W. Watson, *Characterisation and manipulation of docetaxel resistant prostate cancer cell lines*. *Mol Cancer*, 2011. **10**: p. 126.
54. Naot, D. and J. Cornish, *The role of peptides and receptors of the calcitonin family in the regulation of bone metabolism*. *Bone*, 2008. **43**(5): p. 813-818.

55. Russell, F.A., R. King, S.J. Smillie, X. Kodji, and S.D. Brain, *Calcitonin gene-related peptide: physiology and pathophysiology*. *Physiol Rev*, 2014. **94**(4): p. 1099-142.
56. Kitamura, K., K. Kangawa, M. Kawamoto, Y. Ichiki, S. Nakamura, H. Matsuo, and T. Eto, *Adrenomedullin: a novel hypotensive peptide isolated from human pheochromocytoma*. *Biochem Biophys Res Commun*, 1993. **192**(2): p. 553-60.
57. Poyner, D.R., P.M. Sexton, I. Marshall, D.M. Smith, R. Quirion, W. Born, R. Muff, J.A. Fischer, and S.M. Foord, *International Union of Pharmacology. XXXII. The mammalian calcitonin gene-related peptides, adrenomedullin, amylin, and calcitonin receptors*. *Pharmacol Rev*, 2002. **54**(2): p. 233-46.
58. Desai, A.J., D.J. Roberts, G.O. Richards, and T.M. Skerry, *Role of Receptor Activity Modifying Protein 1 in Function of the Calcium Sensing Receptor in the Human TT Thyroid Carcinoma Cell Line*. *PLoS ONE*, 2014. **9**(1): p. e85237.
59. Pi, M., P. Faber, G. Ekema, P.D. Jackson, A. Ting, N. Wang, M. Fontilla-Poole, R.W. Mays, K.R. Brunden, J.J. Harrington, and L.D. Quarles, *Identification of a novel extracellular cation-sensing G-protein-coupled receptor*. *J Biol Chem*, 2005. **280**(48): p. 40201-9.
60. Desai, A., *Novel insights into the interaction of the Calcium Sensing Receptor with the Receptor Activity Modifying Proteins.*, in *Faculty of Medicine, Dentistry and Health*. 2013, University of Sheffield: Sheffield, UK.
61. Wei, J., T. Hanna, N. Suda, G. Karsenty, and P. Ducy, *Osteocalcin promotes beta-cell proliferation during development and adulthood through Gprc6a*. *Diabetes*, 2014. **63**(3): p. 1021-31.
62. Pi, M., K. Kapoor, Y. Wu, R. Ye, S.E. Senogles, S.K. Nishimoto, D.J. Hwang, D.D. Miller, R. Narayanan, J.C. Smith, J. Baudry, and L.D. Quarles, *Structural and Functional Evidence for Testosterone Activation of GPRC6A in Peripheral Tissues*. *Mol Endocrinol*, 2015. **29**(12): p. 1759-73.
63. Christopoulos, A., G. Christopoulos, M. Morfis, M. Udawela, M. Laburthe, A. Couvineau, K. Kuwasako, N. Tilakaratne, and P.M. Sexton, *Novel receptor partners and function of receptor activity-modifying proteins*. *Journal of Biological Chemistry*, 2003. **278**(5): p. 3293-3297.

64. Zudaire, E., A. Martinez, and F. Cuttitta, *Adrenomedullin and cancer*. *Regulatory Peptides*, 2003. **112**(1-3): p. 175-183.
65. Ritchie, C.K., K.G. Thomas, L.R. Andrews, D.J. Tindall, and L.A. Fitzpatrick, *Effects of the calciotropic peptides calcitonin and parathyroid hormone on prostate cancer growth and chemotaxis*. *Prostate*, 1997. **30**(3): p. 183-187.
66. Hay, D.L., C.S. Walker, and D.R. Poyner, *Adrenomedullin and calcitonin gene-related peptide receptors in endocrine-related cancers: opportunities and challenges*. *Endocrine-Related Cancer*, 2011. **18**(1): p. C1-C14.
67. Cornish, J. and D. Naot, *Amylin and adrenomedullin: novel regulators of bone growth*. *Curr Pharm Des*, 2002. **8**(23): p. 2009-2021.
68. Cornish, J., K.E. Callon, U. Bava, S.A. Kamona, G.J.S. Cooper, and I.R. Reid, *Effects of calcitonin, amylin, and calcitonin gene-related peptide on osteoclast development*. *Bone*, 2001. **29**(2): p. 162-168.
69. Bunton, D.C., M.C. Petrie, C. Hillier, F. Johnston, and J.J. McMurray, *The clinical relevance of adrenomedullin: a promising profile?* *Pharmacol Ther*, 2004. **103**(3): p. 179-201.
70. Kitamura, K., K. Kangawa, and T. Eto, *Adrenomedullin and PAMP: discovery, structures, and cardiovascular functions*. *Microsc Res Tech*, 2002. **57**(1): p. 3-13.
71. Kitamura, K., K. Kangawa, Y. Ishiyama, H. Washimine, Y. Ichiki, M. Kawamoto, N. Minamino, H. Matsuo, and T. Eto, *Identification and hypotensive activity of proadrenomedullin N-terminal 20 peptide (PAMP)*. *FEBS Lett*, 1994. **351**(1): p. 35-7.
72. McLatchie, L.M., N.J. Fraser, M.J. Main, A. Wise, J. Brown, N. Thompson, R. Solari, M.G. Lee, and S.M. Foord, *RAMPs regulate the transport and ligand specificity of the calcitonin-receptor-like receptor*. *Nature*, 1998. **393**(6683): p. 333-9.
73. Ogoshi, M., K. Inoue, K. Naruse, and Y. Takei, *Evolutionary history of the calcitonin gene-related peptide family in vertebrates revealed by comparative genomic analyses*. *Peptides*, 2006. **27**(12): p. 3154-64.

74. Breeze, A.L., T.S. Harvey, R. Bazzo, and I.D. Campbell, *Solution structure of human calcitonin gene-related peptide by 1H NMR and distance geometry with restrained molecular dynamics*. *Biochemistry*, 1991. **30**(2): p. 575-82.
75. Hague, S., L. Zhang, M.K. Oehler, S. Manek, I.Z. MacKenzie, R. Bicknell, and M.C. Rees, *Expression of the hypoxically regulated angiogenic factor adrenomedullin correlates with uterine leiomyoma vascular density*. *Clin Cancer Res*, 2000. **6**(7): p. 2808-14.
76. Martinez, A., M.J. Miller, E.J. Unsworth, J.M. Siegfried, and F. Cuttitta, *Expression of adrenomedullin in normal human lung and in pulmonary tumors*. *Endocrinology*, 1995. **136**(9): p. 4099-105.
77. Miller, M.J., A. Martinez, E.J. Unsworth, C.J. Thiele, T.W. Moody, T. Elsasser, and F. Cuttitta, *Adrenomedullin expression in human tumor cell lines. Its potential role as an autocrine growth factor*. *J Biol Chem*, 1996. **271**(38): p. 23345-51.
78. Satoh, F., K. Takahashi, O. Murakami, K. Totsune, M. Sone, M. Ohneda, K. Abe, Y. Miura, Y. Hayashi, and H. Sasano, *Adrenomedullin in human brain, adrenal glands and tumor tissues of pheochromocytoma, ganglioneuroblastoma and neuroblastoma*. *The Journal of Clinical Endocrinology & Metabolism*, 1995. **80**(5): p. 1750-1752.
79. Calvo, A., I. Abasolo, N. Jimenez, Z. Wang, and L. Montuenga, *Adrenomedullin and proadrenomedullin N-terminal 20 peptide in the normal prostate and in prostate carcinoma*. *Microsc Res Tech*, 2002. **57**(2): p. 98-104.
80. Rocchi, P., F. Boudouresque, A.J. Zamora, X. Muracciole, E. Lechevallier, P.M. Martin, and L. Ouafik, *Expression of adrenomedullin and peptide amidation activity in human prostate cancer and in human prostate cancer cell lines*. *Cancer Res*, 2001. **61**(3): p. 1196-206.
81. Abrahamsson, P.A., *Neuroendocrine differentiation in prostatic carcinoma*. *Prostate*, 1999. **39**(2): p. 135-48.
82. Berenguer, C., F. Boudouresque, C. Dussert, L. Daniel, X. Muracciole, M. Grino, D. Rossi, K. Mabrouk, D. Figarella-Branger, P.M. Martin, and L.H. Ouafik, *Adrenomedullin, an autocrine/paracrine factor induced by androgen*

- withdrawal, stimulates 'neuroendocrine phenotype' in LNCaP prostate tumor cells. Oncogene, 2008. 27(4): p. 506-518.*
83. Abasolo, I., Z. Wang, L.M. Montuenga, and A. Calvo, *Adrenomedullin inhibits prostate cancer cell proliferation through a cAMP-independent autocrine mechanism. Biochemical and Biophysical Research Communications, 2004. 322(3): p. 878-886.*
 84. Martinez, A., M. Vos, L. Guedez, G. Kaur, Z. Chen, M. Garayoa, R. Pio, T. Moody, W.G. Stetler-Stevenson, H.K. Kleinman, and F. Cuttitta, *The effects of adrenomedullin overexpression in breast tumor cells. J Natl Cancer Inst, 2002. 94(16): p. 1226-37.*
 85. Berenguer-Daize, C., F. Boudouresque, C. Bastide, A. Tounsi, Z. Benyahia, J. Acunzo, N. Dussault, C. Delfino, N. Baeza, L. Daniel, M. Cayol, D. Rossi, A. El Battari, D. Bertin, K. Mabrouk, P.M. Martin, and L. Ouafik, *Adrenomedullin blockade suppresses growth of human hormone-independent prostate tumor xenograft in mice. Clin Cancer Res, 2013. 19(22): p. 6138-50.*
 86. Wang, L., M. Gala, M. Yamamoto, M.S. Pino, H. Kikuchi, D.S. Shue, S. Shirasawa, T.R. Austin, M.P. Lynch, B.R. Rueda, L.R. Zukerberg, and D.C. Chung, *Adrenomedullin is a therapeutic target in colorectal cancer. International journal of cancer. Journal international du cancer, 2014. 134(9): p. 2041-2050.*
 87. Iwasaki, H., M. Shichiri, F. Marumo, and Y. Hirata, *Adrenomedullin stimulates proline-rich tyrosine kinase 2 in vascular smooth muscle cells. Endocrinology, 2001. 142(2): p. 564-72.*
 88. Semplicini, A., G. Ceolotto, E. Baritono, L.K. Malendowicz, P.G. Andreis, M. Sartori, G.P. Rossi, and G.G. Nussdorfer, *Adrenomedullin stimulates DNA synthesis of rat adrenal zona glomerulosa cells through activation of the mitogen-activated protein kinase-dependent cascade. J Hypertens, 2001. 19(3 Pt 2): p. 599-602.*
 89. Shichiri, M., N. Fukai, N. Ozawa, H. Iwasaki, and Y. Hirata, *Adrenomedullin is an autocrine/paracrine growth factor for rat vascular smooth muscle cells. Regul Pept, 2003. 112(1-3): p. 167-73.*

90. Sun, Y., W.Z. Liu, T. Liu, X. Feng, N. Yang, and H.F. Zhou, *Signaling pathway of MAPK/ERK in cell proliferation, differentiation, migration, senescence and apoptosis*. J Recept Signal Transduct Res, 2015. **35**(6): p. 600-4.
91. Abasolo, I., L.M. Montuenga, and A. Calvo, *Adrenomedullin prevents apoptosis in prostate cancer cells*. Regul Pept, 2006. **133**(1-3): p. 115-22.
92. Nakamura, M., B. Han, O. Nunobiki, and K. Kakudo, *Adrenomedullin: a tumor progression factor via angiogenic control*. Curr Cancer Drug Targets, 2006. **6**(7): p. 635-43.
93. Nikitenko, L.L., S.B. Fox, S. Kehoe, M.C. Rees, and R. Bicknell, *Adrenomedullin and tumour angiogenesis*. Br J Cancer, 2006. **94**(1): p. 1-7.
94. Fukushi, J., M. Ono, W. Morikawa, Y. Iwamoto, and M. Kuwano, *The activity of soluble VCAM-1 in angiogenesis stimulated by IL-4 and IL-13*. J Immunol, 2000. **165**(5): p. 2818-23.
95. Nishimura, Y., T. Nitto, T. Inoue, and K. Node, *IL-13 attenuates vascular tube formation via JAK2-STAT6 pathway*. Circ J, 2008. **72**(3): p. 469-75.
96. Pomorski, P., *[Calcium regulation of cell migration]*. Postepy Biochem, 2009. **55**(2): p. 163-70.
97. Bodding, M., *TRP proteins and cancer*. Cell Signal, 2007. **19**(3): p. 617-24.
98. Gkika, D. and N. Prevarskaya, *TRP channels in prostate cancer: the good, the bad and the ugly?* Asian J Androl, 2011. **13**(5): p. 673-6.
99. Monet, M., V. Lehen'kyi, F. Gackiere, V. Firlej, M. Vandenberghe, M. Roudbaraki, D. Gkika, A. Pourtier, G. Bidaux, C. Slomianny, P. Delcourt, F. Rassendren, J.P. Bergerat, J. Ceraline, F. Cabon, S. Humez, and N. Prevarskaya, *Role of cationic channel TRPV2 in promoting prostate cancer migration and progression to androgen resistance*. Cancer Res, 2010. **70**(3): p. 1225-35.
100. Oulidi, A., A. Bokhobza, D. Gkika, F. Vanden Abeele, V. Lehen'kyi, L. Ouafik, B. Mauroy, and N. Prevarskaya, *TRPV2 mediates adrenomedullin stimulation of prostate and urothelial cancer cell adhesion, migration and invasion*. PLoS One, 2013. **8**(5): p. e64885.

101. Suzuki, K., Y. Kobayashi, and T. Morita, *Significance of serum calcitonin gene-related peptide levels in prostate cancer patients receiving hormonal therapy*. *Urologia Internationalis*, 2009. **82**(3): p. 291-295.
102. Suzuki, K., Y. Kobayashi, and T. Morita, *Serum calcitonin gene-related peptide levels in untreated prostate cancer patients*. *Int J Urol*, 2006. **13**(6): p. 781-4.
103. Nagakawa, O., M. Ogasawara, H. Fujii, K. Murakami, J. Murata, H. Fuse, and I. Saiki, *Effect of prostatic neuropeptides on invasion and migration of PC-3 prostate cancer cells*. *Cancer Lett*, 1998. **133**(1): p. 27-33.
104. Nagakawa, O., M. Ogasawara, J. Murata, H. Fuse, and I. Saiki, *Effect of prostatic neuropeptides on migration of prostate cancer cell lines*. *Int J Urol*, 2001. **8**(2): p. 65-70.
105. Logan, M., P.D. Anderson, S.T. Saab, O. Hameed, and S.A. Abdulkadir, *RAMP1 is a direct NKX3.1 target gene up-regulated in prostate cancer that promotes tumorigenesis*. *American Journal of Pathology*, 2013. **183**(3): p. 951-963.
106. Feng, J., X. Xu, B. Li, E. Brown, A.B. Farris, S.Y. Sun, and J.J. Yang, *Prostate cancer metastatic to bone has higher expression of the calcium-sensing receptor (CaSR) than primary prostate cancer*. *Receptors Clin Investig*, 2014. **1**(6).
107. Pi, M. and L.D. Quarles, *GPRC6A regulates prostate cancer progression*. *Prostate*, 2012. **72**(4): p. 399-409.
108. Thiel, G., A. Lesch, and A. Keim, *Transcriptional response to calcium-sensing receptor stimulation*. *Endocrinology*, 2012. **153**(10): p. 4716-28.
109. Yu, X.J., C.Y. Li, K.Y. Wang, and H.Y. Dai, *Calcitonin gene-related peptide regulates the expression of vascular endothelial growth factor in human HaCaT keratinocytes by activation of ERK1/2 MAPK*. *Regul Pept*, 2006. **137**(3): p. 134-9.
110. Ho, C.C.K., P.K. Seong, Z.M. Zainuddin, M.R.A. Manaf, M. Parameswaran, and A.H.A. Razack, *Retrospective Study of Predictors of Bone Metastasis in Prostate Cancer Cases*. *Asian Pacific Journal of Cancer Prevention*, 2013. **14**(5): p. 3289-3292.

111. Nimptsch, K., S. Rohrmann, A. Nieters, and J. Linseisen, *Serum undercarboxylated osteocalcin as biomarker of vitamin K intake and risk of prostate cancer: a nested case-control study in the Heidelberg cohort of the European prospective investigation into cancer and nutrition*. *Cancer Epidemiol Biomarkers Prev*, 2009. **18**(1): p. 49-56.
112. Liu, M., Y.Y. Zhao, F. Yang, J.Y. Wang, X.H. Shi, X.Q. Zhu, Y. Xu, D. Wei, L. Sun, Y.G. Zhang, K. Yang, Y.C. Qu, X. Wang, S.Y. Liang, X. Chen, C.X. Zhao, L. Zhu, L. Tang, C.G. Zheng, and Z. Yang, *Evidence for a role of GPRC6A in prostate cancer metastasis based on case-control and in vitro analyses*. *Eur Rev Med Pharmacol Sci*, 2016. **20**(11): p. 2235-48.
113. Long, Q.Z., Y.F. Du, X.Y. Ding, X. Li, W.B. Song, Y. Yang, P. Zhang, J.P. Zhou, and X.G. Liu, *Replication and fine mapping for association of the C2orf43, FOXP4, GPRC6A and RFX6 genes with prostate cancer in the Chinese population*. *PLoS One*, 2012. **7**(5): p. e37866.
114. Takata, R., S. Akamatsu, M. Kubo, A. Takahashi, N. Hosono, T. Kawaguchi, T. Tsunoda, J. Inazawa, N. Kamatani, O. Ogawa, T. Fujioka, Y. Nakamura, and H. Nakagawa, *Genome-wide association study identifies five new susceptibility loci for prostate cancer in the Japanese population*. *Nat Genet*, 2010. **42**(9): p. 751-4.
115. Owan, I. and K. Ibaraki, *The Role of Calcitonin-Gene-Related Peptide (Cgrp) in Macrophages - the Presence of Functional Receptors and Effects on Proliferation and Differentiation into Osteoclast-Like Cells*. *Bone and Mineral*, 1994. **24**(2): p. 151-164.
116. Cornish, J. and I.R. Reid, *Effects of amylin and adrenomedullin on the skeleton*. *Journal of musculoskeletal & neuronal interactions*, 2001. **2**(1): p. 15-24.
117. Theoleyre, S., Y. Wittrant, S.K. Tat, Y. Fortun, F. Redini, and D. Heymann, *The molecular triad OPG/RANK/RANKL: involvement in the orchestration of pathophysiological bone remodeling*. *Cytokine Growth Factor Rev*, 2004. **15**(6): p. 457-75.
118. Wittrant, Y., S. Theoleyre, C. Chipoy, M. Padrines, F. Blanchard, D. Heymann, and F. Redini, *RANKL/RANK/OPG: new therapeutic targets in*

- bone tumours and associated osteolysis*. Biochim Biophys Acta, 2004. **1704**(2): p. 49-57.
119. Zheng, Y., D. Basel, S.O. Chow, C. Fong-Yee, S. Kim, F. Buttgerit, C.R. Dunstan, H. Zhou, and M.J. Seibel, *Targeting IL-6 and RANKL signaling inhibits prostate cancer growth in bone*. Clin Exp Metastasis, 2014. **31**(8): p. 921-33.
120. Zheng, Y., S.O. Chow, K. Boernert, D. Basel, A. Mikuscheva, S. Kim, C. Fong-Yee, T. Trivedi, F. Buttgerit, R.L. Sutherland, C.R. Dunstan, H. Zhou, and M.J. Seibel, *Direct crosstalk between cancer and osteoblast lineage cells fuels metastatic growth in bone via auto-amplification of IL-6 and RANKL signaling pathways*. J Bone Miner Res, 2014. **29**(9): p. 1938-49.
121. Coffey, D.S., *Similarities of prostate and breast cancer: Evolution, diet, and estrogens*. Urology, 2001. **57**(4 Suppl 1): p. 31-8.
122. Lopez-Otin, C. and E.P. Diamandis, *Breast and prostate cancer: an analysis of common epidemiological, genetic, and biochemical features*. Endocr Rev, 1998. **19**(4): p. 365-96.
123. Hansen, R.R., V. Vacca, T. Pitcher, A.K. Clark, and M. Malcangio, *Role of extracellular calcitonin gene-related peptide in spinal cord mechanisms of cancer-induced bone pain*. Pain, 2016. **157**(3): p. 666-76.
124. Jimenez-Andrade, J.M., A.P. Bloom, J.I. Stake, W.G. Mantyh, R.N. Taylor, K.T. Freeman, J.R. Ghilardi, M.A. Kuskowski, and P.W. Mantyh, *Pathological sprouting of adult nociceptors in chronic prostate cancer-induced bone pain*. J Neurosci, 2010. **30**(44): p. 14649-56.
125. Lamb, D.J. and L. Zhang, *Challenges in prostate cancer research: animal models for nutritional studies of chemoprevention and disease progression*. J Nutr, 2005. **135**(12 Suppl): p. 3009S-3015S.
126. Stone, K.R., D.D. Mickey, H. Wunderli, G.H. Mickey, and D.F. Paulson, *Isolation of a human prostate carcinoma cell line (DU 145)*. Int J Cancer, 1978. **21**(3): p. 274-81.
127. Paul, R. and J. Breul, *Antiandrogen withdrawal syndrome associated with prostate cancer therapies: incidence and clinical significance*. Drug Saf, 2000. **23**(5): p. 381-90.

128. Bastide, C., C. Bagnis, P. Mannoni, J. Hassoun, and F. Bladou, *A Nod Scid mouse model to study human prostate cancer*. Prostate Cancer Prostatic Dis, 2002. **5**(4): p. 311-5.
129. Nemeth, J.A., J.F. Harb, U. Barroso, Jr., Z. He, D.J. Grignon, and M.L. Cher, *Severe combined immunodeficient-hu model of human prostate cancer metastasis to human bone*. Cancer Res, 1999. **59**(8): p. 1987-93.
130. Horoszewicz, J.S., S.S. Leong, T.M. Chu, Z.L. Wajsman, M. Friedman, L. Papsidero, U. Kim, L.S. Chai, S. Kakati, S.K. Arya, and A.A. Sandberg, *The LNCaP cell line--a new model for studies on human prostatic carcinoma*. Prog Clin Biol Res, 1980. **37**: p. 115-32.
131. Gleave, M.E., J.T. Hsieh, A.C. von Eschenbach, and L.W. Chung, *Prostate and bone fibroblasts induce human prostate cancer growth in vivo: implications for bidirectional tumor-stromal cell interaction in prostate carcinoma growth and metastasis*. J Urol, 1992. **147**(4): p. 1151-9.
132. Lim, D.J., X.L. Liu, D.M. Sutkowski, E.J. Braun, C. Lee, and J.M. Kozlowski, *Growth of an androgen-sensitive human prostate cancer cell line, LNCaP, in nude mice*. Prostate, 1993. **22**(2): p. 109-18.
133. Thalmann, G.N., P.E. Anezinis, S.M. Chang, H.E. Zhau, E.E. Kim, V.L. Hopwood, S. Pathak, A.C. von Eschenbach, and L.W. Chung, *Androgen-independent cancer progression and bone metastasis in the LNCaP model of human prostate cancer*. Cancer Res, 1994. **54**(10): p. 2577-81.
134. Kaighn, M.E., K.S. Narayan, Y. Ohnuki, J.F. Lechner, and L.W. Jones, *Establishment and characterization of a human prostatic carcinoma cell line (PC-3)*. Invest Urol, 1979. **17**(1): p. 16-23.
135. Pettaway, C.A., S. Pathak, G. Greene, E. Ramirez, M.R. Wilson, J.J. Killion, and I.J. Fidler, *Selection of highly metastatic variants of different human prostatic carcinomas using orthotopic implantation in nude mice*. Clin Cancer Res, 1996. **2**(9): p. 1627-36.
136. Stephenson, R.A., C.P. Dinney, K. Gohji, N.G. Ordonez, J.J. Killion, and I.J. Fidler, *Metastatic model for human prostate cancer using orthotopic implantation in nude mice*. J Natl Cancer Inst, 1992. **84**(12): p. 951-7.

137. Shevrin, D.H., S.C. Kukreja, L. Ghosh, and T.E. Lad, *Development of skeletal metastasis by human prostate cancer in athymic nude mice*. Clin Exp Metastasis, 1988. **6**(5): p. 401-9.
138. Wu, X., S. Gong, P. Roy-Burman, P. Lee, and Z. Culig, *Current mouse and cell models in prostate cancer research*. Endocr Relat Cancer, 2013. **20**(4): p. R155-70.
139. Logothetis, C.J. and S.H. Lin, *Osteoblasts in prostate cancer metastasis to bone*. Nat Rev Cancer, 2005. **5**(1): p. 21-8.
140. Romanuik, T.L., T. Ueda, N. Le, S. Haile, T.M. Yong, T. Thomson, R.L. Vessella, and M.D. Sadar, *Novel biomarkers for prostate cancer including noncoding transcripts*. Am J Pathol, 2009. **175**(6): p. 2264-76.
141. Fire, A., S. Xu, M.K. Montgomery, S.A. Kostas, S.E. Driver, and C.C. Mello, *Potent and specific genetic interference by double-stranded RNA in Caenorhabditis elegans*. Nature, 1998. **391**(6669): p. 806-11.
142. Lin, A., C.J. Giuliano, N.M. Sayles, and J.M. Sheltzer, *CRISPR/Cas9 mutagenesis invalidates a putative cancer dependency targeted in on-going clinical trials*. Elife, 2017. **6**.
143. Liang, F., M. Han, P.J. Romanienko, and M. Jasin, *Homology-directed repair is a major double-strand break repair pathway in mammalian cells*. Proceedings of the National Academy of Sciences, 1998. **95**(9): p. 5172-5177.
144. Klug, A., *The discovery of zinc fingers and their applications in gene regulation and genome manipulation*. Annu Rev Biochem, 2010. **79**: p. 213-31.
145. Bogdanove, A.J. and D.F. Voytas, *TAL effectors: customizable proteins for DNA targeting*. Science, 2011. **333**(6051): p. 1843-6.
146. Mak, A.N., P. Bradley, A.J. Bogdanove, and B.L. Stoddard, *TAL effectors: function, structure, engineering and applications*. Curr Opin Struct Biol, 2013. **23**(1): p. 93-9.
147. Cermak, T., E.L. Doyle, M. Christian, L. Wang, Y. Zhang, C. Schmidt, J.A. Baller, N.V. Somia, A.J. Bogdanove, and D.F. Voytas, *Efficient design and*

- assembly of custom TALEN and other TAL effector-based constructs for DNA targeting*. Nucleic Acids Res, 2011. **39**(12): p. e82.
148. Ishino, Y., H. Shinagawa, K. Makino, M. Amemura, and A. Nakata, *Nucleotide sequence of the iap gene, responsible for alkaline phosphatase isozyme conversion in Escherichia coli, and identification of the gene product*. J Bacteriol, 1987. **169**(12): p. 5429-33.
149. Barrangou, R., C. Fremaux, H. Deveau, M. Richards, P. Boyaval, S. Moineau, D.A. Romero, and P. Horvath, *CRISPR provides acquired resistance against viruses in prokaryotes*. Science, 2007. **315**(5819): p. 1709-12.
150. Jinek, M., K. Chylinski, I. Fonfara, M. Hauer, J.A. Doudna, and E. Charpentier, *A programmable dual-RNA-guided DNA endonuclease in adaptive bacterial immunity*. Science, 2012. **337**(6096): p. 816-21.
151. Cong, L., F.A. Ran, D. Cox, S. Lin, R. Barretto, N. Habib, P.D. Hsu, X. Wu, W. Jiang, L.A. Marraffini, and F. Zhang, *Multiplex genome engineering using CRISPR/Cas systems*. Science, 2013. **339**(6121): p. 819-23.
152. Mali, P., L. Yang, K.M. Esvelt, J. Aach, M. Guell, J.E. DiCarlo, J.E. Norville, and G.M. Church, *RNA-guided human genome engineering via Cas9*. Science, 2013. **339**(6121): p. 823-6.
153. van der Meer, R., H.Y. Song, S.H. Park, S.A. Abdulkadir, and M. Roh, *RNAi screen identifies a synthetic lethal interaction between PIM1 overexpression and PLK1 inhibition*. Clin Cancer Res, 2014. **20**(12): p. 3211-21.
154. Song, J., D. Yang, J. Xu, T. Zhu, Y.E. Chen, and J. Zhang, *RS-1 enhances CRISPR/Cas9- and TALEN-mediated knock-in efficiency*. Nat Commun, 2016. **7**: p. 10548.
155. Maruyama, T., S.K. Dougan, M.C. Truttmann, A.M. Bilate, J.R. Ingram, and H.L. Ploegh, *Increasing the efficiency of precise genome editing with CRISPR-Cas9 by inhibition of nonhomologous end joining*. Nat Biotechnol, 2015. **33**(5): p. 538-42.
156. Ribeiro, S., J. Mairhofer, C. Madeira, M.M. Diogo, C. Lobato da Silva, G. Monteiro, R. Grabherr, and J.M. Cabral, *Plasmid DNA size does affect nonviral gene delivery efficiency in stem cells*. Cell Reprogram, 2012. **14**(2): p. 130-7.

157. Sheng, Y., V. Mancino, and B. Birren, *Transformation of Escherichia coli with large DNA molecules by electroporation*. *Nucleic Acids Res*, 1995. **23**(11): p. 1990-6.
158. Ichikawa-Shindo, Y., T. Sakurai, A. Kamiyoshi, H. Kawate, N. Iinuma, T. Yoshizawa, T. Koyama, J. Fukuchi, S. Iimuro, N. Moriyama, H. Kawakami, T. Murata, K. Kangawa, R. Nagai, and T. Shindo, *The GPCR modulator protein RAMP2 is essential for angiogenesis and vascular integrity*. *J Clin Invest*, 2008. **118**(1): p. 29-39.
159. Hsu, P.D., D.A. Scott, J.A. Weinstein, F.A. Ran, S. Konermann, V. Agarwala, Y. Li, E.J. Fine, X. Wu, O. Shalem, T.J. Cradick, L.A. Marraffini, G. Bao, and F. Zhang, *DNA targeting specificity of RNA-guided Cas9 nucleases*. *Nat Biotechnol*, 2013. **31**(9): p. 827-32.
160. Pattanayak, V., S. Lin, J.P. Guilinger, E. Ma, J.A. Doudna, and D.R. Liu, *High-throughput profiling of off-target DNA cleavage reveals RNA-programmed Cas9 nuclease specificity*. *Nat Biotechnol*, 2013. **31**(9): p. 839-43.
161. Zhang, X.-H., L.Y. Tee, X.-G. Wang, Q.-S. Huang, and S.-H. Yang, *Off-target Effects in CRISPR/Cas9-mediated Genome Engineering*. *Molecular Therapy - Nucleic Acids*, 2015. **4**(Supplement C): p. e264.
162. Cho, S.W., S. Kim, Y. Kim, J. Kweon, H.S. Kim, S. Bae, and J.-S. Kim, *Analysis of off-target effects of CRISPR/Cas-derived RNA-guided endonucleases and nickases*. *Genome Research*, 2014. **24**(1): p. 132-141.
163. Ost, P., K. Decaestecker, B. Lambert, V. Fonteyne, L. Delrue, N. Lumen, F. Ameye, and G. De Meerleer, *Prognostic factors influencing prostate cancer-specific survival in non-castrate patients with metastatic prostate cancer*. *Prostate*, 2014. **74**(3): p. 297-305.
164. Seyfried, T.N., *On the Origin of Cancer Metastasis*. 2013. **18**(1-2): p. 43-73.
165. Bhowmick, N.A., E.G. Neilson, and H.L. Moses, *Stromal fibroblasts in cancer initiation and progression*. *Nature*, 2004. **432**(7015): p. 332-337.
166. Cheng, N., A. Chytil, Y. Shyr, A. Joly, and H.L. Moses, *Transforming growth factor-beta signaling-deficient fibroblasts enhance hepatocyte growth factor signaling in mammary carcinoma cells to promote scattering and invasion*. *Mol Cancer Res*, 2008. **6**(10): p. 1521-33.

167. Goltz, D., M. Montani, M. Braun, S. Perner, N. Wernert, K. Jung, M. Dietel, C. Stephan, and G. Kristiansen, *Prognostic relevance of proliferation markers (Ki-67, PHH3) within the cross-relation of ERG translocation and androgen receptor expression in prostate cancer*. *Pathology*, 2015. **47**(7): p. 629-36.
168. Tennant, J.R., *EVALUATION OF THE TRYPAN BLUE TECHNIQUE FOR DETERMINATION OF CELL VIABILITY*. *Transplantation*, 1964. **2**(6): p. 685-694.
169. Papadimitriou, E. and P.I. Lelkes, *Measurement of cell numbers in microtiter culture plates using the fluorescent dye Hoechst 33258*. *Journal of Immunological Methods*, 1993. **162**(1): p. 41-45.
170. Cory, A.H., T.C. Owen, J.A. Barltrop, and J.G. Cory, *Use of an aqueous soluble tetrazolium/formazan assay for cell growth assays in culture*. *Cancer Communications*, 1991. **3**(7): p. 207-212.
171. Adams, J.M. and S. Cory, *The Bcl-2 apoptotic switch in cancer development and therapy*. *Oncogene*, 2007. **26**(9): p. 1324-37.
172. Olsson, M. and B. Zhivotovsky, *Caspases and cancer*. *Cell Death Differ*, 2011. **18**(9): p. 1441-9.
173. Sueur, S., M. Pesant, L. Rochette, and J.-L. Connat, *Antiapoptotic effect of calcitonin gene-related peptide on oxidative stress-induced injury in H9c2 cardiomyocytes via the RAMP1/CRLR complex*. *Journal of Molecular and Cellular Cardiology*, 2005. **39**(6): p. 955-963.
174. Liu, D., C. Li, Y. Chen, C. Burnett, X.Y. Liu, S. Downs, R.D. Collins, and J. Hawiger, *Nuclear import of proinflammatory transcription factors is required for massive liver apoptosis induced by bacterial lipopolysaccharide*. *J Biol Chem*, 2004. **279**(46): p. 48434-42.
175. Poręba, M., A. Strózyk, G.S. Salvesen, and M. Drag, *CASPASE SUBSTRATES AND INHIBITORS*. *Cold Spring Harbor perspectives in biology*, 2013. **5**(8): p. a008680-a008680.
176. Schaeffer, D., J.A. Somarelli, G. Hanna, G.M. Palmer, and M.A. Garcia-Blanco, *Cellular migration and invasion uncoupled: increased migration is not an inexorable consequence of epithelial-to-mesenchymal transition*. *Mol Cell Biol*, 2014. **34**(18): p. 3486-99.

177. Benton, G., I. Arnaoutova, J. George, H.K. Kleinman, and J. Koblinski, *Matrigel: from discovery and ECM mimicry to assays and models for cancer research*. *Adv Drug Deliv Rev*, 2014. **79-80**: p. 3-18.
178. Nagakawa, O., M. Ogasawara, H. Fujii, K. Murakami, J. Murata, H. Fuse, and I. Saiki, *Effect of prostatic neuropeptides on invasion and migration of PC-3 prostate cancer cells*. *Cancer Letters*, 1998. **133**(1): p. 27-33.
179. Paget, S., *The distribution of secondary growths in cancer of the breast*. 1889. *Cancer Metastasis Rev*, 1989. **8**(2): p. 98-101.
180. Crowley, L.C. and N.J. Waterhouse, *Measuring Survival of Hematopoietic Cancer Cells with the Colony-Forming Assay in Soft Agar*. *Cold Spring Harb Protoc*, 2016. **2016**(8): p. pdb.prot087189.
181. Kan, C., G. Vargas, F. Le Pape, and P. Clézardin, *Cancer Cell Colonisation in the Bone Microenvironment*. *International Journal of Molecular Sciences*, 2016. **17**(10): p. 1674.
182. Shiozawa, Y., A.M. Havens, Y. Jung, A.M. Ziegler, E.A. Pedersen, J. Wang, J. Wang, G. Lu, G.D. Roodman, R.D. Loberg, K.J. Pienta, and R.S. Taichman, *Annexin II/annexin II receptor axis regulates adhesion, migration, homing, and growth of prostate cancer*. *Journal of cellular biochemistry*, 2008. **105**(2): p. 370-380.
183. Garcia-Calvo, M., E.P. Peterson, D.M. Rasper, J.P. Vaillancourt, R. Zamboni, D.W. Nicholson, and N.A. Thornberry, *Purification and catalytic properties of human caspase family members*. *Cell Death Differ*, 1999. **6**(4): p. 362-9.
184. LaValle, C.R., L. Zhang, S. Xu, J.L. Eiseman, and Q.J. Wang, *Inducible Silencing of Protein Kinase D3 Inhibits Secretion of Tumor-Promoting Factors in Prostate Cancer*. *Molecular Cancer Therapeutics*, 2012. **11**(7): p. 1389.
185. Stepanenko, A.A. and V.V. Dmitrenko, *Pitfalls of the MTT assay: Direct and off-target effects of inhibitors can result in over/underestimation of cell viability*. *Gene*, 2015. **574**(2): p. 193-203.
186. Ellsworth, D.L., H.L. Blackburn, C.D. Shriver, S. Rabizadeh, P. Soon-Shiong, and R.E. Ellsworth, *Single-cell sequencing and tumorigenesis: improved understanding of tumor evolution and metastasis*. *Clinical and Translational Medicine*, 2017. **6**(1): p. 15.

187. Rajasekhar, V.K., L. Studer, W. Gerald, N.D. Socci, and H.I. Scher, *Tumour-initiating stem-like cells in human prostate cancer exhibit increased NF-kappaB signalling*. *Nat Commun*, 2011. **2**: p. 162.
188. Moltzahn, F. and G.N. Thalmann, *Cancer stem cells in prostate cancer*. *Translational Andrology and Urology*, 2013. **2**(3): p. 242-253.
189. Bubendorf, L., A. Schopfer, U. Wagner, G. Sauter, H. Moch, N. Willi, T.C. Gasser, and M.J. Mihatsch, *Metastatic patterns of prostate cancer: an autopsy study of 1,589 patients*. *Hum Pathol*, 2000. **31**(5): p. 578-83.
190. Long, X., C. Cui, P. Chen, S. Wang, D. Wang, G. Xu, X. Yao, and B. Shi, *[Impact and related mechanism of exogenous receptor activity modifying protein 1 on calcitonin gene-related peptide modified bone marrow mesenchymal stem cells on the migration of vascular smooth muscle cells in vitro]*. *Zhonghua Xin Xue Guan Bing Za Zhi*, 2015. **43**(6): p. 537-41.
191. Friedl, P. and S. Alexander, *Cancer Invasion and the Microenvironment: Plasticity and Reciprocity*. *Cell*. **147**(5): p. 992-1009.
192. Kleinman, H.K. and G.R. Martin, *Matrigel: basement membrane matrix with biological activity*. *Semin Cancer Biol*, 2005. **15**(5): p. 378-86.
193. Tiwari, N., A. Gheldof, M. Tataru, and G. Christofori, *EMT as the ultimate survival mechanism of cancer cells*. *Seminars in Cancer Biology*, 2012. **22**(3): p. 194-207.
194. Franken, N.A., H.M. Rodermond, J. Stap, J. Haveman, and C. van Bree, *Clonogenic assay of cells in vitro*. *Nat Protoc*, 2006. **1**(5): p. 2315-9.
195. Ruoslahti, E., *Fibronectin in cell adhesion and invasion*. *Cancer Metastasis Rev*, 1984. **3**(1): p. 43-51.
196. Muller, P.A.J. and K.H. Vousden, *p53 mutations in cancer*. *Nature Cell Biology*, 2013. **15**: p. 2.
197. Wong, R.S.Y., *Apoptosis in cancer: from pathogenesis to treatment*. *Journal of Experimental & Clinical Cancer Research : CR*, 2011. **30**(1): p. 87-87.
198. Nagakawa, O., M. Ogasawara, J. Murata, H. Fuse, and I. Saiki, *Effect of prostatic neuropeptides on migration of prostate cancer cell lines*. *International Journal of Urology*, 2001. **8**(2): p. 65-70.

199. Cairns, P., K. Okami, S. Halachmi, N. Halachmi, M. Esteller, J.G. Herman, J. Jen, W.B. Isaacs, G.S. Bova, and D. Sidransky, *Frequent inactivation of PTEN/MMAC1 in primary prostate cancer*. *Cancer Res*, 1997. **57**(22): p. 4997-5000.
200. Lee, S.H., D. Johnson, R. Luong, and Z. Sun, *Crosstalking between Androgen and PI3K/AKT Signaling Pathways in Prostate Cancer Cells*. *The Journal of Biological Chemistry*, 2015. **290**(5): p. 2759-2768.
201. Wegiel, B., A. Bjartell, Z. Culig, and J.L. Persson, *Interleukin-6 activates PI3K/Akt pathway and regulates cyclin A1 to promote prostate cancer cell survival*. *Int J Cancer*, 2008. **122**(7): p. 1521-9.
202. Lou, W., Z. Ni, K. Dyer, D.J. Tweardy, and A.C. Gao, *Interleukin-6 induces prostate cancer cell growth accompanied by activation of stat3 signaling pathway*. *Prostate*, 2000. **42**(3): p. 239-42.
203. Akimoto, S., A. Okumura, and H. Fuse, *Relationship between serum levels of interleukin-6, tumor necrosis factor-alpha and bone turnover markers in prostate cancer patients*. *Endocr J*, 1998. **45**(2): p. 183-9.
204. Sim, H.G. and C.W. Cheng, *Changing demography of prostate cancer in Asia*. *Eur J Cancer*, 2005. **41**(6): p. 834-45.
205. Siegel, R., D. Naishadham, and A. Jemal, *Cancer statistics, 2012*. *CA Cancer J Clin*, 2012. **62**(1): p. 10-29.
206. Lin, D.W., M. Porter, and B. Montgomery, *Treatment and survival outcomes in young men diagnosed with prostate cancer: a Population-based Cohort Study*. *Cancer*, 2009. **115**(13): p. 2863-71.
207. Sobel, R.E. and M.D. Sadar, *Cell lines used in prostate cancer research: a compendium of old and new lines--part 1*. *J Urol*, 2005. **173**(2): p. 342-59.
208. Fridman, R., M.C. Kibbey, L.S. Royce, M. Zain, M. Sweeney, D.L. Jicha, J.R. Yannelli, G.R. Martin, and H.K. Kleinman, *Enhanced tumor growth of both primary and established human and murine tumor cells in athymic mice after coinjection with Matrigel*. *J Natl Cancer Inst*, 1991. **83**(11): p. 769-74.
209. Veldscholte, J., C. Ris-Stalpers, G.G. Kuiper, G. Jenster, C. Berrevoets, E. Claassen, H.C. van Rooij, J. Trapman, A.O. Brinkmann, and E. Mulder, *A mutation in the ligand binding domain of the androgen receptor of human*

- LNCaP cells affects steroid binding characteristics and response to anti-androgens.* Biochem Biophys Res Commun, 1990. **173**(2): p. 534-40.
210. Heinlein, C.A. and C. Chang, *Androgen receptor in prostate cancer.* Endocr Rev, 2004. **25**(2): p. 276-308.
211. Kochuparambil, S.T., B. Al-Husein, A. Goc, S. Soliman, and P.R. Somanath, *Anticancer efficacy of simvastatin on prostate cancer cells and tumor xenografts is associated with inhibition of Akt and reduced prostate-specific antigen expression.* J Pharmacol Exp Ther, 2011. **336**(2): p. 496-505.
212. Kerbel, R.S., *Human tumor xenografts as predictive preclinical models for anticancer drug activity in humans: better than commonly perceived-but they can be improved.* Cancer Biol Ther, 2003. **2**(4 Suppl 1): p. S134-9.
213. Ibrahim, T., E. Flamini, L. Mercatali, E. Sacanna, P. Serra, and D. Amadori, *Pathogenesis of osteoblastic bone metastases from prostate cancer.* Cancer, 2010. **116**(6): p. 1406-18.
214. Parisotto, M. and D. Metzger, *Genetically engineered mouse models of prostate cancer.* Molecular Oncology, 2013. **7**(2): p. 190-205.
215. Marker, P.C., A.A. Donjacour, R. Dahiya, and G.R. Cunha, *Hormonal, cellular, and molecular control of prostatic development.* Dev Biol, 2003. **253**(2): p. 165-74.
216. Reeves, K.J., J.E. Hurrell, M. Cecchini, G. van der Pluijm, J.M. Down, C.L. Eaton, F. Hamdy, P. Clement-Lacroix, and N.J. Brown, *Prostate cancer cells home to bone using a novel in vivo model: modulation by the integrin antagonist GLPG0187.* Int J Cancer, 2015. **136**(7): p. 1731-40.
217. Kalikin, L.M., A. Schneider, M.A. Thakur, Y. Fridman, L.B. Griffin, R.L. Dunn, T.J. Rosol, R.B. Shah, A. Rehemtulla, L.K. McCauley, and K.J. Pienta, *In vivo visualization of metastatic prostate cancer and quantitation of disease progression in immunocompromised mice.* Cancer Biol Ther, 2003. **2**(6): p. 656-60.
218. Park, S.I., S.J. Kim, L.K. McCauley, and G.E. Gallick, *Pre-Clinical Mouse Models of Human Prostate Cancer and their Utility in Drug Discovery.* Current protocols in pharmacology / editorial board, S.J. Enna (editor-in-chief) ... [et al.], 2010. **51**: p. 14.15-14.15.27.

219. Schneider, A., L.M. Kalikin, A.C. Mattos, E.T. Keller, M.J. Allen, K.J. Pienta, and L.K. McCauley, *Bone Turnover Mediates Preferential Localization of Prostate Cancer in the Skeleton*. *Endocrinology*, 2005. **146**(4): p. 1727-1736.
220. Kim, M.J., R. Bhatia-Gaur, W.A. Banach-Petrosky, N. Desai, Y. Wang, S.W. Hayward, G.R. Cunha, R.D. Cardiff, M.M. Shen, and C. Abate-Shen, *Nkx3.1 mutant mice recapitulate early stages of prostate carcinogenesis*. *Cancer Res*, 2002. **62**(11): p. 2999-3004.
221. Wang, S., J. Gao, Q. Lei, N. Rozengurt, C. Pritchard, J. Jiao, G.V. Thomas, G. Li, P. Roy-Burman, P.S. Nelson, X. Liu, and H. Wu, *Prostate-specific deletion of the murine Pten tumor suppressor gene leads to metastatic prostate cancer*. *Cancer Cell*, 2003. **4**(3): p. 209-21.
222. DeRose, Y.S., G. Wang, Y.C. Lin, P.S. Bernard, S.S. Buys, M.T. Ebbert, R. Factor, C. Matsen, B.A. Milash, E. Nelson, L. Neumayer, R.L. Randall, I.J. Stijleman, B.E. Welm, and A.L. Welm, *Tumor grafts derived from women with breast cancer authentically reflect tumor pathology, growth, metastasis and disease outcomes*. *Nat Med*, 2011. **17**(11): p. 1514-20.
223. Morton, C.L. and P.J. Houghton, *Establishment of human tumor xenografts in immunodeficient mice*. *Nat Protoc*, 2007. **2**(2): p. 247-50.
224. Zhao, X., Z. Liu, L. Yu, Y. Zhang, P. Baxter, H. Voicu, S. Gurusiddappa, J. Luan, J.M. Su, H.C. Leung, and X.N. Li, *Global gene expression profiling confirms the molecular fidelity of primary tumor-based orthotopic xenograft mouse models of medulloblastoma*. *Neuro Oncol*, 2012. **14**(5): p. 574-83.
225. Fleming, J.M., T.C. Miller, M.J. Meyer, E. Ginsburg, and B.K. Vonderhaar, *Local regulation of human breast xenograft models*. *J Cell Physiol*, 2010. **224**(3): p. 795-806.
226. Talmadge, J.E., R.K. Singh, I.J. Fidler, and A. Raz, *Murine models to evaluate novel and conventional therapeutic strategies for cancer*. *Am J Pathol*, 2007. **170**(3): p. 793-804.
227. Taurozzi, A.J., R. Beekharri, M. Wantoch, M.-C. Labarthe, H.F. Walker, R.I. Seed, M. Simms, G. Rodrigues, J. Bradford, G. van der Horst, G. van der Pluijm, and A.T. Collins, *Spontaneous development of Epstein-Barr Virus*

- associated human lymphomas in a prostate cancer xenograft program. PLoS ONE*, 2017. **12**(11): p. e0188228.
228. Ho, T.W., K.M. Connor, Y. Zhang, E. Pearlman, J. Koppenhaver, X. Fan, C. Lines, L. Edvinsson, P.J. Goadsby, and D. Michelson, *Randomized controlled trial of the CGRP receptor antagonist telcagepant for migraine prevention. Neurology*, 2014. **83**(11): p. 958-66.
229. Ho, T.W., M.D. Ferrari, D.W. Dodick, V. Galet, J. Kost, X. Fan, H. Leibensperger, S. Froman, C. Assaid, C. Lines, H. Koppen, and P.K. Winner, *Efficacy and tolerability of MK-0974 (telcagepant), a new oral antagonist of calcitonin gene-related peptide receptor, compared with zolmitriptan for acute migraine: a randomised, placebo-controlled, parallel-treatment trial. The Lancet*. **372**(9656): p. 2115-2123.
230. ter Haar, E., C.M. Koth, N. Abdul-Manan, L. Swenson, J.T. Coll, J.A. Lippke, C.A. Lepre, M. Garcia-Guzman, and J.M. Moore, *Crystal structure of the ectodomain complex of the CGRP receptor, a class-B GPCR, reveals the site of drug antagonism. Structure*, 2010. **18**(9): p. 1083-93.
231. Bankhead, P., M.B. Loughrey, J.A. Fernandez, Y. Dombrowski, D.G. McArt, P.D. Dunne, S. McQuaid, R.T. Gray, L.J. Murray, H.G. Coleman, J.A. James, M. Salto-Tellez, and P.W. Hamilton, *QuPath: Open source software for digital pathology image analysis. Sci Rep*, 2017. **7**(1): p. 16878.
232. Sinclair, S.R., S.A. Kane, B.J. Van der Schueren, A. Xiao, K.J. Willson, J. Boyle, I. de Lepeleire, Y. Xu, L. Hickey, W.S. Denney, C.-C. Li, J. Palcza, F.H.M. Vanmolkot, M. Depré, A. Van Hecken, M.G. Murphy, T.W. Ho, and J.N. de Hoon, *Inhibition of capsaicin-induced increase in dermal blood flow by the oral CGRP receptor antagonist, telcagepant (MK-0974). British Journal of Clinical Pharmacology*, 2010. **69**(1): p. 15-22.
233. Han, T.H., R.L. Blanchard, J. Palcza, J.B. McCrea, T. Laethem, K. Willson, Y. Xu, S. Ermlich, J. Boyle, C. Lines, M. Gutierrez, L. Van Bortel, A.J. Xiao, S. Sinclair, L. Hickey, D. Panebianco, and M.G. Murphy, *Single- and multiple-dose pharmacokinetics and tolerability of telcagepant, an oral calcitonin gene-related peptide receptor antagonist, in adults. J Clin Pharmacol*, 2010. **50**(12): p. 1367-76.

234. Wright, P.T., S. Schobesberger, and J. Gorelik, *Studying GPCR/cAMP pharmacology from the perspective of cellular structure*. *Frontiers in Pharmacology*, 2015. **6**: p. 148.
235. Moore, E.L. and C.A. Salvatore, *Targeting a family B GPCR/RAMP receptor complex: CGRP receptor antagonists and migraine*. *British Journal of Pharmacology*, 2012. **166**(1): p. 66-78.
236. Sanders, J.L., N. Chattopadhyay, O. Kifor, T. Yamaguchi, and E.M. Brown, *Ca(2+)-sensing receptor expression and PTHrP secretion in PC-3 human prostate cancer cells*. *Am J Physiol Endocrinol Metab*, 2001. **281**(6): p. E1267-74.
237. Dackor, R., K. Fritz-Six, O. Smithies, and K. Caron, *Receptor activity-modifying proteins 2 and 3 have distinct physiological functions from embryogenesis to old age*. *J Biol Chem*, 2007. **282**(25): p. 18094-9.
238. Dackor, R.T., K. Fritz-Six, W.P. Dunworth, C.L. Gibbons, O. Smithies, and K.M. Caron, *Hydrops Fetalis, Cardiovascular Defects, and Embryonic Lethality in Mice Lacking the Calcitonin Receptor-Like Receptor Gene*. *Molecular and Cellular Biology*, 2006. **26**(7): p. 2511-2518.
239. Fritz-Six, K.L., W.P. Dunworth, M. Li, and K.M. Caron, *Adrenomedullin signaling is necessary for murine lymphatic vascular development*. *J Clin Invest*, 2008. **118**(1): p. 40-50.
240. Tsujikawa, K., K. Yayama, T. Hayashi, H. Matsushita, T. Yamaguchi, T. Shigeno, Y. Ogitani, M. Hirayama, T. Kato, S. Fukada, S. Takatori, H. Kawasaki, H. Okamoto, M. Ikawa, M. Okabe, and H. Yamamoto, *Hypertension and dysregulated proinflammatory cytokine production in receptor activity-modifying protein 1-deficient mice*. *Proc Natl Acad Sci U S A*, 2007. **104**(42): p. 16702-7.
241. Mazzocchi, G., L.K. Malendowicz, A. Ziolkowska, R. Spinazzi, P. Rebuffat, F. Aragona, E. Ferrazzi, P.P. Parnigotto, and G.G. Nussdorfer, *Adrenomedullin (AM) and AM receptor type 2 expression is up-regulated in prostate carcinomas (PC), and AM stimulates in vitro growth of a PC-derived cell line by enhancing proliferation and decreasing apoptosis rates*. *International journal of oncology*, 2004. **25**(6): p. 1781-1787.

242. Kaur, G. and J.M. Dufour, *Cell lines: Valuable tools or useless artifacts*. Spermatogenesis, 2012. **2**(1): p. 1-5.
243. Gibson, T.J., M. Seiler, and R.A. Veitia, *The transience of transient overexpression*. Nat Methods, 2013. **10**(8): p. 715-21.
244. Suzuki, K., Y. Kobayashi, and T. Morita, *Significance of serum calcitonin gene-related peptide levels in prostate cancer patients receiving hormonal therapy*. Urol Int, 2009. **82**(3): p. 291-5.
245. Antal, C.E., A.M. Hudson, E. Kang, C. Zanca, C. Wirth, N.L. Stephenson, E.W. Trotter, L.L. Gallegos, C.J. Miller, F.B. Furnari, T. Hunter, J. Brognard, and A.C. Newton, *Cancer-Associated Protein Kinase C Mutations Reveal Kinase's Role as Tumor Suppressor*. Cell, 2015. **160**(3): p. 489-502.
246. Castro, N.P., N.D. Fedorova-Abrams, A.S. Merchant, M.C. Rangel, T. Nagaoka, H. Karasawa, M. Klauzinska, S.M. Hewitt, K. Biswas, S.K. Sharan, and D.S. Salomon, *Cripto-1 as a novel therapeutic target for triple negative breast cancer*. Oncotarget, 2015. **6**(14): p. 11910-11929.
247. Choi, P.S. and M. Meyerson, *Targeted genomic rearrangements using CRISPR/Cas technology*. Nature communications, 2014. **5**: p. 3728-3728.
248. Ofude, M., A. Mizokami, M. Kumaki, K. Izumi, H. Konaka, Y. Kadono, Y. Kitagawa, M. Shin, J. Zhang, E.T. Keller, and M. Namiki, *Repression of cell proliferation and androgen receptor activity in prostate cancer cells by 2'-hydroxyflavanone*. Anticancer Res, 2013. **33**(10): p. 4453-61.
249. Mol, A.J., A.A. Geldof, G.A. Meijer, H.G. van der Poel, and R.J. van Moorselaar, *New experimental markers for early detection of high-risk prostate cancer: role of cell-cell adhesion and cell migration*. J Cancer Res Clin Oncol, 2007. **133**(10): p. 687-95.
250. Kunz, T.H., S. Mueller-Steiner, K. Schwerdtfeger, P. Kleinert, H. Troxler, J.M. Kelm, L.M. Ittner, J.A. Fischer, and W. Born, *Interaction of receptor-activity-modifying protein1 with tubulin*. Biochim Biophys Acta, 2007. **1770**(8): p. 1145-50.
251. Martin, S.K., M. Kamelgarn, and N. Kyprianou, *Cytoskeleton targeting value in prostate cancer treatment*. American Journal of Clinical and Experimental Urology, 2014. **2**(1): p. 15-26.

252. Zhu, M.-L., C. Horbinski, M. Garzotto, D.Z. Qian, T.M. Beer, and N. Kyprianou, *Tubulin-Targeting Chemotherapy Impairs Androgen Receptor Activity in Prostate Cancer*. *Cancer research*, 2010. **70**(20): p. 7992-8002.
253. Gravdal, K., O.J. Halvorsen, S.A. Haukaas, and L.A. Akslen, *A switch from E-cadherin to N-cadherin expression indicates epithelial to mesenchymal transition and is of strong and independent importance for the progress of prostate cancer*. *Clin Cancer Res*, 2007. **13**(23): p. 7003-11.
254. Asiedu, M.K., *Targeting Breast Cancer Stem Cells generated through Epithelial-Mesenchymal Transition: The roles of AXL and ADM/RAMP3 Pathways*. 2011.
255. Jin, J.-K., F. Dayyani, and G.E. Gallick, *Steps in Prostate Cancer Progression that lead to Bone Metastasis*. *International journal of cancer. Journal international du cancer*, 2011. **128**(11): p. 2545-2561.
256. Festuccia, C., V. Dolo, F. Guerra, S. Violini, P. Muzi, A. Pavan, and M. Bologna, *Plasminogen activator system modulates invasive capacity and proliferation in prostatic tumor cells*. *Clin Exp Metastasis*, 1998. **16**(6): p. 513-28.
257. Kumano, M., H. Miyake, M. Muramaki, J. Furukawa, A. Takenaka, and M. Fujisawa, *Expression of urokinase-type plasminogen activator system in prostate cancer: correlation with clinicopathological outcomes in patients undergoing radical prostatectomy*. *Urol Oncol*, 2009. **27**(2): p. 180-6.
258. Rovin, J.D., H.F. Frierson, Jr., W. Ledin, J.T. Parsons, and R.B. Adams, *Expression of focal adhesion kinase in normal and pathologic human prostate tissues*. *Prostate*, 2002. **53**(2): p. 124-32.
259. Tremblay, L., W. Hauck, A.G. Aprikian, L.R. Begin, A. Chapdelaine, and S. Chevalier, *Focal adhesion kinase (pp125FAK) expression, activation and association with paxillin and p50CSK in human metastatic prostate carcinoma*. *Int J Cancer*, 1996. **68**(2): p. 164-71.
260. Tuo, Y., X. Guo, X. Zhang, Z. Wang, J. Zhou, L. Xia, Y. Zhang, J. Wen, and D. Jin, *The biological effects and mechanisms of calcitonin gene-related peptide on human endothelial cell*. *J Recept Signal Transduct Res*, 2013. **33**(2): p. 114-23.

261. Salvatore, C.A., J.C. Hershey, H.A. Corcoran, J.F. Fay, V.K. Johnston, E.L. Moore, S.D. Mosser, C.S. Burgey, D.V. Paone, A.W. Shaw, S.L. Graham, J.P. Vacca, T.M. Williams, K.S. Koblan, and S.A. Kane, *Pharmacological characterization of MK-0974 [N-[(3R,6S)-6-(2,3-difluorophenyl)-2-oxo-1-(2,2,2-trifluoroethyl)azepan-3-yl]-4-(2-oxo-2,3-dihydro-1H-imidazo[4,5-b]pyridin-1-yl)piperidine-1-carboxamide], a potent and orally active calcitonin gene-related peptide receptor antagonist for the treatment of migraine*. *J Pharmacol Exp Ther*, 2008. **324**(2): p. 416-21.
262. Pienta, K.J., C. Abate-Shen, D.B. Agus, R.M. Attar, L.W. Chung, N.M. Greenberg, W.C. Hahn, J.T. Isaacs, N.M. Navone, D.M. Peehl, J.W. Simons, D.B. Solit, H.R. Soule, T.A. VanDyke, M.J. Weber, L. Wu, and R.L. Vessella, *The current state of preclinical prostate cancer animal models*. *Prostate*, 2008. **68**(6): p. 629-39.
263. Rea, D., V. del Vecchio, G. Palma, A. Barbieri, M. Falco, A. Luciano, D. De Biase, S. Perdonà, G. Facchini, and C. Arra, *Mouse Models in Prostate Cancer Translational Research: From Xenograft to PDX*. *BioMed Research International*, 2016. **2016**: p. 9750795.
264. Allocca, G., A.P. Kusumbe, S.K. Ramasamy, and N. Wang, *Confocal/two-photon microscopy in studying colonisation of cancer cells in bone using xenograft mouse models*. *Bonekey Rep*, 2016. **5**: p. 851.
265. Wang, N., K.J. Reeves, H.K. Brown, A.C.M. Fowles, F.E. Docherty, P.D. Ottewell, P.I. Croucher, I. Holen, and C.L. Eaton, *The frequency of osteolytic bone metastasis is determined by conditions of the soil, not the number of seeds; evidence from in vivo models of breast and prostate cancer*. *Journal of Experimental & Clinical Cancer Research : CR*, 2015. **34**: p. 124.
266. Yi, K.H. and J. Lauring, *Recurrent AKT mutations in human cancers: functional consequences and effects on drug sensitivity*. *Oncotarget*, 2016. **7**(4): p. 4241-4251.
267. Chung, T.D., J.J. Yu, T.A. Kong, M.T. Spiotto, and J.M. Lin, *Interleukin-6 activates phosphatidylinositol-3 kinase, which inhibits apoptosis in human prostate cancer cell lines*. *Prostate*, 2000. **42**(1): p. 1-7.

268. Lee, S.O., W. Lou, M. Hou, F. de Miguel, L. Gerber, and A.C. Gao, *Interleukin-6 promotes androgen-independent growth in LNCaP human prostate cancer cells*. Clin Cancer Res, 2003. **9**(1): p. 370-6.
269. Gu, L., P. Talati, P. Vogiatzi, A.L. Romero-Weaver, J. Abdulghani, Z. Liao, B. Leiby, D.T. Hoang, T. Mirtti, K. Alanen, M. Zinda, D. Huszar, and M.T. Nevalainen, *PHARMACOLOGICAL SUPPRESSION OF JAK1/2 BY JAK1/2 INHIBITOR AZD1480 POTENTLY INHIBITS IL-6-INDUCED EXPERIMENTAL PROSTATE CANCER METASTASES FORMATION*. Molecular cancer therapeutics, 2014. **13**(5): p. 1246-1258.
270. Pencik, J., R. Wiebringhaus, M. Susani, Z. Culig, and L. Kenner, *IL-6/STAT3/ARF: the guardians of senescence, cancer progression and metastasis in prostate cancer*. Swiss Med Wkly, 2015. **145**: p. w14215.
271. Wong, A.L.A., J.L. Hirpara, S. Pervaiz, J.Q. Eu, G. Sethi, and B.C. Goh, *Do STAT3 inhibitors have potential in the future for cancer therapy?* Expert Opin Investig Drugs, 2017. **26**(8): p. 883-887.
272. Ahearn, T.U., N. Tchrakian, K.M. Wilson, R. Lis, E. Nuttall, H.D. Sesso, M. Loda, E. Giovannucci, L.A. Mucci, S. Finn, and I.M. Shui, *Calcium-Sensing Receptor Tumor Expression and Lethal Prostate Cancer Progression*. J Clin Endocrinol Metab, 2016. **101**(6): p. 2520-7.
273. Manning, A.T., N. O'Brien, and M.J. Kerin, *Roles for the calcium sensing receptor in primary and metastatic cancer*. Eur J Surg Oncol, 2006. **32**(7): p. 693-7.
274. Liao, J., A. Schneider, N.S. Datta, and L.K. McCauley, *Extracellular calcium as a candidate mediator of prostate cancer skeletal metastasis*. Cancer Res, 2006. **66**(18): p. 9065-73.
275. Greenberg, N.M., F. DeMayo, M.J. Finegold, D. Medina, W.D. Tilley, J.O. Aspinall, G.R. Cunha, A.A. Donjacour, R.J. Matusik, and J.M. Rosen, *Prostate cancer in a transgenic mouse*. Proc Natl Acad Sci U S A, 1995. **92**(8): p. 3439-43.
276. Halse, J., S. Greenspan, F. Cosman, G. Ellis, A. Santora, A. Leung, N. Heyden, S. Samanta, S. Doleckyj, E. Rosenberg, and A.E. Denker, *A phase 2, randomized, placebo-controlled, dose-ranging study of the calcium-sensing*

- receptor antagonist MK-5442 in the treatment of postmenopausal women with osteoporosis.* J Clin Endocrinol Metab, 2014. **99**(11): p. E2207-15.
277. Aggarwal, A., M. Prinz-Wohlgenannt, S. Tennakoon, J. Hobaus, C. Boudot, R. Mentaverri, E.M. Brown, S. Baumgartner-Parzer, and E. Kallay, *The calcium-sensing receptor: A promising target for prevention of colorectal cancer.* Biochim Biophys Acta, 2015. **1853**(9): p. 2158-67.
278. Johansson, H., M.W. Boesgaard, L. Norskov-Lauritsen, I. Larsen, S. Kuhne, D.E. Gloriam, H. Brauner-Osborne, and D. Sejer Pedersen, *Selective Allosteric Antagonists for the G Protein-Coupled Receptor GPRC6A Based on the 2-Phenylindole Privileged Structure Scaffold.* J Med Chem, 2015. **58**(22): p. 8938-51.
279. Schaffner, F., A.M. Ray, and M. Dontenwill, *Integrin alpha5beta1, the Fibronectin Receptor, as a Pertinent Therapeutic Target in Solid Tumors.* Cancers (Basel), 2013. **5**(1): p. 27-47.
280. Tai, Y.L., L.C. Chen, and T.L. Shen, *Emerging roles of focal adhesion kinase in cancer.* Biomed Res Int, 2015. **2015**: p. 690690.
281. Pi, M., K. Kapoor, R. Ye, D.J. Hwang, D.D. Miller, J.C. Smith, J. Baudry, and L.D. Quarles, *Computationally identified novel agonists for GPRC6A.* PLoS One, 2018. **13**(4): p. e0195980.